Impact of Wettability on Rock Mechanics and Oil Recovery

A Comparative Study on Different Outcrop Chalks

by

Jaspreet Singh Sachdeva

Thesis submitted in fulfilment of
the requirements for the degree of
PHILOSOPHIAE DOCTOR
(PhD)

Faculty of Science and Technology
Department of Energy Resources
2020

University of Stavanger
NO-4036 Stavanger
NORWAY
www.uis.no

ISBN: 978-82-7644-905-1
ISSN: 1890-1387
PhD: Thesis UiS No. 502

This dissertation is dedicated to my parents who instilled in me the virtues of perseverance and commitment and relentlessly encouraged me to strive for excellence.

Acknowledgements

I would like to express my sincere gratitude to everyone who helped and encouraged me in various ways in carrying out my PhD work. Their contributions are sincerely appreciated and gratefully acknowledged.

First and foremost, I would like to thank Dr. Anders Nermoen, Prof. Merete Vadla Madland and Dr. Reidar Inge Korsnes for their guidance, advices and suggestions throughout the term of my PhD. Without their valuable assistance, always generously and unstintingly given, the completion of this work would have been immeasurably more difficult. Dr. Korsnes' cheerful mood and love for the same taste in music as me made my time spent in the laboratories completely worthwhile.

I am also indebted to The National IOR Centre of Norway for introducing me to so many industry stalwarts in Improved Oil Recovery and Rock Mechanics field of studies and helping me learn so much more than what I had wished for at the start of my PhD. I would also like to thank everyone at the Department of Energy Resources and Department of Energy and Petroleum Engineering, University of Stavanger, for their support and cooperation.

I would also like to give my special thanks to Dr. Kim Andre Vorland and Dr. Ola Kjetil Siqveland for their invaluable help in carrying out the experimental work. During this work, the constant association with all my PhD colleagues, especially Tijana Voake, Dhruvit Satishchandra Berawala and Shreyansh Divyankar, and their valuable suggestions are highly appreciated. I would also like to thank *Folken* in Stavanger for providing me with a second home in Norway.

I really appreciate the time spent with the Hibernia EOR group at the Memorial University of Newfoundland, Canada, as an exchange researcher and would like to extend my heartiest gratitude to Prof. Lesley Anne James and Mr. Edison Sripal for teaching me so much through

experimental studies and long discussions. The time spent in St. John's also provided me with an opportunity to meet many new people, including Rishikesh Nair, which I will cherish forever.

My special thanks go to my parents Mr. Amarjeet Singh Sachdeva and Mrs. Kulvinder Kaur Sachdeva for their continuous encouragement, love and support during my thesis work. Their morale boosting support during these years cannot be described in words. I also express my gratitude to my brother Mr. Darshanjeet Singh Sachdeva, my sister-in-law Ms. Harkirtan Kaur Sachdeva and my beautiful niece Suhaavi Kaur Sachdeva for continuously inspiring me to achieve new heights.

I am also very grateful to all my extended family members and friends across the globe for believing in me and for providing their support at all times.

I, once again, thank everyone for their never-ending support and encouragement that they have provided me at various stages of my PhD period.

Jaspreet Singh Sachdeva

Summary

Chalk reservoirs are highly fractured and are known for their remarkable storage capacity as a reservoir rock for the petroleum industry. Chalk is a sedimentary carbonate rock primarily made up of calcium carbonate (calcite, $CaCO_3$) and is a very important reservoir rock in the Norwegian and Danish Continental Shelfs. Water flooding has been used as a secondary production method in chalk reservoirs as it provides pressure maintenance to the reservoir and is a proven improved oil recovery (IOR) method to produce more oil from the production facilities. Ekofisk field in the Norwegian Continental Shelf is a successful example of production by water flooding method, where seawater is used as the injection fluid. The initial estimated oil recovery was 18% as mentioned in the initial development plan of the field and today's estimates lie well above 50%.

However, seawater has also shown to enhance reservoir compaction due to water weakening of the chalk formation. It can, for example, lead to buckling and loss of well pipes, arching of overburden rocks leading to stress redistributions, and the porosity/permeability decline of the producible formation, all physical effects that alter the ultimate recovery and recovery rates of oil-bearing chalk reservoirs.

The detection of subsidence of the Ekofisk field in the Norwegian North Sea around 35 years ago has been linked to the compaction of chalk formations due to porosity reduction associated with field production. It attracted the attention of oil and gas researchers across the globe and since that time, considerable research has been carried out concerning chalk behavior, especially on how the pore fluid composition alters the mechanical properties of chalk.

Research on chalk, so far, has primarily been carried out on water-wet systems. The studies have shown that when reactive brines are injected through chalk at elevated temperatures, chemical reactions occur

between the rock and the injected brine, which affects chalk mechanical stability. It has been found that the divalent ions, such as magnesium (Mg^{2+}), calcium (Ca^{2+}) and sulfate (SO_4^{2-}) play an important role in defining chalk mechanics. Mg^{2+} ions in the injected brines lead to dissolution of calcite, which in turn leads to precipitation of new mineral phases such as magnesite, huntite, talc, anhydrite etc. Both Mg^{2+} and SO_4^{2-} ions also adsorb on the chalk surface leading to a reduction in the strength of the rock.

This project deals with the mechanical effects and oil production upon brine injection through wettability-altered samples from two chalk types. **Paper I** and **Paper III** give the results from the mechanical tests performed on Kansas chalk and Mons chalk, respectively. Both chalk types were saturated by a mixture of oil (60% - 40% by volume of Heidrun oil and heptane) and 1.1 M sodium chloride (NaCl) brine and aged for three weeks at 90°C. The wettability index of the altered samples was estimated using chromatographic separation tests by co-injecting sulfate ions, that adsorb on the water-wet mineral surfaces, and non-affine tracer. A good repeatability was observed for both chalk types.

In the triaxial test program, unaged water-wet and aged wettability-altered samples were hydrostatically loaded to 1.5 times yield stress so stiffness and strength could be determined. The samples were kept at the same stress level over time to monitor the volumetric creep. After a stagnant creep period of 15 days, magnesium chloride ($MgCl_2$) brine was flushed through both chalk types. A different set of Kansas samples from the same chalk block were also flooded by seawater. The effluents were taken at frequent intervals of time and tested using Ion Chromatography for effluent concentration. The oil production from the wettability-altered samples was also continuously monitored.

The combined observations of the bulk volume, oil volume and estimated solid volume (from effluent analyses) were used to calculate pore volume and thereby oil saturation with time.

Paper I showed that the wettability-altered Kansas chalk samples were stiffer and stronger than the water-wet samples, and when the stress was kept at 1.5 times yield the creep curves overlapped. During the flow-through period, the changes in ion composition were insensitive to the presence of oil, and ongoing water weakening for wettability-altered samples was the same as in the water-wet samples. Further, it was found that oil was only produced during the first 2–3 pore volumes (PVs) of injected brine. Afterwards, no oil was produced even though the chemical reactions took place and pore volume reduced.

Paper III showed that both water wet and wettability-altered Mons chalk samples gave comparable trends during the stagnant phase and the following $MgCl_2$ injection phase when the stress was kept at 1.5 times yield. They also showed that the non-equilibrium chemical reactions were insensitive to the initial wettability. The oil production observations, however, showed that 43% of the total oil was recovered during early-stage compaction from Mons chalk with no flow, whereas Kansas chalk did not produce any oil. No tail-end oil production was observed due to compaction or non-equilibrium brine flow in any of the two chalk types.

Paper II dealt with evaluating the extent to which chemical interactions induced by the $MgCl_2$ brine injection modify the water wetness of wettability-altered chalk samples. These tests were performed at low effective stresses. In situ wettability measurements were carried out using chromatographic separation and were performed every 10 days to estimate the evolution in mineral surface area in contact with water. The results showed an increased delay time for the sulfate ion, linked to an increase of the mineral surface area, which was observed in both water-wet and wettability-altered cores but was found to be more dominating

in the wettability-altered samples. This implied that oil, which was adsorbed on the mineral surfaces, got mobilized in addition to an increased overall specific surface area as new magnesium-bearing minerals precipitated and grew during the $MgCl_2$ brine flow. This was supported by continuous effluent analysis displaying a reduced magnesium and increased calcium concentration. As in **Paper I** and **Paper III**, the nonequilibrium chemical reactions did not lead to additional oil recovery.

The main objective of **Paper IV** was to evaluate the degree to which the wettability in chalk core samples can be controlled in the laboratory. Kansas chalk samples saturated with the same 1.1M NaCl brine and oil mixture (60% - 40% by volume of Heidrun oil and heptane), as in Paper I, II and III, were aged at a constant temperature of 90°C with aging time as the laboratory control variable. A multimodal method incorporating contact angle measurements, wettability index via USBM test, and SEM-MLA analysis was applied in evaluating wettability. It was observed that an aging period of 21 days was enough to obtain a stable wettability at the specified aging conditions.

Paper V dealt with exploring elastic and plastic parameters during deviatoric loading and time-dependent deformation. A series of experiments were performed at 130°C to study the effect of four different fluids, viz., distilled water (DW), NaCl-brine, $MgCl_2$-brine and seawater (SSW), on Mons outcrop chalk. The cores were deviatorically loaded and left to creep at a constant value of 69-73% of the axial yield stress obtained from reference tests with the same brine. The results showed that SSW had the lowest yield stress followed by NaCl and $MgCl_2$, and highest for DW. The final creep strain was highest for SSW and was 1.3-1.5 times higher than for other brines. The core initially saturated by SSW showed the highest plastic component of the total strain inferring that the ions in SSW does play an important role in inducing permanent damage.

The main aim of **Paper VI** was to check how the mechanical strength of chalk depends on the chemistry of pore fluids. Experiments were performed at uni-axial strain conditions maintaining constant overburden stress during pore pressure depletion and subsequent compaction phase. Significant differences were observed during the depletion and time-dependent compaction phase. The oil-saturated core was stronger than core saturated by brine-oil mixture, while the brine-saturated core accumulated most strain. During compaction, seawater was injected that led to additional strain; most so in the oil-saturated core, intermediate additional strain in the brine-oil mixed core, and least additional strain was observed in the brine-saturated core. This is in line with earlier results on how the ion composition of seawater significantly impacted chalk mechanics. It was also observed that the seawater induced weakening is abrupt, and it is more prominent when there is less water in the core originally.

Abbreviations and Symbols

W_i	Wettability index
A_1	Area under the secondary drainage capillary pressure curve
A_2	Area under the primary imbibition capillary pressure curve
S_w	Water saturation
A_{mw}	Area between thiocyanate and sulfate concentration curves for wettability-altered sample
A_{ww}	Area between thiocyanate and sulfate concentration curves for water-wet sample
σ	Stress / Stress tensor
σ_{ij}	Normal components of stress
τ_{ij}	Shear components of stress
r	Radial direction
θ	Tangential direction
z	Axial direction
ε	Strain / Strain tensor
t	Time
L_o	Original length of sample
$L(t)$	Length of sample at time t

ΔL	Change in length of sample
ε_{ij}	Normal components of strain
Γ_{ij}	Shear components of strain
σ'	Effective stress
α	Biot coefficient
P_f	Pore pressure
E	Young's / Elastic modulus
ν	Poisson's ratio
ε_{vol}	Volumetric strain
V_o	Original volume of sample
ΔV	Change in volume of sample
ε_r	Radial strain
ε_θ	Tangential strain
ε_z	Axial strain
r_o	Original radius of sample
Δr	Change in radius of sample
X	Conversion factor to convert axial strain to volumetric strain
σ'_{hyd}	Effective hydrostatic stress
K	Bulk modulus of material

P_{conf} / σ_{rad}	Confining pressure
f_{area}	Area factor that relates the area of the core plug to the area of the chamber in the triaxial cell
P_{pist}	Hydraulic pressure in the piston chamber of the triaxial cell
P_{fric}	Friction of the piston / friction pressure in the triaxial cell
$\sigma_{elastic}$	Linear elastic stress
V_b	Bulk volume of sample
ε_p	Strain component due to change in pore volume of sample
ε_s	Strain component due to change in solid volume of sample
ΔV_s	Change in the solid volume of sample
$M_{s,o}$	Original solid mass of core plug
$M_s(t)$	Mass evolution of core plug with time
$\rho_{s,o}$	Original solid density of core plug
$\rho_s(t)$	Density evolution of core plug with time
$m_{Ca}(t)$	Amount of calcium produced from the core plug at time t
$m_{Ca,total}$	Total amount of calcium produced from the core plug
$\rho_{s,f}$	Final solid density of core plug
η	Fitting parameter that makes the observed replacement of calcium by magnesium from ion chromatography data match the observed loss in dry mass before and after test

q_{in} / Q	Injection flow rate
n_{Mg}	Molar weight of magnesium = 24 g/mol
n_{Ca}	Molar weight of calcium = 40 g/mol
$c_{in,Mg}$	Inlet molar concentration of magnesium
$c_{out,Mg}$	Outlet molar concentration of magnesium
$c_{in,Ca}$	Inlet molar concentration of calcium
$c_{out,Ca}$	Outlet molar concentration of calcium
V_s	Solid volume of sample
V_p	Pore volume of sample
ΔV_p	Change in the pore volume of sample
ΔV_b	Change in the bulk volume of sample
$V_{b,o}$	Original bulk volume of sample
$V_{p,o}$	Original pore volume of sample
φ	Porosity of the core plug
S_{wi}	Irreducible / Initial water saturation
P_c	Capillary pressure
ω	Angular rotation speed of centrifuge
$\widehat{C_k}$	Reduced concentrations of sulfate and thiocyanate ions
Mg^{2+}	Magnesium ion
Ca^{2+}	Calcium ion

SO_4^{2-}	Sulfate ion
Na^+	Sodium ion
Cl^-	Chloride ion
SCN^-	Thiocyanate ion
BET	Brunauer–Emmett–Teller
BSE	BackScattered Electron
$CaCO_3$	Calcium Carbonate / Calcite
DW	Distilled Water
EDX	Energy Dispersive X-ray
EOR	Enhanced Oil Recovery
FEG	Field Emission Gun
FEG-SEM	Field Emission Gun Scanning Electron Microscopy
HFW	High Full Well
IC	Ion Chromatography
IOR	Improved Oil Recovery
LVDT	Linear Voltage Differential Transducer
$MgCO_3$	Magnesium Carbonate / Magnesite
$MgCl_2$	Magnesium Chloride
NaCl	Sodium Chloride
PV	Pore Volume

PV_i	Initial Pore Volume
SCAL	Special Core Analysis
SEM-MLA	Scanning Electron Microscope - Mineral Liberation Analysis
SSA	Specific Surface Area
SSW	Synthetic Seawater
USBM	United States Bureau of Mines

List of publications

Paper I:

Sachdeva, J.S., Nermoen, A., Korsnes, R.I., and Madland, M.V. (2019). Impact of Initial Wettability and Injection Brine Chemistry on Mechanical Behaviour of Kansas Chalk. *Transport in Porous Media*, **128**(2), 755-795. https://doi.org/10.1007/s11242-019-01269-z.

Paper II:

Sachdeva, J.S., Muriel, H., Nermoen, A., Korsnes, R.I., and Madland, M.V. (2019). Chalk Surface Area Evolution during Flow of Reactive Brines: Does Oil Play a Role? *Energy & Fuels*, **33**(6), 4890-4908. https://doi.org/10.1021/acs.energyfuels.9b00515.

Paper III:

Sachdeva, J.S., Nermoen, A., Korsnes, R.I., and Madland, M.V. (2019). Effect of Initial Wettability on Rock Mechanics and Oil Recovery: Comparative Study on Outcrop Chalks. Submitted to *Transport in Porous Media*, publication under review.

Paper IV:

Sachdeva, J.S., Sripal, E.A., Nermoen, A., Korsnes, R.I., Madland, M.V., and James, L.A. (2018). A Laboratory Scale Approach to Wettability Restoration in Chalk Core Samples. Paper SCA2018-117 presented at the International Symposium of the Society of Core Analysts, Trondheim, Norway, 27-30 August.

Paper V:

Sachdeva, J.S., Nermoen, A., Korsnes, R.I., and Madland, M.V. (2017). Elastic and Plastic Behavior of Chalks at Deviatoric Stress Condition: Experiments Performed with Four Different Brines. Paper Tu P030 presented at the IOR Norway 2017 – 19th European Symposium on Improved Oil Recovery, Stavanger, Norway, 24-27 April.

Paper VI:

Sachdeva, J.S., Nermoen, A., Madland, M.V., and Korsnes, R.I. (2016). How Wetting Conditions Dictate Chalk Mechanics at Uni-axial Strain Conditions – Insights from Experiments Performed at In-situ Stress, Temperature and Pore Pressure. Paper SCA2016-068. *International Symposium of the Society of Core Analysts 2016*, Snowmass, Colorado, USA.

Additional contributions

Sachdeva, J.S., Nermoen, A., Korsnes, R.I., and Madland, M.V. (2019). Impact of Initial Wettability and Injection Brine Chemistry on Chalk Mechanics of Kansas and Mons Outcrops. *IOR Norway 2019*, Stavanger, Norway.

Sachdeva, J.S., Nermoen, A., Korsnes, R.I., and Madland, M.V. (2019). Impact of Wettability on Geomechanics and Oil Recovery / Observations on Outcrop Chalk. *Workshop on Wettability Characterization and Alteration of Heterogeneous Carbonate Reservoir Rocks*, NORCE, Stavanger, Norway, March 18.

Sachdeva, J.S., Nermoen, A., Korsnes, R.I., and Madland, M.V. (2018). How the Presence of Oil and Water Affects Chalk Mechanics at Isotropic Stresses. Extended Abstract. *80th EAGE Conference and Exhibition 2018*, Copenhagen, Denmark.

Sachdeva, J.S., Nermoen, A., Korsnes, R.I., and Madland, M.V. (2018). Effect of presence of oil and water on chalk mechanics. *IOR Norway 2018*, Stavanger, Norway.

Minde, M.W., Sachdeva, J.S., Zimmermann, U., Madland, M.V., Korsnes, R.I., and Nermoen, A. (2018). Mineral alterations in water wet and mixed wet chalk due to flooding of seawater-like brines. *IOR Norway 2018*, Stavanger, Norway.

Sachdeva, J.S., Nermoen, A., Madland, M.V., and Korsnes, R.I. (2016). How Wetting Conditions Dictate Chalk Mechanics at Uni-axial Strain Conditions – Insights from Experiments Performed at In-situ Stress, Temperature and Pore Pressure. Lunch and Learn. *University of Stavanger 2016*.

Sachdeva, J.S., Nermoen, A., Madland, M.V., Korsnes, R.I., and Siqveland, O.K. (2016). Which processes are at play during wettability alteration and water induced compaction of chalks? *IOR Norway 2016*, Stavanger, Norway.

Table of Contents

List of Figures

List of Tables

1 Introduction

Approximately 50-60% of the known oil and gas reserves worldwide are found in rocks made up of calcium carbonate ($CaCO_3$) originating from the deposition of the shells or skeletal material in shallow, warm ocean waters (Roehl and Choquette 1985; Lucia 1992; Flügel 2004; Burchette 2012). Due to a decrease in the amount of recoverable reserves using current technologies / strategies, it is of paramount importance to develop and implement measures that could increase the recovery of oil from such reservoirs. This, in turn, would also guide the ways to effectively produce from the reservoirs which are still undiscovered or undeveloped. This will help to increase the recovery rates and reduce the environmental footprint.

Several major oil and gas fields on the Norwegian Continental Shelf (NCS) are producing from chalk reservoirs. Chalks are often found in deep basins as well as on drowned shelves developed from lithification of fine-grained skeletons of planktonic microorganisms, that contain the calcite, during diagenetic processes (Lucia 1992). Chalk rocks of today can be characterised as soft, white, porous sedimentary carbonate rocks formed in marine environments by the sedimentation of calcite shells. They are very fascinating granular materials because their mechanical properties depend on the physico-chemical interplay with the pore fluids. In addition to being a rock-type that contain great hydrocarbon potential, chalks can also be used to study the organisms living in the ocean and the paleoclimate at which the sediments were deposited. They are often highly porous and low permeable because of the sub-micrometer sizes of the pores and skeletal remains.

Seawater is often injected into chalk reservoirs as means of pressure support and secondary means of improved oil recovery. However, seawater injection into chalk leads to enhanced compaction of the reservoir rock. This compaction is a result of both pore pressure

depletion early in the field life, and water weakening induced by seawater injection at later stages (Gauer et al. 2002). The compaction by pore volume reduction has been suggested to be an important driving mechanism for mobilizing resident fluids towards production facilities and, hence compaction is of great potential for improving oil recovery, especially if oils are mobile (Sulak and Danielsen 1989; Sulak 1991; Hermansen et al. 2000). Now the mobility of the different fluids is a function of the surface affinity of oil and water, so it is not self-evident that pore volume reduction leads to improved oil recovery rates. This is one of the hypotheses that is put to test in this study.

Reservoir compaction, however, has also shown to induce seafloor subsidence affecting the equipment resting on the sea floor (Sulak and Danielsen 1989; Maury et al. 1996; Nagel 1998; Sylte et al. 1999; Gauer et al. 2002). Seafloor subsidence was detected at the Ekofisk field in the Norwegian North Sea in 1984 (Wiborg and Jewhurst 1986; Sulak and Danielsen 1989). Serious concerns were raised relating to buckling and loss of well pipes, arching of overburden rocks leading to stress redistributions, and the porosity/permeability decline of the producible formation, all physical effects that alter the ultimate recovery and recovery rates of oil bearing chalk reservoirs (Thomas et al. 1987; Teufel et al. 1991; Maury et al. 1996; Hermansen et al. 1997; Nagel 1998; Kristiansen et al. 2005; Doornhof et al. 2006). This subsidence had a consequence on the safety of the equipment, as well as safety of the personnel on the platforms. The height of the platform deck above sea was not enough to avoid the highest waves, hence the platforms were jacked-up by six meters (Overview Greater Ekofisk Area 2019). Since then, considerable research has been carried out concerning chalk behavior in general, and mechanical properties in particular. Johnson and Rhett (1986) and Schroeder and Shao (1996) concluded that the pore collapse deformation of high porosity chalk accounted for most of the reservoir compaction and subsidence. Piau and Maury (1994) mentioned the action of local shear forces exerted by oil/water menisci on grains

(Andersen et al. 1992) and suggested the existence of very localized and quasi-instantaneous chemical actions of brines on grain-to-grain contacts as possible weakening mechanisms. Lord et al. (1998), Heugas and Charlez (1990), and Piau and Maury (1994) pointed out that mineral dissolution at grain-to-grain contacts was needed to be considered in order to explain the water weakening effect.

Later, research focused on understanding how the mechanical behavior of chalk is dictated by the pore fluid chemistry (Risnes 2001; Hellmann et al. 2002a, 2002b; Risnes et al. 2003; Madland et al. 2008; Korsnes et al. 2008; Neveux et al. 2014a, 2014b). These studies dealt with how aqueous chemistry affected mechanical stiffness and plastic failure strength during hydrostatic stress build-up, and the time-dependent deformation during creep. The analysis of the effluent brines and the chemical and micro-structural changes to the minerals in the rock have shown that the injected brines are not in equilibrium with the rock surface. As such, over time changes of the load bearing framework affect the creep deformation rates at constant stress condition during continuous brine flow (Korsnes et al. 2006a, 2006b, 2008; Madland et al. 2008, 2011; Megawati et al. 2011, 2013).

The chemical composition and microscopic structure of the mineral phases that constitutes the chalk, i.e. the load bearing structure, are subject to change when being exposed to continuous flooding of reactive brines over significant times. A reactive brine is composed of surface-active divalent ions, such as magnesium (Mg^{2+}), calcium (Ca^{2+}) and sulfate (SO_4^{2-}), that interacts with the calcite surface and changes its microscopic structural framework, whereas a weakly reactive brine consists of monovalent ions such as sodium (Na^{+}) and chloride (Cl^{-}) that show a lower affinity for calcite surface compared to the divalent ions.

Heggheim et al. (2005) observed that sulfate ions in the injected synthetic seawater (SSW) brine led to a reduced yield and caused weakening of chalk. The point to be noted here is that these tests were run at ambient

conditions and there was no flooding during loading phase. The cores were aged for four weeks at 130°C. Korsnes et al. (2008) also observed the same effect by demonstrating that flooding SSW containing sulfate ions through chalk yielded at a significantly lower stress compared to the samples flooded by SSW without sulfate ions. This reduction in yield, at that time, was concluded to have been caused due to the precipitation of anhydrite. Megawati et al. (2013) further showed using sodium sulfate as the injection brine that if the brine contains only sulfate as the surface-active ion, the reduction in yield is due to its adsorption on the charged calcite surface. The interaction between neighbouring charged surfaces (electrical double layer) gives rise to repulsive electrostatic forces. This leads to a disjoining pressure between grains that eases grain re-organization and allows for pore collapse at lower stresses because the normal load between grain-grain reduces the frictional forces. This process has been employed to explain (a) yielding at lower effective stresses than when saturated by brines without surface-active ions (Korsnes et al. 2008; Liteanu et al. 2013) and (b) additional rates of compaction (Nermoen et al. 2014) when seawater was injected.

When magnesium chloride ($MgCl_2$) brine is injected through chalk, dissolution of calcite $CaCO_3$ and precipitation of magnesite $MgCO_3$ occur (Madland et al. 2011; Nermoen et al. 2015; Zimmermann et al. 2015; Minde et al. 2017, 2018a, 2018b; Andersen et al. 2018). These dissolution/precipitation processes lead to enhanced bulk volume creep rates in chalk compared to when flooded with weakly reactive sodium chloride (NaCl) brine (Madland et al. 2009, 2011). Megawati et al. (2011) also showed similar results while flooding chalk with $MgCl_2$ brine. Further, Nermoen et al. (2015) showed that the compaction rate was sensitive to the injection rate. At higher flooding rates, the rate of dissolution of calcite and precipitation of Mg-bearing minerals increased. The solid volume changed because the sample lost mass and the mineral density increased (density of magnesite is 3.0 g/cm^3 and calcite is 2.7 g/cm^3). Further, the solid volume changes led to a reduction

in bulk volume, and the grains unlocked and reorganized to reduce pore volume. Long-term $MgCl_2$ flooding tests (516 days and 1072 days) on Liège water-wet chalk (Belgium) altered the mineralogy from calcite to Mg-bearing minerals dominated by magnesite (Nermoen et al. 2015; Zimmermann et al. 2015; Minde et al. 2017; Borromeo et al. 2018). These observations are in line with modeling results reported in Hiorth et al. (2013).

In addition, the divalent magnesium ions have also shown to adsorb on available surface sites leading to desorption of calcium ions from the internal calcite surface (Ahsan and Fabricius 2010; Alam et al. 2010; Nermoen et al. 2018a), resulting in stiffening and strengthening of chalk due to a lower internal repulsive electrostatic force.

It has also been suggested that chemical reactions between the injected non-equilibrium brines and chalk surface lead to additional oil recovery (Hiorth et al. 2010) either due to rock dissolution or change in the surface charge during brine injection that affects rock wettability. For chemical reactions to be non-negligible, tens (or hundreds) of pore volumes are required. So, for chemical reactions to play a role in enhancing the oil recovery, it must be to mobilize oil after the initial displacement.

Megawati et al. (2015) and Andersen et al. (2018) studied five different chalk types and found a dependence of the non-carbonate content on how the mechanical creep behavior was affected by $MgCl_2$ brine injection. Injecting this brine into impure chalks (Liège, Aalborg and Kansas) led to an immediate increased creep rate. However, in pure chalks (Mons and Stevns Klint) the creep response was delayed by a time lag of several weeks before a tertiary-like creep developed. These rock samples were never exposed to oil, which enabled the aqueous solution to contact the minerals directly.

Both ongoing adsorption/desorption and dissolution/precipitation processes, that describe the interactions between the pore fluid and the mineralogical surfaces, have shown to change several of the parameters

that describe chalk mechanical behavior, such as elastic stiffness, plastic strength and time-dependent deformation rates.

Further on, wettability of chalk has been studied to understand how wettability affects multiphase fluid flow, and how alterating the wetting state impacts oil production (Standnes and Austad 2000a, 2000b; Zhang and Austad 2005; Zhang et al. 2006; Strand et al., 2007; Fathi et al. 2010). Prior to flooding and imbibition experiments, reservoir chalk or outcrop chalk is cleaned with solvents and distilled water rendering it water wet. The water-wet chalk surface prefers water coating the grains, and will spontaneously imbibe water, which on pore level controls the flow of oil. Hence, to obtain realistic oil production curves, the wettability of these chalk samples must be changed to a neutral-wet / oil-wet state. This is a standard routine in these experiments and is done by flooding crude oil and water, and then aging over time at high temperature before the wettability can be determined and any additional experiments can be performed. The aged core samples are, then, imbibed and/or flooded and the oil production is quantified as a function of the injected brine composition.

1.1 Objectives

Most of the geomechanical experiments performed so far have exclusively been performed on samples that have never been exposed to oil such that the mineral phases were considered water wet. This has enabled the aqueous solution to contact the minerals directly, and as such, the applicability of the water weakening mechanism to oil reservoir samples has been debated. The question has been to what degree the load bearing structure, especially the grain contacts, are prone to the documented water weakening because the minerals within an oil reservoir chalk sample can sometimes be partially or completely covered with organic oil components that inhibit the adsorption and dissolution/precipitation processes.

Therefore, this study deals with the combined effect of initial wettability and injection brine chemistry on the mechanical response in chalk. Figure 1 shows how wettability, rock mechanics, multiphase flow in porous media and chemical reactions by rock-fluid interactions define the chalk core dynamics.

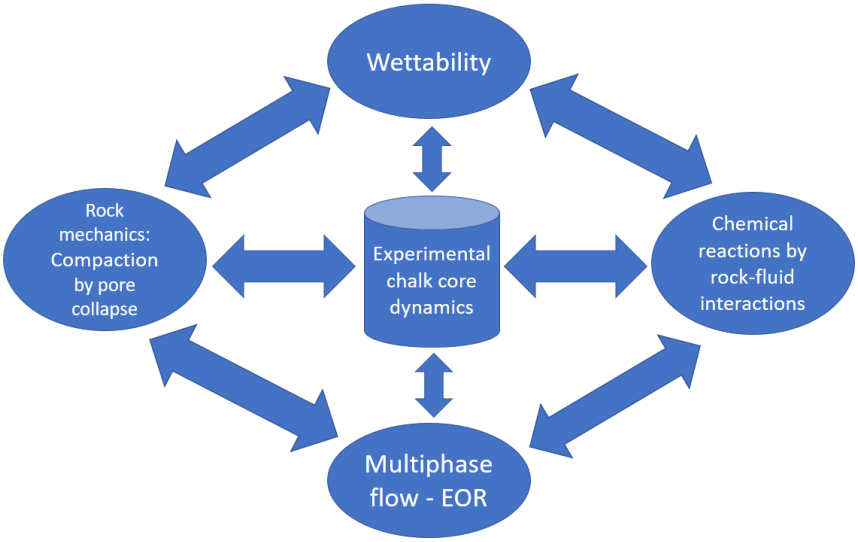

Figure 1. Relationship of chalk core dynamics to various experimentally derived parameters.

Hence, the main research goals of this study are defined in the following points:

1. Defining and evaluating the impact of initial wettability on chalk mechanics.
2. Defining and evaluating the effect of injection brine chemistry on the mechanical response in wettability-altered chalk.
3. Quantifying and understanding the effect of compaction on enhanced oil recovery.
4. Understanding the effect of non-equilibrium rock-fluid interactions on enhanced oil recovery.

1.2 Thesis Outline

This thesis is divided into five main sections. They are:

Section 2 covers the theory related to rock mechanics that has been applied in this work. It includes the basics of stress and strain, their relationship using Hooke's law and the definition of the elastic moduli. It also includes the explanation of drained conditions used in this study. Section 3 covers the materials and methods used in this work, while section 4 presents the main results from the work performed and the discussion of these results. The last section, section 5, provides the concluding remarks and the scope of future work.

Three journal papers (**Paper I**, **Paper II** and **Paper III**) and one conference proceeding (**Paper IV**), that document the main body of this PhD thesis, are attached in the end. Two more conference proceedings (**Paper V** and **Paper VI**) are also attached, however they are not discussed in the main body of this thesis as they do not directly complement the main objective of this work but are performed as extra work during the tenure of the PhD.

2 Theory

In this chapter, the key underlying processes of rock mechanics, used in this study of how chalk mechanics, multiphase flow and mineral wettability are related, are presented.

Rock Mechanics is an applied science of the mechanical behavior of rock masses. It is the study of deformation resulting from the strain of rocks in response to applied stresses. Most materials have an ability to resist and recover from deformations produced by forces. This ability is called elasticity. It is the foundation for all aspects of rock mechanics.

2.1 Stress and strain

Stress is defined as force per unit area. A stress tensor is used to describe the stresses in a porous body. For a cylindrical core plug, a stress tensor σ is defined by,

$$\sigma_{ij} = \begin{bmatrix} \sigma_{rr} & \tau_{r\theta} & \tau_{rz} \\ \tau_{\theta r} & \sigma_{\theta\theta} & \tau_{\theta z} \\ \tau_{zr} & \tau_{z\theta} & \sigma_{zz} \end{bmatrix} \quad (1)$$

where τ_{ij} defines the shear components and σ_{ij} defines the normal components of stress, with $ij = \{r, \theta, z\}$ denoting the radial (r), tangential (θ) and axial (z) directions. When there is no net translational or rotational force acting in the solid body (i.e., $\tau_{r\theta} = \tau_{\theta r}$, $\tau_{rz} = \tau_{zr}$ and $\tau_{\theta z} = \tau_{z\theta}$), a stress tensor can be defined by six independent components only. The off-diagonal elements vanish (τ_{ij}) when the stress tensor is rotated to find the principal directions. For every point inside a body under static equilibrium there are three directions, called the principal directions, where the stress vector is normal to the plane and there is no shear component. These normal stress vectors are called principal stresses. In cylindrical geometries, the principal directions align with the r, θ and z directions.

Now, when a force is applied on a body, there is some change in the dimensions. The most commonly accepted definition of strain defines it as the ratio of elongation in the length of the body ΔL to its original length L_o. Hence, the strain ε at any given time t is given by,

$$\varepsilon(t) = -\frac{L(t) - L_o}{L_o} = -\frac{\Delta L}{L_o} \tag{2}$$

where $L(t)$ is the length of the body at time t. This sign convention is consistent with that of positive compressive stresses, i.e. a positive strain is associated with contraction. This definition of strain is applicable to small finite deformations. In cylindrical coordinates, a strain tensor ε is defined by,

$$\varepsilon_{ij} = \begin{bmatrix} \varepsilon_{rr} & \Gamma_{r\theta} & \Gamma_{rz} \\ \Gamma_{\theta r} & \varepsilon_{\theta\theta} & \Gamma_{\theta z} \\ \Gamma_{zr} & \Gamma_{z\theta} & \varepsilon_{zz} \end{bmatrix} \tag{3}$$

where Γ_{ij} defines the shear components and ε_{ij} defines the normal components of strain. As is the case with the stress tensor, the shear strains also balance each other (i.e., $\Gamma_{r\theta} = \Gamma_{\theta r}$, $\Gamma_{rz} = \Gamma_{zr}$ and $\Gamma_{\theta z} = \Gamma_{z\theta}$), thereby reducing the number of parameters required to describe the deformation of a volume to six. The off-diagonal elements vanish (Γ_{ij}) when the strain tensor is rotated to find the principal directions.

2.2 Effective stresses - Biot coefficient

In porous rocks, the external load is transmitted through the solids at inter-granular contacts. At the same time, some of the externally applied load is carried by the fluid pressure within the pores, thereby reducing the influence of the applied stress. The observed deformation is therefore subjected to the interaction between the fluid pressure and the solid stresses into the effective stress relation. The magnitude of the fluid-to-solid force exchange is given by the fluid-solid contact area. This area is related to the degree of cementation and the spacing between grain

contacts. Hence, an equivalent effective stress variable σ' is calculated from the applied stress σ minus a fraction of the pore pressure P_f. This fraction α is given by the cemented cross-area and is termed the Biot coefficient, which always lies between 0 and 1. Hence, the effective stress is defined by,

$$\sigma' = \sigma - \alpha P_f \tag{4}$$

In tensor form, the effective stress is given by,

$$\sigma' = \begin{bmatrix} \sigma_{rr} - \sigma P_f & \tau_{r\theta} & \tau_{rz} \\ \tau_{\theta r} & \sigma_{\theta\theta} - \sigma P_f & \tau_{\theta z} \\ \tau_{zr} & \tau_{z\theta} & \sigma_{zz} - \sigma P_f \end{bmatrix} \tag{5}$$

2.3 Elastic moduli

For small stresses and/or strains (i.e. in the limit of linear elasticity) and assuming homogeneous and isotropic materials, Hooke's law can be used to relate stresses and strains. It assumes that the deformation is immediate, linear and reversible. The elastic parameters that describe the stress-strain relation of a volume element along the principal directions are given via the matrix equation,

$$\begin{bmatrix} \varepsilon_r \\ \varepsilon_\theta \\ \varepsilon_z \end{bmatrix} = \frac{1}{E} \begin{bmatrix} 1 & -\nu & -\nu \\ -\nu & 1 & -\nu \\ -\nu & -\nu & 1 \end{bmatrix} \begin{bmatrix} \sigma_r' \\ \sigma_\theta' \\ \sigma_z' \end{bmatrix} \tag{6}$$

where E defines the Young's/Elastic modulus and ν defines the Poisson's ratio. In cylindrical coordinates, the volumetric strain can be expressed by the radial ε_r, axial ε_z and tangential ε_θ strains.

Young's modulus E is a measure of the stiffness of the sample, i.e. the sample resistance against being compressed by a uniaxial stress. For a spatial direction r, Young's modulus is defined by,

$$\varepsilon_r = \frac{1}{E}\sigma_r \tag{7}$$

This is applicable only when a sample behaves linearly to the applied stress, which is sometimes the case for small stress and strain increments.

Poisson's ratio ν is a measure of lateral expansion in the perpendicular directions relative to longitudinal contraction due to the applied stress in the r direction,

$$\nu = -\frac{\varepsilon_\theta}{\varepsilon_r} = -\frac{\varepsilon_z}{\varepsilon_r} \tag{8}$$

For hydrostatic tests, the stresses in all spatial directions are equal, hence $\sigma'_r = \sigma'_\theta = \sigma'_z = \sigma'_{hyd}$ where σ'_{hyd} is used to define the effective hydrostatic stress. Hence equation (6) becomes,

$$\varepsilon_{vol} E = 3(1 - 2\nu)\sigma'_{hyd} \tag{9}$$

where ε_{vol} defines the volumetric strain. Equation (9) can be written as,

$$K\varepsilon_{vol} = \sigma'_{hyd} \tag{10}$$

where K defines the bulk modulus of a material in the elastic region in hydrostatic tests. Thus, $E = 3(1 - 2\nu)K$.

2.4 Time-dependent deformation (creep)

Creep is defined as the time-dependent deformation at constant stress condition. In the plastic phase during pore collapse, the material strength is associated with the rate of creep. The creep rate is simply given by the partial derivative with respect to time of the observed volumetric creep,

$$\dot{\varepsilon_{vol}} = \frac{\partial \varepsilon_{vol}}{\partial t} \tag{11}$$

There are three stages of creep following a change in the stress state (Figure 2). These are:

- Primary creep (steadily declining creep rate),
- Secondary creep (constant creep rate), and
- Tertiary creep (accelerated creep rate).

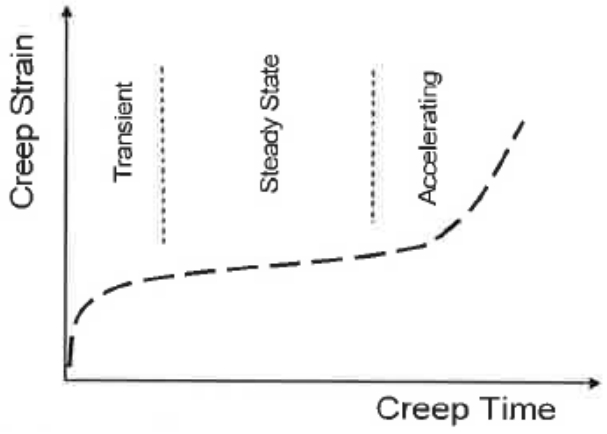

Figure 2. Strain versus time for a creeping material (Fjær et al., 2008).

2.5 Drained test conditions

In testing of low permeability materials, e.g. chalk, drained condition means that the flooding rate of injection fluids must be kept sufficiently low in order to avoid unacceptable pressure build-up when the sample deforms.

In drained tests (Fjær et al. 2008) the pore pressure inside the sample is maintained at a prescribed value by keeping the outlet through the pistons and the cells open, and the fluids can escape (hence constant effective stress). There are two types of tests usually performed:

a) when the outlets are kept open to the atmosphere so that the pore pressure will be zero ($P_f = 0$). In that case from equation (4),

$$\sigma' = \sigma \tag{12}$$

b) when the tests are run at prescribed and constant pore pressure conditions or at actual reservoir conditions. Then the pore pressure must be kept at that prescribed value or at the reservoir pressure level.

The drained tests performed in this study on chalk were run at a prescribed pore pressure value of 0.7 MPa.

2.6 Yield analysis

During stress build-up, the axial and radial strains in the sample are measured. The onset of plastic behavior is identified as the departure from linearity in a plot of effective stress as function of observed strain. For low stress changes, the stress-strain relation is more-or-less linear in accordance with Hooke's law. A linear curve can be fitted to the measurements made in the linear elastic regime, which is then extended into the plastic regime. The onset of yield (i.e. when non-linearity is observed in the stress-strain relation) has been defined to occur when the residual stress R, defined as the difference between the extrapolated linear elastic stress ($\sigma_{elastic} = c_e \varepsilon_z + b_e$) and the imposed effective stress, *i.e.* $R = |\sigma_{elastic} - \sigma_z'|$, exceeds a certain threshold.

2.7 Bulk volume estimates for hydrostatic tests due to non-uniform deformation

After hydrostatic testing, the plug is non-homogenously deformed such that the bulk volume is given by the sum of truncated wedges. The diameter D_i is measured at intervals h_i along the plug and any variations in the diameter is incorporated in the total bulk volume V_b estimated by,

$$V_b = \sum_i \frac{\pi h_i}{12} (D_i^2 + D_{i+1}^2 + D_i D_{i+1}) \tag{13}$$

2.8 Time-dependent evolution of volumetric strain

The volumetric strain ε_{vol} is defined as the ratio of the volumetric change ΔV divided by the original volume V_o,

$$\varepsilon_{vol} = -\frac{\Delta V}{V_o} \tag{14}$$

In some of the experiments in this study, only the axial strain development was measured. Hence, an assumption was introduced in order to convert the axial strain measurements to estimate the volumetric strain. A conversion factor X was introduced such that,

$$\varepsilon_{vol} = X\varepsilon_{ax} \tag{15}$$

which was assumed to be constant throughout the test. The conversion factor was determined by matching the volumetric strain to the volume of the core after the experiment.

In compressive hydrostatic systems, the porous rocks deform by reducing its bulk volume. The total bulk volume change is caused by changes in both pore and solid volumes. Hence, the volumetric strain can be additively partitioned into a mechanical component and a chemical component given by (Nermoen et al. 2016),

$$\varepsilon_{vol} = \varepsilon_p + \varepsilon_s \tag{16}$$

where ε_p is the strain component due to change in the pore volume and ε_s is the strain component due to change in the solid volume. This is valid in a porous material of solids and voids where the pore volume reduction is associated with re-organization of grains during compaction, and the solid volume reduction is associated with rock-fluid interactions during reactive flow.

2.9 Evolution in solid volume with time

The evolution of the solid mass over time is calculated from the difference in the concentrations of the injected fluid and the produced effluent fluids. Now if the density evolution of the solid mass is known, the change in solid volume ΔV_s can be calculated by,

$$\Delta V_s(t) = \frac{M_s(t)}{\rho_s(t)} - \frac{M_{s,o}}{\rho_{s,o}} \tag{17}$$

In this equation, the mass (M_s) and the density (ρ_s) before ($M_{s,o}$ and $\rho_{s,o}$, respectively) and after the triaxial test are measured quantities. As function of time, however, the values of mass ($M_s(t)$) and density ($\rho_s(t)$) must be calculated.

- To calculate the density at a given time during the experiment $\rho_s(t)$, a function is used that depends on the amount of calcium produced from the plug at that time $m_{Ca}(t)$, and the initial ($\rho_{s,o}$) and final ($\rho_{s,f}$) densities such that,

$$\rho_s(t) = \rho_{s,o} + ((\rho_{s,f} - \rho_{s,o})(m_{Ca}(t)/m_{Ca,total})) \tag{18}$$

- The solid volume evolution with time was estimated from the ion chromatography (IC) using equation (17) in which the solid rock mass and the average density is varied with time. The IC data for magnesium (Mg) and calcium (Ca) is used to interpolate the mass of the core at a given time t according to,

$$M_s(t) = M_{s,0} + \eta \int_0^t q_{in}(n_{Mg}(c_{in,Mg} - c_{out,Mg}) - n_{Ca}(c_{in,Ca} - c_{out,Ca})).dt \tag{19}$$

  where η is a fitting parameter that makes the observed replacement of Ca by Mg from IC-data match the observed loss in dry mass before and after test, q_{in} is the injected flow rate

(liter/day), molar weights $n_{Mg} = 24$ g/mol and $n_{Ca} = 40$ g/mol, and c_{in} and c_{out} are the inlet and outlet molar concentrations in (mol/liter) of Mg and Ca, and t is measured in days.

2.10 Porosity evolution during compaction and flow of non-equilibrium brines

The basic equations used to quantify the porosity evolution through time are given based on the work presented by Nermoen et al. (2015, 2018b). The bulk volume of a porous material V_b is given by,

$$V_b = V_s + V_p \tag{20}$$

where V_s is the solid volume and V_p is the pore volume of the material. Any changes in the solid and pore volumes lead to changes in the bulk volume, hence,

$$\Delta V_b = \Delta V_s + \Delta V_p \tag{21}$$

Porosity (φ) is the percentage of pore space in a rock. It is defined as the ratio of the pore volume to the bulk volume and is given by,

$$\varphi = \frac{V_p}{V_b} = 1 - \frac{V_s}{V_b} \tag{22}$$

Hence, if during an experiment both pore and bulk volumes are changing dynamically, the time evolution of porosity is given by,

$$\varphi(t) = \frac{V_{p,o} + \Delta V_p(t)}{V_{b,o} + \Delta V_b(t)} \tag{23}$$

where the original pore volume $V_{p,o}$ and bulk volume $V_{b,o}$ of the rock/material are known quantities.

Replacing equation (21) in equation (23),

$$\varphi(t) = \frac{V_{p,o} + \Delta V_b(t) - \Delta V_s(t)}{V_{b,o} + \Delta V_b(t)} \tag{24}$$

Now volumetric strain ε_{vol} at any given time t is given by,

$$\varepsilon_{vol}(t) = -\frac{\Delta V_b(t)}{V_{b,o}} \tag{25}$$

The negative sign in the volumetric strain is in line with the geotechnical engineering that inward deformation is positive. The original porosity is given by equation (22),

$$\varphi_o = \frac{V_{p,o}}{V_{b,o}} \tag{26}$$

Hence, equation (24) becomes,

$$\varphi(t) = \frac{\varphi_o - \varepsilon_{vol}(t) - \Delta V_s(t)/V_{b,o}}{1 - \varepsilon_{vol}(t)} \tag{27}$$

This equation is used to analyze how the porosity evolves with time when the overall bulk and solid volumes change through time.

3 Materials and Methods

3.1 Model rock material

In the presented study, chalk is used as a model rock material. This model material is selected because of its economic and technological relevancy as host rock for hydrocarbon resources. The phenomenon that its geomechanical property is affected by the injection of brines is not unique to chalk, this has also been observed for other rocks. However, since the specific surface area of chalk material is high, the surface-processes also affect the bulk behavior.

Other examples that also possess a huge surface area include clays (that have even a higher surface area than chalk material), while other siliciclastic rocks (beach deposits, riverbeds etc.) have larger rounded grains with lower surface area making the rock-fluid interactions less dominating for the overall observed behavior.

A typical picture of the structure of chalk material from Kansas outcrop is presented in Figure 3.

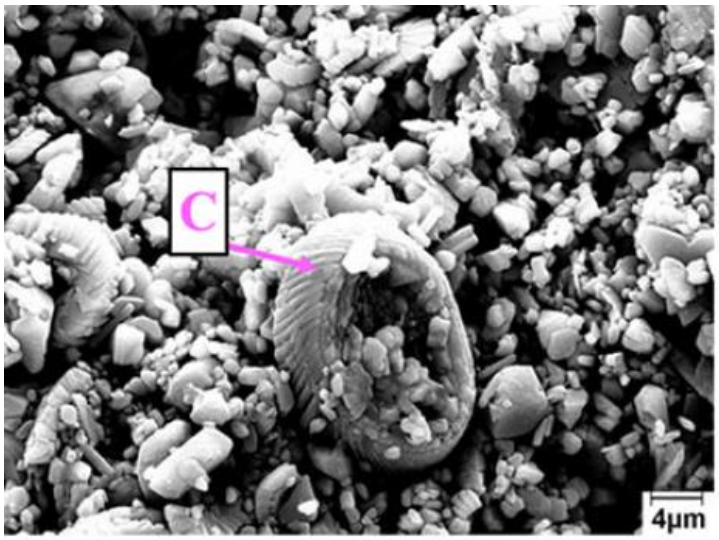

Figure 3. Scanning Electron Microscope (SEM) image of unflooded Kansas outcrop chalk material. 'C' denotes the coccolithophore ring observed in the sample surrounded by diagenetic calcite and clay minerals (Andersen et al. 2018).

3.1.1 Outcrop chalks in this study

It is relatively easy to obtain reservoir cores using well established coring methods. However, due to the capital linked to the extraction of the cores and limited availability, experimental studies are mostly performed on outcrop materials used as analogue models for the reservoir rocks. It is believed that the observed behavior of the interplay between geomechanics, multiphase transport (oil/water and EOR), chemical interactions, and wettability changes on outcrops are also applicable to reservoir cases. There are several outcrops across the globe and their applicability to various North Sea chalk reservoirs is always up for discussion. These outcrop chalk samples differ in their chemical composition and mechanical properties (Hjuler and Fabricius 2009).

Two types of outcrop chalks have been used in this study. They are collected from quarries in Kansas, USA (Niobrara Formation) and Mons,

Belgium (Trivières Formation). These two outcrop chalks are the endmember cases where the Kansas chalk is stiffer with a low porosity and has gone through more chemical reworking, while the Mons chalk is softer possessing a high porosity and has been exposed to lesser amount of diagenetic overprint.

3.1.1.1 Kansas: Niobrara Formation

Chalk samples were collected from the Fort Hays Member of the Niobrara Formation from west-central Kansas (USA). This chalk is from Late Cretaceous geological age. The Kansas chalk type is reported to have a non-carbonate content of 1-3% (Tang and Firoozabadi 2001; Megawati et al. 2013) and mainly consist of quartz, clay and pyrite (Runnels and Dubins 1949; Hattin and Cobban 1977; Longman et al. 1998). Porosity of chalk from the Niobrara Formation is in the range 35-39% (**Paper I**, **Paper II**, **Paper IV and Paper VI**) and permeability has been reported in the range 1-4 mD (**Paper IV**; Korsnes et al. 2006a; Megawati et al. 2013; Andersen et al. 2018). Tang and Firoozabadi (2001) argue that it is a good analogue to some clean North Sea reservoir chalks in regard to porosity, capillary pressure, and absolute and relative permeability.

3.1.1.2 Mons: Trivières Formation

The chalk from Mons is taken from the Trivières Formation. This chalk belongs to Late Cretaceous geological age and is very pure (> 99 weight percent (wt %) calcite). Porosity is in the range 41-44% (**Paper III** and **Paper V**). The chalk from the Trivières Formation has a high degree of intact coccoliths (Richard et al. 2005). Mons chalk is pure coccolithic mudstone. Large amounts of very small coccoliths and broken calcite crystals of organic origin form the solid framework for this type of chalk (Andersen et al. 2018).

3.2 Core preparation

Cylindrical core samples were drilled in parallel from single Kansas and Mons chalk blocks and were radially adjusted to a diameter of 38.1 mm. The samples were then cut to desired lengths and dried at 110°C overnight after which the initial dry mass was measured. The carbonate mineralogy is not affected by the drying conditions (MacDonald 1956). They were vacuumed before saturation by distilled water (DW) within the vacuum chamber, before saturated mass measurement. The mass difference between the dry and saturated sample was used to estimate the pore volume and saturation porosity.

The samples were divided into two test series:

- Samples for wettability determination by comparing chromatographic separation of reference unaged water-wet samples (Kansas Kww1 to Kww7, refer **Paper I**; Kansas KA1, refer **Paper II**; and Mons Mww1 to Mww3, refer **Paper III**) to wettability-altered samples (Kansas Kmw1 to Kmw4, refer **Paper I**; Kansas KA2 to KA4, refer **Paper II**; and Mons Mmw1 to Mmw3, refer **Paper III**).
- Samples for chemo-mechanical compaction during flow in triaxial cell. These samples were divided into two sub-series: a) 100% water saturated samples ('water-wet samples'): Kansas K1, K2, K5 and K6, refer **Paper I**, and Mons M1 and M2, refer **Paper III**; and b) wettability-altered samples containing a non-zero oil saturation ('wettability-altered samples'): Kansas K3, K4, K7 and K8, refer **Paper I**, and Mons M3 and M4, refer **Paper III**.

The detailed properties of the samples used in this work are mentioned in **Paper I**, **Paper II** and **Paper III**. The properties of the samples mentioned in **Paper IV**, **Paper V** and **Paper VI** provide additional information to supplement this work.

It is assumed that the wettability index results obtained from the wettability-altered samples through the wettability determination program apply to the wettability-altered samples used in the triaxial test program.

3.3 Description of fluids

3.3.1 Brines used

In the wettability determination program, two versions of artificial seawater were used (**Paper I**, **Paper II** and **Paper III**). The SW1T brine contained SO_4^{2-} and SCN^- tracer ions, while SW0T did not (Table 1). Total dissolved solids of SW1T and SW0T equal the SSW case. Four other brines were used during the triaxial test program (Table 1):

- 1.1 M NaCl brine for initial saturation was used to simulate initial resident formation fluids (**Paper I**, **Paper II**, **Paper III**, **Paper IV**, **Paper V** and **Paper VI**). This brine was also used as the injection brine in **Paper VI**.
- 0.657 M NaCl (**Paper II** and **Paper V**) and 0.219 M $MgCl_2$ (**Paper I**, **Paper III** and **Paper V**) brines, with equal ionic strength to seawater (0.657), were used as injection brines. These two brines were used to simulate the fluid injection at Ekofisk. $MgCl_2$ brine injection also focusses on the adsorption / desorption and dissolution / precipitation effects from the Ca-Mg exchange (Madland et al. 2009, 2011).
- SSW (**Paper I**, **Paper V** and **Paper VI**) was also used as an injection brine to model the processes occurring when seawater contacts the Ekofisk hydrocarbon reservoir. SSW interacts with the chalk by both adsorption of surface-active divalent sulfate ions and dissolution / precipitation processes due to presence of magnesium ions (Madland et al. 2011). It is also active in precipitation processes (such as anhydrite precipitation) even in the absence of magnesium ions.

Table 1. Composition of brines used in the tracer tests and during flow-through tests.

	Wettability determination program		**Triaxial test program**			
Ions	**SW0T**	**SW1T**	**1.1 M NaCl**	**0.657 M NaCl**	**0.219 M $MgCl_2$**	**SSW**
	mol/l	**mol/l**	**mol/l**	**mol/l**	**mol/l**	**mol/l**
HCO_3^-	0.002	0.002	0	0	0	0.002
Cl^-	0.583	0.492	1.100	0.657	0.438	0.525
SO_4^{2-}	0	0.024	0	0	0	0.024
SCN^-	0	0.024	0	0	0	0
Mg^{2+}	0.045	0.045	0	0	0.219	0.045
Ca^{2+}	0.013	0.013	0	0	0	0.013
Na^+	0.46	0.393	1.100	0.657	0	0.450
Li^+	0	0.024	0	0	0	0
K^+	0.010	0.034	0	0	0	0.010
Ionic Strength	0.643	0.647	1.100	0.657	0.657	0.657
TDS (g/l)	33.39	33.39	64.28	38.40	44.52	33.39

3.3.2 Oil used

A 60%-40% volume mixture of crude oil from the Heidrun field offshore Norway and heptane was used (**Paper I**, **Paper II**, **Paper III**, **Paper IV** and **Paper VI**) for two main reasons: (a) Lowering the acid number: high acid number leads to more oil-wet cores, and (b) Reducing the oil viscosity: less pressure is required to displace the oil. After the dilution, the oil was centrifuged and filtered through a 5 μm Millipore filter to remove any asphaltene precipitates.

The properties of Heidrun crude oil are reported in Table 2. The acid number of the Heidrun oil was 2.82 mg KOH/g and oil mixture was 2.12 mg KOH/g measured according to the Fan and Buckley (2007) procedure.

Table 2. Properties of Heidrun Crude oil at 25°C

Color	**Density (kg/m^3)**	**Viscosity (cP)**	**TAN (mg KOH/g)**	**Asphaltene content (%)**
Light brown	858	6	2.82	< 1

3.4 Triaxial cells

Cylindrical plugs were mounted into the triaxial cell that allowed for continuous measurements of the axial and radial strains at elevated stresses and temperature (Figure 4). The triaxial cell was equipped with a heating element and a regulating system with precise temperature control. Three pumps were connected to the triaxial cell to control the piston pressure (P_{pist}), confining pressure (P_{conf} / σ_{rad}) and flow rate (Q). The pore pressure on the downstream side (P_p) was controlled by a back-pressure regulator ensuring constant pore pressure (0.7 MPa). An external Linear Voltage Differential Transducer (LVDT) monitored the change in length of the core plug (L) and an internal extensometer monitored the change in diameter of the core plug. The way in which the experimental setup was designed, the axial stress was given by P_{conf} plus P_{pist} minus the friction of the piston (P_{fric}) times an area-factor (f_{area}) that relates the area of the plug to the area of the piston in upper chamber,

$$\sigma_z = P_{conf} + f_{area}(P_{pist} - P_{fric}) \tag{28}$$

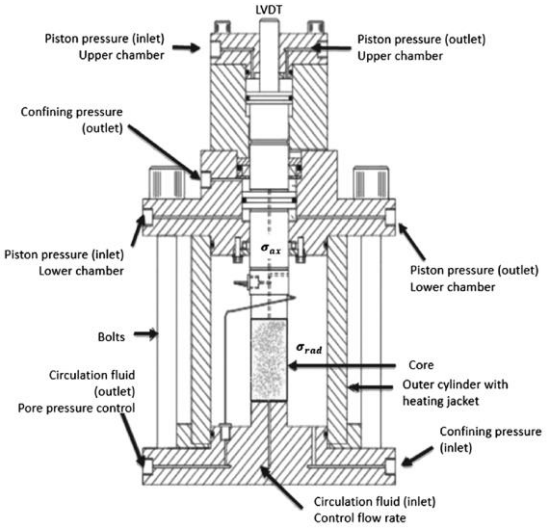

Figure 4. Sketch of the triaxial cell

3.5 Experimental procedure

This section describes the experimental procedures followed for wettability alteration, wettability determination, geomechanical tests, ion chromatography on the effluent samples, oil volume measurements, and density and specific surface area determination.

3.5.1 Initial saturation and wettability alteration procedure

3.5.1.1 Cores used in wettability determination program by chromatographic separation technique and triaxial tests

The water-wet samples were saturated by 1.1 M NaCl brine. The wettability-altered samples were prepared according to the following procedure:

i) Saturation by 1.1 M NaCl brine;
ii) Mounted in Hassler cell and heated to 50°C;
iii) Flooded two PVs of the oil mixture in each direction at 0.7 MPa back pressure and 1.6 MPa confining pressure during

which the produced brine was collected and measured to estimate the irreducible water saturation S_{wi}.

iv) Submerged the samples in the same oil mixture in aging containers and left for 21 days at 90°C.

3.5.1.2 Cores used in wettability determination program by contact angle, United States Bureau of Mines (USBM) and Scanning Electron Microscope – Mineral Liberation Analysis (SEM-MLA) methods

3.5.1.2.1 Centrifuge for Primary Drainage

Seven cylindrical core samples of 38.1 mm diameter and 50 mm length, and 5 mm length end pieces from both ends (top and bottom, 14 in total) were saturated by 1.1 M NaCl brine. The brine saturated cores, including the 14 top and bottom end pieces with filter paper in between, were mounted into the core holders of the centrifuge (*Rotosilenta 630RS* centrifuge from Vinci Technologies). An overburden of 1.38 MPa was used, and the centrifuge was operated in drainage mode to displace the brine with oil to S_{wi}. Drainage was performed in seven steps from 500 rpm to 3500 rpm in increments of 500 rpm with three hours of equilibration time for each step. The capillary pressure was calculated at any position, r, along the core length using the Hassler-Brunner equation (Hassler and Brunner 1945):

$$P_c(r) = \frac{1}{2}\Delta\rho\omega^2(r_1^2 - r^2) \qquad (29)$$

where $\Delta\rho = \rho_{out} - \rho_{in}$ is the density difference between the fluid expelled from the core (ρ_{out}) and the fluid entering the core (ρ_{in}), ω is the angular rotation speed of the centrifuge, and $r_1 \simeq 22.1$ cm (for drainage mode of centrifuge) and 16.5 cm (for imbibition mode of centrifuge) and r (varying from 0 to 5 cm) are the distances from the rotational axis to the outlet face and any point along the core length, respectively.

After reaching an equilibrium between the oil / water saturation and capillary pressure, i.e. when no more brine was being produced, the brine expelled from the core was measured and the average water saturation for each rotation speed was obtained. This water saturation was plotted against the capillary pressure estimated from equation (29) to produce the capillary pressure curve.

3.5.1.2.2 Aging

After the centrifuge the overburden was reduced to 0.7 MPa and the core holders with cores and end pieces inside were placed in the oven to age at 90°C for aging time ranging from 6 to 30 days (Table 3).

Table 3. Aging time for different cores

Core No.	**Saturation porosity (%)**	**Aging Time (days)**
1	38.6	6
2	38.5	9
3	37.8	12
4	36.9	15
5	38.0	18
6	38.1	21
7	37.6	30

After aging, the seven full sized cores were used for USBM wettability measurement, and the seven top and seven bottom end pieces were used for the contact angle measurements and SEM-MLA analyses, respectively.

3.5.2 Establishing wettability

3.5.2.1 Chromatographic separation technique

The chromatographic separation procedure is based on the idea that the water wet areas of the chalk surface attract SO_4^{2-} ions that are present in the injected brine, i.e. SO_4^{2-} ions adsorb on the calcite surfaces that are

in contact with water. Therefore, when a brine containing SO_4^{2-} and SCN^- tracer is injected (into a sample saturated by non-sulfate and non-tracer brine) the sulfate is delayed compared to the non-affine tracer during frequent sampling of the effluent fluids. The key premise in this work is that the area spanned by the sulfate concentration curve compared to the tracer curve of the effluent samples is proportional to the surface area available for the sulfate ions to adsorb. The ratio of the area between curves for a mixed-wet sample divided by the reference area of a water-wet sample defines the wetting index (W_i),

$$W_i = \frac{A_{mw}}{A_{ww}} \tag{30}$$

where A_{mw} and A_{ww} are the areas between the SO_4^{2-} and SCN^- curves for mixed-wet and water wet samples, respectively. The areas under the SO_4^{2-} and SCN^- curves were determined using the trapeze method in this study.

The wettability determination could not be performed on the cores used in the triaxial test program since the flow of fluids used in the wettability determination could alter the wettability, as sulfate is a wettability modifier (Strand et al. 2006; Zhang and Austad 2006; Zhang et al. 2007). It would also displace oil from the core prior to the mechanical test. Therefore, several wettability tests were performed in order to check the repeatability and obtain confidence that all cores had similar wettability. Hence, the assumption that the wettability determined from the wettability determination program also applies to the wettability-altered cores in the triaxial test program held strong ground.

Wettability determination was performed in Hassler (**Paper I** and **Paper III**) and triaxial (**Paper II**) cells by (i) flooding four PVs of SW0T brine, (ii) injecting SW1T brine for 500 minutes with a flow rate of 0.2 ml/min. During the SW1T brine injection, 36 to 40 samples were collected using a Gilson fraction sampler. Each sample contained 2 ml of fluids collected over 10.0 minutes, with 2.5 minutes waste time between each sample.

For each fluid sample, the thiocyanate and sulfate concentrations were determined using ion chromatography (IC). The concentration c_k of each species k (SCN^- and SO_4^{2-}) is rescaled by the SCN^- and SO_4^{2-} concentrations of SW0T c_{k0} (in this case zero) and SW1T $c_{k1} = 0.024$ mol/liter, such that a reduced concentration $\widehat{C_k}$ could be obtained,

$$\widehat{C_k} = \frac{c_k - c_{k0}}{c_{k1} - c_{k0}} \tag{31}$$

This reduced concentration varies between zero and one, and when the effluent concentration equals the inlet concentration it gives $\widehat{C_k} = 1$. This enables the thiocyanate and sulfate curves to be plotted together. The area between these curves was estimated by integration using the trapeze method. Further, larger cores will have a larger total surface area than the smaller ones, so the areas are reported in per gram of the core for accurate comparison.

3.5.2.2 Contact angle method

The top end pieces of the aged core samples were mounted in a *Vinci IFT 700* instrument to measure the contact angle by sessile drop method. The same NaCl brine, used to saturate the samples initially, was used as the droplet fluid and each droplet was of size $\sim 5 \cdot 10^{-4}$ ml (radius of 0.5 mm). 8-10 photographs were acquired over two minutes each enabling us to observe how the droplet obtained a stable geometry over time. The top end pieces were at the oil front during the primary imbibition process and hence, it was assured that the saturation was uniform. Contact angle was measured at multiple spots (about 10 to 12) on the surface of the piece and an average value was taken as the contact angle for that sample. The generally accepted contact angle wettability classification is given in Table 4.

Table 4. Contact angle wettability classification (McPhee et al. 2015).

	Water Wet	**Neutral Wet**	**Oil Wet**
Minimum	0°	60-75°	105-120°
Maximum	60-75°	105-120°	180°

3.5.2.3 USBM method

After the primary drainage and aging, the NaCl brine was forcibly imbibed (primary imbibition) into the cores using the centrifuge in imbibition mode to obtain residual oil saturation (S_{or}) before a secondary drainage was performed to reach S_{wi} (Donaldson et al. 1969, 1980; Donaldson 1981; McPhee et al. 2015). The receiving tubes, coupling cups to core holders, were saturated by the same fluid as the cups holding the fluid that enters the cores. A confining pressure of 1.38 MPa and seven centrifugal steps from 500 to 3500 rpm, with 500 rpm increments and three hours equilibration time, were used. The trapezoidal method was used to estimate the area under the secondary drainage (A_1) and primary imbibition (A_2) capillary pressure curves, and the wettability index W_i was calculated from the following equation,

$$W_i = \log \frac{A_1}{A_2} \tag{32}$$

In conjunction to equation (32), the wettability index W_i is greater than 0 for water-wet, smaller than 0 for oil-wet and around 0 for neutral-wet systems.

3.5.2.4 SEM-MLA analysis

The bottom end pieces of the aged core samples were used for SEM-MLA analysis (Sripal and James 2016, 2018).

A *FEI Quanta 650 Field Emission Gun (FEG) Scanning Electron Microscope (SEM)* equipped with Bruker high throughput energy dispersive X-ray (EDX) system and backscattered electron detectors was used. Imaging on the flat sample surfaces was carried out at very low vacuum conditions (0.6 Torr). Additionally, the samples were not subjected to any metallic or carbon coating on the surface, except for a liquid graphite coating on the sample holder. Instrument conditions and parameters included a high voltage of 25 kV, spot size of 5.75, working distance of 13.5 mm, 10 nA beam current, 16 µs BackScattered Electron (BSE) dwell time, 10 pixel minimum size (400 pixel frame resolution for 1-mm high full well (HFW)), and 12-ms spectrum dwell for EDX. Each of these Mineral Liberation Analysis (MLA) acquisitions was completed using version 3.1.4.683 MLA software and took between 3 and 4 hours per sample.

Prior to testing the individual aged end pieces, two pure chalk pieces, one with a drop of the oil mixture and another with a drop of 1.1M NaCl-brine on it, were analyzed to determine the oil and NaCl-brine (termed 'halite') signatures and added to the SEM mineral database. The aged end pieces were, then, analyzed to determine the relative quantity of oil, halite and carbonate in percent. The results for individual samples were acquired as a digital map of the minerals and a data table listing their mineral composition. The mineralogy was determined using GXMAP measurement mode within FEI mineral liberation analyzer software, equipped on the SEM. Each mineral identified was within an 80% match to a known standard X-ray. The premise was to link the oil/halite concentrations to the overall wetness of the mineral surface, which in this study was controlled by the aging time.

3.5.3 Hydrostatic tests in a triaxial cell

The $MgCl_2$ flow-through experiments in **Paper I** and **Paper III** were conducted according to the following stages:

1. Mounted the cores in the triaxial cell (K1 to K4 in **Paper I**, and M1 to M4 in **Paper III**); kept the bypass valve open with no flow-through the cores.
2. Increased confining pressure (σ_{rad}) to 1.2 MPa and pore pressure (P_f) to 0.7 MPa simultaneously.
3. Increased temperature to 130°C.
4. σ_{rad} increased to approximately 1.5 times above yield at a loading rate of 0.045 MPa/min with bypass open. The onset of yield stress was determined when the hydrostatic stress - volumetric strain curve deviated by more than 0.7 MPa for Kansas chalk and more than 0.5 MPa for Mons chalk from the straight elastic line used to determine the bulk modulus (K).
5. Observed creep; for the first 15 days of creep period bypass valve was kept open.
6. Afterwards bypass valve was closed and $MgCl_2$ brine flooding was commenced through cores at a flow rate of 0.010 ml/min.
7. Increased $MgCl_2$ brine flooding rate to 0.040 ml/min for all tests after a certain number of days.
8. Decreased flow rate back to 0.010 ml/min for some of the cores.
9. Cleaned the cores with four PVs of DW at the end of the test.
10. Used toluene to remove the leftover oil from wettability-altered cores, followed by flooding methanol to remove toluene. Toluene was flooded till the effluent became completely transparent in color. Afterwards, DW was used to remove methanol from these cores.
11. Chromatographic separation tests were performed on all Mons samples after mechanical tests (**Paper III**). These tests were not performed on Kansas samples.
12. Demounted all cores from triaxial cell.

After demounting, the wet mass, dry mass, length and diameter were measured. Afterwards, the samples were cut into six sections of almost equal length and tested for density and specific surface area using gas

pycnometer and Brunauer–Emmett–Teller (BET) theory, respectively (see sections 3.5.7 and 3.5.8).

Flow-through experiments were also performed on Kansas chalk samples with SSW (K5 to K8 in **Paper I**). The procedure followed was the same as with $MgCl_2$ brine, except that the cores were flooded only at 0.010 ml/min flow rate. For details, the reader is referred to **Paper I**. Flow-through experiments with SSW were not performed on Mons chalk samples in this study.

3.5.4 Triaxial tests at low effective stresses with frequent tracer tests to evaluate chalk surface area evolution with time

Tracer tests were performed in triaxial cells at frequent intervals of time on a separate set of Kansas chalk samples, drilled from the same chalk block as for the hydrostatic tests, to evaluate the extent to which chemical interactions induced by the continuous $MgCl_2$ brine injection modify the water wetness of the chalk samples. One water wet (KA1) and three mixed wet (KA2 to KA4) samples were flooded by $MgCl_2$ brine at low effective stresses and tracer tests were performed after 7 days each for KA1 and 10 days each for KA2 to KA4 using chromatographic separation technique.

Readers are advised to refer to **Paper II** for the detailed experimental procedures followed for the water wet sample KA1 and the mixed wet samples KA2, KA3 and KA4.

3.5.5 Measurement of oil production

During the hydrostatic tests (**Paper I** and **Paper III**) and the triaxial tests at low effective stresses (**Paper II**), the oil produced was collected in a burette / separator placed on the downstream side of the experimental setup and read by eye at frequent intervals.

3.5.6 Ion Chromatography (IC)

The effluent samples acquired were diluted 500 times with de-ionized water to meet the linear regime of the *Dionex IC S-5000+ Ion Chromatography* system. The samples were diluted using the *Gilson GX-271* liquid handler operated by the *Trilution* software. Once the analysis finished, a series of peaks, corresponding to each ion in the effluent sample, was obtained. The area under each peak was assumed to be proportional to the ion concentration in the fluid when compared to known standards with known concentrations.

3.5.7 Mineral density determination

Samples were cut into six sections of almost equal length after mechanical tests. These sections were kept in the oven at 110°C overnight. Next morning these sections were taken out and placed in a vacuum sealed container to cool down. Each section was, then, weighted and inserted, one-by-one, into the *Micromeritics AccuPyc II 1340 Gas Pycnometer* (using helium) to measure the solid volume. With mass and solid volume known, the mineral density of each section was estimated.

3.5.8 Specific surface area (SSA) determination

The SSA was estimated by Brunauer–Emmett–Teller (BET) theory, which works on the principle of physical adsorption of gas molecules on a solid surface (Brunauer et al. 1938). The SSA measurements were carried out on *Micromeritics TriStar II* instrument using liquid nitrogen, as it does not chemically react with the chalk. Two grams of powdered chalk were added to the sample glass tube and degassed for 5 hours at 110°C on *Micromeritics VacPrep 061 Sample Degas System*. A stable vacuum pressure of 20-30 mTorr was attained for all tested samples before the sample tubes were attached to the BET apparatus. The specific surface area was measured automatically by the *TriStar II 3020* software.

4 Results and Discussion

This section presents the results from the experimental studies performed on both Kansas and Mons chalks, followed by a detailed discussion of these results.

4.1 Results of wettability determination

4.1.1 Impact of aging time on qualitative analysis of wettability using contact angle method

It was not possible to obtain a stable and time-independent contact angle measurement for samples with 6 and 9 aging days as the droplet initially had a maximal contact angle of around 65° and 66°, but within only a few seconds, it spread out and got sucked into chalk developing into a contact angle of 0° with time. Samples aged 12 and 15 days formed sessile droplets enabling stable contact angle measurements of 78° and 85°, respectively. Increasing the aging time to 18, 21 and 30 days the contact angle increased to 102°, 110°, and 108°, respectively (Figure 5 and Figure 6 (left), Table 5). Hence, as the aging time was increased to 18 days and beyond, the contact angle reached a plateau of more than 100° which is in-line with oil wet characteristics, said to be greater than 105° (Anderson 1986; Cuiec et al. 1994).

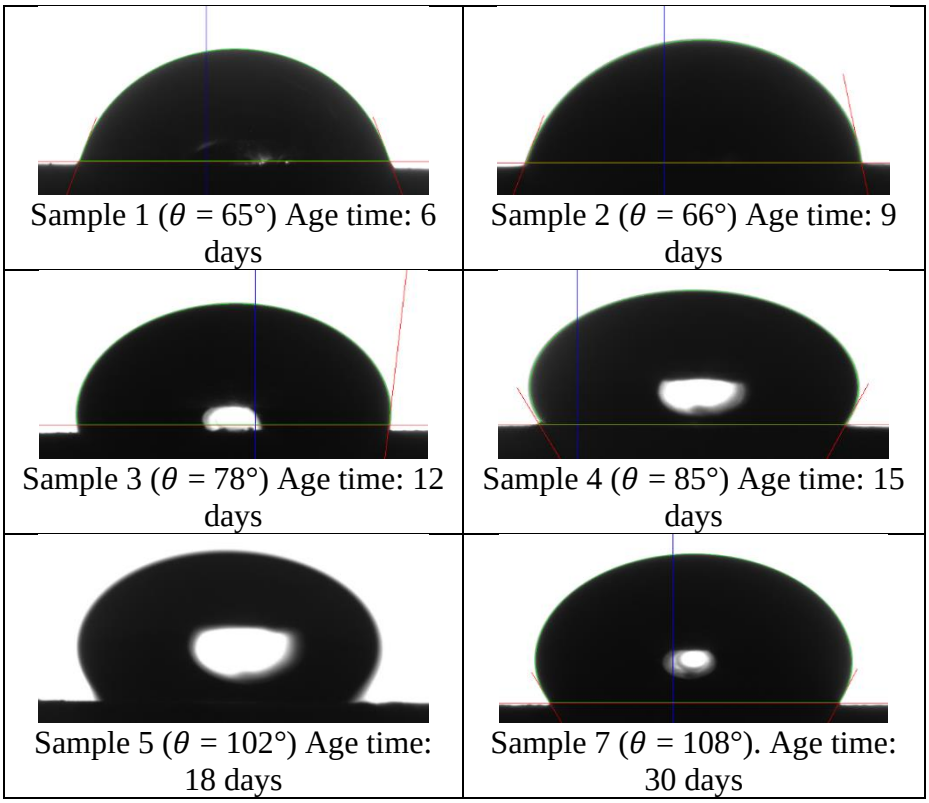

Figure 5. Brine droplet of size $\sim 5 \cdot 10^{-4}$ ml placed onto the aged top end piece. The contact angle is shown for differently aged chalk samples (see **Paper IV**).

4.1.2 Impact of aging time on quantitative analysis of wettability using USBM method

After the samples were aged they were imbibed by NaCl brine (primary imbibition) from S_{wi} to the residual oil saturation (S_{or}, Figure 7 and Table 5). The area under the P_c vs S_w curve during primary imbibition is termed A_2. The cores were, then, taken out of the core holders which were switched to drainage mode before secondary drainage was performed (in which oil expelled brine). The area under the P_c vs S_w curve during secondary drainage is termed A_1.

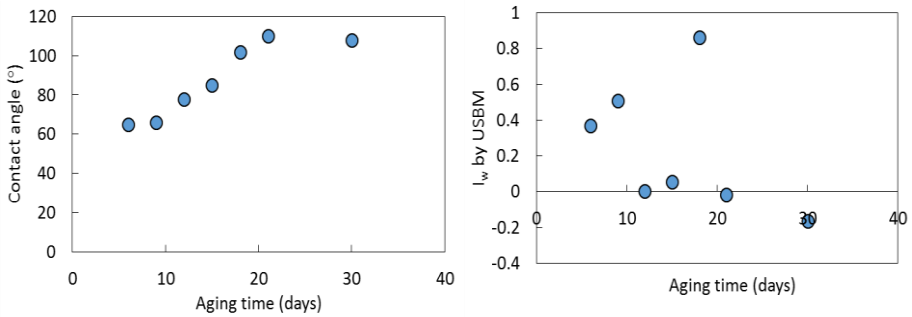

Figure 6. Left: Contact angle on the top end piece of aged chalk cores as a function of aging time. Right: Wettability index measurement using USBM method as a function of aging time (see **Paper IV**).

The wettability index I_w from USBM method was estimated using the log10 of the ratio A_1 by A_2 in equation (32). From the I_w reported in Table 5, it can be seen that, except from core number 5 (18 days), an increasing aging time leads to a lowered wettability index, ranging from 0.37 and 0.51 for 6 and 9 days aging to around zero for 12, 15 and 21 days, and -0.16 for 30 days aging. Figure 6 (right) gives a plot of wettability index estimated by USBM method as a function of aging time. The abnormality with result from sample aged 18 days is quite uncertain and is likely caused by either excess confining pressure or due to the presence of natural fractures within chalk, which led to further disintegration during the primary imbibition and secondary drainage tests.

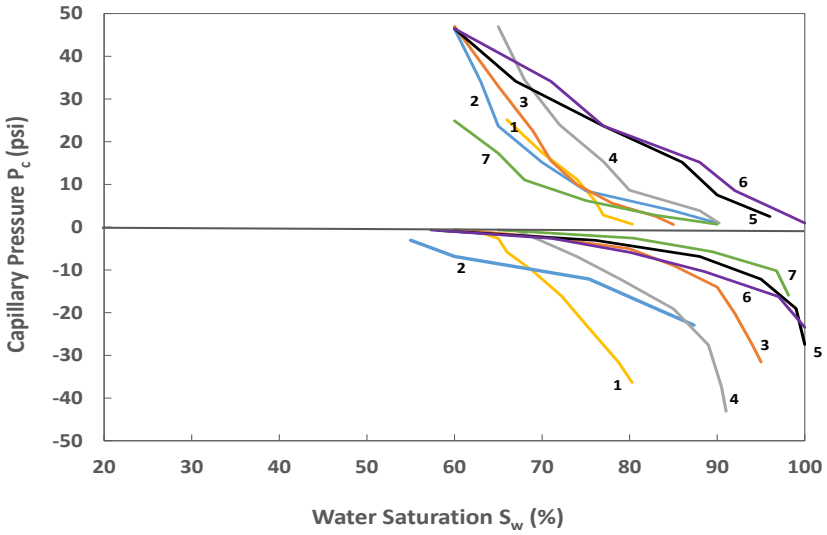

Figure 7. Primary imbibition (brine displacing oil, $P_c < 0$) and secondary drainage (oil displacing brine, $P_c > 0$) for Kansas chalk samples 1 to 7, number of aging days in parenthesis: 1 (6-yellow), 2 (9-blue), 3 (12-orange), 4 (15-grey), 5 (18-black), 6 (21-purple) and 7(30-green) (see **Paper IV**).

Note: For samples 5 and 6, the primary imbibition data was adjusted to 100% maximum saturation as the experiments overestimated the saturations to beyond 100%. The S_{or} reported for samples 5 and 6 in Table 5 are assumed to be the penultimate points after the saturations were adjusted to 100%.

4.1.3 Impact of aging time on qualitative analysis of wettability using SEM-MLA analysis

The lower end pieces were analyzed using SEM–MLA in which the oil/brine content of the surface of the samples was determined (Table 5). Based on the individual surface measurements (reported in Table 6) for the amount of oil/brine/calcite of the aged chalk samples, the SEM-MLA wettability estimates are reported in Table 5. Figure 8 provides two examples of mineral/fluid MLA maps and SEM images of samples aged for 6 days and 30 days showing how an increasing aging time results in an increased oil signature on the chalk samples. Standnes and Austad

(2000a, 2000b) also concluded that the increase in aging time increased the affinity of oil towards the chalk surface.

Table 5. Experimental measurements for Kansas chalk (see **Paper IV**)

Core No.	**Aging Time (days)**	S_{wi} **(%)**	**Contact Angle (º)***	**SEM-MLA oil %**	I_w **(USBM)**
1	6	64.71	65 (29.4)	10	0.368
2	9	54.32	66 (26.8)	19	0.510
3	12	58.10	78 (9.1)	27	0.005
4	15	62.61	85 (7.5)	37	0.053
5	18	54.15	102 (6.2)	37	0.864
6	21	54.33	110 (4.2)	39	-0.018
7	30	58.64	108 (4.5)	46	-0.165

*150 to 300 data points were collected with average value reported and standard deviation presented in brackets

Table 6. Mineral list from the SEM-MLA analysis for Kansas chalk samples 1 to 7, number of aging days in parenthesis: 1(6), 2(9), 3(12), 4(15), 5(18), 6(21) and 7(30) (see **Paper IV**).

Color	Mineral	% Area coverage by sample						
		#1	#2	#3	#4	#5	#6	#7
	Carbonate	8	21	61	3	57	50	31
	Halite	82	60	12	60	6	11	23
	Oil	10	19	27	37	37	39	46
	Others	0	3	3	4	3	1	2

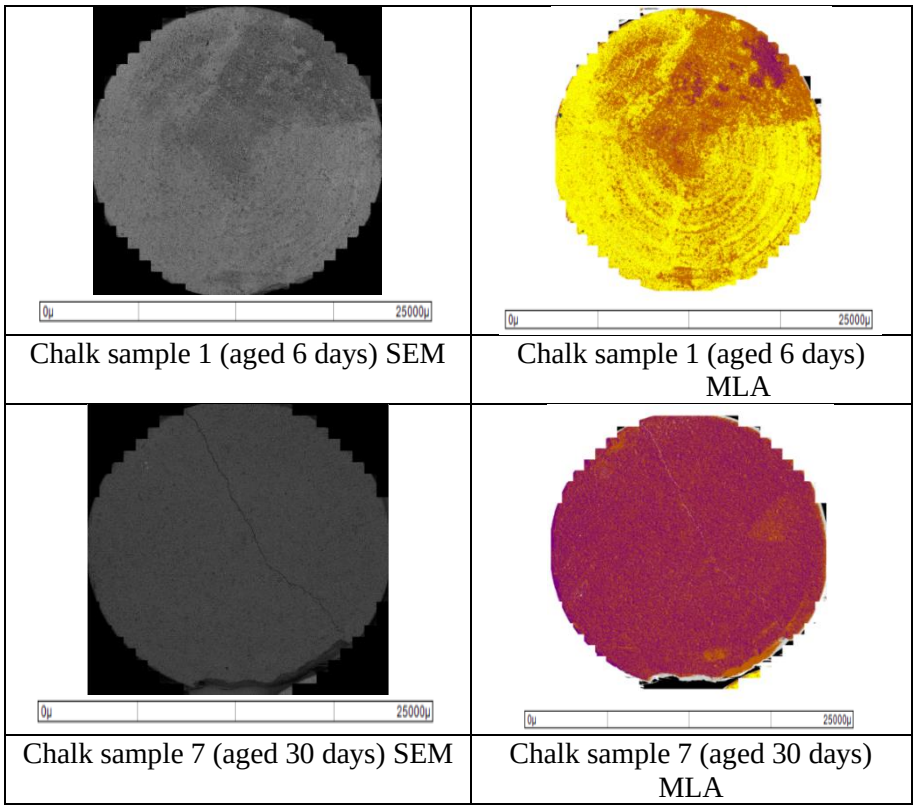

Chalk sample 1 (aged 6 days) SEM	Chalk sample 1 (aged 6 days) MLA
Chalk sample 7 (aged 30 days) SEM	Chalk sample 7 (aged 30 days) MLA

Figure 8. SEM and MLA images of different aged chalk samples (see **Paper IV**).

Comparison of results from contact angle, USBM and SEM-MLA methods

The wettability measurements reported here, from the three methods, imply that an aging time exceeding 21 days was enough to ensure that the Kansas chalks are oil wet when the samples were saturated by 1.1 M NaCl brine and 2.12 mg KOH/g oil and aged at 90°C. The results from these methods, especially contact angle and USBM methods, show that the cores attained neutral wet state and were on the oil wet side.

Similar work had been carried out previously on Rørdal chalk samples (Graue et al. 1999), wherein the chalk samples were submerged into crude oil for wettability alteration, and then after aging the crude oil was

flushed out by decahydronapthalene, which subsequently was flushed out by decane for imbibition tests. Graue et al. (1999) reported that a stable wettability was obtained for cores aged more than 14 days using this set of fluids.

4.1.4 Results of wettability estimation from chromatographic separation technique

Chromatographic separation technique was applied to both Kansas (**Paper I**) and Mons (**Paper III**) chalk types.

4.1.4.1.1 Initial wettability of Kansas chalk

For Kansas chalk, the average area for water-wet and wettability-altered cores was found to be $(1.59 \pm 0.07) \cdot 10^{-3}$ PV/g and $(0.88 \pm 0.05) \cdot 10^{-3}$ PV/g, respectively. This corresponds to an average W_i of 0.55 ± 0.05 for the wettability-altered samples, meaning they are close to neutral-wet condition but on the water-wet side. An example of two chromatographic separations of a completely water-wet (Kww7) and a wettability-altered sample (Kmw3) is shown in Figure 9(a) and (b), respectively. Here, the reduced ion concentration is plotted against PVs of SW1T flooded. Each dot reflects a single effluent water sample and the separation between the sulfate ion and thiocyanate tracer ion can be visualized. Figure 9(c) displays the difference between the measured thiocyanate and sulfate concentrations for the water-wet core (Kww7) and wettability-altered core (Kmw3).

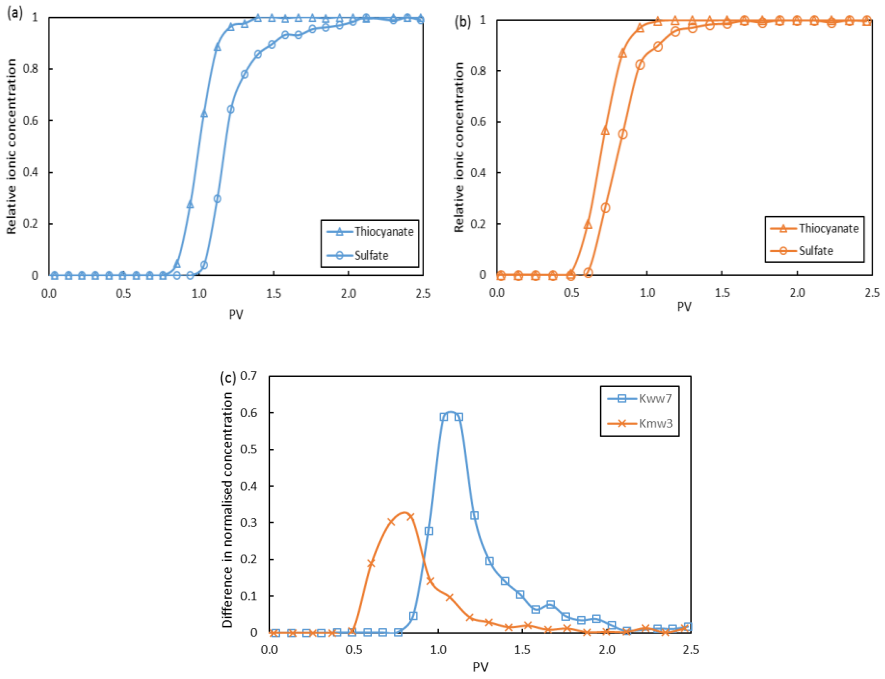

Figure 9. Chromatographic separation on (a) water-wet core (Kww7, blue) and (b) wettability-altered core (Kmw3, orange). The plots (a) and (b) show how the increase in sulfate concentration is delayed compared to the thiocyanate concentration after SW1T is injected. The plot (c) shows the difference in normalized concentrations between the thiocyanate and sulfate curves for the water-wet (blue) and wettability-altered cores (orange). The integrated separation area for Kww7 and Kmw3 was 1.71×10^{-3} PV/g and 0.92×10^{-3} PV/g, respectively (see **Paper I)**.

4.1.4.1.2 Initial wettability of Mons chalk

Similarly, for Mons chalk, the average area for water-wet and wettability-altered samples was estimated to be 1.48 ± 0.08 PV/g and 0.93 ± 0.04 PV/g, respectively. This corresponds to an average W_i of 0.63 ± 0.07 for the wettability-altered samples, which also means that they are close to neutral-wet condition but on the water wet side. Figure 10(a) and (b) shows two chromatographic separation tests performed on

a completely water-wet sample (Mww2) and a wettability-altered sample (Mmw3). Figure 10(c) displays the difference between the measured thiocyanate and sulfate concentrations for the water-wet sample (Mww2, blue) and wettability-altered sample (Mmw3, green).

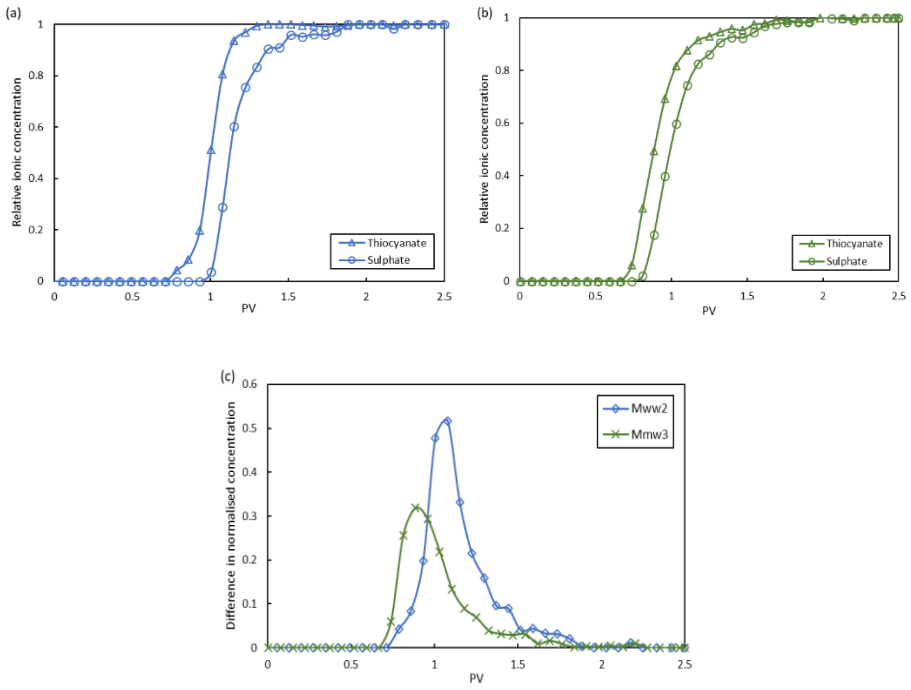

Figure 10. Chromatographic separation on (a) water-wet core (Mww2, blue) and (b) wettability-altered core (Mmw3, green). The plots (a) and (b) show how the increase in sulfate concentration is delayed compared to the thiocyanate concentration after SW1T is injected. The plot (c) shows the difference in normalized concentrations between the thiocyanate and sulfate curves for the water-wet (blue) and wettability-altered cores (green). The integrated separation area for Mww2 and Mmw3 was 1.43×10^{-3} PV/g and 0.98×10^{-3} PV/g, respectively (see **Paper III**).

Readers are advised to refer to **Paper I** and **Paper III** for the estimated individual areas for the Kansas and Mons water-wet and wettability-altered samples.

Comparison of wettability determination results from Kansas and Mons chalks

It is observed that these two chalk types differ in their wettability values with the same aging procedure. The wettability for the wettability-altered Kansas chalk was found to be 0.55 ± 0.05, whereas wettability-altered Mons chalk gave the wetting index of 0.63 ± 0.07, which shows that Mons chalk was more water wet compared to Kansas chalk at the start of the hydrostatic loading at 130°C. This shows that the mineralogy of the two chalks play a role in determining how wettability of the two types is changed after aging at same temperature for the same period of time with same brine and oil compositions. It is likely that the presence of silicates and clay in Kansas chalk make it more oil wet compared to Mons chalk which is very pure. It may also be due to the higher initial water saturation for Mons chalk that they were left more water wet to start with after aging at similar conditions.

Standnes and Austad (2000a) reported that the wettability induced by crude oils on chalk surfaces is related to the number of acidic components in the crude oil, i.e. crude oils with high acid numbers have a greater potential to turn the chalk oil-wet. Zhang and Austad (2005) also showed that the acid number affect the wetting state. Hence, a deviation in the AN from 2.12 mg KOH/g used in this study to any other value may change the wetness of the chalk cores for the same aging time.

Comparison of results from contact angle and USBM methods with the results from chromatographic separation technique

The results from contact angle and USBM methods show that the cores were neutral wet, but on the oil wet side, after aging for 21 days at 90°C. The chromatographic separation technique also showed that the cores were neutral wet state, but on the water wet side, with same aging conditions. This small difference in the wettability determination between these methods is likely within the margin of error, but further studies are needed using contact angle, USBM and SEM-MLA methods to check for the repeatability of the results.

4.2 Impact of wettability on fluid flow in porous media and mechanical response in chalk

Wettability affects the flow and distribution of reservoir fluids in the rock and plays a significant role in determining how immiscible fluids move through reservoirs, deciding production rates of oil and water and the ultimate oil recovery. Consider an oil wet reservoir rock, where oil is bonded to the mineral surfaces, flooded by water. The injected water flows through the center of the pores, expelling the mobile oil here. This behavior subsequently leads to a rapid water breakthrough, and a high water cut later on leaving significant immobile oil volumes behind. The immobile oil volumes would further depend upon the specific surface area and the oil film thickness. If the same reservoir rock was water-wet, i.e. oil being the non-wetting phase, the oil will occupy the center of the larger pores. During waterflooding the injected water will tend to imbibe into the smaller pores, moving oil into the larger pores where it can be displaced. Oil, then, moves ahead of the waterfront, which results in increased primary oil recovery before water breakthrough occurs. After water breakthrough, almost all the remaining oil becomes immobile. The disconnected residual oil is in the form of oil droplets trapped by capillary forces, arising from the surface energy between oil, water and mineral surface, where the curvature of the oil droplet is larger than the pore throat diameter.

Wettability may also be important to the mechanical behavior of rock. The mechanical response of the material to imposed stress is dictated by the load bearing structure. In a water-wet system, the grains have a larger affinity to water, hence water weakening of chalk has been observed due to chemical reactions occurring between the minerals constituting chalk and reactive brines. In an oil wet system where oil coat the chalk surface, it is envisioned that oil prevents the water phase to get in contact and react with mineral grains, thereby keeping the chalk rock strong and stiff. In a wettability-altered system, however, it is expected that the detailed spatial distribution of oil and water along the pore walls will control the

link between wettability index and sample stiffness and strength. In this study, the work has been performed on outcrop chalk samples and the effect of wettability on chalk mechanics at hydrostatic conditions has been quantified.

4.2.1 Impact of wettability on elastic stiffness and plastic strength

The stress-strain curve during loading and the position of yield stresses for Kansas cores K1 to K8 and Mons cores M1 to M4 are shown in Figure 11 and Figure 12, respectively. The bulk moduli, and the yield and creep stresses used further in the experiments are reported in Table 7 and Table 8, respectively, for both chalk types.

During hydrostatic loading from 1.2 MPa to approximately 1.5 times the yield at 130°C and 0.7 MPa pore pressure, the inlet was closed, NaCl brine was bypassed and the initial saturation fluids only moved towards the outlet due to compaction. The elastic stiffness (bulk modulus) and plastic strength (onset of yield) were observed to be affected by the oil/water saturation and wetness of the cores (Figure 11 and Figure 12). Further on, the wettability-altered Kansas samples were found to be 33% stiffer and 35% stronger than the water-wet Kansas samples (Figure 11), meaning that the stiffness and strength are correlated with each other resulting in stiffer wettability-altered cores to be stronger than the water-wet samples. Similar correlations between stiffness and strength were also shown for 100% water saturated chalk at both 30°C and 130°C (Nermoen et al. 2018a) and for Stevns Klint chalk at ambient temperature (Katika et al. 2015). For Mons chalk, on the other hand, the water-wet and the wettability-altered samples showed similar stiffnesses and strengths (Figure 12).

Table 7. Bulk modulus of both Kansas and Mons cores during hydrostatic loading used in the triaxial test program.

Chalk Type	**Injection brine***	**Core**	**Wetting state**	S_{wi} **(-)**	**Bulk modulus (GPa)**
Kansas	$MgCl_2$ flow	K1	Water wet	1	1.3±0.005
		K2		1	1.9±0.008
		K3	Wettability-altered	0.28	2.6±0.006
		K4		0.29	2.2±0.008
	SSW flow	K5	Water wet	1	2.2±0.007
		K6		1	1.9±0.020
		K7	Wettability-altered	0.27	2.5±0.007
		K8		0.28	2.3±0.005
Mons	$MgCl_2$ flow	M1	Water wet	1	1.3±0.008
		M2		1	1.8±0.034
		M3	Wettability-altered	0.34	1.0±0.006
		M4		0.36	1.1±0.009

*Note: During hydrsostatic loading, the inlet was closed and the initial saturation fluids (NaCl brine for water wet and NaCl brine + oil mixture for wettability altered) were only allowed to move towards the outlet due to compaction. The injection brines are given here just to distininguish between the samples that were flooded by $MgCl_2$ and SSW later on.

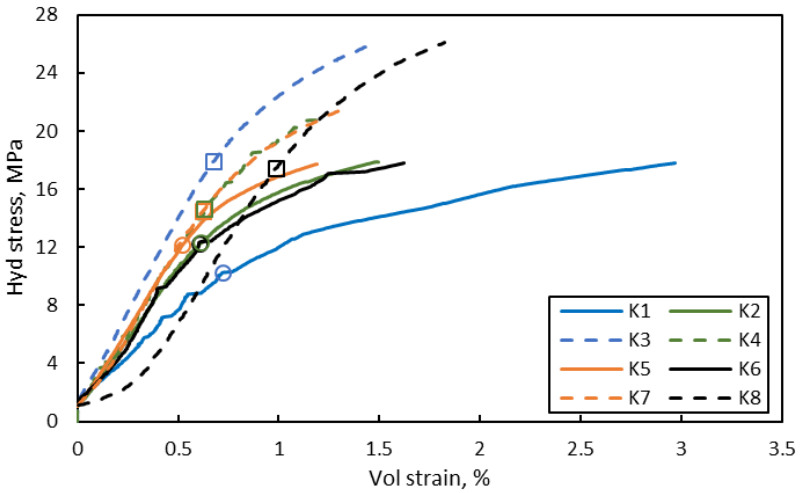

Figure 11. Hydrostatic stress versus volumetric strain for Kansas cores used in the triaxial test program. Solid and dashed lines represent water-wet and wettability-altered cores, respectively. Yield stresses for these cores are displayed in their corresponding curves (circles for water-wet and squares for wettability-altered cores) (see **Paper I**).

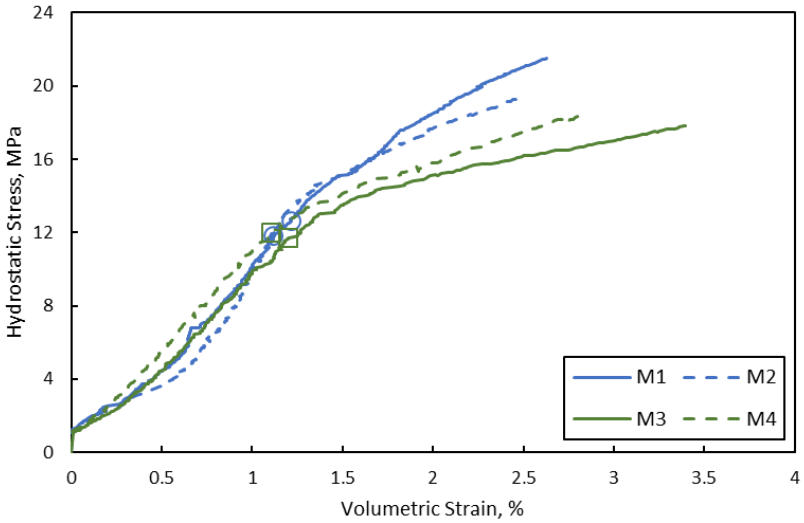

Figure 12. Hydrostatic stress versus volumetric strain for Mons cores used in the triaxial test program. Blue solid and dashed lines represent water-wet cores and green solid and dashed lines represent wettability-altered cores. Yield stresses for these cores are displayed in their corresponding curves (circles for water-wet and squares for wettability-altered cores) (see **Paper III**).

Table 8. Onset of yield stresses and creep stresses are given for Kansas and Mons cores used in the triaxial test program.

Chalk Type	**Injection brine***	**Core**	**Wetting state**	**Onset of yield stress (MPa)**	**Creep stress (MPa)**
Kansas	$MgCl_2$ flow	K1	Water wet	10.3	17.9
		K2		12.9	17.9
		K3	Wettability-altered	17.9	26.1
		K4		14.6	20.8
	SSW flow	K5	Water wet	12.5	17.8
		K6		12.4	17.9
		K7	Wettability-altered	14.5	21.6
		K8		17.7	26.1
Mons	$MgCl_2$ flow	M1	Water wet	14.4	21.5
		M2		13.3	19.3
		M3	Wettability-altered	12.4	17.8
		M4		12.3	18.3

*Note: During hydrsostatic loading, the inlet was closed and the initial saturation fluids (NaCl brine for water wet and NaCl brine + oil mixture for wettability altered) were only allowed to move towards the outlet due to compaction. The injection brines are given here just to distininguish between the samples that were flooded by $MgCl_2$ and SSW later on.

A significant difference in the loading stiffness and yield strength, beyond the experimental uncertainty, was not observed in Mons chalk. The initial soft behavior at low stresses, i.e. the initial large strains of the water-wet samples, can be caused by closure of micro-cracks and fractures formed due to the sample handling. Further experiments are required to identify if the mechanical parameters for Mons samples can be altered by aging, e.g. with a more acidic oil, higher aging temperature/time, or by lowering S_{wi} even more before oil is injected (a lower value of S_{wi} could make the core more oil-wet).

Oil adsorption impact particle-particle contact forces

The thickness of the charged diffusive layer on calcite surfaces is characterized by the Debye length (Lyklema 2005; Megawati et al. 2013; Voake et al. 2019) that increases with increasing temperature (Andreassen and Fabricius 2010). A thickening of the layer (Debye length) increases the repulsive area between particles causing further weakening of water-saturated samples. Voake et al. (2019) further reported a Debye length of around 200 nm at 130°C using Debye-Huckel theory.

The force between particles in the presence of water is dictated by the sum of attractive van der Waals forces and repulsive electrostatic forces from the overlapping diffusive layer. When oil replace water on surface areas where the double layers would otherwise interact (regions with electrostatic repulsion), the disjoining pressure would reduce and the overall force balance between particles would change. When the normal force between two grains increase (in the case of oil adsorption), it becomes harder for particles to re-organize. This seems to have occurred in Kansas, which has a Biot coefficient of 0.91 (Voake et al. 2019) and smaller pore size (characterized by the lower relaxation time T_2 estimated from the NMR studies, Voake et al. 2019) than Mons with a Biot coefficient of 0.95 (Figure 13(a) and Table 13 in Appendix). If oil adsorbs on mineral surfaces but not on nearby particle contacts, the geomechanical parameters would remain un-affected. This seems to have occurred in Mons (Figure 13(b)).

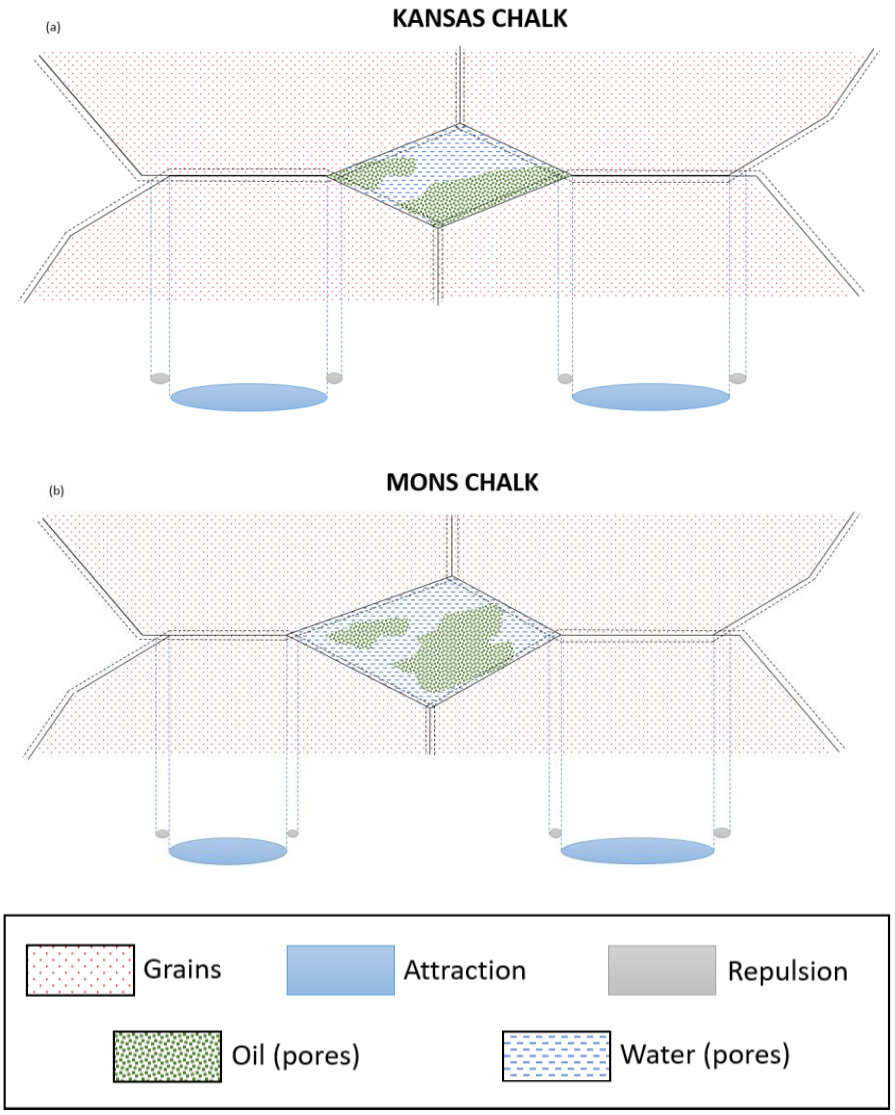

Figure 13. Partitioning of oil and water in pores for (a) Kansas and (b) Mons chalks. Attractive van der Waals and repulsive electrostatic forces present between calcite grains are also shown. Mons chalk has larger pore size and Biot coefficient compared to Kansas chalk (Voake et al. 2019) (see **Paper III**).

With the same oil, brine composition and aging temperature, it has been reported that Kansas chalk remains water-wet if the aging time is less than 6 days, and aging for 21 days was enough to obtain a stable neutral-wettability (**Paper IV**). It remains to be tested how mechanical parameters change for the same oil/water saturation for unaged samples. If the aging conditions were modified, the Mons chalk may become more mixed/oil wet thereby affecting stiffness and strength differently than in this study.

4.2.2 Impact of wettability on creep behavior

The creep stress for all eight Kansas cores and four Mons cores was set to be 1.5 times yield stress so that the development could be compared to each other. Since the yield stress was determined with the naked eye during hydrostatic loading, the creep stress chosen deviated from the factor 1.5 times yield stress (Table 8). The actual creep stresses (in Figure 14, Figure 15 and Figure 16) varied between a factor of 1.4 and 1.7 times yield stress for Kansas cores, and 1.4 and 1.5 times yield stress for Mons cores.

During the first 15 days of creep period, the inlet valve was kept closed and NaCl brine was bypassed. The initial resident fluids were able to flow through core due to compaction only and could leave the core on the downstream side. NaCl brine weakly interacts with the mineral surfaces in chalk and leads to minor calcite dissolution. Madland et al. (2011) showed the effect of flooding NaCl brine through water-wet Liège chalk and observed that the calcium concentration in the effluent was as low as 0.004 mol/l throughout the experiment. Andersen et al. (2018) showed negligible mineral precipitation effects for both water-wet Kansas and Mons chalks flooded by NaCl brine. In the hydrostatic tests performed in this work, the cores were only initially saturated by NaCl, and not flooded. The interactions between chalk and stagnant NaCl brine were observed to be negligible as the amount of dissolved

calcite, due to interaction of chalk with NaCl brine, amounted to less than 0.01% in mass compared to the initial dry mass of the samples.

4.2.2.1 Kansas chalk

The volumetric creep strain for the four water-wet (100% NaCl brine saturated) and four wettability-altered cores (with initial NaCl brine saturation ranging from 27% to 29%) during the first 15 days followed approximately the same creep trend when stress was set to 1.5 times the yield (Figure 14 and Figure 15). The samples were not flooded during this time interval, and the fluid movement was controlled by pore volume reduction. The observation that how creep is evolving for both water-wet and wettability-altered chalks may imply that oil wetness is not affecting the way in which the grains re-organize. These observations exemplify how different mechanical parameters correlate to each other.

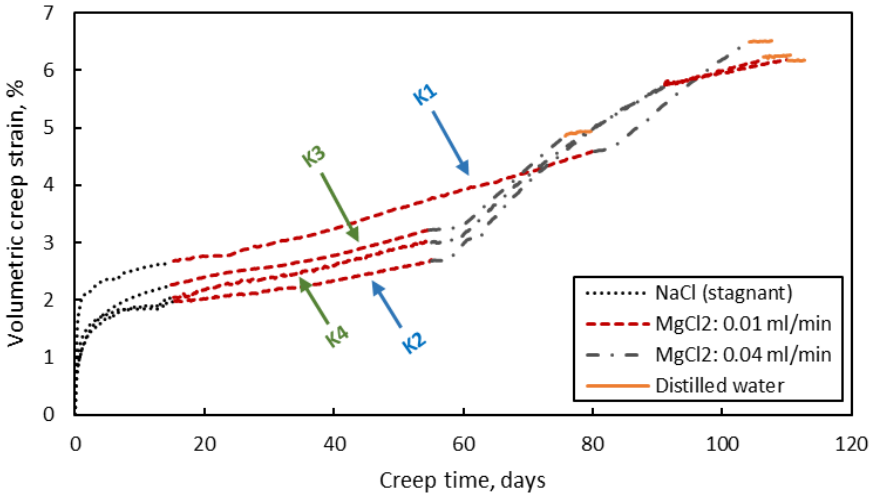

Figure 14. Volumetric creep strain with time during $MgCl_2$ flow through water-wet Kansas cores K1 and K2 (blue arrows), and wettability-altered Kansas cores K3 and K4 (green arrows) (see **Paper I**).

From 16th day the injection of $MgCl_2$ and SSW started. The injection of $MgCl_2$ brine has shown to induce chemical reactions leading to

additional creep rates, and more chemical reactions taking place during a time interval leads to an increased creep rate (Nermoen et al. 2015). When $MgCl_2$ brine was injected at the lower rate of 0.010 ml/min (approx. 0.5 initial PVs (PV_i) per day), the strain curve went from having a negative second derivative to a straight line with a more-or-less constant strain rate. Quadrupling the flow rate to 0.040 ml/min, after a certain number of days, increased the linear creep rate by a factor of 2.5 to 4. This is in line with the analysis of the effluent fluids (Figure 17) that display how the loss rate (in grams per day) of Ca and gain rate of Mg also increased by a factor of 2 to 4 after the flow rate was quadrupled. This shows how chemical reactions drive reduction in the solid volume by reducing the overall mass and increasing the mineral density, and how this behavior is linked to the creep rate with time (Nermoen et al. 2016; Andersen et al. 2018). As shown in the presented data, the presence of oil in the pores does not alter the dissolution/precipitation driven water weakening dynamics, neither qualitatively nor quantitatively.

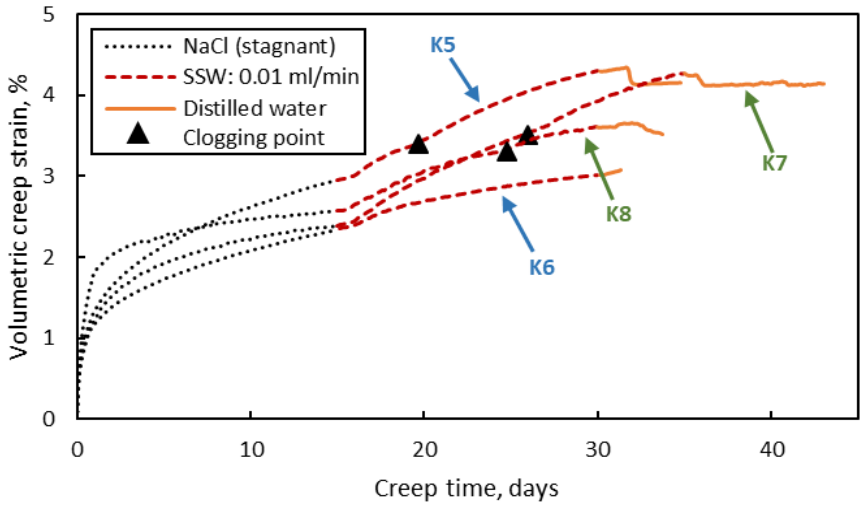

Figure 15. Volumetric creep strain with time during SSW flow through water-wet Kansas cores K5 and K6 (blue arrows), and wettability-altered Kansas cores K7 and K8 (green arrows) (see **Paper I**).

The chalk samples that were flooded with SSW (i.e. K5 to K8, Figure 15) displayed a qualitatively similar behavior as the $MgCl_2$ samples (K1 to K4, Figure 14). Injecting SSW induced chemical reactions and adsorption of surface-active ions leading to immediate additional creep rates. All cores showed comparable volumetric strain curves, irrespective of the initial wettability and oil/water saturation. After clogging (in the water-wet K5 and wettability-altered K7 and K8 samples) after a certain period, the strain rate declined because of reduced effective stress due to pore pressure buildup. The clogging did not occur inside the samples but in the steel tubing on the outlet side, so opening the bypass valve reduced the pore pressure and the strain rate regained its pre-clogging values.

4.2.2.2 Mons chalk

The volumetric creep strain at constant creep stresses (given in Table 8) for different wettability cores followed a comparable trend for all Mons samples throughout the creep period (Figure 16). They showed a similar trend during the stagnant fluid creep period. After the start of $MgCl_2$ injection at 0.010 ml/min flow rate, the strain rate curve stayed negative for around 15 days, after which it stayed constant for the rest of the flooding period at this flow rate (depicted by a zero slope curve, see Figure 16). This is similar to previous observations with clean chalks such as Mons and Stevns Klint (Andersen et al. 2018).

All samples showed an accelerated strain, irrespective of the initial wettability, when the flow rate of $MgCl_2$ injection was increased to 0.040 ml/min (Figure 16). The strain rate increased by a factor of 3 to 8 at the starting of injection period at higher rate. Nonetheless, the strain rate showed fluctuations and decreased by a factor of 1.5 to 2.5 times by the end of the higher rate injection phase. This shows how chemical reactions are independent of the oil/water saturation and the initial wetness of the Mons chalk cores but depend on the chalk mineralogy as these fluctuations were not observed for Kansas cores. During DW

flooding to clean the cores, the strain rate dropped down to zero instantly depicting that no major interactions took place between DW and the rock, and that there was negligible precipitation of any secondary phases.

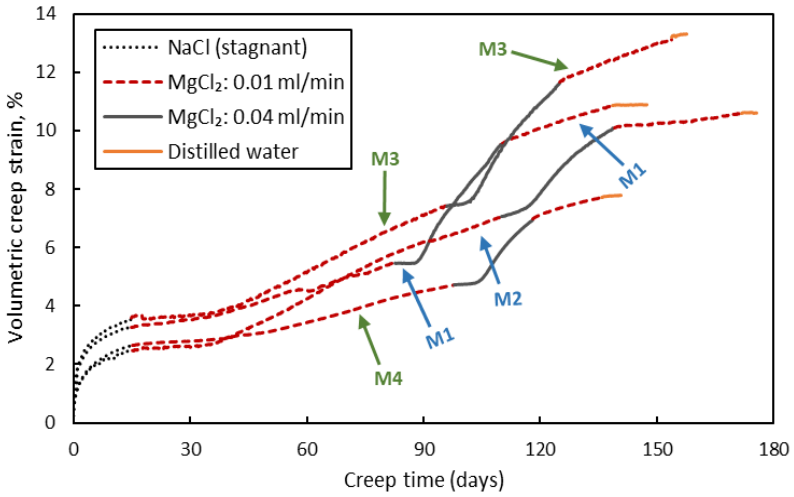

Figure 16. Volumetric creep strain with time during $MgCl_2$ flow through water-wet Mons cores M1 and M2 (blue arrows), and wettability-altered Mons cores M3 and M4 (green arrows) (see **Paper III**).

Impact of DW injection during cleaning of cores

During DW injection to clean the cores of any salts, the strain rate dropped significantly for all cores flooded by $MgCl_2$ brine (Figure 14 and Figure 16), even though the temperature and stress level were the same. The solubility of calcite in DW at 25°C is reported to be 0.013 g/l (Voake et al. 2019) and it decreases with increase in temperature (Coto et al. 2012). This means that 0.00039 g of calcite dissolved per PV of DW flooded through cores (approximate PV of 30 ml) at 25°C. As four PVs of DW were flooded to clean the cores at 130°C, the calcite dissolved amounts to approximately 0.001 % in mass compared to the initial dry mass of the cores (average initial dry mass of 135 g). Hence, it may be concluded that the interactions of DW with calcite are minor in nature.

For SSW flooded cores, a decrease in the strain rate is observed for the cores where clogging occurred due to pore pressure increase (K5, K7 and K8) during flooding by DW to clean the cores. For core K6 (without clogging), an increase in the volumetric creep strain is observed. This was also observed by Korsnes et al. (2006b).

These observations further exemplify how chemical reactions that undergo during the continuous flow of reactive fluids affect the rate of deformation, thereby displaying the link between chemical reactions and the quantitative amount of water weakening. Of special importance to emphasize is that all these observations are insensitive to the initial wettability and brine/oil saturation of the chalks.

4.2.3 Impact of wettability on rock-fluid interactions

4.2.3.1 Rock-fluid interactions during $MgCl_2$ flow

Figure 17 and Figure 18 display the effluent calcium and magnesium ion concentrations for Kansas and Mons chalk, respectively, during $MgCl_2$ brine flow through the two water-wet (a and b) and two wettability-altered (c and d) cores. Since the dominating chemical reactions are attributed to the precipitation of magnesium-bearing minerals and the dissolution of calcium carbonate, the focus is on the calcium and magnesium ions. Besides, magnesium ions can also adsorb on the calcite surface on the expense of calcium desorption. In all, dissolution/precipitation and adsorption/desorption lead to a decrease in the magnesium concentration in the sampled effluent compared to the injected brine concentration and an increase in the calcium concentration.

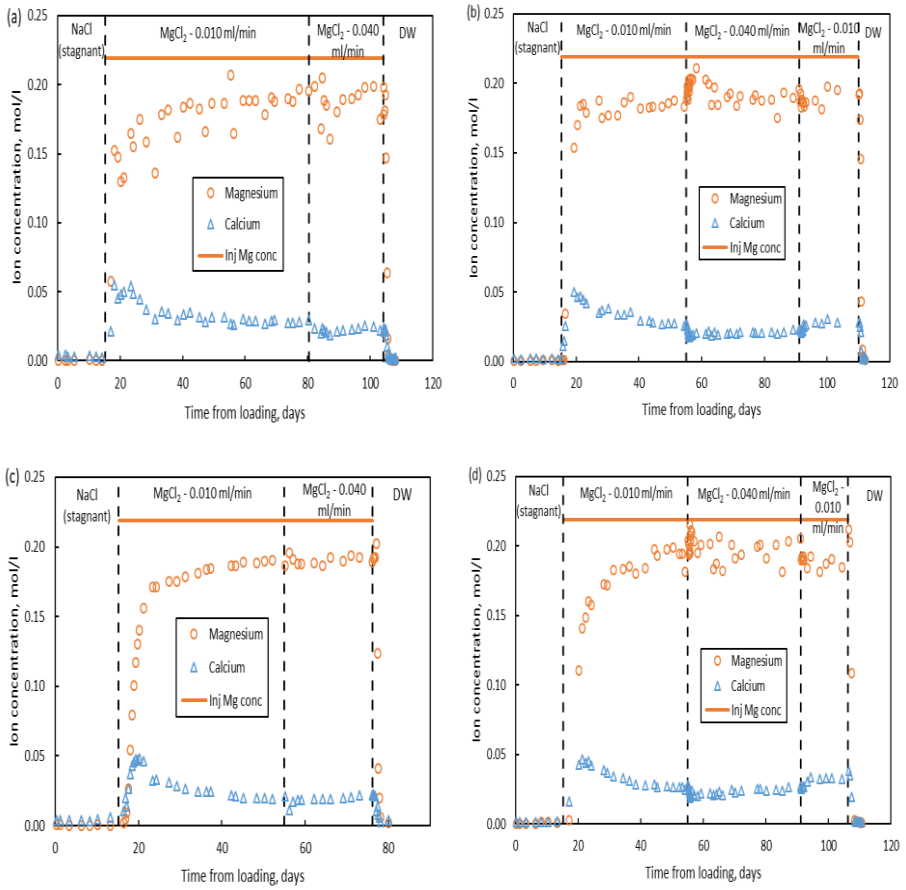

Figure 17. Kansas chalk samples flooded by $MgCl_2$ brine. Effluent ion concentrations of calcium and magnesium ions, and the injected magnesium ion concentration over time are shown for water-wet cores (a) K1 and (b) K2 and wettability-altered cores (c) K3 and (d) K4 (see **Paper I**).

The effluent analyses (Figure 17 and Figure 18) of Kansas and Mons chalks show that the calcium production and magnesium retention rates (in g/day) changed by a factor of 2 to 6 (rates estimated by multiplying the ion concentration in mol/l, flow rate in l/day and molecular weight of calcium and magnesium in g/mol) when the flow rate quadrupled – irrespective of the wettability and oil/water saturation. This shows how chemical reactions may drive reduction in solid volume by reducing the

overall mass and increasing the mineral density, and how this behavior links to the bulk creep strain rate (Nermoen et al. 2016; Andersen et al. 2018).

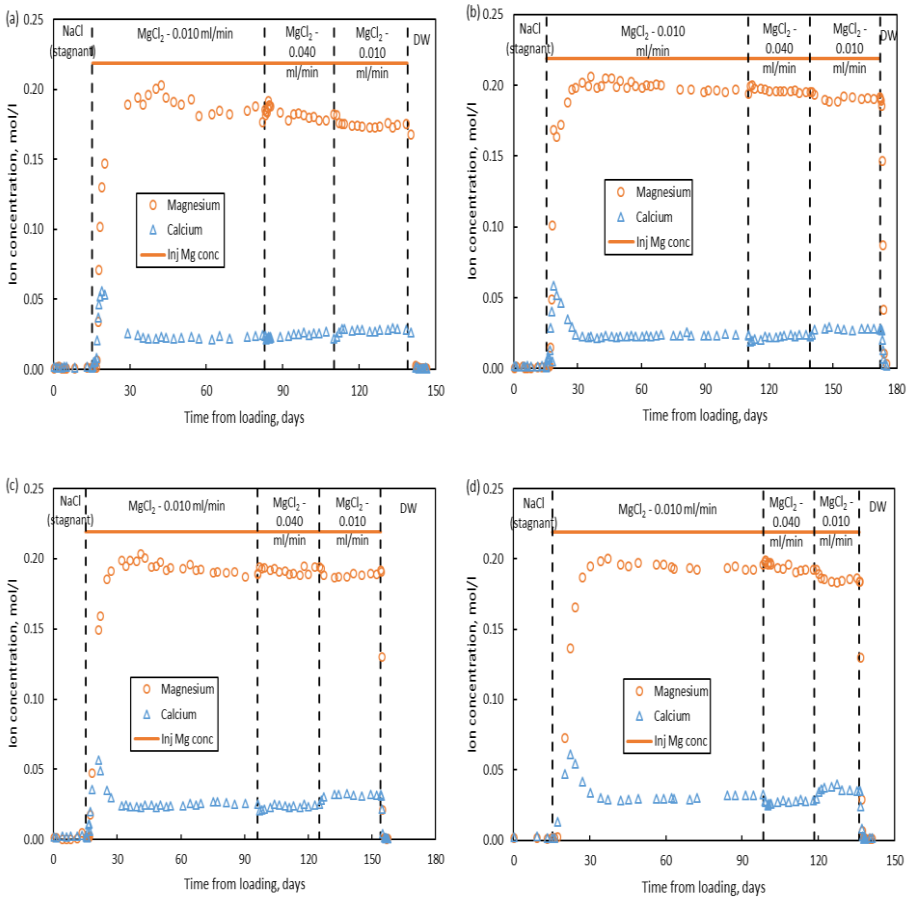

Figure 18. Mons chalk samples flooded by $MgCl_2$ brine. Effluent ion concentrations of calcium and magnesium ions, and the injected magnesium ion concentration over time are shown for water-wet cores (a) M1 and (b) M2, and wettability-altered cores (c) M3 and (d) M4 (see **Paper III**).

The effluent analyses on Kansas and Mons chalks have shown that interactions took place between the pore fluid and the mineralogical surfaces during $MgCl_2$ brine flooding.

At least two water weakening mechanisms are required to understand how the change in fluid composition in the effluent analysis (Figure 17 and Figure 18) and strain rate depend on each other: (i) Chemical reactions between brine and chalk related to dissolution and precipitation, and (ii) the adsorption of surface-active divalent ions (magnesium and sulfate ions) on the chalk surface and desorption of calcium ions. This adsorption changes the electrostatic repulsion thereby changing the inter-particle forces governing grain movements (Megawati et al. 2013). In all cases irrespective of the brine composition, the oil/brine saturation and wettability, the calcium concentration increased and the magnesium concentration decreased in the effluent. This is related to the production of calcium ions resting on the mineral surface and dissolution of calcite as well as precipitation of magnesium carbonate (Madland et al. 2011; Nermoen et al. 2015; Zimmermann et al. 2015; Minde et al. 2017, 2018a, 2018b; Andersen et al. 2018) and adsorption of magnesium ions onto and desorption of calcium ions from the calcite surface (Ahsan and Fabricius 2010; Alam et al. 2010; Nermoen et al. 2018a; Liu et al. 2018). However, only a limited number of surface sites are available, so the adsorption/desorption contribution to the changes in the ion concentrations will not prevail indefinitely. Adsorption/desorption dynamics could only occur within the first few pore volumes of the reactive brine injection in these cases. Afterwards the dissolution/precipitation processes dominate the calcium and magnesium effluent dynamics. Secondary minerals can be identified using SEM. Qualitatively, the mineral replacement seems to be insensitive to the initial water wetness and oil/brine saturation. The described behavior is in-line to what was indicated by X-ray diffraction and SEM studies carried out on chalk after $MgCl_2$ brine flow-through experiments by Madland et al. (2011) and Megawati et al. (2015).

4.2.3.2 Rock-fluid interactions during SSW flow

The chemical interactions between the core and the injected fluid are more complicated when SSW is injected compared to $MgCl_2$ brine. This

is because there are additional ions other than Mg ions present in SSW that interact with chalk leading to more complex chemical interactions. The effluent ion concentrations of sulfate, magnesium and calcium are reported in Figure 19 for the two water-wet (K5 and K6) and one wettability-altered (K8) cores. The effluent analysis of the wettability-altered core K7 is not shown due to lack of data.

In the same way as during $MgCl_2$ flow, magnesium ions are retained in the cores and calcium ions are produced when SSW is injected through Kansas chalk. In addition, sulfate ions are retained in the cores. During the first 15 days of creep period (bypass), magnesium and sulfate concentrations in the effluents are observed to be zero, while a small production of calcium ions can be seen for K5 and K6 (Figure 19(a) and (b)). This may imply that calcite dissolution has taken place within the core, and that these ions are transported *either* by advection together with fluids expelled as the core is compacted *or* by diffusion through the tubing to the bypass valve and then transported along with the fluids from there.

The bypass valve was closed and SSW was flooded through the cores from the 16^{th} day, after which a transient period is observed (Figure 19). In this period the calcium, magnesium and sulfate concentrations increase until 17-18 days after which a stable concentration is reached for core K6 (Figure 19(b)). The concentration of these three ions did not stabilize for cores K5 and K8 (Figure 19(a) and (c)). After a certain period, the system clogged due to precipitation in the steel tubing on the outlet side of the cores (K5, K7 and K8) and the bypass had to be opened to avoid pore pressure buildup.

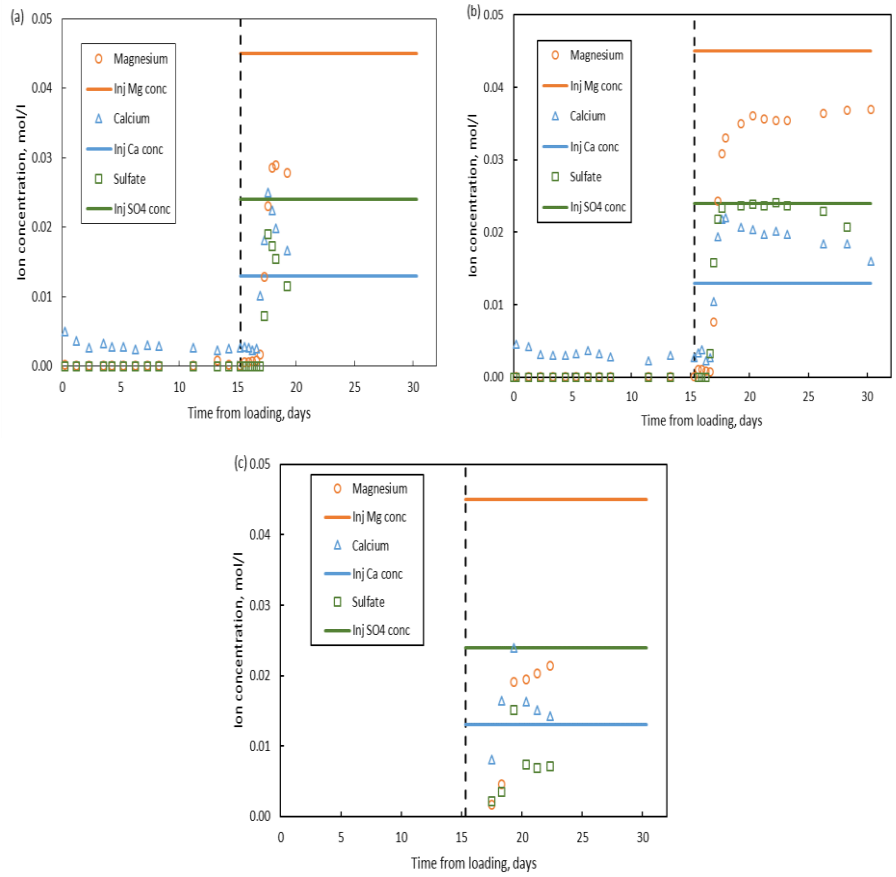

Figure 19. Kansas chalk samples flooded by SSW brine. Injected and effluent ion concentrations of calcium, magnesium and sulfate ions over time are shown for water-wet cores (a) K5 and (b) K6, and wettability-altered core (c) K8. The effluent analysis of the wettability-altered core K7 is not shown due to lack of data. The black dashed vertical line in the plots depict the start of SSW flooding (see **Paper I**).

4.2.4 Impact of wettability on chalk surface area evolution during $MgCl_2$ flow

The initial tracer test was performed on the Kansas water wet sample KA1 before the injection process started, thereafter tracer tests were

performed after NaCl brine had been injected for 7.5 days, and after two injection periods of $MgCl_2$ brine for 7 days each. All the tracer tests were performed at ambient temperature, whereas the temperature during injection of $MgCl_2$ and NaCl was 130°C such that chemical reactions could occur. The aim was to quantify how the two brines affected the area spanned by the sulfate-thiocyanate concentration curves. Figure 20(a) displays the normalized concentration data along y-axis and PV_i of SW1T injected along x-axis. It can be seen how thiocyanate concentration increases ahead of the sulfate concentration and the rise in sulfate concentration is delayed in comparison. The area spanned between the thiocyanate and sulfate curves is displayed in Figure 20(b), whereas the area per gram of the core is reported in Table 9. The integrated area between the curves are given in units of PV per gram to capture the sample size effect.

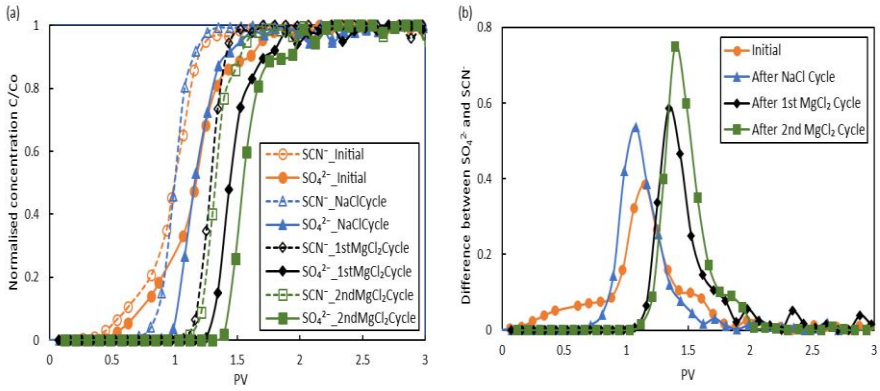

Figure 20. (a) Chromatographic separation during SW1T injection at ambient temperature on KA1. The normalized concentrations for thiocyanate (dashed curves) and sulfate (solid curves) ions are shown for initial tracer test (orange), after 7.5 days of NaCl injection (blue), after 7 days of 1st $MgCl_2$ injection (black) and after 7 days of 2nd $MgCl_2$ injection (green). The integrated areas between thiocyanate and sulfate are given in Table 9. (b) Difference between SCN^- and SO_4^{2-} as a function of PVs injected for each tracer test (see **Paper II**).

The initial tracer test yielded an area (orange curve in Figure 20(b)) of 1.45×10^{-3} PV/g, while after NaCl injection for 7.5 days the curve

changed its shape, but the area increased insignificantly to 1.46×10^{-3} PV/g, i.e. an increase of 0.7%. After $MgCl_2$ brine was injected for 7 days, the area (black curve) increased to 1.60×10^{-3} PV/g, i.e. an increase of 10.3%. After a second $MgCl_2$ brine injection phase for another 7 days, the area increased to 1.75×10^{-3} PV/g, i.e. 20.7% increase compared to the initial tracer test and 9.4% compared to the first $MgCl_2$ injection phase. These results show how the surface area that plays a role in sulfate adsorption increases with time. Figure 20(b) also displays how the difference evolve through time, where the curves shift towards the right, and the maximal difference between the thiocyanate and sulfate tracer increases each time.

Three Kansas mixed wet samples KA2 to KA4 were used to test the hypothesis that $MgCl_2$ brine could modify the wetting state of mixed wet chalk. For the three samples, one, two and four tracer tests were performed. Each tracer test was performed after $MgCl_2$ brine was injected for 10 days in each phase at a rate of $1PV_i$/day at 130°C.

For KA2, KA3 and KA4, the initial tracer test yielded areas of 0.81×10^{-3} PV/g, 0.86×10^{-3} PV/g and, 0.86×10^{-3} PV/g, respectively. This implies a water wetness of 0.56, 0.59 and 0.59 for the three cores (using equation (30)), respectively, by using the area estimated for the water wet reference sample KA1 (1.45×10^{-3} PV/g).

For the three cores after 10 days $MgCl_2$ injection at 130°C, the area between thiocyanate and sulfate concentration curves changed to 1.41×10^{-3} PV/g, 1.38×10^{-3} PV/g, and 1.35×10^{-3} PV/g, respectively. The corresponding wetting indices changed to 0.97, 0.95 and 0.93 for KA2, KA3 and KA4, respectively, which corresponds to an increase in the water wet surface area by a factor of 1.73, 1.61 and 1.57 compared to the surface area before $MgCl_2$ injection started. Then, KA2 was dismantled while further $MgCl_2$ injection of KA3 and KA4 continued.

After another 10 days of $MgCl_2$ injection at 130°C, the water wet surface area of KA3 and KA4 increased to 1.50×10^{-3} PV/g and 1.55×10^{-3} PV/g, namely an increase of the water wet surface available for sulfate adsorption by a factor 1.74 and 1.80 compared to initial measurement. Both these values are greater than the KA1 reference of 1.45×10^{-3} PV/g, implying that the water wet surface area increased to more than the surface area of 100% water wet core. After this second $MgCl_2$ injection phase, the KA3 sample was dismantled.

A third and fourth $MgCl_2$ injection phases of 10 days each were conducted for KA4. Here, the integrated area between the thiocyanate and sulfate curves increased to 1.62×10^{-3} PV/g and 1.71×10^{-3} PV/g, which corresponds to an increase by a factor of 1.88 and 1.99 compared to the initial value. The left column of Figure 21((a), (c) and (e)) displays normalized sulfate and thiocyanate concentrations and the right column ((b), (d) and (f)) displays the difference between sulfate and thiocyanate concentrations as function of number of PVs of SW1T injected for different tracer tests performed on mixed wet samples KA2, KA3 and KA4, respectively.

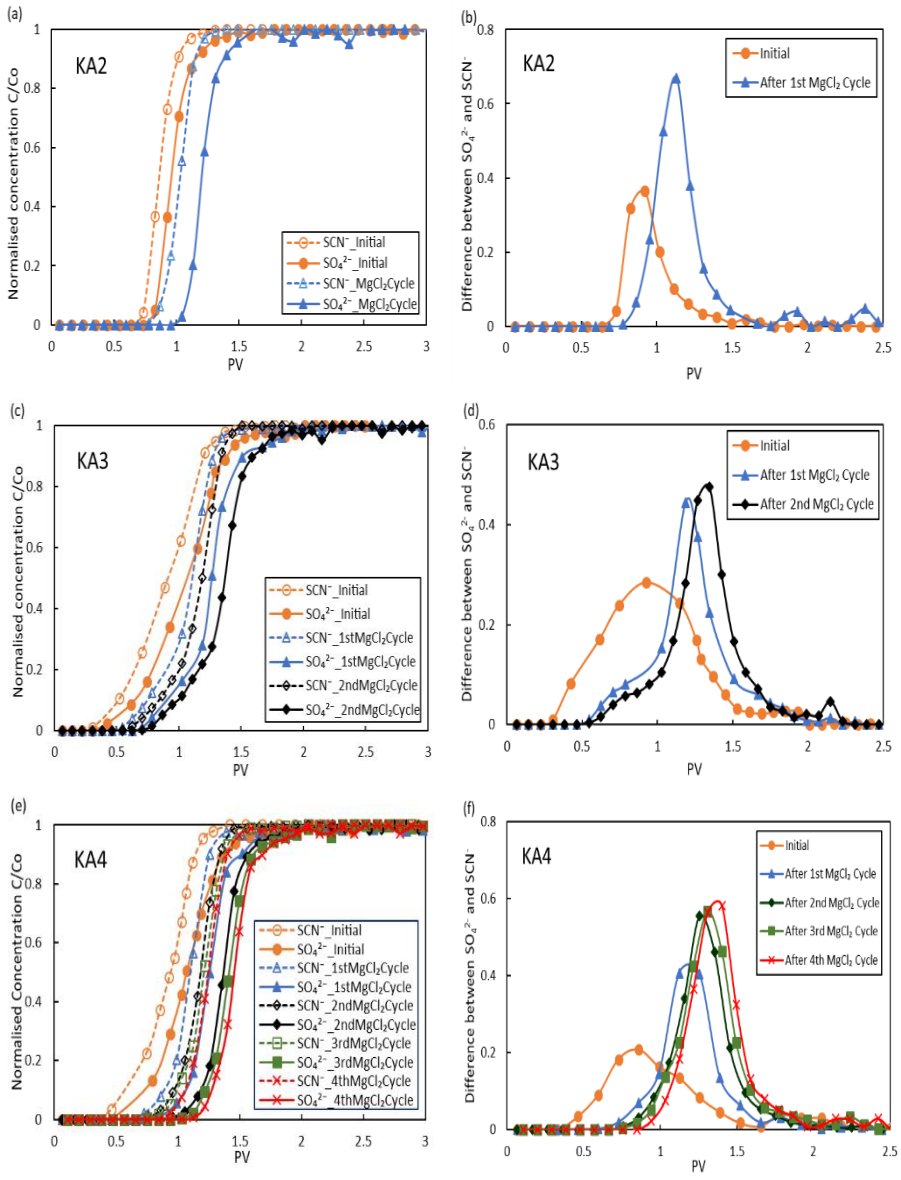

Figure 21. Chromatographic separation test at ambient temperature for the mixed wet samples KA2, KA3 and KA4. The left column ((a), (c) and (e)) displays normalized concentrations for thiocyanate (dashed curves) and sulfate (solid curves) and are shown for the initial tracer test (orange), and after 1st (blue), 2nd (black), 3rd (green), and 4th (red) injection phases of $MgCl_2$ brine each lasting 10 days. The right column ((b), (d) and (f)) displays the difference

between sulfate and thiocyanate. Clear trends in the difference are seen, the area increases, the peak increases and the curve is shifted to the right for each curve, see Table 9 and Figure 22 (see **Paper II**).

The plots (Figure 20 and Figure 21) show how the increase in sulfate concentration is delayed compared to the thiocyanate concentration when SW1T brine is injected. Table 9 summarizes the values of the area obtained between the sulfate and thiocyanate ions during tracer tests for all samples.

Table 9. Estimated integrated areas per gram of the sample for water and mixed wet samples, and the corresponding wettability indices. NaCl and $MgCl_2$ were injected at 130°C for chemical reactions to occur while tracer tests were conducted at ambient temperature.

Sample	**Timing of tracer test**	**Number of injection days at 130°C**	**Integrated sulfate – tracer area per gram sample (10^{-3}PV/g)**	**Wetting index (W_i)**
KA1 Water wet	Initial tracer test	0	1.45	1.00
	NaCl inj.	7.5	1.46	1.01
	1st $MgCl_2$ inj.	14.5	1.60	1.10
	2nd $MgCl_2$ inj.	21.5	1.75	1.21
KA2 Mixed wet	Initial tracer test	0	0.81	0.56
	$MgCl_2$ inj.	10.0	1.41	0.97
KA3 Mixed wet	Initial tracer test	0	0.86	0.59
	1st $MgCl_2$ inj.	10.0	1.38	0.95
	2nd $MgCl_2$ inj.	20.0	1.50	1.03
KA4 Mixed wet	Initial tracer test	0	0.86	0.59
	1st $MgCl_2$ inj.	10.0	1.35	0.93
	2nd $MgCl_2$ inj.	20.0	1.55	1.07
	3rd $MgCl_2$ inj.	30.0	1.62	1.12
	4th $MgCl_2$ inj.	40.0	1.71	1.18

The evolution in the areas spanned by the SCN^- and SO_4^{2-} curves per gram of the water wet KA1 sample in Figure 20(b) and the mixed wet samples KA2, KA3 and KA4 in Figure 21(b), (d) and (f) are displayed together in Figure 22. Here in Figure 22(a), it can be seen how the continuous $MgCl_2$ injection at 1 PV_i per day evolved the water wet area available for sulfate adsorption.

Further on, the estimated wetting index, when compared to the initial surface area of the 100% water wet core, evolved with increased amount of $MgCl_2$ injection (Figure 22(b)). After 20 days of $MgCl_2$ injection both KA3 and KA4 had a surface area exceeding the initial area of KA1, implying that the amount of water wet area in the core has increased. This is an indication that new mineral phases were growing from nucleation seeds within the cores which is in line with what has been observed for water wet chalk samples flooded by $MgCl_2$ brine previously (Andersen et al. 2018).

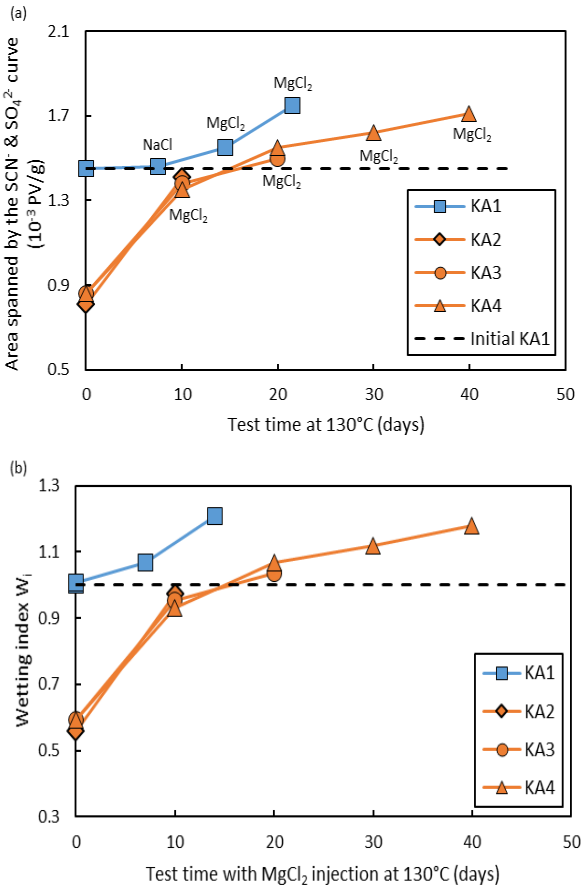

Figure 22. (a) Area spanned by the thiocyanate and sulfate concentration curves for water wet sample KA1 (blue) and mixed wet samples KA2, KA3 and KA4 (orange) as a function of test time at 130°C. (b) Evolution of wetting index as a function of $MgCl_2$ brine injection days at 130°C for all samples. The black dashed line in (b) gives the wetting index of a completely water wet core (equal to one) (see **Paper II**).

For the water wet sample KA1, the area obtained between the thiocyanate and sulfate curves remained the same after flooding NaCl brine as before the flooding, supporting the notion that Na^+ and Cl^- ions are inert to weakly reactive to the mineral surfaces in chalk. This is in-line with Madland et al. (2011). Later when the same sample was flooded

by $MgCl_2$ brine, an increase in this area was observed with time (Table 9). The time-dependent chemical reactions between the brine and calcite minerals displayed in Figure 23 for the water wet sample KA1 are interpreted as a) magnesium adsorption on available surface sites, and b) dissolution of calcite and precipitation of secondary magnesium-bearing minerals, where the effluent magnesium concentration never reaches the injected concentration and triggers mineralogical changes in the chalk framework. The same behaviour has been reported in other similar experimental studies (Madland et al. 2009, 2011; Megawati et al. 2011; Nermoen et al. 2015; Zimmermann et al. 2015; Wang et al. 2016; Minde et al. 2017, 2018a; Andersen et al. 2018).

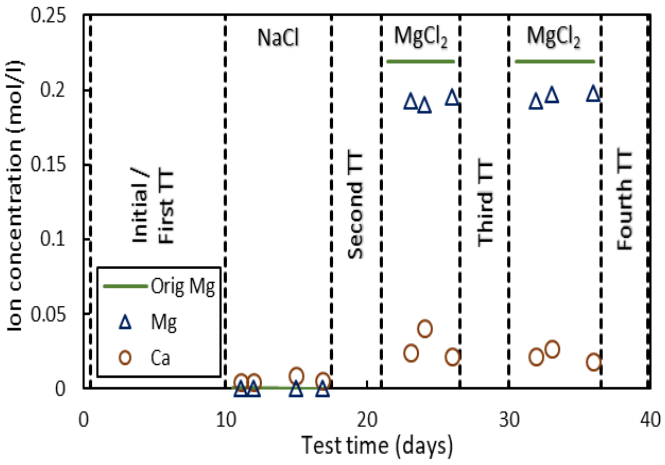

Figure 23. Effluent ion concentrations of calcium and magnesium ions, and the injected magnesium ion concentration over time are shown for the water wet sample KA1. The abbreviation TT stands for tracer test (see **Paper II**).

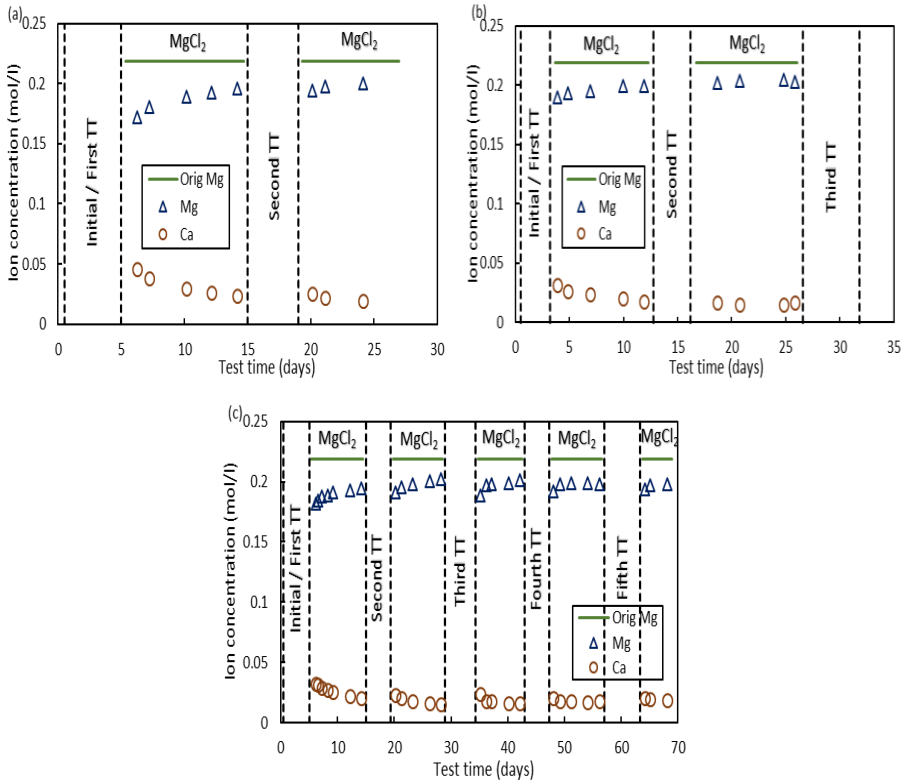

Figure 24. Effluent ion concentrations of calcium and magnesium ions, and the injected magnesium ion concentration over time are shown for the mixed wet samples (a) KA2, (b) KA3 and (c) KA4. The abbreviation TT stands for tracer test (see **Paper II**).

The mixed wet samples KA2, KA3 and KA4, which were also flooded by $MgCl_2$ brine, showed similar results in both IC data and evolution of water wet area where the brine flow increased the water wetness of the cores, as the water wet surface area increased after each 10 day $MgCl_2$ flooding cycle (Table 9). The wettability index of samples KA3 and KA4 exceeded 1 after the second $MgCl_2$ injection phase, implying that the available water wet surface area in these samples exceeded the total mineral area available for the water wet reference sample KA1. From the effluent analysis of these mixed wet samples (Figure 24), it is observed that calcium is produced and magnesium is retained in the samples

throughout the injection period, in-line with the continuous dissolution/precipitation processes taking place in water saturated samples. Precipitated minerals have been documented to grow using Field Emission Gun Scanning Electron Microscopy (FEG-SEM) and EDX studies (Madland et al. 2011; Megawati et al. 2011; Nermoen et al. 2015; Zimmermann et al. 2015; Wang et al. 2016; Minde et al. 2017, 2018a, 2018b; Andersen et al. 2018).

4.2.5 Observations of oil volume development for the wettability-altered cores

The produced oil volume during flow and compaction was measured in a vertical column on the downstream side of the experimental setup and read off by eye at frequent time intervals. The results of the oil production are reported in Table 10. Based on the difference between the pore volume and measured oil volume, the water volumes were estimated through time.

Table 10. Initial and final oil and water volumes in wettability-altered Kansas cores K4 and K7 and Mons core M4.

Chalk type	**Kansas**		**Mons**
Wettability-altered core	**K4**	**K7**	**M4**
Injection brine	**$MgCl_2$**	**SSW**	**$MgCl_2$**
Irreducible water volume before test, ml	8.3	8.0	12.0
Irreducible water saturation S_{wi}, %	28.5	27.4	36.4
Initial oil volume, ml	20.8	21.2	21.0
Total produced oil at the end of the test, ml	8.8	9.8	11.2
Oil volume after test, ml	12.0	11.4	9.8
Oil saturation after test, %	49.4	45.2	41.4
Pore volume before and after test, ml	29.1 and 24.3	29.2 and 25.2	33.0 and 23.7

4.2.5.1 Oil volume development during $MgCl_2$ flow

4.2.5.1.1 Through Kansas chalk

Figure 25(a) shows the oil and water volumes and (b) the change in the saturation of oil inside the core with time from the start of hydrostatic loading for the wettability-altered Kansas core K4.

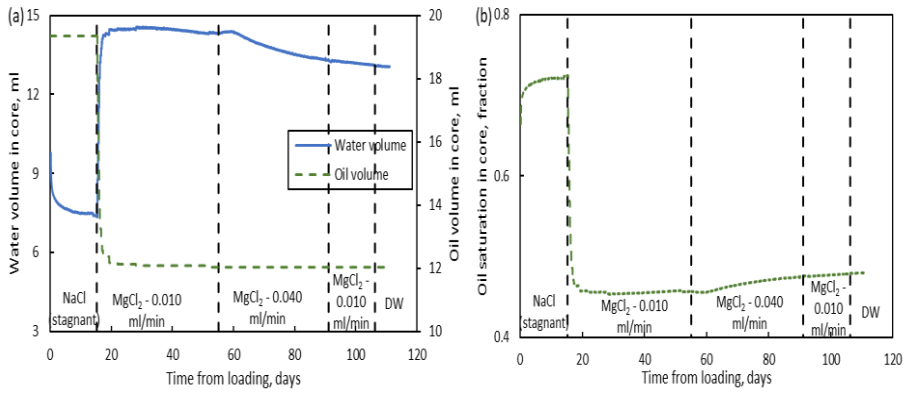

Figure 25. Wettability-altered Kansas sample K4. (a) Oil and water volumes in the core obtained from measurements of the oil volume produced, bulk volume from compaction and solid volume from chemical reactions and (b) oil saturation in the core with time from the start of hydrostatic loading. Black dashed vertical lines depict the time when brine composition and/or flow rate changed (see **Paper I**).

The heating of the cells led to production of oil interpreted to be caused by thermal expansion of oil. However, during loading and subsequent compaction without flow-through (stagnant NaCl brine in the pores), no additional oil was produced implying that, within the error of measurement, only water was expelled during compaction. When $MgCl_2$ flooding started, oil was produced immediately. After a certain time, however, the oil production ceased even though compaction and chemical reactions continued.

The increase in flow rate of $MgCl_2$ brine to 0.04 ml/min on the 56^{th} day did not lead to additional oil production even though more than 57% of the initial oil was left inside the core. The additional dissolution of calcium and precipitation of magnesium triggered by the four-fold increase in flow rate (see Figure 17), and the four-fold increase in pressure drop across the core, did not have any effects on oil production. As observed from Figure 25(b), the oil saturation increases from 60 days and onwards. This is because compaction prevailed with time, but no

more oil was recovered from the core. Therefore, the compaction occurred by reducing the water volume, whilst the oil volume remained constant.

Volumetric compaction by pore volume reduction only contributed to the expulsion of the free moving fluids in the pores, namely water. Even though the core deforms, and the pore volume decreases, neither compaction nor $MgCl_2$ brine induced chemical reactions lead to additional tail-end oil production. Two main reasons are used to interpret this: (1) oil is bonded and trapped on mineral surfaces in 50 nm to 0.1 μm thick oil films (calculated by dividing the immobile residual oil volume to the surface area of the sample), and (2) the oil droplets surrounded by water split up in smaller ganglia in which the pressure difference across is insufficient to overcome the capillary forces halting oil production.

4.2.5.1.2 Through Mons chalk

Figure 26(a) shows the oil and water volumes, and (b) the oil saturation inside the core throughout the duration of the test from the start of hydrostatic loading for the Mons wettability-altered core M4.

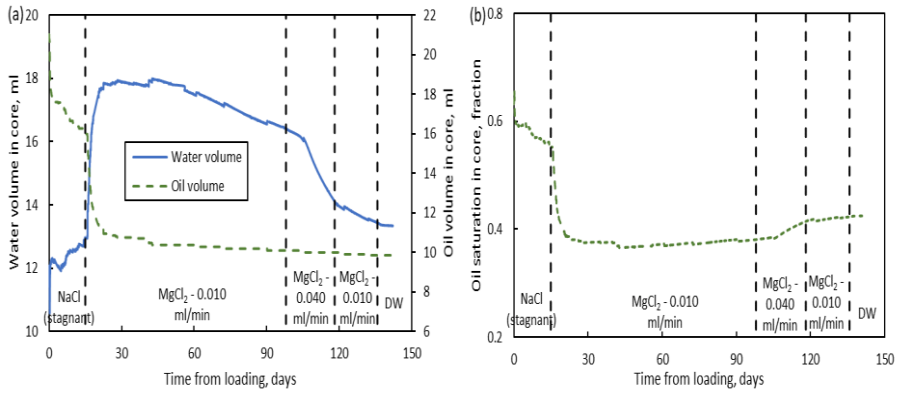

Figure 26. Wettability-altered Mons sample M4. (a) Oil and water volumes in the core obtained from measurements of the oil volume produced, bulk volume from compaction and solid volume from chemical reactions and (b) oil saturation in the core with time from the start of hydrostatic loading. Black dashed vertical lines depict the time when brine composition and/or flow rate changed (see **Paper III**).

During hydrostatic loading and no-flow creep period (up to 15th day), 4.7 ml oil was produced from wettability-altered Mons M4 core. Hence, deformation contributed to 43% of the total oil recovered after the initial thermal expansion. This value is comparable to the bulk volume loss of the sample (i.e. $\Delta V_s = \Delta V_p = \Delta V_{oil}$). Given that the water was not mobilized implies that oil was the mobile phase during compaction. After the first 15 days of creep, $MgCl_2$ was injected. In this phase, all the oil was produced during the initial 2-3 PVs, and after which despite the ongoing chemical reactions and compaction, negligible oil was produced from the core. This shows that the non-equilibrium rock-fluid interactions between the calcite surface and $MgCl_2$ brine did not contribute to any tail-end recovery after the initial displacement.

The increase in flow rate of $MgCl_2$ brine to 0.04 ml/min on the 98th day did not lead to any significant additional oil production. Therefore, the additional dissolution of calcium and precipitation of magnesium triggered by the four-fold increase in flow rate did not have any

significant effect on the oil recovery. Even though pore volume decreased with time, the compaction caused by the imposed stresses led to expelling of only water from the core. Hence, oil saturation increased from 90 days and onwards (Figure 26(b)).

On the other hand, no oil was produced during the loading and the creep phase due to compaction and further no oil was recovered during $MgCl_2$ injection through wettability-altered Kansas chalk after the initial displacement. The recovery of oil from Mons chalk due to compaction is likely due to the fact that it is more water-wet (W_i of 0.63 ± 0.07) to start with compared to the wettability-altered Kansas chalk (W_i of 0.55 ± 0.05). Wettability-altered Mons M4 core also has a larger volumetric strain during loading and creep in the stagnant phase compared to the Kansas wettability-altered cores, which could also have resulted in production of oil. Kansas chalk also has a smaller pore size than Mons (Voake et al. 2019) and due to the capillary forces, they need the extra flow energy from the injection brine to produce oil. However, it remains to be tested how compaction-driven multiphase flow and geomechanical properties are changed for unaged oil/water saturated Kansas and Mons chalk samples.

4.2.5.2 Oil volume development during SSW flow

4.2.5.2.1 Through Kansas chalk

Similar observations were made for SSW flooded K7 core as for $MgCl_2$ flooded K4 sample. Figure 27(a) shows the oil and water volumes with time, and (b) displays the oil saturation inside the wettability-altered Kansas K7 core from the start of hydrostatic loading. No oil was observed during loading and insignificant amount of oil was obtained during the subsequent compaction in the course of the 15 days of bypass period. When SSW flooding started on the 16^{th} day, oil was produced immediately but ceased after a certain time even though compaction and chemical reactions continued.

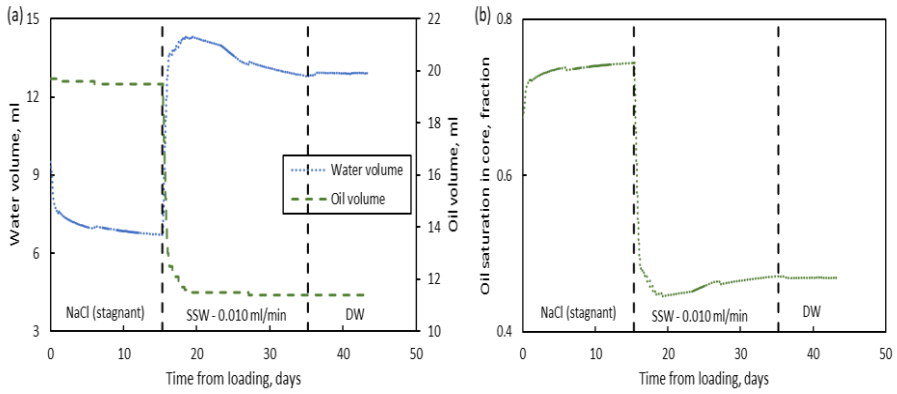

Figure 27. Wettability-altered Kansas sample K7. (a) Oil and water volumes in the core obtained from measurements of the oil volume produced, bulk volume from compaction and solid volume from chemical reactions and (b) oil saturation in the core with time from the start of hydrostatic loading. Black dashed vertical lines depict the time when brine composition changed (see **Paper I**).

The oil recovery observations showed that SSW flood gave 4% more oil recovery than $MgCl_2$ flood during the initial displacement of oil (46.2% oil recovery for K7 and 42.3% oil recovery for K4). This may indicate that SSW alters wettability favorably for oil recovery. However, after the initial displacement of oil during the flooding of these brines, the pore volume reduction did not change the volume of oil in the cores and only water was expelled. Combined observations of oil production during compaction and non-equilibrium flow imply that (a) $MgCl_2$ and SSW brines do not mobilize oil adsorbed on the rock surface, and (b) compaction do not contribute to oil production after the initial displacement. This observation is opposite to the interpretations of the Ekofisk production by Sulak and Danielsen (1989) where they concluded that compaction drive results in increased hydrocarbon recovery.

4.2.6 Observations of specific surface area after tests for all cores

The cores were cut into six equal sections after mechanical tests and tested for SSA using BET technique.

4.2.6.1 Specific surface area changes in Kansas chalk after tests

Measurements of the SSA of unaltered and unflooded Kansas chalk are reported in Table 11 where the untested end pieces are the ones that are left on each side during the cutting of the cylindrical cores. The untested SSAs are compared to six sections of the tested and flooded cores where section 1 represent the sample material placed close to the inlet and section 6 represent the outlet part. SSA measurements were not obtained on SSW flooded samples.

Table 11. Specific surface area measurements of unflooded core material from both sides of the core, and for sections along the core for K1 to K4 after test ($MgCl_2$ flooded samples).

Core	**K1**	**K2**	**K3**	**K4**
Core section	**Water-wet**		**Wettability-altered**	
	SSA, m^2/g	**SSA, m^2/g**	**SSA, m^2/g**	**SSA, m^2/g**
Outlet end-piece (Unflooded)	2.91	2.68	1.80	2.30
6	2.23 & 2.26	3.15 & 3.12	3.56 & 3.56	1.12 & 1.14
5	3.11	3.04	3.17	1.17
4	3.47 & 3.47	2.64	2.43 & 2.45	1.19 & 1.21
3	3.89	2.95 & 2.92	2.26	1.17
2	3.41	2.87	2.25	1.05
1	3.31 & 3.32	3.27 & 3.24	1.97 & 2.01	1.09 &1.04
Inlet end-piece (Unflooded)	3.20	2.98 & 2.99	1.57	2.50
Test time (days)	108.2	112.9	80.2	110.8

The non-homogenous chemical replacement dynamics are observed in the SSA measurements of Kansas cores (Table 11). The change in SSA was non-uniform through the cores. The trends were not clear, except that the SSA of cores K1, K3 and K4 increased from the inlet towards the middle of the samples. This may be because of the initial spatial variability in grain size through the core, and inherent uncertainty in the measurements themselves, so firm conclusions cannot be drawn. Andersen et al. (2018) also observed the non-homogeneous chemical replacement dynamics in $MgCl_2$ brine flooded water wet Kansas samples. They observed that the SSA decreased from the inlet towards the outlet of the samples.

4.2.6.2 Specific surface area changes in Mons chalk after tests

Measurements of the SSA of unaltered and unflooded Mons chalk are reported in Table 12 where the untested end pieces are the ones that are left on each side during the cutting of the cylindrical cores.

Table 12. Specific surface area measurements of unflooded core material from both sides of the core, and for sections along the core for Mons samples M1 to M4 after test ($MgCl_2$ flooded samples).

Core	**M1**	**M2**	**M3**	**M4**
Core section	**Water-wet**		**Wettability-altered**	
	SSA, m^2/g	**SSA, m^2/g**	**SSA, m^2/g**	**SSA, m^2/g**
Outlet end piece (unflooded)	1.82	1.98	2.11	1.96
6	2.33	2.26	2.20	2.02
5	2.47	2.43	2.14	2.08
4	2.45	2.49	2.39	2.44
3	2.45	2.46	2.55	2.45
2	2.47	2.49	3.05	2.82
1	2.18	2.40	3.35	3.02
Inlet end piece (unflooded)	2.13	2.05	2.22	2.17

The non-homogeneous chemical replacement dynamics were also observed in the SSA of Mons samples (Table 12). The SSA of water-wet Mons cores increase towards the middle of the core and then decrease towards the outlet, whereas the SSA of the wettability-altered cores decrease towards the outlet with the highest value observed at the inlet of the samples. Andersen et al. (2018) demonstrated that the SSA of the

water-wet Mons chalk decreased from the inlet to the outlet sections of the samples. This difference in our results may be linked to the initial spatial variability in grain size through the cores, the number of pore volumes flooded through the cores or the flow rates of the injection fluids.

4.3 Implications on the industry

The chalk samples used in this study are analogues to the North Sea chalk reservoirs. The experimental results on both Kansas and Mons outcrop chalks have shown that the compaction rates, during the injection of reactive brines, are independent of the initial wettability and hence the initial oil/water saturation in the cores. This has been further confirmed by the ion chromatography carried out on effluent samples, which gave the observations on the rock-fluid interactions. This shows that the oil present in the pore spaces do not obstruct and block the path of the brine injected during waterflooding to contact the grain-grain contacts. Hence, the results obtained from the wettability-altered cores are similar to those from water-wet cases. Therefore, it is concluded that the results from the water-wet cores obtained from the experimental studies carried out in the past three decades are applicable to the real reservoir systems.

It is further expected that deeply buried and more diagenetically overprinted chalks, such as Ekofisk and Valhall chalk reservoirs in the Norwegian Continental Shelf, are predicted to behave very similar to Kansas outcrop chalk, and thereby show similar strength and stiffness response to injection brines as shown by Kansas chalk.

5 Conclusions and scope of future work

5.1 Conclusions

This study deals with the impact of initial wettability and reactive flow on chalk mechanics and oil recovery. Two different outcrop chalks from Kansas (USA) and Mons (Belgium) quarries were used as model materials in this study. The whole study was divided into two test programs: (a) Wettability determination program to determine the wetting state of the wettability-altered chalk, and (b) Triaxial test program in which the cores were hydrostatically loaded to 1.5 times yield stress and tested for their mechanical response to the applied external stress.

Impact of aging time

A study was performed to deduce the aging time required to obtain a stable wettability in Kansas chalk at the aging temperature of 90°C with 1.1M NaCl brine and oil mixture of 60% - 40% (by volume) Heidrun crude oil - heptane as the saturation fluids. The methods used to determine wettability were contact angle, USBM and SEM-MLA. The results showed that atleast 21 days of aging time is required to obtain a stable wettability at the specified aging conditions. Similar investigations are needed to deduce the aging time for obtaining stable wettability in Mons chalk.

Determining wettability

The wettability of all chalk cores used in the triaxial test program was altered in the same way at the specified conditions and aged for 21 days at 90°C. The wettability was determined using the chromatographic separation method. The wettability-altered Kansas and Mons samples gave a wetting index of 0.55 ± 0.05 and 0.63 ± 0.07, respectively. Even though both obtained a neutral wet state, the wetting indices obtained were still different for the two chalk types. This shows that the mineralogy of the two chalks play a role in determining their wettability

at the same aging conditions. It is likely that the presence of silicates and clay in Kansas chalk make it more oil wet compared to Mons chalk which is very pure.

Elastic and plastic parameters

During loading with no flow-through of NaCl brine and at 130°C, the water-wet and wettability-altered Mons samples showed similar stiffnesses and strengths. On the other hand, the wettability-altered Kansas samples showed 33% higher stiffnesses and 35% higher strengths compared to the water-wet Kansas samples. This is likely due to oil replacing water on surface areas where electrical double layers would interact if only water was found in the pores. This leads to reduced disjoining pressure, and thereby increased normal force between particles, which makes particles re-organizing by sliding more difficult. This is an interpretation for why geomechanical parameters for Kansas chalk are affected by wettability alteration, while they remain unaffected for Mons. The importance of the overlapping double layers is more pronounced for Kansas chalk because of its smaller Biot coefficient and smaller pore size than Mons chalk.

Time dependent deformation

During the creep phase, the strain rates followed a comparable trend independent of wetting state for both Kansas and Mons chalk types. This observation was found to be the same during both the bypass period (first 15 days) and the flow of reactive brines. Injection of reactive brines induced chemical reactions leading to additional creep rates in both chalk types.

Geochemical interactions – on the impact of oil

Geochemical effects (shown by IC of the effluent samples) are also not found to be affected by the presence of oil and the initial wetness of the cores. In all cases irrespective of the brine composition, the initial oil/brine saturation and wettability, the calcium concentration increases and the magnesium concentration decreases in the effluent (in $MgCl_2$

flooded samples). This is linked to the dissolution of calcite as well as precipitation of magnesium carbonate and adsorption of magnesium ions onto and desorption of calcium ions from the calcite surface. Effluent analysis also showed a reduction in the sulfate concentration in the effluents from SSW flooded samples. This is linked to the adsorption of sulfate ions on the charged calcite surfaces. As shown in the presented evidence, the presence of oil in the pores does not alter the dissolution/precipitation driven water weakening dynamics, neither qualitatively nor quantitatively. It is also shown how chemical reactions drive reduction in the solid volume by reducing the overall mass for $MgCl_2$ flooded samples and increasing the mineral density, and how this behavior is linked to the creep rate with time.

Hence, it was shown that as wettability has minimal to no effect on the compaction rates and geochemical effects during the injection of reactive brines through both water-wet and wettability-altered chalk samples, the results from the water-wet cores (obtained from the experimental studies in the past three decades) are applicable to the real reservoir systems.

Multiphase transport – oil production with time

The oil recovery from the wettability-altered Kansas and Mons samples was continuously monitored during the loading and creep periods. The results from Kansas chalk showed that after the initial displacement of mobile oil during injection of $MgCl_2$ and SSW brines, there was no additional oil recovery due to ongoing compaction or non-equilibrium brine flow. On the other hand, wettability-altered Mons samples showed 43% oil recovery through compaction even before the injection of $MgCl_2$ brine started. This oil production may be linked to the partitioning of oil and water in Mons samples after aging, which probably differs from Kansas samples as wettability-altered Mons samples were more water wet to start with compared to Kansas samples. After the displacement of oil during the first 2-3 PVs of $MgCl_2$ injection, no tail-end oil recovery was observed in the later stages. This is likely due to the fact that the injected brines are not able to mobilize the oil bonded on the walls or the

pressure difference across the oil ganglia is insufficient to overcome capillary forces.

Petrophysical changes

The non-homogenous chemical replacement dynamics were observed in the SSA measurements of both Kansas and Mons cores. The trends were not clear for Kansas chalk and further investigations are required to draw any firm conclusion. However, the SSA measurements of Mons chalk after tests have shown to be clearly affected by the wetting state. The wettability-altered Mons cores showed the highest value of SSA at the inlet decreasing towards the outlet whereas the SSA of water-wet Mons cores increased towards the middle and then decreased towards the outlet of the samples.

Overall, the results have shown that although the injection of reactive brines through chalk lead to enhanced compaction, which is found to be insensitive to the wetness of the samples, it does not lead to any tail-end oil recovery.

5.2 Scope of future work

This study opens the scope for a detailed future work which can include:

a) Geochemical analysis of the flooded core samples to compare the changes in the solid framework of water-wet and wettability-altered samples.
b) Tuning wettability in lab since wettability impacts how oil and water are partitioned within the pores, followed by measuring if compaction and chemical reactions would mobilize oil either at lower or higher wettability indexes.
c) Hydrostatic loading of the wettability-altered samples to check for the reproducibility of the geomechanical results in this study at different aging conditions.

d) Hydrostatically loading to different stress levels above yield to check if a similar response in the creep rates is observed with both $MgCl_2$ and SSW brines.
e) Injecting brines with different compositions to optimize the oil recovery and minimize chalk compaction.
f) The wettability impacts how oil and water are partitioned within the pores. Hence, it would be important to check for the effect of this spatial partitioning of oil and water on the enhanced oil recovery by compaction.
g) Analytical and numerical modeling to define strain partitioning in the geomechanical experiments performed on chalk.

6 References

Ahsan, R. and Fabricius, I.L., 2010. Sorption of magnesium and sulfate ions on calcite. In 72nd EAGE Conference and Exhibition incorporating SPE EUROPEC 2010, Extended Abstracts, SP13.

Alam, M.M., Ahsan, R., Shaik, A.K., and Fabricius, I.L., 2010. Surface charge of calcite and its influence on the electrical conductivity in chalk. In 80th Annual International Meeting, Society of Exploration Geophysicists, Expanded Abstracts, 2686-2691.

Andersen, M.A., Foeged, N., and Pedersen, H.F., 1992. The Link between Waterflood-Induced Compaction and Rate-Sensitive Behavior in a Weak North Sea Chalk. In: *Proceedings of the Fourth North Sea Chalk Symposium,* Deauville, France, September.

Andersen, P.Ø., Wang, W., Madland, M.V., Zimmermann, U., Korsnes, R.I., Bertolino, S.R.A., Minde, M., Schulz, B., and Gilbricht, S., 2018. Comparative Study of Five Outcrop Chalks Flooded at Reservoir Conditions: Chemo-mechanical Behaviour and Profiles of Compositional Alteration. *Transport in Porous Media*, **121**(1), 135-181.

Anderson, W.G., 1986. Wettability Literature Survey - Part 1: Rock/Oil/Brine Interactions and the Effects of Core Handling on Wettability. *Journal of Petroleum Technology*, **38**(10), 1125-1144.

Andreassen, K.A. and Fabricius, I.L., 2010. Biot critical frequency applied to description of failure and yield of highly porous chalk with different pore fluids. *Geophysics*, **75**(6), E205-E213.

Borromeo, L., Egeland, N., Minde, M.W., Zimmermann, U., Andò, S., Madland, M.V. and Korsnes, R.I., 2018. Quick, Easy, and Economic Mineralogical Studies of Flooded Chalk for EOR Experiments Using Raman Spectroscopy. *Minerals*, **8**(6), 221. ISSN 2075-163X. https://doi.org/10.3390/min8060221.

Brunauer, S., Emmett, P.H., and Teller, E., 1938. Adsorption of gases in multimolecular layers. *Journal of the American chemical society*, **60**(2), 309-319.

Burchette, T.P., 2012. Carbonate Rocks and Petroleum Reservoirs: A Geological Perspective from the Industry. *Geological Society*, London, Special Publications, **370**(1), 17-37.

Coto, B., Martos, C., Peña, J. L., Rodríguez, R., and Pastor, G., 2012. Effects in the solubility of $CaCO_3$: Experimental study and model description. *Fluid Phase Equilibria*, **324**, 1-7.

Cuiec, L., Bourbiaux, B., and Kalaydjian, F., 1994. Oil recovery by imbibition in low-permeability chalk. *SPE Formation Evaluation (Society of Petroleum Engineers); (United States)*, **9**(3).

Donaldson, E.C., 1981. Oil-water-rock wettability measurement. *Am. Chem. Soc., Div. Pet. Chem., Prepr.; (United States)*, *26*(CONF-810308-(Vol. 1)).

Donaldson, E.C., Kendall, R.F., Pavelka, E.A., and Crocker, M.E., 1980. Equipment and procedures for fluid flow and wettability tests of geological materials (No. DOE/BETC/IC-79/5). Department of Energy, Bartlesville, OK (USA). Bartlesville Energy Technology Center.

Donaldson, E.C., Thomas, R.D., and Lorenz, P.B., 1969. Wettability Determination and Its Effect on Recovery Efficiency. *SPE Journal*, **9**(1), 13–20.

Doornhof, D., Kristiansen, T.G., Nagel, N.B., Pattillo, P.D., and Sayers, C., 2006. Compaction and Subsidence. *Oilfield Review*, **18**, 50-68.

Fan, T. and Buckley, J.S., 2007. Acid number measurements revisited. *SPE Journal*, **12**(04), 496-500.

Fathi, S.J., Austad, T., and Strand, S., 2010. "Smart Water" as a Wettability Modifier in Chalk: The Effect of Salinity and Ionic Composition. *Energy & Fuels*, **24**(4), 2514-2519. http://dx.doi.org/10.1021/ef901304m.

Fjær E., Holt, R.M., Horsrud, P., Raaen, A.M., and Risnes, R., 2008. *Petroleum related rock mechanics*, 2nd Ed., Amsterdam: Elsevier.

Flügel, E., 2004. *Microfacies of Carbonate Rocks: Analysis, Interpretation and Application*. Springer Science & Business Media.

Gauer, P.R., Sylte, J.E., and Nagel, N.B., 2002. Ekofisk Field Well Log Decompaction. Paper SPE/ISRM 78177 presented at the Rock Mechanics Conference, Irving, Texas, October 20-23.

Graue, A., Viksund, B.G., and Baldwin, B.A., 1999. Reproducible wettability alteration of low-permeable outcrop chalk. *SPE Reservoir Evaluation & Engineering*, **2**(02), 134-140.

Hassler, G.L., and Brunner, E., 1945. Measurement of capillary pressures in small core samples. *Trans. AIME*, **160**,114-123.

Hattin, D.E., and Cobban, W.A., 1977. Upper Cretaceous stratigraphy, paleontology, and paleoecology of western Kansas. *The Mountain Geologist* **14**(3-4):175–217

Heggheim, T., Madland, M.V., Risnes, R., and Austad, T., 2005. A Chemical Induced Enhanced Weakening of Chalk by Seawater. *Journal of Petroleum Science and Engineering*, **46**, 171-184.

Hellmann, R., Renders, P.J.N., Gratier, J.P., and Guiguet, R., 2002a. Experimental pressure solution compaction of chalk in aqueous solutions. Part 1. Deformation behavior and chemistry. *Water-Rock Interactions, Ore Deposits, and Environmental Geochemistry: A Tribute to David A. Crerar*, **7**(7), 129–152.

Hellmann, R., Gaviglio, P., Renders, P.J.N., Gratier, J.P., Bekri, S., and Adler, P., 2002b. Experimental pressure solution compaction of chalk in aqueous solutions. Part 2. Deformation examined by SEM, porosimetry, synthetic permeability, and X-ray computerized tomography. *Water-Rock Interactions, Ore Deposits, and Environmental Geochemistry: A Tribute to David A. Crerar*, **7**(7), 153–178.

Hermansen, H., Landa, G.H., Sylte, J.E., and Thomas, L.K., 2000. Experiences after 10 years of waterflooding the Ekofisk field, Norway. *Journal of Petroleum Science and Engineering*, **26**, 11–18.

Hermansen, H., Thomas, L.K., Sylte, J.E., and Aasbøe, B.T., 1997. Twenty Five Years of Ekofisk Reservoir Management. Paper SPE 38927 presented at the SPE Annual Technical Conference and Exhibition, San Antonio, Texas, USA, October 5-8.

Heugas, O. and Charlez, P., 1990. Mechanical effect of the water injection on Ekofisk chalk. In: Third North Sea Chalk Symposium, Copenhagen, Denmark.

Hiorth, A., Cathles, L.M., and Madland, M.V., 2010. The impact of pore water chemistry on carbonate surface charge and oil wettability. *Transport in porous media*, **85**(1), 1-21.

Hiorth, A., Jettestuen, E., Cathles, L.M., and Madland, M.V., 2013. Precipitation, Dissolution, and Ion Exchange Processes Coupled with a Lattice Boltzmann Advection Diffusion Solver. *Geochimica et Cosmochimica Acta*, **104**, 99–110. http://dx.doi.org/10.1016/j.gca.2012.11.019.

Hjuler, M.L., and Fabricius, I.L., 2009. Engineering properties of chalk related to diagenetic variations of Upper Cretaceous onshore and offshore chalk in the North Sea area. *Journal of Petroleum Science and Engineering*, **68**(3-4), 151-170.

Johnson, J.P. and Rhett, D.W., 1986. Compaction Behavior of Ekofisk Chalk as a Function of Stress. Paper SPE 15872 presented at the European Petroleum Conference, London, United Kingdom, October 20-22. doi: 10.2118/15872-MS.

Katika, K., Addassi, M., Alam, M.M., and Fabricius, I.L., 2015. The effect of divalent ions on the elasticity and pore collapse of chalk evaluated from compressional wave velocity and low-field Nuclear Magnetic Resonance (NMR). *Journal of Petroleum Science and Engineering*, **136**, 88-99.

Korsnes, R.I., Madland, M.V., and Austad, T., 2006a. Impact of Brine Composition on the Mechanical Strength of Chalk at High Temperature. *Eurock 2006: Multiphysics Coupling and Long Term Behaviour in Rock Mechanics*, Taylor and Francis, London, 133-140.

Korsnes, R.I., Strand, S., Hoff, O., Pedersen, T., Madland, M.V., and Austad, T., 2006b. Does the Chemical Interaction between Seawater and Chalk affect the Mechanical Properties of Chalk? *Eurock 2006: Multiphysics Coupling and Long Term Behaviour in Rock Mechanics*, Taylor and Francis, London, 427-434.

Korsnes, R.I., Madland, M.V., Austad, T., Haver, S., and Røsland, G., 2008. The Effects of Temperature on the Water Weakening of Chalk by Seawater. *Journal of Petroleum Science and Engineering*, **60**, 183-193.

Kristiansen, T.G., Barkved, O.I., Buer, K., and Bakke, R., 2005. Production-Induced Deformations Outside the Reservoir and Their Impact on 4D Seismic. Paper IPTC 10818 presented at the International Petroleum Technology Conference, Doha, Qatar, November 21-23. http://dx.doi.org/10.2523/IPTC-10818-MS.

Liteanu, E., Spiers, C.J., and de Bresser, J.H.P., 2013. The influence of water and supercritical CO_2 on the failure behavior of chalk, *Tectonophysics*, **599**, 157–169. doi: 10.1016/j.tecto.2013.04.013.

Liu, J., Wani, O.B., Alhassan, S.M., and Pantelides, S.T., 2018. Wettability Alteration and Enhanced Oil Recovery Induced by Proximal Adsorption of Na^+, Cl^-, Ca^{2+}, Mg^{2+}, and SO_4^{2-} Ions on Calcite. *Physical Review Applied*, **10**(3), 034064.

Longman, M.W., B.A. Luneau, and S.M. Landon, 1998. Nature and Distribution of Niobrara Lithologies in the Cretaceous Western Interior of the Rocky Mountain Region. *The Mountain Geologist*, **35**, 137-170.

Lord, C.J., Johlman, C.L., and Rhett, D.W., 1998. Is capillary suction a viable cohesive mechanism in chalk? In: SPE/ISRM Rock Mechanics in Petroleum Engineering, Trondheim, Norway.

Lucia, F.J., 1992, Carbonate Reservoir Models: Facies, Diagenesis, and Flow Characterization: Part 6. Geological Methods, *ME 10: Development Geology Reference Manual*, AAPG Spec. Pub. Type: Methods in Exploration, A095, 269-274.

Lyklema, J., 2005. *Fundamentals of interface and colloid science: soft colloids*, **5**. San Diego, USA: Elsevier, Academic Press.

MacDonald, G.J., 1956. Experimental determination of calcite-aragonite equilibrium relations at elevated temperatures and pressures. *American Mineralogist: Journal of Earth and Planetary Materials*, **41**(9-10), 744-756.

Madland, M.V., Hiorth, A., Korsnes, R.I., Evje, S., and Cathles, L., 2009. Rock Fluid Interactions in Chalk Exposed to Injection of Seawater, $MgCl_2$, and NaCl Brines with Equal Ionic Strength. Paper A22 presented at the 15th European Symposium on Improved Oil Recovery, Paris, France, April 27-29.

Madland, M.V., Hiorth, A., Omdal, E., Megawati, M., Hildebrand-Habel, T., Korsnes, R.I., Evje, S., and Cathles, L.M., 2011. Chemical Alterations Induced by Rock-Fluid Interactions when Injecting Brines in High Porosity Chalks. *Transport in Porous Media*, **87**, 679-702.

Madland, M.V., Midtgarden, K., Manafov, R., Korsnes, R.I., Kristiansen, T.G., and Hiorth, A., 2008. The Effect of Temperature and Brine Composition on the Mechanical Strength of Kansas Chalk. Paper SCA2008-55 presented at the International Symposium of the Society of Core Analysts, Abu Dhabi, UAE, October 29-November 2.

Maury, V., Piau, J.M., and Halle, G., 1996. Subsidence induced by water injection in water sensitive reservoir rocks: The example of Ekofisk. Paper SPE 36890 presented at the SPE European Petroleum Conference, Milan, Italy, October 22-24.

McPhee, C., Reed, J., and Zubizarreta, I., 2015. *Core Analysis: A Best Practice Guide*, **64**, 313-345, Amsterdam: Elsevier.

Megawati, M., Andersen, P.Ø., Korsnes, R.I., Evje, S., Hiorth, A., and Madland, M.V., 2011. The effect of aqueous chemistry pH on the time-dependent deformation behavior of chalk experimental and modelling study. In: Pore2Fluid International Conference. 16–18 Nov, Paris, France.

Megawati, M., Hiorth, A., and Madland, M.V., 2013. The Impact of Surface Charge on the Mechanical Behaviour of High-Porosity Chalk. *Rock Mechanics and Rock Engineering*, **46**(5), 1073-1090.

Megawati, M., Madland, M.V., and Hiorth, A., 2015. Mechanical and Physical Behavior of High-Porosity Chalks Exposed to Chemical Perturbation. *Journal of Petroleum Science and Engineering*, **133**, 313-327.

Minde, M.W., Haser, S., Korsnes, R.I., Zimmermann, U., and Madland, M.V., 2017. Comparative Studies of Mineralogical Alterations of Three Ultra-long-term Tests of Onshore Chalk at Reservoir Conditions. In: 19th European Symposium on Improved Oil Recovery/IOR Norway 2017. European Association of Geoscientists and Engineers. ISBN 978-94-6282-209-2.

Minde, M.W., Zimmermann, U., Madland, M.V., Korsnes, R.I., Schulz, B. and Gilbricht, S., 2018a. Mineral Replacement in Long-Term Flooded Porous Carbonate Rocks. Submitted to *Geochimica et Cosmochimica Acta*, publication under review.

Minde, M.W., Wang, W., Madland, M.V., Zimmermann, U., Korsnes, R.I., Bertolino, S.R., and Andersen, P.Ø., 2018b. Temperature effects on rock engineering properties and rock-fluid chemistry in opal-CT-bearing chalk. *Journal of Petroleum Science and Engineering*, **169**, 454-470.

Nagel, N.B., 1998. Ekofisk Field Overburden Modelling. Paper SPE 47345 presented at the SPE/ISRM Rock Mechanics in Petroleum Engineering, Trondheim, Norway, July 8-10.

Nermoen, A., Korsnes, R.I., Haug, S., Hiorth, A., and Madland, M.V., 2014. The dynamic stability of chalks during flooding of non-equilibrium brines and CO_2, Stavanger: Fourth EAGE CO_2 Geological Storage Workshop, Demonstrating Storage Integrity and Building Confidence in CCS.

Nermoen, A., Korsnes, R.I., Hiorth, A. and Madland, M.V., 2015. Porosity and Permeability Development in Compacting Chalks during Flooding of Non-Equilibrium Brines: Insights from Long-Term Experiment. *Journal of Geophysical Research: Solid Earth*, **120**. https://doi.org/10.1002/2014JB011631

Nermoen, A., Korsnes, R.I., Aursjø, O., Madland, M.V., Kjørslevik, T.A.C., and Østensen, G., 2016. How Stress and Temperature Conditions Affect Rock-Fluid Chemistry and Mechanical Deformation. *Frontiers in Physics*. http://dx.doi.org/10.3389/fphy.2016.00002.

Nermoen, A., Korsnes, R.I., Storm, E.V., Stødle, T., Madland, M.V., and Fabricius, I.L., 2018a. Incorporating electrostatic effects into the effective stress relation – insights from chalk experiments. *Geophysics*, **83**(3), 1-13.

Nermoen, A., 2018b. Porosity Evolution during Chemo-Mechanical Compaction. doi: 10.5772/intechopen.72795.

Neveux, L., Grgic, D., Carpentier, C., Pirnon, J., Truche, L., and Girard, J.P., 2014a. Influence of hydrocarbon injection on the compaction by pressure solution of a carbonate rock: An experimental study under triaxial stresses. *Marine and Petroleum Geology*, **55**, 282–294.

Neveux, L., Grgic, D., Carpentier, C., Pironon, J., Truche, L., and Girard, J.P., 2014b. Experimental simulation of chemomechanical processes during deep burial diagenesis of carbonate rocks. *Journal of Geophysical Research: Solid Earth*, **119**(2), 984–1007. https://doi.org/10.1002/2013JB010516

Overview Greater Ekofisk Area, ConocoPhillips Norway, 2019, http://www.conocophillips.no/our-norway-operations/greater-ekofisk-area/overview/ (viewed on 11.05.2019).

Piau, J.M. and Maury, V., 1994. Mechanical effects of water injection in chalk reservoirs. In: SPE/ISRM Rock Mechanics in Petroleum Engineering, Delft, Netherlands.

Richard, J., Sizun, J.P., and Machhour, L., 2005. Environmental and diagenetic records from a new reference section for the Boreal realm: the Campanian chalk of the Mons basin (Belgium). *Sedimentary Geology*, **178**(1-2), 99-111.

Risnes, R., 2001. Deformation and Yield in High Porosity Outcrop Chalk. *Phys. Chem. Earth* (A), **26**, 53-57.

Risnes, R., Haghighi, H., Korsnes, R.I., and Natvik, O., 2003. Chalk-Fluid Interactions with Glycol and Brines. *Tectonophysics*, **370**, 213-226.

Roehl, P.O. and Choquette, P.W. (Eds.), 1985. *Carbonate Petroleum Reservoirs*. New York: Springer.

Runnels, R.T., and Dubins, I.M., 1949. Chemical and petrographic studies of the Fort Hays Chalk in Kansas. *Kansas Geological Survey Bulletin*, **82**, 1-36.

Schroeder, C. and Shao, J., 1996. Plastic deformation and capillary effects in chalks. In: *Proceedings of the 5th North Sea Chalk Symposium*, Reims, France.

Sripal, E. and James, L.A., 2016. Application of an Optimization Method for Restoration of Core Samples for SCAL Experiments. Paper SCA2016-002 presented at the International Symposium of the Society of Core Analysts, Snowmass, Colorado, USA, August 22–26.

Sripal, E. and James, L.A., 2018. Application of an Optimization Method for the Restoration of Core Samples for SCAL Experiments. *Petrophysics*, **59**(1), 72-81.

Standnes, D.C. and Austad, T., 2000a. Wettability alteration in chalk: 1. Preparation of core material and oil properties. *Journal of Petroleum Science and Engineering*, **28**(3), 111-121.

Standnes, D.C. and Austad, T., 2000b. Wettability alteration in chalk: 2. Mechanism for wettability alteration from oil-wet to water-wet using surfactants. *Journal of Petroleum Science and Engineering*, **28**(3), 123-143.

Strand, S., Standnes, D.C., and Austad, T., 2006. New Wettability Test for Chalk Based on Chromatographic Separation of SCN^- and SO_4^{2-}. *Journal of Petroleum Science and Engineering*, **52**, 187-197.

Strand, S., Hjuler, H.L., Torsvik, R., Pedersen, J.I., Madland, M.V., and Austad, T., 2007. Wettability of chalk: Impact of silica, clay content and mechanical properties. *Petroleum Geoscience*, **13**(1), 69-80.

Sulak, R.M., 1991. Ekofisk Field: The First 20 Years. *Journal of Petroleum Technology*, **43**(10), 1-265.

Sulak, R.M. and Danielsen, J., 1989. Reservoir Aspects of Ekofisk Subsidence. *Journal of Petroleum Technology*, **41**(7), 709-716, SPE 17852-PA.

Sylte, J.E., Thomas, L.K., Rhett, D.W., Bruning, D.D., and Nagel, N.B., 1999. Water Induced Compaction in the Ekofisk Field. Paper SPE 56426 presented at the SPE Annual Technical Conference and Exhibition, Houston, Texas, October 3-6.

Tang, G. and Firoozabadi, A., 2001. Effect of pressure gradient and initial water saturation on water injection in water-wet and mixed-wet fractured porous media. *SPE Reservoir Evaluation & Engineering* **4**(6): p. 516-524.

Teufel, L.W., Rett, D.W., and Farrell, H.E., 1991. Effect of reservoir depletion and pore pressure drawdown in in-situ stress and deformation in the Ekofisk field, North Sea. In: *Proceedings of the 32nd U.S. Rock Mechanics Symposium*, p. 63-72, Norman, Oklahoma, July 10-12.

Thomas, L.K., Dixon, T.N., Evans, C.E., and Vienot, M.E., 1987. Ekofisk Waterflood Pilot. *Journal of Petroleum Technology*, **39**(02), 221-232.

Voake, T., Nermoen, A., Ravnås, C., Korsnes, R.I., and Fabricius, I.L., 2019. Influence of temperature cycling and pore fluid on tensile strength of chalk. *Journal of Rock Mechanics and Geotechnical Engineering*, **11**(2), 277-288.

Wang, W., Madland, M.V., Zimmermann, U., Nermoen, A., Korsnes, R.I., Bertolino, S.R.A., and Hildebrand-Habel, T., 2016. Evaluation of porosity change during chemo-mechanical compaction in flooding experiments on Liège outcrop chalk. *Geological Society, London, Special Publications*, **435**(1), 26 October. https://doi.org/10.1144/SP435.10.

Wiborg, R., and Jewhurst, J., 1986. Ekofisk subsidence detailed and solutions assessed. *Oil & Gas Journal*, **84**(7), 47-51.

Zhang, P. and Austad, T., 2005. The Relative Effects of Acid Number and Temperature on Chalk Wettability. Paper SPE 92999 presented at SPE International Symposium on Oilfield Chemistry, Houstan, Texas, USA, February 2-4.

Zhang, P. and Austad, T., 2006. Wettability and oil recovery from carbonates: Effects of temperature and potential determining ions. *Colloids and Surfaces A: Physicochemical and Engineering Aspects*, **279**(1-3), 179-187.

Zhang, P., Tweheyo, M.T., and Austad, T., 2006. Wettability Alteration and Improved Oil Recovery in Chalk: The Effect of Calcium in the Presence of Sulfate. *Energy & Fuels*, **20**, 2056-2062.

Zhang, P., Tweheyo, M. T., and Austad, T., 2007. Wettability alteration and improved oil recovery by spontaneous imbibition of seawater into chalk: Impact of the potential determining ions Ca^{2+}, Mg^{2+}, and SO_4^{2-}. *Colloids and Surfaces A: Physicochemical and Engineering Aspects*, **301**(1-3), 199-208.

Zimmermann, U., Madland, M.V., Nermoen, A., Hildebrand-Habel, T., Bertolino, S.A.R., Hiorth, A., Korsnes, R.I., Audinot, J.N., and Grysan, P., 2015. Evaluation of the compositional changes during flooding of reactive fluids using scanning electron microscopy, nano-secondary ion mass spectrometry, x-ray diffraction and whole rock geochemistry. *AAPG (Am. Assoc. Pet. Geol.) Bulletin*, **99**(5), 791–805. http://dx.doi.org/10.1306/12221412196.

Appendix

Comparison of Kansas and Mons chalk types.

Table 13. Comparison of Kansas and Mons chalk types.

	Kansas	**Mons**
Carbonate content, %	95-97	> 99
Initial wettability index	0.55 ± 0.05	0.63 ± 0.07
Biot coefficient (Voake et al. 2019)	0.91	0.95
Initial porosity, %	35-38	42-44
Initial water saturation, %	26-29	31-38
Relaxation time T_2 from NMR studies, ms (Voake et al. 2019)	15-80	35-200

Paper I

Sachdeva, J.S., Nermoen, A., Korsnes, R.I., and Madland, M.V. (2019). Impact of Initial Wettability and Injection Brine Chemistry on Mechanical Behaviour of Kansas Chalk. *Transport in Porous Media*, **128**(2), 755-795. https://doi.org/10.1007/s11242-019-01269-z.

Transport in Porous Media (2019) 128:755–795
https://doi.org/10.1007/s11242-019-01269-z

Impact of Initial Wettability and Injection Brine Chemistry on Mechanical Behaviour of Kansas Chalk

Jaspreet S. Sachdeva[1,2] · **Anders Nermoen**[1,3] · **Reidar I. Korsnes**[1,2] · **Merete V. Madland**[1,2]

Received: 5 September 2018 / Accepted: 9 March 2019 / Published online: 16 March 2019

Abstract

The injection of seawater-like brines alters stiffness, strength and time-dependent deformation rates for water-saturated chalks. This study deals with the mechanical effects and oil production upon brine injection through wettability-altered samples. The results from two test programs are presented: (a) 'Wettability determination program' and (b) 'triaxial test program'. Kansas chalk samples were saturated by a mixture of oil and water and aged over time at 90 °C. The wettability index of the altered samples was estimated using chromatographic separation tests by co-injecting sulphate ions that adsorb on the *water-wet* mineral surfaces and non-affine tracer. A good repeatability was observed. In the triaxial test program, unaged *water-wet* and aged *mixed-wet* samples were hydrostatically loaded to 1.5 times yield stress so stiffness and strength could be determined. The samples were kept at the same stress level over time to monitor the volumetric creep. After a stagnant flow period of 15 days, $MgCl_2$ brine and seawater were flushed through the samples so the oil production and ion concentration of the effluent water could be obtained. The combined observations of the bulk volume, oil volume and estimated solid volume (from effluent analyses) enabled us to calculate pore volume and thereby oil saturation with time. The *mixed-wet* samples were found to be stiffer and stronger than the *water-wet* samples, and when the stress was kept at 1.5 times yield the creep curves overlapped. During the flow-through period, the changes in ion composition are insensitive to the presence of oil, and ongoing water weakening for *mixed-wet* samples is the same as in the *water-wet* samples. Further, we found that oil was only produced during the first 2–3 pore volumes (PVs) injected. Afterwards, no oil was produced even though the chemical reactions took place and pore volume reduced.

Keywords Improved oil recovery · Water flooding · Chalk compaction · Wettability · Geomechanics · Oil production measurements

Electronic supplementary material The online version of this article (https://doi.org/10.1007/s11242-019-01269-z) contains supplementary material, which is available to authorized users.

✉ Jaspreet S. Sachdeva
jaspreet.s.sachdeva@uis.no

Extended author information available on the last page of the article

1 Introduction

Approximately 50–60% of the known oil and gas reserves worldwide are found in rocks made up of calcium carbonate (Burchette 2012). Chalk is a soft, white, porous sedimentary carbonate rock formed in marine environments by the sedimentation of calcite shells. It is a very fascinating granular material because its mechanical properties depend on the physico-chemical interplay with the pore fluids. Chalk can also, for example, be used to study the organisms living in the ocean and the paleoclimate at which the sediments were deposited. Freshly deposited calcareous ooze has porosity of approximately 70%. As the ooze gets buried, it is mechanically compacted by overburden stress resulting in pore volume loss and stress build-up at grain contacts. This results in pressure dissolution and formation of chalk (Mimran 1975; Bjørlykke and Høeg 1997; Hellmann et al. 2002a, b; Fabricius 2014; Nermoen et al. 2016). Chalk today can be recognised by the preservation of the coccoliths, foraminifera and algae shells (Fabricius 2003).

Chalk is characterised as a highly porous and a low permeable rock. The injection of seawater into chalk reservoirs leads to enhanced compaction of the reservoir rock, which has proven to be an important driving mechanism for pushing the resident fluids towards production facilities and, hence, of great potential for improving oil recovery (Sulak and Danielsen 1989; Sulak 1991; Hermansen et al. 2000). However, it has also shown to induce seafloor subsidence (Sulak and Danielsen 1989; Maury et al. 1996; Nagel 1998; Sylte et al. 1999; Gauer et al. 2002). This compaction observed in the chalk reservoirs is a result of both pore pressure depletion early in the field life, and water weakening induced by seawater injection at later stages (Gauer et al. 2002).

The detection of subsidence in the Ekofisk field at the Norwegian North Sea around 30 years ago raised serious concerns related to buckling and loss of well pipes, arching of overburden rocks leading to stress redistributions, and the porosity/permeability decline of the producible formation, all physical effects that alter the ultimate recovery and recovery rates of oil-bearing chalk reservoirs (Thomas et al. 1987; Teufel et al. 1991; Maury et al. 1996; Hermansen et al. 1997; Nagel 1998; Kristiansen et al. 2005; Doornhof et al. 2006). Since then, considerable research has been carried out concerning chalk behaviour in general, and mechanical properties in particular (Johnson and Rhett 1986; Heugas and Charlez 1990; Andersen et al. 1992; Piau and Maury 1994; Brignoli et al. 1994; Delage et al. 1996; Schroeder and Shao 1996; Schroeder et al. 1998; Papamichos et al. 1997, Lord et al. 1998).

Later, research focused on understanding how the mechanical behaviour of chalk is dictated by the pore fluid chemistry (Risnes 2001; Hellmann et al. 2002a, b; Risnes et al. 2003; Madland et al. 2008; Korsnes et al. 2008; Neveux et al. 2014a, b). These studies dealt with how aqueous chemistry affected mechanical stiffness and plastic failure strength during hydrostatic stress build-up, and the time-dependent deformation during creep. The analysis of the effluent brines and the chemical and microstructural changes to the minerals in the rock have shown that the injected brines are not in equilibrium with the rock surface. As such, over time changes of the load-bearing framework affect the creep deformation rates at constant stress condition during continuous brine flow (Korsnes et al. 2006a, b, 2008; Madland et al. 2008, 2011; Megawati et al. 2011, 2012).

The chemical composition and microscopic structure of the mineral phases that constitute the chalk, i.e. the load-bearing structure, are subject to change when being exposed to continuous flooding of reactive brines over significant times. A reactive brine is composed of surface-active divalent ions, such as Mg^{2+}, Ca^{2+} and SO_4^{2-}, that interacts with the calcite surface and changes its microscopic structural framework, whereas a weakly reactive

brine consists of monovalent ions such as Na^+ and Cl^- that show a lower affinity for calcite surface compared to the divalent ions.

A study by Korsnes et al. (2008) demonstrated that when synthetic seawater (SSW), containing the divalent sulphate ions, was flooded through chalk cores, the yield strength was found to be significantly lower than those flooded with SSW without sulphate. Megawati et al. (2012) further showed that reduction in yield due to the presence of sulphate in pore fluid is due to its adsorption on the charged calcite surface. The interaction between neighbouring charged surfaces (electrical double layer) gives rise to repulsive electrostatic forces. This leads to a disjoining pressure between grains that eases grain reorganisation and allows for pore collapse at lower stresses because the normal load between grain–grain reduces the frictional forces. This process has been employed to explain (a) yielding at lower effective stresses than when saturated by brines without surface-active ions (Korsnes et al. 2008; Liteanu et al. 2013) and (b) additional rates of compaction (Nermoen et al. 2014) when seawater was injected.

Madland et al. (2009, 2011) demonstrated the dissolution of calcite and precipitation of magnesium-bearing carbonates and silicates during magnesium chloride ($MgCl_2$) brine flooding through Liège and Stevns Klint chalk. It was shown that samples flooded with $MgCl_2$ brine had a higher creep rate than the reference cores flooded with sodium chloride (NaCl) brine. Megawati et al. (2011) also showed similar results for Liège chalk when flooded with $MgCl_2$ brine. Further on, post-experimental analysis of the long-term $MgCl_2$ brine flooding tests (516 and 1072 days) on Liège *water-wet* chalk produced significant mineralogical changes where the cores were completely transformed from calcite to Mg-bearing minerals (Nermoen et al. 2015; Zimmermann et al. 2015; Minde et al. 2017; Borromeo et al. 2018). These observations are in line with modelling results reported in Hiorth et al. (2013).

In addition, the divalent magnesium ions have also shown to adsorb on available surface sites leading to desorption of calcium ions from the internal calcite surface (Ahsan and Fabricius 2010; Alam et al. 2010; Nermoen et al. 2018), resulting in stiffening and strengthening of chalk due to a lower internal repulsive electrostatic force.

Both ongoing adsorption/desorption and dissolution/precipitation processes, that describe the interactions between the pore fluid and the mineralogical surfaces, have shown to change several of the parameters that describe chalk mechanical behaviour. The chemo-mechanical effects in the aqueous phase have been shown on samples acquired from a range quarries from many localities. Most of the experiments that were cited above have exclusively been performed on samples that have never been exposed to oil such that the mineral phases were considered water wet. This has enabled the aqueous solution to contact the minerals directly, and as such, the applicability of the water weakening mechanism to oil reservoir samples has been debated. The question has been to what degree the load-bearing structure, especially the grain contacts, are prone to the documented water weakening, because the minerals within an oil reservoir chalk sample can sometimes be partially or completely covered with organic oil components that inhibit the adsorption and dissolution/precipitation processes.

Further on, wettability of chalk has been studied to understand how wettability affects multiphase fluid flow, in an attempt to enhance oil production (Standnes and Austad 2000a, b; Zhang and Austad 2005; Zhang et al. 2006; Strand et al., 2007; Fathi et al. 2010). Prior to flooding and imbibition experiments, reservoir chalk or outcrop chalk is cleaned with solvents and distilled water rendering it water wet. The *water-wet* chalk surface prefers water coating the grains, and will spontaneously imbibe water, which on pore level controls the flow of oil. Hence, to obtain realistic oil production

curves, the wettability of these chalk samples must be changed to a mixed wet/oil-wet state. This is a standard routine in these experiments and is done by flooding crude oil and water, and then ageing over time at high temperature before the wettability can be determined and any additional experiments can be performed. The aged core samples are, then, flooded and imbibed and the oil production is quantified as a function of the injected brine composition.

These core flooding/imbibition studies on chalk, however, did not take into account the mechanical behaviour of chalk. Hence, a question that has been unanswered so far is the extent to which the results of the previous geomechanical studies, performed on *water-wet* and water-saturated outcrop chalk, may be applied to oil reservoirs. Therefore, this study deals with the effects of changes in wettability on the mechanical response in chalk.

The premise of this study was to alter the wettability of Kansas chalk in a reproducible way and obtain experimental data on the relation between wetting state to stiffness, strength and time-dependent mechanical behaviour. The wetting state of chalk cores was altered to a *mixed-wet* state prior to mechanical testing at high effective stresses and reservoir temperature. Emphasis has been laid on exploring how stagnant non-reactive brines alter the mechanical properties both during loading to high stresses and in the creep phase, and the effects of injection of seawater and $MgCl_2$ brine on the mechanical parameters in the creep phase.

2 Materials and Methods

2.1 Rock Sample Material

19 cylindrical chalk samples were drilled from a single block obtained from an outcrop quarry with Late Cretaceous age in west-central Kansas (USA). An underlying assumption for the validity of this study is that the petrophysical, mechanical, chemical properties, and surface area and its affinity to ions are similar enough for quantitative comparisons to be made. Tang and Firoozabadi (2001) argue that Kansas outcrop chalk shows close similarities with the reservoir chalk from some of the North Sea chalk reservoirs in regards to porosity, permeability, and relative permeability. Kansas chalk has a non-carbonate content ranging from 1 to 3% (Tang and Firoozabadi 2001; Megawati et al. 2012).

All 19 samples were radially adjusted to 38.1 mm diameter and cut at desired lengths before dried at 110 °C overnight, after which the initial dry mass was measured. The samples were then vacuumed before saturated by distilled water (DW) for saturated mass measurements. The mass difference between the dry and saturated sample was used to estimate pore volume and saturation porosity (Tables 1, 3).

The 19 samples were divided into two test series:

- 11 samples were used for wettability determination by comparing chromatographic separation of seven reference *water-wet* samples and four wettability-altered samples.
- 8 samples were used for chemo-mechanical compaction during flow in triaxial cell. These 8 samples were divided into two sub-series: (a) four samples kept water wet and 100% water saturated in which two were flooded with SSW and two with $MgCl_2$ brine; and (b) four samples were wettability-altered containing a nonzero oil saturation, two of which were flooded with SSW and two with $MgCl_2$ brine.

Table 1 Basic properties of cores used in hydrostatic tests and flooded by $MgCl_2$ brine and SSW

	$MgCl_2$ brine flow tests				SSW flow tests			
	Water wet		Mixed wet		Water wet		Mixed wet	
	K1	K2	K3	K4	K5	K6	K7	K8
Core length (mm)	68.6	70.8	71.8	69.5	71.9	69.4	71.1	70.7
Core diameter (mm)	38.1	38.1	38.1	38.1	38.1	38.1	38.1	38.1
Dry mass (g)	130.7	138.0	143.4	135.5	140.5	134.8	140.4	139.3
Saturated mass (g)	160.7	167.7	172.4	164.6	170.6	164.1	169.7	168.4
Pore volume (ml)	30.0	29.7	29.0	29.1	30.1	29.3	29.3	29.1
Bulk volume (ml)	78.2	80.7	81.9	79.2	82.0	79.1	81.1	80.6
Saturation porosity ϕ (%)	38.4	36.8	35.4	36.7	36.7	37.0	36.1	36.1
Specific surface area (m^2/g)[a]	2.91–3.20	2.99–2.68	1.57–1.80	2.50–2.30	N.A.	N.A.	N.A.	N.A.

[a]The specific surface area of the inlet and outlet end pieces from the cutting of the core are given

N.A. not available

We assume that the results from the wettability determination program apply to the samples used in the triaxial test program.

2.2 Description of Fluids

Five brine compositions were used. In the wettability determination program, two versions of artificial seawater were used. The SW1T brine contained sulphate (SO_4^{2-}) and thiocyanate (SCN^-) tracer whilst SW0T did not (Table 2). Total dissolved solids of SW1T and SW0T equal the synthetic seawater (SSW) case. Three other brines were used during the triaxial tests program (Table 2):

Table 2 Composition of brines used in the wettability determination test and during core flooding in triaxial cells

Ions	Wettability determination program		Triaxial test program		
	SW0T (mol/l)	SW1T (mol/l)	1.1 M NaCl (mol/l)	0.219 M $MgCl_2$ (mol/l)	SSW (mol/l)
HCO_3^-	0.002	0.002	0	0	0.002
Cl^-	0.583	0.492	1.1	0.438	0.525
SO_4^{2-}	0	0.024	0	0	0.024
SCN^-	0	0.024	0	0	0
Mg^{2+}	0.045	0.045	0	0.219	0.045
Ca^{2+}	0.013	0.013	0	0	0.013
Na^+	0.46	0.393	1.1	0	0.45
Li^+	0	0.024	0	0	0
K^+	0.01	0.034	0	0	0.01
Ionic strength	0.643	0.647	1.1	0.657	0.657
TDS (g/l)	33.39	33.39	64.28	44.52	33.39

- 1.1 M NaCl brine was used for initial saturation to resemble resident formation fluids, i.e. its molar strength equals Ekofisk formation brine.
- 0.219 M $MgCl_2$ brine, with equal ionic strength to seawater (0.657), was used as a flooding brine for first series of cores. This is injected to focus on the dissolution and precipitation effects from the Ca–Mg exchange (Madland et al. 2009, 2011).
- SSW was used as a flooding brine for second series of cores to model the processes occurring when seawater is injected into hydrocarbon reservoirs. SSW interacts with the chalk by both dissolution/precipitation and adsorption of surface-active ions (Madland et al. 2011).

The oil used was a 60–40% volume mixture of crude oil from the Heidrun field offshore Norway and heptane. The acid number of the Heidrun oil was measured to be 2.82 mg KOH/g, whilst the acid number of the 60–40% volume mixture was 2.12 mg KOH/g. The titration procedure developed by Fan and Buckley (2007) was used to estimate the acid number.

2.3 Wettability Alteration and Fluid Saturations

A consequence of submerging chalk cores in oil over prolonged periods at high temperature is that oil components adsorb onto the mineral surfaces in the chalk, thereby making the mineral surfaces more hydrophobic, i.e. mixed wet. The wettability-altered samples (4 samples in the wettability determination program and 4 samples in the triaxial test program) were treated according to the following procedure:

- Saturation by 1.1 M NaCl brine.
- Mounted in a Hassler cell and heated to 50 °C. Flooded two pore volumes (PVs) in each direction by the oil mixture during which the produced brine was collected and the volume of water was measured to estimate the initial water saturation S_{wi}.
- Submerged the samples in the same oil mixture in ageing containers and left for 21 days at 90 °C.

In Sachdeva et al. (2018), the same chalk type was altered with the same fluids and temperature for different ageing times. The wettability was quantified using a series of techniques and obtained a stable value after 21 ageing days.

The wettability-altered samples were termed K3&K4, and, K7&K8 for those flooded by $MgCl_2$ brine and SSW, respectively (Table 1), in the triaxial test program, and Kmw1 to Kmw4 in the wettability determination program (Table 3).

The *water-wet* samples, four in the triaxial test program (K1&K2 flooded by $MgCl_2$ brine and K5&K6 flooded by SSW, Table 1) and seven in the wettability determination program (Kww1 to Kww7, see Table 3), were saturated by 1.1 M NaCl brine before tests.

2.4 Description of the Chromatographic Separation for Wettability Determination

Chromatographic separation refers to how the effluent concentration profile of non-affine tracers differs from the dynamic concentration profile of surface-active ions that adsorb onto charged, *water-wet* mineral surface sites. Strand et al. (2006) developed the chromatographic wettability procedure for chalk rocks. This method has also found its use for

Table 3 Basic properties of *water-wet* and *mixed-wet* cores used for wettability estimation

Core	Wetting state	Length (mm)	Diameter (mm)	Dry mass (g)	Saturated mass (g)	Pore volume (ml)	Porosity (%)
Kww1	Water wet	71.9	38.1	138.8	169.5	30.7	37.5
Kww2		72.9	38.1	141.3	172.3	31.0	37.3
Kww3		72.9	38.1	139.9	170.9	31.0	37.3
Kww4		70.0	38.1	136.2	165.7	29.5	37.0
Kww5		68.6	38.1	136.8	164.4	27.6	35.3
Kww6		68.8	38.1	134.2	163.0	28.8	36.7
Kww7		67.9	38.1	134.4	162.0	27.6	35.7
Kmw1	Mixed wet	72.5	38.1	139.2	170.4	31.2	37.7
Kmw2		73.2	38.1	140.8	172.2	31.4	37.6
Kmw3		74.4	38.1	148.4	178.5	30.1	35.5
Kmw4		72.0	38.1	139.8	170.1	30.3	36.9

Irreducible water saturations are given in Table 4

the analysis of limestone reservoirs (Fathi et al. 2010). The effluent ion concentration was determined by ion chromatography (IC).

The divalent sulphate anions (SO_4^{2-}) replace the monovalent anions on the positively charged calcite surface sites, as on the typical calcite form, there is an equal number of positively and negatively charged sites (Stipp 1999). The sulphate adsorption will only occur on the mineral areas in contact with the water phase, hence surfaces covered by oil will not capture sulphate. By co-injecting the adsorbing sulphate anions and non-affine thiocyanate (SCN^-) tracer, the two concentration profiles will split. The area spanned by the difference between the two concentration profiles (the concentration as function of ml injected) is then interpreted to be proportional to the mineral surface in contact with water. Further, if oil is bound to parts of the calcite minerals in a *mixed-wet* sample, the sulphate-tracer profile separation area is reduced compared to that for the *water-wet* samples. The ratio of the areas for the *mixed-wet* sample (A_{mw}) and the reference *water-wet* sample (A_{ww}) defines the wettability index (W_i),

$$W_i = \frac{A_{mw}}{A_{ww}} \tag{1}$$

A wettability index of 1, that the two areas are the same, means that the sample has the same number of surface sites for sulphate adsorption as the reference case making it completely water wet. A W_i of zero stems from overlapping sulphate and tracer curves which imply that the water cannot contact the minerals and thus the sample is termed completely oil wet.

The number of reactive surface sites on the calcite surface N is given by

$$N = W_i M_{dry} S n \times 10^{18} \tag{2}$$

where M_{dry} is the dry weight of the core, S is the specific surface area in m^2/g, and n is the number of surface sites per nm^2. Values of 3 m^2/g for specific surface area and 5 positive surface sites per nanometer square have been reported for Kansas chalk (Megawati et al. 2012). These sites may be occupied by different ions such as SO_4^{2-}, Cl^-, HCO_3^- (present

in injection brines) and CO_3^{2-} (arising from the calcite dissolution). A competitive adsorption takes place depending on different conditions such as surface affinity, temperature, brine injection rate.

Other values of W_i could imply that minerals inside the sample are partially covered by oil (mixed wet) making those regions unavailable for sulphate adsorption, or that reactive flow changes the specific surface area because of rock-fluid interactions. This is because dissolution and precipitation reactions can increase or reduce the number of surface sites available for adsorption, even when oil is present within the core, by changing the specific surface area of the rock.

2.5 Quantifying the Wettability Alteration by Ageing

The number of sulphate ions adsorbed compared to the tracer flow profile was quantified on four aged and seven unaged samples from the same block as the 8 samples used in the triaxial test program. The wettability modification procedure by ageing was equivalent for all cores in both 'wettability determination program' and the 'triaxial test program'. The wettability determination could not be done on the cores used in the triaxial tests before the experiments are run since the fluids used in the wettability determination could alter the wettability (sulphate is a wettability modifier). An underlying assumption is that the wettability determined, from the area spanned by the tracer and sulphate for the four aged cores and seven unaged cores, also applies to the four aged cores in the triaxial test program.

The wettability determination was performed in a Hassler cell by (1) flooding four PVs of the SW0T brine, (2) injecting SW1T brine for 500 min with a flow rate of 0.2 ml/min. During the SW1T injection, 40 samples were collected using a Gilson fraction sampler. Each sample contained 2 ml of fluids collected for 10.0 min each, with a 2.5 min waste time in between each sample. For each fluid sample (40 for each test), the concentration of thiocyanate and sulphate was determined using ion chromatography. For each sample, the concentration c_k of each species k (i.e. SCN^- and sulphate), is rescaled by the sulphate and SCN^- concentrations of SW0T c_{k0}(both being zero) and the concentrations for SW1T $c_{k1} = 0.024$ mol/l, such that a reduced concentration for each species $\widehat{C_k}$ could be obtained,

$$\widehat{C_k} = \frac{c_k - c_{k0}}{c_{k1} - c_{k0}} \tag{3}$$

This reduced concentration varies between zero and one, and when the effluent concentration equals the inlet concentration of the SW1T brine it gives $\widehat{c_k} = 1$. This enables the thiocyanate and sulphate curves to be plotted together. The difference between these curves, then, gives the area by integration using the trapeze method. As noted in Eq. 2, the number of surface sites (n) remains the same (reported to be 4.95 sites per nm^2 by Heberling et al. (2011)) and the area between the thiocyanate and sulphate curves is thus assumed to be directly proportional to the surface area available for sulphate on the chalk surface (i.e. $M_{\mathrm{dry}}S$). Larger cores will have a larger total surface area than smaller ones such that for accurate comparison these areas are reported in per gram of the core. The wettabilities of the samples used in the 'triaxial test program' (Tables 1, 5) were assumed to be equal to those obtained from the 'wettability determination program' (see Tables 3, 4).

Table 4 Estimated integrated areas per gram of the core for *water-wet* and *mixed-wet* samples, and the corresponding wettability indexes

	Core	Estimated area between sulphate and tracer (PV)	Integrated sulphate—tracer area per gram core ($\times 10^{-3}$ PV/g)	Wettability index (W_i)	Irreducible water saturation
Water wet	Kww1	0.221	1.59	1	1
	Kww2	0.222	1.57	1	1
	Kww3	0.231	1.65	1	1
	Kww4	0.215	1.58	1	1
	Kww5	0.218	1.59	1	1
	Kww6	0.194	1.45	1	1
	Kww7	0.230	1.71	1	1
	Average		$(1.59 \pm 0.07) \times 10^{-3}$ PV/g		
Mixed wet	Kmw1	0.126	0.90	0.57 ± 0.03	0.27
	Kmw2	0.112	0.80	0.50 ± 0.02	0.28
	Kmw3	0.137	0.92	0.58 ± 0.03	0.27
	Kmw4	0.126	0.90	0.57 ± 0.03	0.26
	Average:		$(0.88 \pm 0.05) \times 10^{-3}$ PV/g	0.55 ± 0.05	

2.6 Ion Chromatography

The effluent samples were diluted 500 times with de-ionised water on a *Gilson GX-271* machine to meet the linear region of the calibration curve of the *Dionex ICS-5000+Ion Chromatograph*. The columns used were *Dionex IonPac AS20* and *Dionex IonPac CS19* and the detector used was *Thermo Scientific™ Dionex™ ICS-5000+CD Conductivity Detector*. The areas under the chromatographic curves were used to calculate the concentration of anions and cations by assuming linear regime of the chromatograph such that,

$$\frac{c_i}{c_{\mathrm{std},i}} = \frac{A_i}{A_{\mathrm{std},i}} \tag{4}$$

where c denotes the concentration, A denotes the area under the chromatograph curve, i is the chemical species under test, and std represent standard samples with given concentration ($c_{\mathrm{std},i}$) and a fixed area ($A_{\mathrm{std},i}$) of the chromatographic curve.

2.7 The Triaxial Cell Setup for Mechanical Flow-Through Tests

Cylindrical plugs were mounted into the triaxial cell that allowed for continuous measurements of the axial and radial strains at elevated stresses and temperature (Fig. 1). The triaxial cell was equipped with a heating element and a regulating system with precise temperature control. Three pumps were connected to the triaxial cell to control the piston pressure (P_{pist}), confining pressure (σ_{rad}) and flooding rate (Q). The pore pressure on the downstream side (P_p) was controlled by a back-pressure regulator ensuring constant pore pressure (0.7 MPa) and the sampling of effluent fluids exiting the sample can be used for

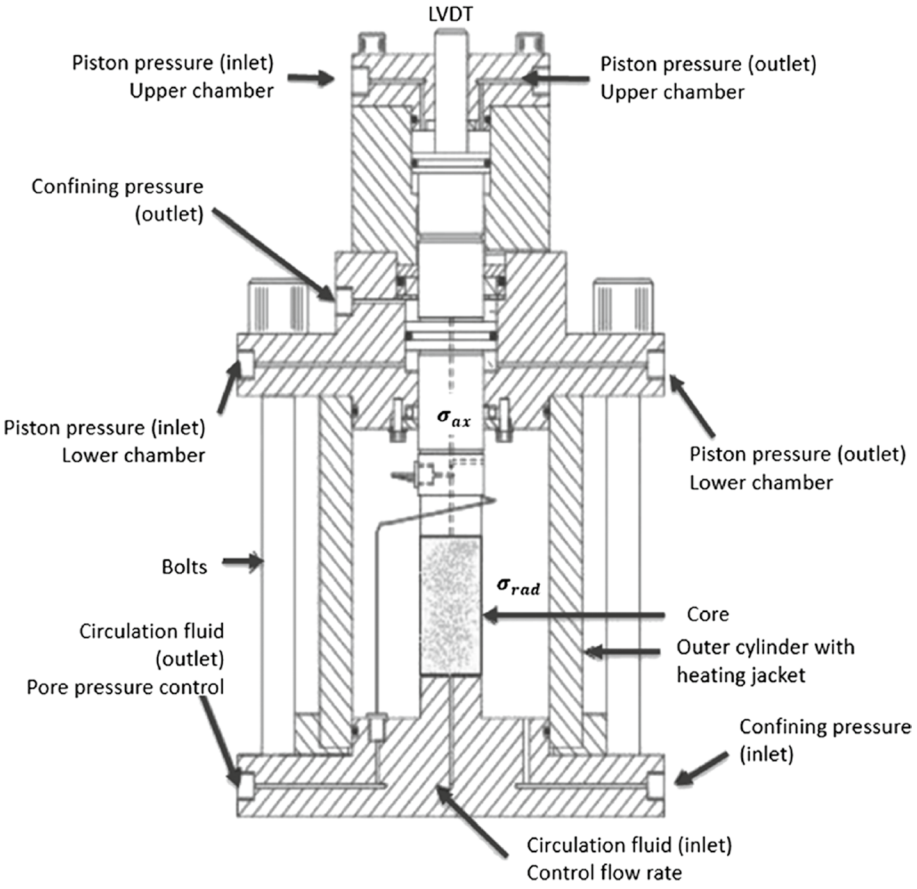

Fig. 1 Sketch of the triaxial cell

ion chromatography. An external Linear Voltage Differential Transducer (LVDT) monitored the change in length of the core plug (L) and an internal extensometer monitored the change in diameter of the core plug, and hence axial and radial strain, respectively.

The axial stress was calculated using confining pressure (radial stress), piston pressure, frictional pressure of the piston movement in the triaxial cell, and an area factor for the piston pressure chamber and the cross area of the plug ($f_{\text{area}} = 1.28$):

$$\sigma_{\text{ax}} = \sigma_{\text{rad}} + f_{\text{area}}\left(P_{\text{pist}} - P_{\text{fric}}\right) \tag{5}$$

In the hydrostatic phase, the stresses are equal in all spatial directions, so the bulk modulus K is given by:

$$K = \Delta\sigma'_{\text{ax}} \Big/ \Delta\varepsilon_{\text{vol}} = \Delta\sigma'_{\text{ax}} \Big/ \left(\Delta\varepsilon_{\text{ax}} + 2\Delta\varepsilon_{\text{rad}}\right) \tag{6}$$

Here, $\Delta\sigma'_{\text{ax}}$ is the change in effective stress in axial direction, where the effective stress is given by the imposed stress in radial and axial direction minus a fraction α times the pore pressure ($\sigma' = \sigma - \alpha P_{\text{pore}}$). We assume the Biot coefficient α to be one in these

experiments. $\Delta\varepsilon_{vol}$ is the change in volumetric strain, $\Delta\varepsilon_{ax}$ is the change in strain in axial direction and $\Delta\varepsilon_{rad}$ is the change in radial strain.

Axial (ε_{ax}), radial (ε_{rad}) and volumetric (ε_{vol}) strains are estimated from the length diameter and bulk volume measurements,

$$\varepsilon_{ax} = -\frac{L - L_o}{L_o} \tag{7}$$

$$\varepsilon_{rad} = -\frac{D - D_o}{D_o} \tag{8}$$

$$\varepsilon_{vol} = -\frac{V_b - V_{b,o}}{V_{b,o}} \tag{9}$$

where L_o, D_o and $V_{b,o}$ define the original length, diameter and bulk volume of the core, respectively, and L, D and V_b define the length, diameter and bulk volume of the core, respectively, at any given time during the experiment.

2.8 Constitutive Equations

The volume of the bulk, pore and solid over time are linked through the constitutive equation $V_b = V_s + V_p$. During the test, the porosity and hence the pore volume are not directly measured. Since porosity is determined by the ratio of pore volume (V_p) to bulk volume (V_b),

$$\phi = \frac{V_p}{V_b} = 1 - \frac{V_s}{V_b} \tag{10}$$

we may use solid volume (V_s) development estimated from the chemical reactions determined from the IC analysis and the bulk compaction to estimate the porosity development using (Nermoen et al. 2015),

$$\phi(t) = \frac{\phi_o + \varepsilon_{vol} - \Delta V_s / V_{b,o}}{1 + \varepsilon_{vol}} \tag{11}$$

2.8.1 Evolution in Bulk Volume with Time

The radial strain was measured only at the middle of the core, although radial deformation is not equal along the length of the core in hydrostatic tests (Nermoen et al. 2015). To obtain an improved volumetric strain estimate, the volumetric strain was estimated from the axial strain via the factor X,

$$\varepsilon_{vol} = X\varepsilon_{ax} \tag{12}$$

which is assumed to remain constant throughout the test. The factor X is determined from the length to volume changes measured directly on the core sample after the test. Thus, the bulk volume can be estimated with time using,

$$V_{b,t} = V_{b,o}\left(1 - \varepsilon_{vol}\right) = V_{b,o}\left(1 - X\varepsilon_{ax}\right) \tag{13}$$

2.8.2 Evolution in Solid Volume with Time

The evolution of the solid mass over time is calculated from the difference in the concentrations of the injected fluid and the produced effluent fluids. Given that the average density evolution of the solids is known, the change in solid volume ΔV_s can be calculated by,

$$\Delta V_s(t) = \frac{M_s(t)}{\rho_s(t)} - \frac{M_{s,o}}{\rho_{s,o}} \tag{14}$$

In this equation, the mass (M_s) evolution and the density (ρ_s) before and after the triaxial test are measured quantities. As function of time, however, the values of density and mass were calculated from the observed ion chromatography.

- The density evolution during the experiment $\rho_s(t)$ is estimated from a function that depends on the amount of calcium produced from the sample at a given time $m_{Ca}(t)$, and the initial $(\rho_{s,o})$ and final $(\rho_{s,f})$ densities via,

$$\rho_s(t) = \rho_{s,o} + \left(\left(\rho_{s,f} - \rho_{s,o}\right)\left(m_{Ca}(t)/m_{Ca,total}\right)\right) \tag{15}$$

  where $m_{Ca,total}$ is the total amount of calcium produced at the end of the test. The initial and final mineral densities were obtained from pycnometry measurements of untested and tested material.
- The dry mass of the sample and density after the triaxial tests and the difference throughout are given in the section 'Analysis of core after test (all tests)'. These values were used to interpolate the mass evolution of the sample via,

$$M_s(t) = M_{s,0} + \eta \int_0^t q_{in}\left(n_{mg}\left(c_{in,Mg} - c_{out,Mg}\right) - n_{ca}\left(c_{in,Ca} - c_{out,Ca}\right)\right)\mathrm{d}t \tag{16}$$

  where η is a fitting parameter that makes the observed replacement of Ca by Mg from IC-data match the observed loss in dry mass before and after test, q_{in} is the injected flow rate (litre/day), molar weights $n_{Mg} = 24$ g/mol and $n_{Ca} = 40$ g/mol, and c_{in} and c_{out} are the inlet and outlet molar concentrations in (mol/l) of Mg and Ca, and t is given in days.

2.8.3 Evolution in Pore Volume with Time

The pore volume is estimated from the calculations of bulk volume minus solid volume, hence,

$$\phi(t) = \frac{V_p(t)}{V_b(t)} = \frac{V_b(t) - V_s(t)}{V_b(t)} \tag{17}$$

2.9 Triaxial Test Program

The mechanical tests with $MgCl_2$ brine were performed at hydrostatic conditions according to the following procedure:

1. Mounted the cores in the triaxial cell; kept the bypass valve open with no flow-through the cores.

2. Increased confining pressure (σ_{rad}) to 1.2 MPa and pore pressure (P_p) to 0.7 MPa simultaneously.
3. Increased temperature to 130 °C.
4. Piston pressure set to 0.30 MPa above the friction pressure and σ_{rad} increased to 1.5 times above yield at a loading rate of 0.045 MPa/min. The creep stress was determined with the naked eye during hydrostatic loading phase.
5. Observed creep; for the first 15 days of creep period bypass valve was kept open. As such, any fluid movement was caused by pore volume reduction because of compaction and not differential pressure (dP) across the sample.
6. Afterwards bypass valve closed and $MgCl_2$ brine flooding started through cores with a flow rate of 0.010 ml/min.
7. Increased $MgCl_2$ brine flooding rate to 0.040 ml/min for all tests after a certain number of days.
8. Decreased flow rate back to 0.010 ml/min for cores K2&K4.
9. Cleaned the cores with four PVs of DW at the end of the test.
10. Used toluene to remove the leftover oil from cores K3&K4, followed by flooding methanol to remove toluene.
11. Used DW to remove methanol from these cores. A single iteration was performed for the cleaning of these cores with toluene and methanol.
12. Demounted all cores from triaxial cell and measured saturated mass. Kept them in an oven at 110 °C overnight.
13. Measured the dry weights, lengths, and diameters the next morning.
14. Cut the cores into 6 sections of almost equal lengths. The density and specific surface area of these sections and of the unflooded end pieces were measured using gas pycnometer and Brunauer–Emmett–Teller (BET) theory, respectively.

Effluent samples were taken approximately three times a week during steps 5–9 and were tested for ionic composition using ion chromatography.

The mechanical tests with synthetic seawater (SSW) were performed at hydrostatic conditions according to the following procedure:

1. Steps 1–5 are the same as above.
6. Closed bypass valve and started flooding SSW through cores with a flow rate of 0.010 ml/min.
7. Cleaned the cores with four PVs of DW at the end of the test.
8. Used toluene to remove the leftover oil from cores K7&K8, followed by flooding methanol to remove toluene.
9. Used DW to remove methanol from these cores. A single iteration was performed for the cleaning of these cores with toluene and methanol.
10. Demounted all cores from triaxial cell and measured saturated mass. Kept them in the oven at 110 °C overnight.
11. Measured the dry weights, lengths, and diameters the next morning.
12. Saturated K7&K8 with SW0T brine and mounted them in a Hassler core holder.
13. Performed chromatographic separation test on cores K7&K8.
14. Demounted the cores from the Hassler core holder after the chromatographic separation test.
15. Cut the cores into 6 sections of almost equal lengths. The density of these sections and of the unflooded end pieces was measured using gas pycnometer.

Effluent samples were taken approximately three times a week during steps 5–7 for cores K5 and K6. Only one effluent sample was taken for core K7, and six samples were taken for core K8 during step 6.

The oil production with time was measured for all *mixed-wet* cores, K3&K4 and K7&K8, using a separator on the downstream side of the triaxial test apparatus. With the oil production known at different times, the remaining oil saturation inside the cores was estimated.

2.10 Density and Specific Surface Area Determination

The cut sections were kept at 110 °C overnight. Next morning the sections were taken out and placed in a vacuum sealed container to cool down. The dry mass was, then, measured and each section was inserted, one-by-one, into the *Micromeritics AccuPyc II 1340 Gas Pycnometer* to measure the solid volume (used helium as a reference). From the solid volume and dry mass known, the solid density was estimated for each section.

The specific surface area was estimated based on Brunauer–Emmett–Teller (BET) theory, which works on the principle of physical adsorption of gas molecules on a solid surface (Brunauer et al. 1938). The measurements were carried out on *Micromeritics TriStar II* instrument. Liquid nitrogen was used during the measurement, as it does not chemically react with chalk. Two grams of powdered chalk was added to the sample glass tube and degassed for 5 h at 110 °C on *Micromeritics VacPrep 061 Sample Degas System*. A stable vacuum pressure of 20–30 mTorr was attained for all tested samples. Afterwards these sample tubes were attached to the BET apparatus and the specific surface area was measured automatically by the *TriStar II 3020* software. A few selected samples were tested twice to check for repeatability.

3 Results

The experimental results are presented in the following sections: (1) Wettability determination based on seven reference *water-wet* samples and four *mixed-wet* samples; (2) stiffness and strength measurements from the hydrostatic loading tests; (3) volumetric deformation during creep; (4) effluent sample analyses using ion chromatography; (5) oil volume observations for the *mixed-wet* samples; and (6) sample analysis after tests for the eight samples used in the triaxial test program.

3.1 Wettability Determination Program

Figure 2a and b displays the chromatographic separations of sulphate and thiocyanate tracer for the *water-wet* (Kww7) and *mixed-wet* sample (Kmw3), respectively. Here, the reduced ion concentration is plotted against PVs of SW1T flooded. Each dot reflects a single effluent water sample and the separation between the sulphate and tracer can be seen in Fig. 2c where the difference for the two cores is displayed. The curve for the *water-wet* sample is delayed and has a larger integrated area compared to that of the *mixed-wet* sample. For direct and accurate comparisons, the integrated areas were divided by the weight of the core since the lengths of the cores differed. The estimated areas of all seven *water-wet* and four *mixed-wet* cores are given in Table 4. The average areas for the *water-wet* and *mixed-wet* cores were $(1.59 \pm 0.07) \times 10^{-3}$ PV/g and $(0.88 \pm 0.05) \times 10^{-3}$ PV/g, respectively.

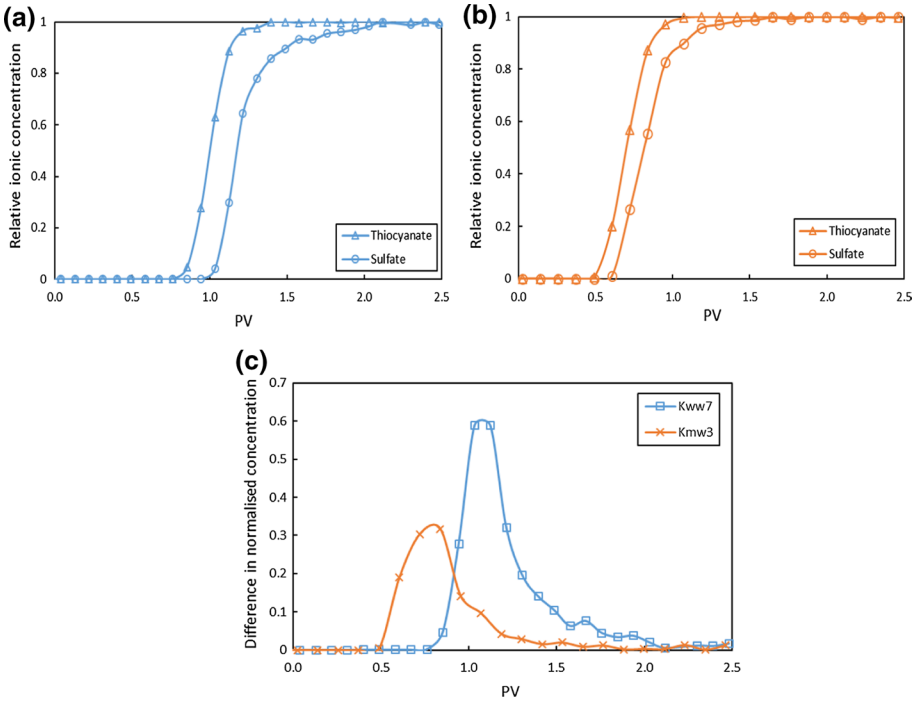

Fig. 2 Chromatographic separation test from the start of SW1T brine flow (after 4 PVs of SW0T) on **a** *water-wet* core (Kww7, blue) and **b** *mixed-wet* core (Kmw3, orange). The plots **a** and **b** show how the increase in sulphate concentration is delayed in the effluent compared to thiocyanate. The plot **c** shows the concentration difference between thiocyanate and sulphate curves with PVs of SW1T for the *water-wet* core Kww7 (blue) and *mixed-wet* core Kmw3 (orange). See Table 4 for all tests

This corresponds to an average W_i of $(0.88 \pm 0.05)/(1.59 \pm 0.07) = 0.55 \pm 0.05$ for the four cores, with the variations seen in Table 4.

It is further assumed that the W_i of the *mixed-wet* cores K3&K4 and K7&K8 used in the triaxial test program that were drilled from the same block and treated in the same way would also be equal to 0.55 ± 0.05.

3.2 Stiffness and Strength Determination with Initial Resident Fluids: Impact of Wettability and Oil/Water Saturation

During hydrostatic loading from 1.2 MPa to approximately 1.5 times the yield at 130 °C and 0.7 MPa pore pressure, the bypass valve was kept open and no fluids were flooded through cores but the initial resident fluids could flow out of the samples. The onset of yield was determined when the stress–strain curve deviated by more than 0.7 MPa from the straight elastic line used to determine the bulk modulus (K). The stress–strain curve during loading and the position of yield stresses for all cores K1 to K8 are shown in Fig. 3, and the yield stress, bulk modulus, and creep stress used further in the experiments are reported in Table 5. The initial water saturation of the wettability-altered cores ranged between 0.27 and 0.29.

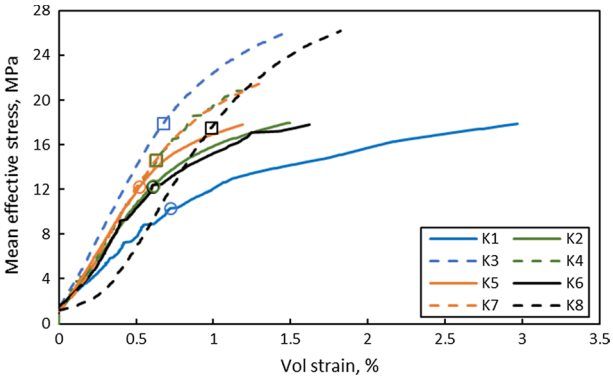

Fig. 3 Mean effective stress versus volumetric strain for all eight cores. Solid and dashed lines represent *water-wet* and *mixed-wet* cores, respectively. Yield stresses for these cores are displayed in their corresponding curves (circle markers for *water-wet* cores and square markers for *mixed-wet* cores)

Table 5 Bulk modulus, onset of yield and creep stress of cores K1 to K8 during hydrostatic loading

	Core	Wetting state	Irreducible water saturation (fraction)	Onset of yield stress (MPa)	Creep stress (MPa)	Bulk modulus (GPa)	Uncertainty in bulk modulus ($\times 10^{-1}$ GPa)
$MgCl_2$ flow	K1	Water wet	1	10.3	17.9	1.3	0.05
	K2		1	12.9	17.9	1.9	0.08
	K3	Mixed wet	0.28	17.9	26.1	2.6	0.06
	K4		0.29	14.6	20.8	2.2	0.08
SSW flow	K5	Water wet	1	12.5	17.8	2.2	0.07
	K6		1	12.4	17.9	1.9	0.20
	K7	Mixed wet	0.27	14.5	21.6	2.5	0.07
	K8		0.28	17.7	26.1	2.3	0.05

All experiments were performed at 130 °C

3.2.1 Stiffness Observations (Bulk Modulus *K*)

The linear region in Fig. 3 from 4 to 8 MPa hydrostatic stress was used to estimate bulk modulus for all cores. The bulk moduli *K* of *water-wet* cores (K1&K2, and K5&K6) were estimated to be 1.8 ± 0.3 GPa and that of *mixed-wet* cores (K3&K4, and K7&K8) was estimated to be 2.4 ± 0.2 GPa. Hence, the *mixed-wet* cores were found to be 33% stiffer than the *water-wet* cores (see Table 5 for all samples).

3.2.2 Strength Observations (Onset of Yield)

The stresses at onset of yield for all eight samples in the triaxial test program were determined from the stress–strain plots (Fig. 3) when the curves deviated by more than 0.7 MPa from the line used to estimate *K* (see Table 5). The circles and squares in Fig. 3 denote the yield stresses for *water-wet* and *mixed-wet* cores, respectively. The *water-wet* cores (K1&K2, and K5&K6) yielded at 12.0 ± 1.0 MPa, whilst the *mixed-wet* cores (K3&K4, and K7&K8) yielded at 16.2 ± 1.6 MPa. Hence, the yield strength of *mixed-wet* cores was found to be 35% higher than that of the *water-wet* cores. Further, it was observed that the

water-wet core K1 with the lowest yield stress and bulk modulus (Table 5 and Fig. 3) had a porosity significantly higher than the rest of the cores (Table 1).

The strength and stiffness relationship for all samples is shown in Fig. 4 and a clear distinction between the *water-wet* cores and the *mixed-wet* cores can be seen. This implies that the stiffer *mixed-wet* cores are stronger than the *water-wet* cores, displaying how either the presence of oil and/or the wettability of the samples mechanically impact chalk.

3.3 Volumetric Deformation During Creep of *Water-Wet* and *Mixed-Wet* Cores

3.3.1 Creep Observations—$MgCl_2$ Brine Series

The creep stress for all four cores was set to be 1.5 times yield stress so that the development could be compared to each other. Since the yield stress was determined with the naked eye during the loading, the creep stress chosen may deviate from the factor 1.5 times yield stress (see Table 5). The actual creep stress (in Figs. 5, 6) varied between a factor of 1.4 and 1.7 times yield stress. The volumetric creep strain for different wettability cores followed a similar trend during the stagnant (bypassed NaCl brine) creep period (black dotted line, Fig. 5) in which the fluid movement is controlled by pore volume reduction. During this time, the creep curve is recognised by a decline in creep rate. After 15 days the bypass was closed and the cores were flooded with 0.219 M $MgCl_2$ brine at a rate of 0.010 ml/min (approximately 0.5 PV/day). During this time, the creep curves displayed similar almost linear behaviour with the same trend irrespective of initial pore fluid composition (red dashed line). After a certain number of days that differed for the four samples, the $MgCl_2$ brine was injected with a fourfold increase in flow rate (0.040 ml/min). In response to that, all four samples, irrespective of their initial oil/water pore fluid composition and wettability, displayed an acceleration in the observed strain, and the strain rate attained a higher value in response to the increased flow rate (dark grey dash-dotted line).

After the $MgCl_2$ brine flow at 0.040 ml/min, the flow rate was reduced back to 0.010 ml/min for the K2 (water wet) and K4 (mixed wet) cores, and consequently the strain rate was immediately reduced for both. This displays how chemical reactions induced by $MgCl_2$ brine drive deformation with time. Before demounting, the cores were flooded by DW to remove salt water from the pores. This led to an immediate drop in strain rate (Fig. 6). The volumetric creep strains at the end of the experiments were K1: 6.52% after 107.6 creep

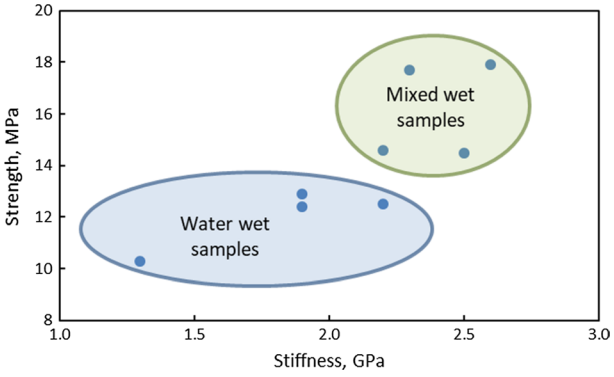

Fig. 4 Relationship of strength (onset of yield) with stiffness (bulk modulus)

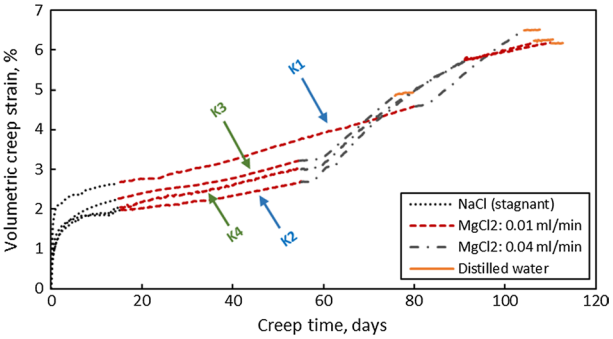

Fig. 5 $MgCl_2$ brine series: Volumetric creep strain versus time for *water-wet* cores K1 and K2 (blue arrows) and *mixed-wet* cores K3 and K4 (green arrows). The temperature was 130 °C and the stress levels were set to 1.4–1.7 times the yield stress (Table 5). The stagnant creep period with the initial fluids is shown by black dotted line, the $MgCl_2$ flooding period of 0.010 ml/min flow rate by red dashed lines, the $MgCl_2$ flooding period of 0.040 ml/min flow rate by dark grey dash-dotted line and the DW flooding period by orange solid line

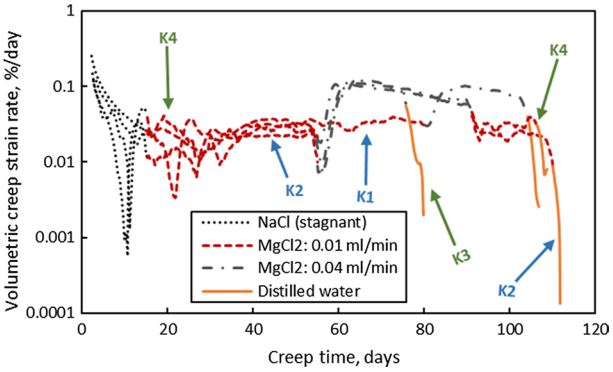

Fig. 6 $MgCl_2$ brine series: Volumetric creep strain rate versus time for *water-wet* cores K1 and K2 (blue arrows) and *mixed-wet* cores K3 and K4 (green arrows). The stagnant creep period with the initial fluids is shown by black dotted line, the $MgCl_2$ flooding period of 0.010 ml/min flow rate by red dashed lines, the $MgCl_2$ flooding period of 0.040 ml/min flow rate by dark grey dash-dotted line and the DW flooding period by orange solid line

days, K2: 6.17% after 112.7 creep days, K3: 4.93% after 79.7 creep days, and K4: 6.26% after 110.5 creep days.

The strain rate observations (Fig. 6) show that when flow rate of $MgCl_2$ brine injection is increased from the lower rate of 0.010 ml/min to the higher rate of 0.040 ml/min, the strain rate increased from 0.025–0.040%/day to around 0.100%/day for all cases. During flooding of DW to clean the cores of any salts before demounting, the strain rate dropped significantly and instantly for all cores to almost zero. In all cases, the correlation between (a) injected fluid flow rate and (b) strain rate shows that Mg-triggered chemical reactions (shown in the forthcoming sections) influence compaction rate irrespective of the presence of oil. This is evident from the start of $MgCl_2$ flooding at the higher rate of 0.040 ml/min when all four samples, both water wet and mixed wet, showed similar increase in the strain rate and the strain rate curves overlapped.

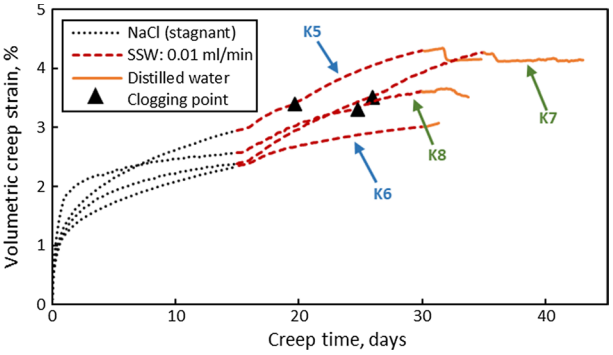

Fig. 7 SSW series: Volumetric creep strain versus time for *water-wet* cores K5 and K6 (blue arrows) and *mixed-wet* cores K7 and K8 (green arrows). Black triangles display the time when the outlet tube clogged. No clogging was observed for core K6. The temperature was 130 °C and the stress levels were set to 1.4–1.7 times the yield stress (Table 5). The stagnant creep period with NaCl brine is shown by black dotted line, the SSW flooding creep period at a flow rate of 0.010 ml/min by red dashed line and the DW flooding creep period by orange solid line

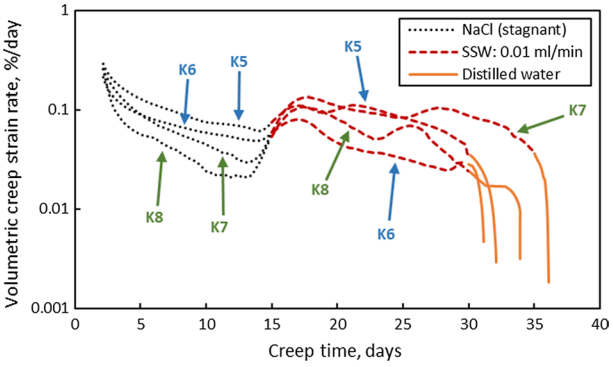

Fig. 8 SSW series: Volumetric creep strain rate versus time for *water-wet* cores K5 and K6 (blue arrows) and *mixed-wet* cores K7 and K8 (green arrows). The stagnant creep period with NaCl brine is shown by black dotted line, the SSW flooding creep period at a flow rate of 0.010 ml/min by red dashed line and the DW flooding creep period by orange solid line

3.3.2 Creep Observations—SSW Brine Series

The creep stresses for the four cores flooded by SSW (K5 to K8) are given in Table 5. During the first 15 days with stagnant fluids (bypassed NaCl brine) inside the core, the creep curves follow a similar trend (Fig. 7). At the end of the 15th day, the bypass was closed and the flow-through of SSW at a flow rate of 0.010 ml/min started. SSW was flooded for 15 days through cores K5, K6 and K8, and for 19.9 days for core K7. As soon as the SSW flood started, the creep strain rate increased rapidly the first few days for all four cores. This was observed irrespective of the wettability and initial saturation displaying how seawater induces abrupt weakening in contrast to when flooded with $MgCl_2$ brine where the weakening is displayed, as shown in Fig. 5. After the initial acceleration, the deformation rate decreased with time (Fig. 8), which was also different to the $MgCl_2$ flooded samples where the deformation rate was constant during flow-through.

As has been experienced before, the outlet tube got clogged during SSW brine injection. It is interpreted that anhydrite forms when the produced fluids enter the steel tubing. For sample K5 this occurred after 4.7 days, for K7 after 10.9 days and for K8 after 9.9 days of SSW flow (black filled triangles in Fig. 7). After this period, the bypass was opened to

maintain a constant pore pressure inside the cores and reduce the SSW flux through cores to zero. Clogging was not observed for core K6.

The final volumetric creep strains at the end of SSW flooding for cores K5 to K8 are 4.15% (after 36 creep days), 3.66% (after 32 creep days), 4.15% (after 43 creep days) and 3.52% (after 33.7 creep days), respectively. Before demounting, all cores were flooded by DW to remove salt water from the pores by increasing the maximum pressure for the flooding pumps. The flow rate during DW injection was 3 to 4 PVs/day for cleaning, even though this led to a high differential pressure across the cores because the outlet tube was clogged. For core K6, which was not clogged, we see an increase in the creep strain after the start of DW flooding, as also documented by Korsnes et al. (2006a). For the remaining cores K5, K7 and K8, the strain became zero because the outlet was clogged, thereby leading to an increase in the pore pressure, and subsequent lowering of the effective stress. The strain rate observations (Fig. 8) show that flooding of SSW induces a strain rate of around 0.03–0.10%/day irrespective of the initial wettability of cores.

3.4 Ion Concentration Using Ion Chromatography

This section displays the observations of the changes in the effluent ion concentrations due to rock-fluid interactions. Effluents were sampled two to three times per week for all tests during creep phase.

3.4.1 Ion Concentration of the Effluent: $MgCl_2$ Brine Series

Figure 9 displays the effluent calcium and magnesium ion concentrations during flow of $MgCl_2$ brine through the two *water-wet* (a and b) and two *mixed-wet* (c and d) cores. Since the dominating chemical reactions are attributed to the precipitation of magnesium-bearing minerals and the dissolution of calcium carbonate, the focus is on the calcium and magnesium ions. Besides, magnesium ions can also adsorb on the calcite surface on the expense of calcium desorption. In all, dissolution/precipitation and adsorption/desorption lead to a decrease in the magnesium concentration in the sampled effluent compared to the injected brine concentration and an increase in the calcium concentration.

Calcium is produced and magnesium is retained in the cores during flooding of $MgCl_2$ brine. From the start of $MgCl_2$ flow (15 days onward), a transient period in the calcium production and magnesium retention is observed until a stable production/retention plateau is reached after around 30 days. When comparing the ion concentration production curves *with* and *without* oil in the pores, the retention of Mg and production of Ca are the same. Further on, in Fig. 9a, b and d it can be seen that the calcium concentration decreased from ~0.027 to ~0.020 mol/l when the flow rate of was increased fourfold. The increased flow rate reduced the retention time for the $MgCl_2$ brine inside the core thereby reducing the time to equilibrate with the chalk. This was not that clearly seen in core K3 (Fig. 9c). Similar results were also reported by Nermoen et al. (2015). The change in magnesium concentration is less sensitive to flow rate.

During DW flooding, calcium and magnesium concentrations fall drastically to almost zero for all cores, confirming that negligible to minor interactions took place compared to during $MgCl_2$ flow.

By multiplying the differences in ion concentration, the molar weights and the flow rates, the magnesium and calcium production rates can be calculated (Fig. 10). The analysis

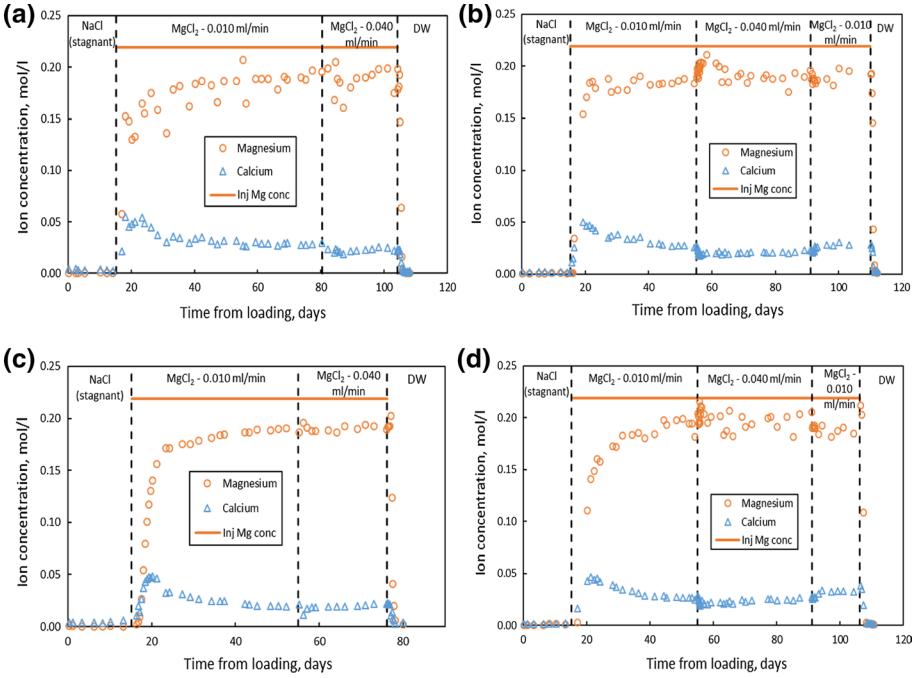

Fig. 9 Samples flooded by $MgCl_2$ brine. Effluent ion concentrations of calcium and magnesium ions, and the injected magnesium ion concentration over time are shown for *water-wet* cores **a** K1 and **b** K2 and *mixed-wet* cores **c** K3 and **d** K4

is done based upon the cores' perspective, such that magnesium retained in the cores is shown as positive numbers and calcium produced from the cores is shown on the negative scale. After $MgCl_2$ brine flooding started, the production and retention rates increased abruptly and with time the magnesium retention rate stabilised at 0.008 g/day for K1 and 0.010 g/day for K2, K3 and K4 after 5–10 days. The loss of Mg and production of Ca seem to be independent of the presence of oil inside the core.

Increasing the flow rate by a factor 4 to 0.040 ml/min, the retention rate of magnesium jumped to 0.020 g/day for K1, 0.030 g/day for K2, 0.040 g/day for K3 and 0.020 g/day for K4. Hence, an increase in the retention rate by a factor of 2–4 times is observed. The flow rate in K2 and K4 was then decreased again to 0.010 ml/min and the retention rate of magnesium dropped to 0.01 g/day for both, i.e. a drop by a factor 2–3.

The same trends were observed for calcium produced, which stabilised at 0.016 g/day for K1 and K2, 0.01 g/day for K3 and 0.02 g/day for K4. When the flow rate was increased, the calcium dissolution rate jumped to 0.054 g/day for K1, 0.048 g/day for K2, 0.04 g/day for K3 and 0.05 g/day for K4. It again decreased to 0.016 g/day and 0.020 g/day in K2 and K4, respectively, when the flow rate was lowered to 0.010 ml/min.

The integrated total magnesium retained for the *water-wet* cores was 0.07 mol (1.78 g) for K1 and 0.08 mol (2.02 g) for K2. For the *mixed-wet* cores, it was 0.06 mol (1.50 g) for K3 and 0.07 mol (1.77 g) for K4. Similarly, the integrated total calcium dissolved and produced from the cores was 0.06 mol (2.54 g) for K1, 0.07 mol (2.82 g) for K2 for the

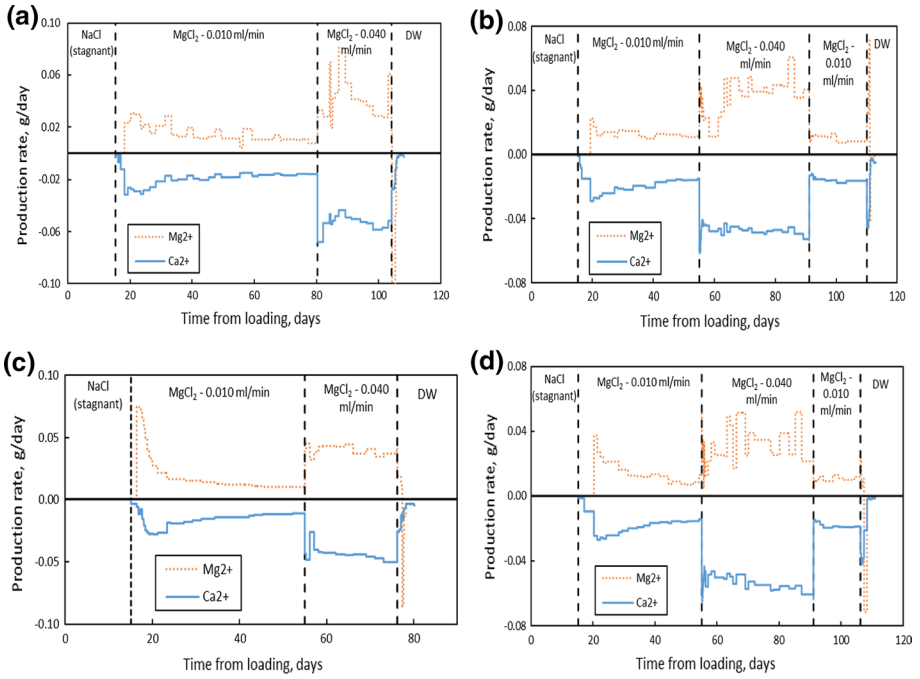

Fig. 10 Samples flooded by $MgCl_2$ brine. Evolution in the production in rates (in g/day) of Mg^{2+} and Ca^{2+} ions over time for *water-wet* cores **a** K1 and **b** K2 and *mixed-wet* cores **c** K3 and **d** K4

water-wet cores, whilst for the *mixed-wet* cores 0.04 mol (1.58 g) for K3, and 0.07 mol (2.99 g) for K4 of Ca was produced.

3.4.2 Ion Concentration in the Effluent: SSW Brine Series

The chemical interactions between the core and the injected fluid are more complicated when SSW is injected compared to $MgCl_2$ brine. This is because there are additional ions other than Mg ions present in SSW, that interact with the chalk leading to more complex chemical interactions. The effluent ion concentrations of sulphate, magnesium and calcium were reported in Fig. 11 for the two *water-wet* (K5 and K6) and one *mixed-wet* (K8) cores. The effluent analysis of the *mixed-wet* core K7 is not shown due to lack of data.

In the same way as during $MgCl_2$ flow, magnesium is retained in the cores and calcium ions are produced when SSW is injected. In addition, sulphate ions are retained in the core. During the first 15 days of bypass, magnesium and sulphate concentrations were zero, whilst a small increase in calcium concentration can be seen for K5 and K6 (Fig. 11a, b). This may imply that calcite dissolution has taken place within the core, and that these ions are transported *either by* advection together with fluids expelled as the core is compacted, *or* diffusion through the tubing to the bypass valve and then transported along with the fluids from there.

The bypass valve was closed and SSW was flooded through the cores from the 15th day, after which a transient period is observed (Fig. 11). In this period the calcium, magnesium and sulphate concentrations increase until 17–18 days after which a stable concentration

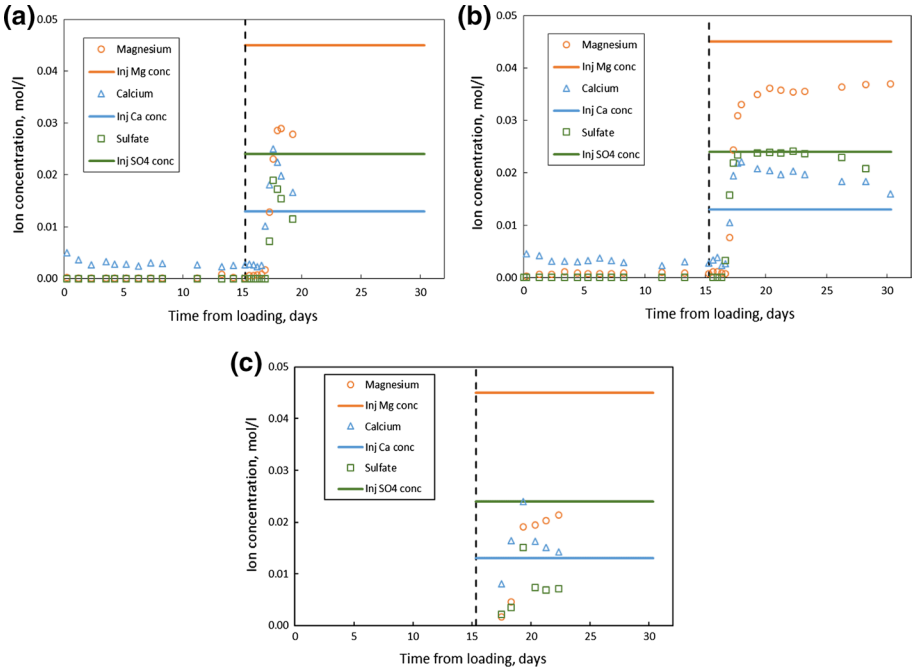

Fig. 11 Samples flooded by SSW brine. Injected and effluent ion concentrations of magnesium, calcium and sulphate ions over time are shown for *water-wet* cores **a** K5 and **b** K6 and *mixed-wet* core **c** K8. The black dashed vertical line in the plots depicts the start of SSW flooding. The effluent analysis of the *mixed-wet* core K7 is not shown due to lack of data

is reached for cores K6 and K8 (Fig. 11b, c). The concentration of these three ions did not stabilise for core K5 (Fig. 11a). After a certain period, the system clogged due to precipitation in the steel tubing on the outlet side of the core and the bypass had to be opened to avoid pore pressure build-up (for the *water-wet* K5 and *mixed-wet* K7 and K8 samples).

The integrated total magnesium retained for the *water-wet* cores K5 and K6 was 0.009 mol (0.214 g) and 0.012 mol (0.300 g), respectively, whilst for the *mixed-wet* core K8 it was 0.009 mol (0.216 g). Similarly, the integrated total sulphate retained in the *water-wet* cores K5 and K6 was 0.006 mol (0.565 g) and 0.005 mol (0.493 g), respectively, whilst for the *mixed-wet* core K8 it was 0.003 mol (0.244 g). Further on, the calcium dissolved and produced from the cores was 0.002 mol (0.080 g) for K5, 0.002 mol (0.075 g) for K6 for the *water-wet* cores, whilst for the *mixed-wet* core K8 0.001 mol (0.029 g) of Ca was produced.

3.5 Oil Volume Development for the *Mixed-Wet* Core K4 During $MgCl_2$ Brine Flow

The produced oil volume during flow and compaction was measured at frequent time intervals (Fig. 12). Based on the difference between the estimated pore volumes and measured oil volumes, the water volumes were also determined and shown in Fig. 12, whilst the initial and final oil and water volumes are reported in Table 6. The oil production measurement of K3 was highly uncertain because of fluctuations in pore pressure, oil received was

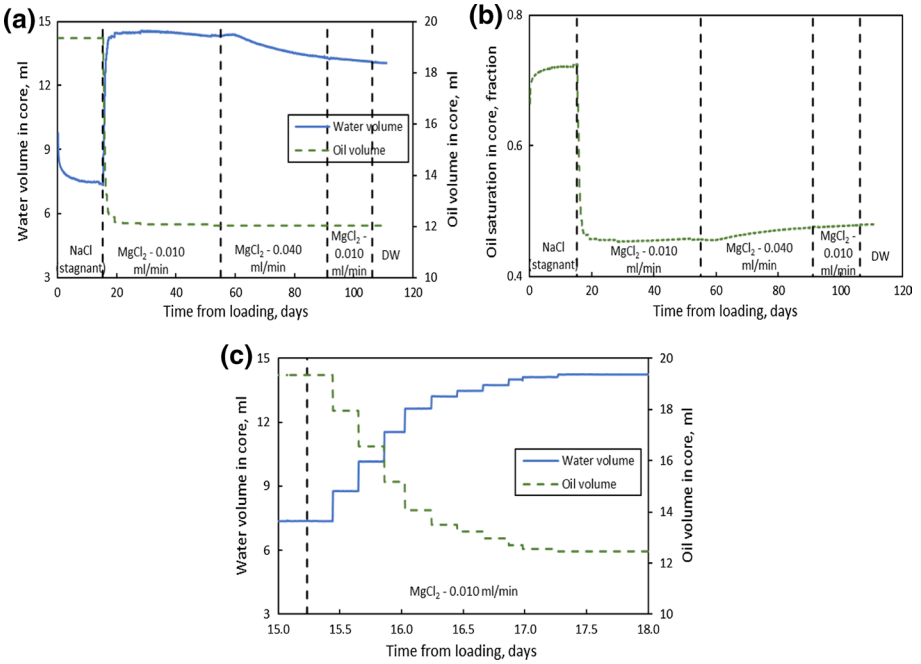

Fig. 12 **a** Observed oil and water volumes, **b** Oil saturation with time, and **c** zoomed into oil and water volumes from day 15 to day 18 for K4 core from the start of hydrostatic loading. The plots show the volumes and saturation inside the core at the corresponding given times. The black dashed vertical lines in the plots depict the time of change in the brine composition and/or change in the flow rate of the brine. This line in plot **c** depicts the start of $MgCl_2$ brine flooding at the rate of 0.010 ml/min

Table 6 Initial and final oil and water volumes in *mixed-wet* core (K4) during $MgCl_2$ brine flow

Core	K4
Irreducible water volume before test	8.3 ml
Irreducible water saturation S_{wi}	28.5%
Initial oil volume	20.8 ml
Total produced oil at the end of the test	8.8 ml
Oil volume after test	12.0 ml
Oil saturation after test	49.4%
Pore volume before and after test	29.1 ml and 24.3 ml

mostly in form of emulsions with water, so the K3 oil measurements are disregarded from this section.

The irreducible water saturation for this core was 28.5%, thus the initial oil in place was 20.8 ml. 1.5 ml oil was produced due to expansion of oil as temperature was increased from ambient to 130 °C. Figure 12a shows the oil and water volumes and b the change in the saturation of oil inside the core with time from the start of hydrostatic loading. At the start of loading, the oil and water volumes inside the core were 19.3 ml and 9.8 ml, respectively. No oil was produced during loading, so the pore volume loss is attributed to

a decrease in the water volume (to 9.0 ml). Further, no oil was produced during the first 15 days of creep with zero flow-through the core, so the pore volume loss led to a decrease in the water volume to 7.4 ml by the end of the 15th day. After the bypass was closed and the flooding of $MgCl_2$ brine started, 5.3 ml oil was produced within the first 20 h followed by 1.5 ml oil in the next 24 h and another 0.4 ml of oil in the subsequent 5 days, reducing the oil volume inside the core to 12.1 ml. An increase in the water volume was observed from 7.4 ml to 14.5 ml in the same period. From the 23rd day till the end of the test on the 111th day, a total of only additional 0.1 ml oil was produced, reducing the oil volume inside the core to 12.0 ml, and the water volume reduced from 14.5 ml to 13.1 ml due to further decrease in the pore volume. In total, 8.8 ml of oil (42.3% of the initial oil in place) was produced from the core at the end of the test. Figure 12b provides the corresponding saturation of oil in the core with time. As can be seen, the oil saturation increases from 60 days and onwards. This is because compaction prevailed with time, but no more oil was recovered from the core. Therefore, the compaction occurred by reducing the water volume, whilst the oil volume remained constant. Figure 12c provides a zoomed version of (a) from day 15 to day 18.

The increase in flow rate of $MgCl_2$ brine to 0.04 ml/min on the 56th day did not lead to additional oil production even though more than 57% of the initial oil was left inside the core. The additional dissolution of calcium and precipitation of magnesium triggered by the fourfold increase in flow rate (see Fig. 12), and the fourfold increase in pressure drop across the core, did not have any effects on oil production. Further on, compaction did not expel oil, only water from the core. This may imply that even though the core deforms and the pore volume decreases, neither compaction nor $MgCl_2$ brine induced chemical reactions lead to additional tail-end oil production.

3.6 Oil Volume Development for the *Mixed-Wet* Core K7 During SSW Flow

Oil and water volumes were measured through time for the K7 core, and the initial and final oil and water volumes are reported in Table 7. Here, the oil production in K8 was highly uncertain because of oil sticking to the walls of the burette and any oil production from K8 was omitted. Thereafter, a new separator technique was installed for oil production measurement from K7.

For the core K7 the irreducible water saturation was 27.4%, thus the initial oil in place was 21.2 ml. 1.5 ml oil was produced during heating to 130 °C due to expansion of oil. Figure 13a shows the oil and water volumes with time, and b displays the oil saturation inside the core from the start of hydrostatic loading when the oil and water volumes inside

Table 7 Initial and final oil and water volumes in *mixed-wet* (K7) core during SSW flow

Core	K7
Irreducible water volume before test	8.0 ml
Irreducible water saturation S_{wi}	27.4%
Initial oil volume	21.2 ml
Total produced oil at the end of the test	9.8 ml
Oil volume left in the core	11.4 ml
Oil saturation after test	45.2%
Pore volume before and after test	29.2 ml and 25.2 ml

Tubing on the outlet side got clogged after 23 days

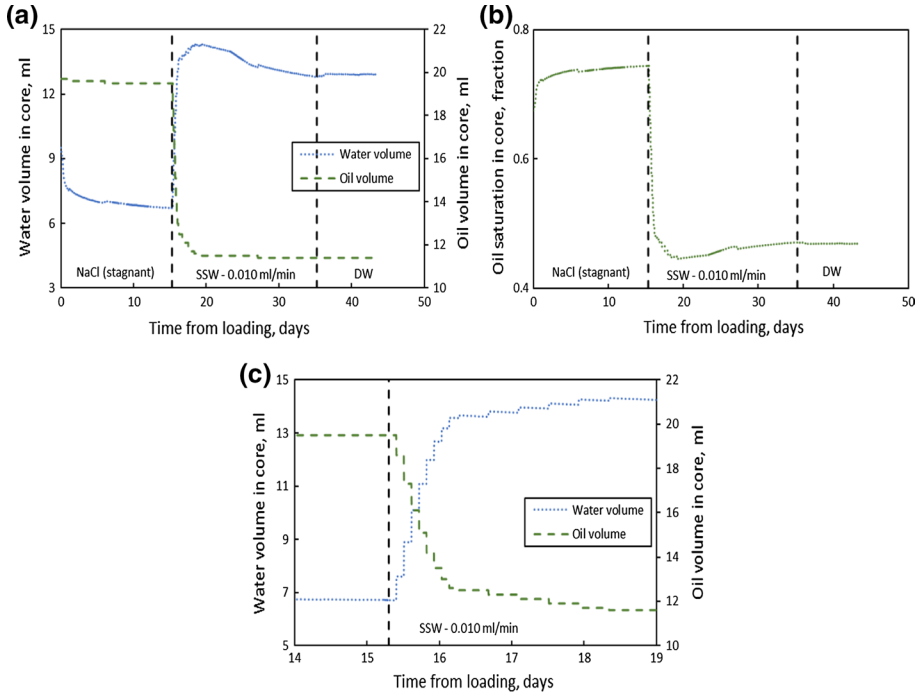

Fig. 13 **a** Observed oil and water volumes, **b** Oil saturation with time, and **c** zoomed into oil and water volumes from day 14 to day 19 for K7 core from the start of hydrostatic loading. The plots show the volumes and saturation inside the core at the corresponding given times. The black dashed vertical lines in the plots depict the change in the brine and/or change in the flow rate of the brine. This line in plot **c** depicts the start of SSW flooding at the rate of 0.010 ml/min

the core were 19.7 ml and 9.5 ml, respectively. The water volume in the core decreased to 8.5 ml during the loading phase with no change in the oil volume. 0.2 ml oil was produced during the first 15 days of creep with the bypass valve open (no flow-through core), whilst the water volume in the core further decreased to 6.7 ml (from the pore volume and oil measurements) by the end of the 15th day. When the SSW flooding started, 7 ml oil was produced within the first 24 h. Further, 0.9 ml oil produced during the subsequent 3 days, reducing the oil volume inside the core to 11.6 ml. The water volume inside the core increased from 6.7 ml to 14.3 ml in the same period as oil is replaced by water and the pore volume is reduced. From 19th day until the opening of bypass on the 26th day, an additional 0.2 ml oil was produced reducing the oil volume to 11.4 ml in the core, whilst the water volume reduced from 14.3 ml to 13.3 ml due to pore volume reduction by compaction. No additional oil was produced after the outlet tube was clogged and the bypass was reopened (the inlet tube was not affected by clogging) until the end of the test. During the rest of the compaction, the water volume decreased to 12.7 ml at the end of the test such that a final oil saturation of 45.2% was obtained. In total, 9.8 ml of oil (46.2% of the initial oil in place) was produced from the core at the end of the test. Figure 13(b) provides the corresponding saturation of oil in the core with time. Figure 13c provides a zoomed version of (a) from day 14 to day 19 after the start of SSW flooding.

3.7 Core Analysis After Tests

Basic measurements were done on all eight cores after the completion of the mechanical tests and the measured quantities are reported in Table 8. The *mixed-wet* cores were cleaned by using toluene to flush out oil, followed by methanol to flush out toluene. Afterwards they were flooded by DW to flush out methanol from the cores. Hence, all cores were saturated by DW before demounting. After demounting, the DW saturated mass was measured and then the cores were kept in a heating cabinet overnight before measuring the dry mass providing the saturation pore volume after test. The bulk volume was estimated from lengths and diameters of the core samples after test. The saturation porosity was estimated from the ratio of the pore volume to the bulk volume.

Measurements of the specific surface area of unaltered and unflooded Kansas chalk are reported in Table 9 where the untested end pieces are the ones that are left on each side during the cutting of the cylindrical cores. The untested specific surface areas are compared to six sections of the tested and flooded core where Sect. 1 represent the sample material placed close to the inlet and Sect. 6 represent the outlet part. For a few selected samples, the specific surface area was measured twice to check the repeatability. In three of four tests the inlet surface area increased, whilst in K4 it reduced from 2.5 to 1.1 m^2/g. Further on in all tests, the specific surface area increased from the inlet towards the middle of the samples. SSA measurements were only obtained on the $MgCl_2$ flooded samples.

3.8 Chromatographic Separation After Tests

Chromatographic separation tests were performed on the SSW flooded *mixed-wet* cores K7 and K8 after the mechanical tests. The sulphate and thiocyanate concentrations versus PVs of SW1T flooded are shown in Fig. 14.

The area between the sulphate and thiocyanate curves was found to be 0.225 PV (1.63×10^{-3} PV/g) for core K7 and 0.243 PV (1.76×10^{-3} PV/g) for core K8. Hence, both cores showed an increase in the area by a factor of two compared to the initial area of the four *mixed-wet* samples in the wettability determination program (Kmw1 to Kmw4) which had a surface area of 0.88×10^{-3} PV/g. This result reflects how dissolution/precipitation effects and the mobilisation of oil during SSW flow change the number of mineral surfaces in contact with water.

4 Discussion

Wettability affects the flow and distribution of reservoir fluids in the rock and plays a significant role in determining how immiscible fluids move through reservoirs, deciding production rates of oil and water and the ultimate oil recovery. Consider an oil-wet reservoir rock, where oil is bonded to the mineral surfaces, flooded by water. The injected water flows through the centre of the pores, expelling the mobile oil here. This behaviour subsequently leads to a rapid water breakthrough, and a high water cut later on leaving significant immobile oil volumes behind. The immobile oil volumes would further depend upon the specific surface area and the oil film thickness. If the same reservoir rock was water wet, i.e. oil being the non-wetting phase, the oil will occupy the centre of the larger pores. During waterflooding the injected water will tend to imbibe into the smaller pores, moving

Table 8 Basic properties of cores measured after tests

	$MgCl_2$				SSW			
	Water wet		Mixed wet		Water wet		Mixed wet	
	K1	K2	K3	K4	K5	K6	K7	K8
Length (mm)	66.0	68.3	70.0	67.2	70.5	68.3	69.7	69.3
Average diameter (mm)	37.1	37.3	37.4	37.3	37.5	37.7	37.5	37.4
New dry mass and ΔM_s (g)	129.0 & − 1.7	136.1 & − 1.9	141.4 & − 2.0	132.6 & − 2.9	140.1 & − 0.4	134.4 & − 0.4	138.2 & − 2.2	138.4 & − 0.9
Saturated mass (g)	152.3	161.1	166.0	156.9	166.3	159.9	163.4	163.1
New bulk volume and ΔV_b (cm^3)	71.3 & − 6.9	74.6 & − 6.1	76.9 & − 5.0	73.4 & − 5.8	77.9 & − 4.1	76.2 & − 2.9	77.0 & − 4.1	76.1 & − 4.5
New pore volume and ΔV_p (cm^3)	23.3 & − 6.7	25.0 & − 4.7	24.6 & − 4.4	24.3 & − 4.8	26.2 & − 3.9	25.5 & − 3.8	25.2 & − 4.1	24.7 & − 4.4
New porosity (%)	32.7	33.5	32.0	33.1	33.6	33.5	32.7	32.5
Initial porosity (%)	38.4	36.8	35.4	36.7	36.7	37.0	36.1	36.1
New solid density and $\Delta \rho_s$ (g/cm^3) (Pycnometry)	2.74 & 0.04	2.74 & 0.04	2.73 & 0.02	2.74 & 0.04	2.71 & 0.01	2.71 & 0.01	2.72 & 0.02	2.71 & 0.01
New solid volume and ΔV_s (cm^3) (Pycnometry)	47.1 & − 1.3	49.7 & − 1.4	51.8 & − 1.1	48.4 & − 1.8	51.7 & − 0.3	49.6 & − 0.3	50.8 & − 1.2	51.1 & − 0.5
Ratio of volumetric to axial strain (X)	2.33	2.13	2.55	2.23	2.74	2.56	2.73	2.75
Test time (days)	108.2	112.9	80.2	110.8	35.0	34.2	44.0	34.2

Table 9 Specific surface area measurements of unflooded core material from both sides of the core, and for sections along the core for K1 to K4 after test ($MgCl_2$ flooded samples)

	Core	K1	K2	K3	K4
	Core section	Water wet		Mixed wet	
		SSA, m^2/g	SSA, m^2/g	SSA, m^2/g	SSA, m^2/g
	Outlet end-piece (Unflooded)	2.91	2.68	1.80	2.30
Outlet	6	2.23 & 2.26	3.15 & 3.12	3.56 & 3.56	1.12 & 1.14
↑	5	3.11	3.04	3.17	1.17
Inlet	4	3.47 & 3.47	2.64	2.43 & 2.45	1.19 & 1.21
	3	3.89	2.95 & 2.92	2.26	1.17
	2	3.41	2.87	2.25	1.05
	1	3.31 & 3.32	3.27 & 3.24	1.97 & 2.01	1.09 &1.04
	Inlet end-piece (unflooded)	3.20	2.98 & 2.99	1.57	2.50
	Test time (days)	108.2	112.9	80.2	110.8

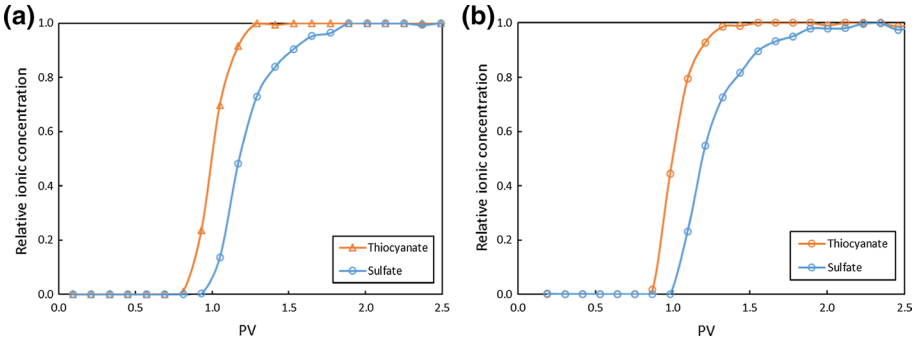

Fig. 14 Chromatographic separation tests performed on *mixed-wet* cores **a** K7 and **b** K8 at ambient temperature after mechanical tests. The plots show reduced ion concentrations of the thiocyanate and sulphate ions for SW1T brine plotted as a function of PVs injected

oil into the larger pores where it can be displaced. Oil, then, moves ahead of the waterfront, which results in increased primary oil recovery before water breakthrough occurs. After water breakthrough, almost all the remaining oil becomes immobile. The disconnected residual oil is in the form of oil droplets trapped by capillary forces, arising from the surface energy between oil, water and mineral surface, where the curvature of the oil droplet is larger than the pore throat diameter.

Wettability can also be important to the mechanical behaviour, as shown here, where the stiffness, strength and time-dependent deformation rate are affected. The mechanical response of the material to imposed stress is dictated by the load-bearing structure. In a *water-wet* system, the grains have a larger affinity to water, hence water weakening of chalk has been observed due to chemical reactions occurring between the minerals constituting chalk and reactive brines. In an oil-wet system where oil coat the chalk surface, it is envisioned that oil prevents the water phase to get in contact and react with mineral grains, thereby keeping the chalk rock strong and stiff.

In a *mixed-wet* system, however, it is expected that detailed spatial distribution of oil and water along the pore walls will control the link between wettability index and sample stiffness and strength. If the particle–particle contacts remain water wet, i.e. the injected oil during wettability alteration cannot enter the pore throats, it is expected that the mechanical behaviour is less sensitive to wettability, than if the opposite case occurred, i.e. the oil wets the smallest pore sizes between neighbouring particles. This argument relies on the premise that the mechanical properties of a porous sample are dictated by the forces holding neighbouring particles together, i.e. the attractive van der Waals forces and the repulsive electrostatic forces. Over time, the mechanical response during injection of different brines will be determined by the same effect as above: if oil is wetting the load frame, i.e. particle contacts, then it is expected that the mechanical response is insensitive to the injected fluid, and vice versa, if water is wetting the particle contacts the ions will diffuse into the grain contacts and alter the force balance between neighbouring grains. Remark that the characteristic time of ion diffusion in water on ~ 1 μm length scale is in the order of seconds to a minute.

4.1 Quantifying the Number of Available Surface Sites for Sulphate Adsorption

The number of positively charged calcite surface sites for sulphate adsorption can be estimated. On calcite surfaces, the divalent sulphate anions replace the monovalent anions, primarily on mineral areas in contact with water. Calcite surfaces covered by oil will not capture sulphate; however, it has been shown that Ca^{2+} can diffuse through oil films, and thereby alter wettability by releasing adsorbed oil (Zhang et al. 2007).

The number of sulphate ions adsorbed within the core during SW1T brine flooding was estimated for all cores using the estimated area between tracer and sulphate (Tables 4, 10) and the original concentration of SO_4^{2-} in SW1T brine (0.024 mol/l). Using a specific surface area of 3 m^2/g, 5 sites per nm^2 (Megawati et al. 2012) and that all sites are occupied by sulphate, the estimated number of adsorbed sulphate ions (Eq. 2) were ~ 21 to 25 times higher for *water-wet* cores, and ~ 37 to 41 times higher for *mixed-wet* cores than calculated from IC (Table 10). Thus, either one or several of the three premises is violated. Using 0.2 surface sites per nm^2 the estimated number of sulphate ions adsorbed matches with the measured.

As can be seen from Fig. 2a, the elution curve for SCN^- passes through point where the normalised concentration is 0.5 when 1 PVs of SW1T is flooded through the *water-wet* core. This indicates that the injected fluid is contacting the total PV of the core (Strand et al. 2006). The sulphate is produced later due to adsorption and hence its dispersion front is wider. In the case of a *mixed-wet* core (Fig. 2b), the normalised concentration of SCN^- is above 0.95 after 1 PV of SW1T. This is because the tracer travels only through the water phase and does not interact with the oil. Hence the tracer is produced earlier in a *mixed-wet* core than in a *water-wet* core. This is applicable for sulphate ions also, the only difference is that the number of sulphate ions adsorbed are less in the *mixed-wet* cores than in the *water-wet* cores.

4.2 Stiffness and Strength Observations

During loading with stagnant and inert NaCl brine inside the pores, the observed elastic stiffness (bulk modulus) and plastic strength (onset of yield) are affected by the oil/water saturation and wetness of the core (Table 5 and Fig. 3). Further on, the stiffness and

Table 10 Number of sulphate SO_4^{2-} ions adsorbed in *water-wet* and *mixed-wet* cores during SW1T-brine flooding

Core	Estimated area between sulphate and tracer (PV)	PV of the cores (ml)	Amount of SW1T flooded through core to obtain the estimated area (ml)	Actual no. of SO_4^{2-} adsorbed ($\times 10^{-3}$ mol)	Measured no. of SO_4^{2-} ions adsorbed from IC	Estimated no. of SO_4^{2-} ions (Eq. 2) (using $S = 3\ m^2/g$ and $n = 5 = 5$)	Factor	Estimated no. of SO_4^{2-} ions (Eq. 2) (using $S = 3\ m^2/g$ and $n = 0.2$)	Factor
Kww1	0.221	30.6	6.8	0.2	9.8E+19	2.1E+21	21.3	8.3E+19	0.9
Kww2	0.222	31.0	6.9	0.2	1.0E+20	2.1E+21	21.3	8.5E+19	0.9
Kww3	0.231	31.0	7.2	0.2	1.0E+20	2.1E+21	20.2	8.4E+19	0.8
Kww4	0.215	29.5	6.3	0.2	9.2E+19	2.0E+21	22.3	8.2E+19	0.9
Kww5	0.218	27.5	6.0	0.1	8.7E+19	2.1E+21	23.6	8.2E+19	0.9
Kww6	0.194	28.8	5.6	0.1	8.1E+19	2.0E+21	24.9	8.1E+19	1.0
Kww7	0.230	27.6	6.3	0.2	9.2E+19	2.0E+21	22.0	8.1E+19	0.9
Kmw1	0.126	31.2	3.9	0.1	5.7E+19	2.1E+21	36.9	8.4E+19	1.5
Kmw2	0.112	31.4	3.5	0.1	5.1E+19	2.1E+21	41.4	8.4E+19	1.7
Kmw3	0.137	30.2	4.1	0.1	6.0E+19	2.2E+21	37.2	8.9E+19	1.5
Kmw4	0.126	30.3	3.8	0.1	5.5E+19	2.1E+21	38.1	8.4E+19	1.5

The original concentration of SO_4^{2-} in SW1T brine is 0.024 mol/l and Avogadro's number is 9.022×10^{23}

strength are correlated with each other, implying that stiffer oil-saturated cores are likely to be strong. Similar correlations between stiffness and strength were also shown for 100% water-saturated chalk at both 30 °C and 130 °C (Nermoen et al. 2018) and for Stevns Klint chalk at ambient temperature (Katika et al. 2015). We also observe that the oil and brine saturated *mixed-wet* cores are stiffer and stronger than the 100% brine saturated *water-wet* cores (Fig. 4).

4.3 Creep Observations

The volumetric creep strain for the 4 *water-wet* (100% NaCl brine saturated) and 4 *mixed-wet* cores (with initial NaCl brine saturation ranging from 27% to 29%) during the first 15 days followed approximately the same creep trend when stress was set to 1.5 times the yield strength (Figs. 5, 7). The samples were not flooded during this time interval, and the only migration fluid was due to the compaction and pore loss and the thermal expansion from the heating of the cell. The observation that the creep evolution is proportional to the yield stress was valid both for *water-wet* and *mixed-wet* chalks. It may imply that oil wetness is not affecting the way in which the grains reorganise given that the stress level exceeds the yield stress. These observations exemplify how seemingly unrelated mechanical parameters correlate with each other in this case when chemical reactions are not taking place.

NaCl brine also interacts with the mineral surfaces in chalk and leads to calcite dissolution. Madland et al. (2011) showed the effect of flooding NaCl brine through *water-wet* Liège chalk and observed that the calcium concentration in the effluent was 0.004 mol/l throughout the experiment. In the presented test series, the cores were only initially saturated by NaCl, and not flooded, and it was observed that the produced calcium concentration varied between 0.003 and 0.005 mol/l. Hence 1 PV of NaCl, used to completely saturate a *water-wet* sample (with an approximate PV of 30 ml), dissolved less than 0.00015 mol (0.015 g) of calcite, which amounted to approximately 0.01% in mass compared to the initial dry mass of the samples (average initial dry mass of 137.8 g). The amount of calcite dissolved due to its interaction with NaCl brine would be even less for the *mixed-wet* samples as their initial water saturation was in the range 27–29%. Therefore, it was concluded that the interactions between chalk and stagnant NaCl brine were negligible.

From 16th day the injection of $MgCl_2$ and SSW started. The injecting $MgCl_2$ brine has shown to induce chemical reactions leading to additional creep rates, and more chemical reactions taking place during a time interval leads to an increased creep rate (Nermoen et al. 2015). When $MgCl_2$ brine is injected at the lower rate of 0.010 ml/min (approx. 0.5 initial PVs per day), the strain curve went from having a negative second derivative to a straight line with a more-or-less constant strain rate (Fig. 6). Quadrupling the flow rate to 0.040 ml/min, after a different number of days for different experiments, increased the linear creep rate by a factor of 2.5 to 4. This is in line with the analysis of the effluent fluids (Fig. 10) that display how the loss rate (in grams per day) of Ca and gain in Mg also increased by a factor of 2 to 4 after the flow rate was quadrupled. This shows how chemical reactions drive reduction in the solid volume by reducing the overall mass and increasing the mineral density, and how this behaviour is linked to the creep rate with time (Nermoen et al. 2016; Andersen et al. 2017). As shown in the presented evidence, the presence of oil in the pores does not alter the dissolution/precipitation driven water weakening dynamics, neither qualitatively nor quantitatively.

Based on the analysis performed by Zimmermann et al. (2015), it is likely that the chemical reactions dominate at the inlet because at this position the fluid is furthest away from chemical equilibrium. As a fluid interacts with the rock whilst moving downstream through the core, the fluid equilibrates with the sample, and at the outlet side the volumetric compaction is most likely dominated by pore volume reduction rather than solid volume effects. The non-homogenous chemical replacement dynamics can also be seen in the specific surface area measurements as reported in Table 9, where the change in specific surface area is non-uniform through the core. The trends are not clear, compared to the natural variation in the presented SSA results. This may be because of the initial spatial variability in grain size through the core, and inherent uncertainty in the measurements themselves, so firm conclusions cannot be drawn.

During DW injection to clean the cores of any salts, the strain rate dropped significantly for all cores (Fig. 6), even though the temperature and stress level were the same. The solubility of calcite in DW at 25 °C is reported to be 0.013 g/l (Voake et al. 2019) and it decreases with increase in temperature (Coto et al. 2012). This means that 0.00039 g of calcite dissolved per PV of DW flooded through cores (approximate PV of 30 ml) at 25 °C. As four PVs of DW were flooded to clean the cores at 130 °C, the calcite dissolved amounts to approximately 0.001% in mass compared to the initial dry mass of the cores (average initial dry mass of 137.8 g). Hence, it may be concluded that the interactions of DW with calcite are minor in nature. This observation further exemplifies how chemical reactions that undergo during the continuous flow of reactive fluids affect the rate of deformation, thereby displaying the link between chemical reactions and the quantitative amount of water weakening. Of special importance to emphasise is that all these observations are insensitive to the initial wettability and brine/oil saturation of the chalks.

The chalk samples that were flooded with SSW (i.e., K5 to K8, Fig. 7) displayed a qualitatively similar behaviour as the $MgCl_2$ samples (K1 to K4). Injecting SSW induced chemical reactions and adsorption of surface-active ions leading to immediate additional creep rates. Until clogging, all cores showed comparable volumetric strain curves, irrespective of the initial wettability and oil/water saturation. Prior to clogging (K5, K7 and K8) the strain rate declined because of reduced effective stress due to pressure build-up. The clogging did not occur inside the samples but in the steel tubing on the outlet side, so opening the bypass valve reduced the flow to zero and the strain rate regained its pre-clogging values. During flooding by DW to clean the cores before demounting, we observe a decrease in the strain rate for the cores where clogging occurred due to pore pressure increase. For core K6 (without clogging), we observe an increase in the volumetric creep strain.

At least two water weakening mechanisms are required to understand how the change in fluid compositions in the effluent analyses (Figs. 9, 11) and strain rate depend on each other: (1) Chemical reactions between brine and chalk related to dissolution and precipitation, especially during $MgCl_2$ flow and also in the SSW experiments, and (2) the adsorption of surface-active divalent ions (magnesium and sulphate ions) on the chalk surface and desorption of calcium ions. This adsorption changes the electrostatic repulsion thereby changing the inter-particle forces governing grain movements (Megawati et al. 2012). In all cases irrespective of the brine composition, the oil/brine saturation and wettability, the calcium concentration increases and the magnesium concentration decreases in the effluent. This is related to the production of calcium ions resting on the mineral surface and dissolution of calcium carbonate as well as precipitation of magnesium carbonate and adsorption of magnesium ions onto the calcite surface. However, only a limited number of surface sites are available, so the adsorption/desorption contribution to the changes in the ion concentrations will not prevail indefinitely. Sachdeva

et al. (2019) showed that desorption and adsorption dynamics could only occur within the first few pore volumes of the reactive brine injection in these cases. Afterwards the dissolution/precipitation processes dominate the calcium and magnesium effluent dynamics. Secondary minerals can be identified using Scanning Electron Microscope (SEM) (see Fig. 15). Qualitatively, the mineral replacement seem to be insensitive to the initial water wetness and oil/brine saturation. The described behaviour is in-line to what was indicated by X-ray diffraction and SEM studies carried out on chalk after $MgCl_2$ brine flow-through experiments by Madland et al. (2011) and Megawati et al. (2015). Megawati et al. (2012) showed the effect of sulphate adsorption on the mechanical behaviour of Kansas chalk at 130 °C.

The effluent analyses imply that stoichiometry is important. However, some clear deviations between Mg–Ca stoichiometry and the measurements are observed: (a) the magnesium concentration varied from sample to sample, more than the calcium concentration that displayed a smoother trend, (b) magnesium did not show the same flow rate dependency as calcium (Fig. 10), and (c) the number of moles of calcium produced is different than the number of moles of magnesium precipitated in all cases. When accounting for produced Ca and retained Mg, we see that the estimated mass evolution from IC does not match the direct core weight measurements of dry core before and after testing. These discrepancies imply that the chemical replacement mechanisms within the core are more complicated than only calcite dissolution and magnesite precipitation. A more complex geochemical process occurred that calls for a more complete and detailed investigation. Similar results were also demonstrated by Nermoen et al. (2015). However, a significant result from the discussed evidence is that the geochemical effects were neither found to be dependent on the wetting state nor the presence of oil. This implies that results obtained from the *water-wet* cores in the past are applicable to real reservoir systems.

During flooding with SSW, three out of four cores got clogged in the outlet tube. The implications of this observation may create large operational problems in actual field conditions. During water flooding by SSW for pressure maintenance, scales from the produced water, consisting of calcium carbonate and calcium sulphate, may deposit on the steel tubing and near wellbore formation to impair production from the production wells.

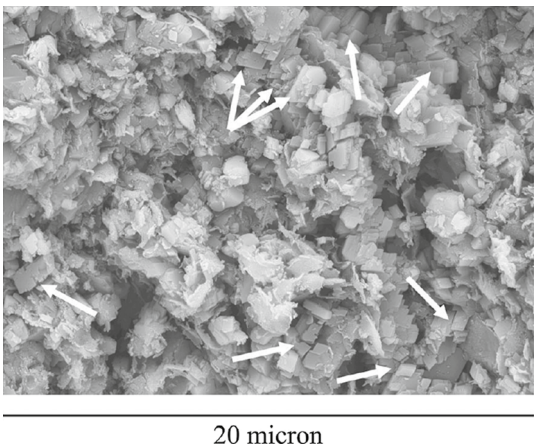

Fig. 15 SEM image of a $MgCl_2$ brine flooded Liege chalk material showing occurrence of magnesite crystals with rhombic habit (arrows) and absence of coccolith remains (Zimmermann et al. 2015)

4.4 Oil Production Observations

The heating of the cells led to production of oil interpreted to be caused by thermal expansion of oil. However, during loading and subsequent compaction without flow-through (stagnant NaCl brine in the pores), no additional oil was produced implying that, within the error of measurement, only water was expelled during compaction. When $MgCl_2$ and SSW flooding started, oil was produced immediately. After a certain time, however, the oil production ceased even though compaction and chemical reactions continued. In the case of $MgCl_2$ brine, no oil production was observed even when the flow rate was increased to 0.040 ml/min. Volumetric compaction by pore volume reduction only contributed to the expulsion of the free moving fluids in the pores, namely water. Two main reasons are used to interpret this: (1) oil is bonded and trapped on mineral surfaces in 50 nm to 0.1 μm thick oil films (calculated by dividing the immobile residual oil volume to the surface area of the sample), and (2) the oil droplets surrounded by water split up in smaller ganglia in which the pressure difference across is insufficient to overcome the capillary forces halting oil production.

The oil recovery observations showed that SSW flood gave 4% more oil recovery than $MgCl_2$ flood during the initial displacement of oil (46.2% oil recovery for K7 and 42.3% oil recovery for K4). This may indicate that SSW alters wettability favourably for oil recovery. However, after the initial displacement of oil during the flooding of these brines, the pore volume reduction did not change the volume of oil in the core and only water was expelled. Combined observations of oil production during compaction and non-equilibrium flow imply that (a) $MgCl_2$ and SSW brines do not mobilise oil adsorbed on the rock surface, and (b) compaction do not contribute to oil production after the initial displacement. This observation is opposite to the interpretations of the Ekofisk production by Sulak and Danielsen (1989) where they concluded that compaction drive results in increased hydrocarbon recovery.

5 Conclusion

The focus in this paper has been to investigate how injection of brines that contain monovalent ions (Na^+ and Cl^- in NaCl) and divalent ions (Ca^{2+}, Mg^{2+} and SO_4^{2-} in $MgCl_2$ and SSW) impact (a) hydrostatic stress and volumetric strain load curves for stiffness and strength measurement, (b) time-dependent deformation at constant stress, (c) chemical reaction from IC analysis, (d) oil production and (e) petrophysical changes after test (specific surface area, density, porosity and wettability). The triaxial tests were performed in two phases: (1) with stagnant fluids (NaCl brine and oil mixture) during the first 15 days, and (2) during continuous flow of seawater and $MgCl_2$ brines afterwards. The triaxial experiments were performed on both four *water-wet* (100% NaCl brine saturated) and four *mixed-wet* (NaCl brine and oil saturated) Kansas chalk samples. In all, eight *mixed-wet* samples were prepared in parallel, and four of these samples were used in the wettability determination program. This is because sulphate adsorption change the wettability, so the cores used in the triaxial test program were not tested for wettability before mechanical tests. The wettability determination program showed a repeatable wettability index.

Wettability alteration and oil/water saturation affected the elastic stiffness (bulk modulus) and plastic strength (onset of yield) during loading with stagnant pore fluids. The wettability-altered samples were found to be stiffer and stronger than *water-wet* samples.

All samples were hydrostatically loaded and kept at a stress level of 150% of the yield stress. The volumetric creep strain for different wettability cores followed a similar trend during the stagnant fluid period and during the injection of the reactive brines. This shows that if the yield stress is known, then the creep curve over time can be estimated given that the same fluid is injected. The proposed correlation between yield stress and creep curve with time indicate the related deformation mechanisms during hydrostatic loading and hydrostatic creep. This is irrespective of the presence of oil/water and wetness of the samples, and that yield stress can be considered a controlling parameter for creep. Further investigations are, however, required to check the validity of this observation.

Injecting $MgCl_2$ and SSW into chalk induced chemical reactions leading to additional creep rates, both for the *water-wet* and *mixed-wet* samples. We found the mechanical dependency of the imposed fluids to be insensitive to the initial wettability. These results indicate that the presence of oil in pores does not prevent brines to access intergranular contacts, which presumably affects mechanical strength. Further on, the chemical replacement observed by the ion chromatography is insensitive to the presence of oil in the pores, indicating that the application of dissolution/precipitation estimates into hydrocarbon reservoirs, when based on *water-wet* scale experiments, is valid.

The observations of oil production with time during compaction and non-equilibrium flow imply that after the initial displacement of oil during flooding of the reactive brines, no additional oil is mobilised. Neither volumetric compaction by the estimated pore volume reduction nor the brine chemistry impacted the oil recovery. Further we found that SSW flooding recovered 4% more oil compared to $MgCl_2$ flooding during initial oil displacement. Our results imply that enhanced oil production driven by pore compaction mobilise only fluids placed in the centre of the pores when enough pressure drive is created to overcome capillary forces. Since wettability impacts how oil and water are partitioned within the pores, it would be important, in the future, to tune wettability in laboratory and then measure if compaction and chemical reactions would mobilise oil either at lower or higher wettability indexes.

Acknowledgements The authors acknowledge the Research Council of Norway and the industry partners, ConocoPhillips Skandinavia AS, Aker BP ASA, Eni Norge AS, Equinor ASA, Neptune Energy Norge AS, Lundin Norway AS, Halliburton AS, Schlumberger Norge AS, Wintershall Norge AS, and DEA Norge AS, of The National IOR Centre of Norway for support.

Compliance with Ethical Standards

Availability of Data The raw data that support the findings of this study are available as supplementary material.

Appendix

Experimental Uncertainty

The experimental uncertainties that are linked to the key experimental findings and corresponding conclusions, and an evaluation of magnitude of the error are given below:

a. Measurement of brine volumes to estimate S_{wi} produced during the wettability alteration procedure: A volumetric burette was used to collect the brine on the downstream side of the Hassler cell. The accuracy of this burette is in the order of 0.1 ml.
b. Dilution of samples during IC analysis: A given variation of 2% corresponding to a variation of 5×10^{-4} mol/l is expected from the ion chromatography.
c. Measurement of oil volumes through the separator: During the first 15 days of bypass open and with stagnant fluids inside the *mixed-wet* cores, we compactify the grain by pore volume reduction, which results in expulsion of oil and water from the pores. The dead volume of the outlet tubing to the separator was less than 1 ml. If some oil had produced during the first 15 days of compaction into this tubing, this oil should have been produced immediately when the brine flooding through the cores started on the 16th day, but in all cases, it took more than this dead volume to be flooded into the core to get the first drop of oil out into the separator. Hence, it was concluded that no oil was produced during the first 15 days of compaction.
d. Area estimate from chromatographic separation test: The errors linked to the estimation of areas between thiocyanate and sulphate for the reference *water-wet* cores and the *mixed-wet* cores were found to be 0.03×10^{-3} PV/g and 0.02×10^{-3} PV/g, respectively.
e. Pycnometry: The solid volume measurements using pycnometry were done twice for a few selected samples to check for the repeatability. The standard deviation for the solid volume measurements was estimated by the Gas Pycnometer itself and was found to be in the range of ± 0.002 cm^3 to ± 0.009 cm^3.
f. Specific surface area: SSA determination was carried out two times on most of the samples to check for the repeatability of the results. The repeatability was found to be very good with a variation of ± 0.05 m^2/g.
g. Porosity determination by saturation: The dry mass and the wet mass for all samples before and after test were determined using a weighing machine. The error linked to that machine is in the order of ± 0.002 g.
h. Bulk volume estimate as a function of time: The lengths and diameters of the cores before and after test were measured using a Digital Caliper and the error associated with this caliper is in the range of 0.01 mm to 0.02 mm. Further on, the radial strain was measured only at the middle of the core, and not along the whole length. Hence a factor X was introduced to relate axial strain to volumetric strain and was assumed to be constant throughout the duration of the test. The error linked to the calculation of X was estimated to be ± 0.08, which means that the error linked to the estimation of bulk volume with time is also the same, i.e. ± 0.08 cm^3.

References

Ahsan, R., Fabricius, I.L.: Sorption of magnesium and sulfate ions on calcite. In: 72nd EAGE Conference and Exhibition Incorporating SPE EUROPEC 2010, Extended Abstracts, SP13 (2010). https://doi.org/10.3997/2214-4609.201401335

Alam, M.M., Ahsan, R., Shaik, A.K., Fabricius, I.L.: Surface charge of calcite and its influence on the electrical conductivity in chalk. In: 80th Annual International Meeting, Society of Exploration Geophysicists, Expanded Abstracts, pp. 2686–2691 (2010). https://doi.org/10.1190/1.3513399

Andersen, M.A., Foeged, N., Pedersen, H.F.: The link between waterflood-induced compaction and rate-sensitive behavior in a weak north sea chalk. In: Proceedings of the Fourth North Sea Chalk Symposium, Deauville, France, Sept 1992

Andersen, P.Ø., Wang, W., Madland, M.V., Zimmermann, U., Korsnes, R.I., Bertolino, S.R.A., Minde, M., Schulz, B., Gilbricht, S.: Comparative study of five outcrop chalks flooded at reservoir conditions: chemo-mechanical behaviour and profiles of compositional alteration. Transp. Porous Media **120**, 1–47 (2017)

Bjørlykke, K., Høeg, K.: Effect of burial and diagenesis on stresses, compaction and fluid flow in sedimentary basins. Mar. Pet. Geol. **14**, 267–276 (1997)

Borromeo, L., Egeland, N., Minde, M.W., Zimmermann, U., Andò, S., Madland, M.V., Korsnes, R.I.: Quick, easy, and economic mineralogical studies of flooded chalk for EOR experiments using Raman spectroscopy. Minerals **8**(6), 221 (2018). https://doi.org/10.3390/min8060221

Brignoli, M., Santarelli, F.J., Righetti, C.: Capillary phenomena in an impure chalk. In: Rock Mechanics in Petroleum Engineering, Delft, Netherlands. Society of Petroleum Engineers (1994). https://doi.org/10.2118/28135-MS

Brunauer, S., Emmett, P.H., Teller, E.: Adsorption of gases in multimolecular layers. J. Am. Chem. Soc. **60**(2), 309–319 (1938)

Burchette, T.P.: Carbonate rocks and petroleum reservoirs: a geological perspective from the industry. Geol. Soc. Lond. Spec. Publ. **370**(1), 17–37 (2012)

Coto, B., Martos, C., Peña, J.L., Rodríguez, R., Pastor, G.: Effects in the solubility of $CaCO_3$: experimental study and model description. Fluid Phase Equilib. **324**, 1–7 (2012)

Delage, P., Schroeder, C., Cui, Y.J.: Subsidence and Capillary Effects in Chalks, pp. 1291–1298. Eurock, ISRM International Symposium, Torino (1996)

Doornhof, D., Kristiansen, T.G., Nagel, N.B., Pattillo, P.D., Sayers, C.: Compaction and subsidence. Oilfield Rev. **18**, 50–68 (2006)

Fabricius, I.L.: How burial diagenesis of chalk sediments controls sonic velocity and porosity. Am. Assoc. Pet. Geol. Bull. **87**(11), 1755–1778 (2003)

Fabricius, I.L.: Burial stress and elastic strain of carbonate rocks. Geophys. Prospect. **62**, 1327–1336 (2014). https://doi.org/10.1111/1365-2478.12184

Fan, T., Buckley, J.S.: Acid number measurements revisited. SPE J. **12**(04), 496–500 (2007)

Fathi, S.J., Austad, T., Strand, S.: "Smart water" as a wettability modifier in chalk: the effect of salinity and ionic composition. Energy Fuels **24**(4), 2514–2519 (2010). https://doi.org/10.1021/ef901304m

Gauer, P.R., Sylte, J.E., Nagel, N.B.: Ekofisk field well log decompaction. Paper SPE/ISRM 78177 Presented at the Rock Mechanics Conference, Irving, Texas, 20–23 Oct 2002

Heberling, F., Trainor, T.P., Lützenkirchen, J., Eng, P., Denecke, M.A., Bosbach, D.: Structure and reactivity of the calcite–water interface. J. Colloid Interface Sci. **354**(2), 843–857 (2011)

Hellmann, R., Renders, P.J.N., Gratier, J.P., Guiguet, R.: Experimental pressure solution compaction of chalk in aqueous solutions. Part 1. Deformation behavior and chemistry. In: Water-Rock Interactions, Ore Deposits, and Environmental Geochemistry: A Tribute to David A. Crerar, vol. 7, pp. 129–152. The Geochemical Society, Special Publication (2002a)

Hellmann, R., Gaviglio, P., Renders, P.J.N., Gratier, J.P., Bekri, S., Adler, P.: Experimental pressure solution compaction of chalk in aqueous solutions. Part 2. Deformation examined by SEM, porosimetry, synthetic permeability, and X-ray computerized tomography. In: Water-Rock Interactions, Ore Deposits, and Environmental Geochemistry: A Tribute to David A. Crerar, vol. 7, pp. 153–178. The Geochemical Society, Special Publication (2002b)

Hermansen, H., Thomas, L.K., Sylte, J.E., Aasboe, B.T., 1997. Twenty Five Years of Ekofisk Reservoir Management. p. 873–885. http://dx.doi.org/10.2118/38927-ms

Hermansen, H., Landa, G.H., Sylte, J.E., Thomas, L.K.: Experiences after 10 years of waterflooding the Ekofisk field, Norway. J. Pet. Sci. Eng. **26**, 11–18 (2000)

Heugas, O., Charlez, P.: Mechanical effect of the water injection on Ekofisk chalk. In: Third North Sea Chalk Symposium, Copenhagen, Denmark (1990)

Hiorth, A., Jettestuen, E., Cathles, L.M., Madland, M.V.: Precipitation, Dissolution, and ion exchange processes coupled with a lattice Boltzmann advection diffusion solver. Geochim. Cosmochim. Acta **104**, 99–110 (2013). https://doi.org/10.1016/j.gca.2012.11.019

Johnson, J.P., Rhett, D.W.: Compaction behavior of Ekofisk chalk as a function of stress. Paper SPE 15872 Presented at the European Petroleum Conference, London, United Kingdom, 20–22 Oct 1986. https://doi.org/10.2118/15872-ms

Katika, K., Addassi, M., Alam, M.M., Fabricius, I.L.: The effect of divalent ions on the elasticity and pore collapse of chalk evaluated from compressional wave velocity and low-field Nuclear Magnetic Resonance (NMR). J. Pet. Sci. Eng. **136**, 88–99 (2015)

Korsnes, R.I., Madland, M.V., Austad, T.: Impact of Brine Composition on the Mechanical Strength of Chalk at High Temperature. Eurock, Multiphysics Coupling and Long Term Behaviour in Rock Mechanics, pp. 133–140. Taylor and Francis, London (2006a)

Korsnes, R.I., Strand, S., Hoff, O., Pedersen, T., Madland, M.V., Austad, T.: Does the Chemical Interaction Between Seawater and Chalk Affect the Mechanical Properties of Chalk? Eurock 2006: Multiphysics Coupling and Long Term Behaviour in Rock Mechanics, pp. 427–434. Taylor and Francis, London (2006b)

Korsnes, R.I., Madland, M.V., Austad, T., Haver, S., Røsland, G.: The effects of temperature on the water weakening of chalk by seawater. J. Pet. Sci. Eng. **60**, 183–193 (2008)

Kristiansen, T.G., Barkved, O.I., Buer, K., Bakke, R.: Production-induced deformations outside the reservoir and their impact on 4D seismic. Paper IPTC 10818 Presented at the International Petroleum Technology Conference, Doha, Qatar, 21–23 Nov 2005. http://dx.doi.org/10.2523/IPTC-10818-MS

Liteanu, E., Spiers, C.J., de Bresser, J.H.P.: The influence of water and supercritical CO_2 on the failure behavior of chalk. Tectonophysics **599**, 157–169 (2013). https://doi.org/10.1016/j.tecto.2013.04.013

Lord, C.J., Johlman, C.L., Rhett, D.W.: Is capillary suction a viable cohesive mechanism in chalk? In: SPE/ISRM Rock Mechanics in Petroleum Engineering, Trondheim, Norway (1998)

Madland, M.V., Hiorth, A., Korsnes, R.I., Evje, S., Cathles, L.: Rock fluid interactions in chalk exposed to injection of seawater, $MgCl_2$, and NaCl brines with equal ionic strength. Paper A22 Presented at the 15th European Symposium on Improved Oil Recovery, Paris, France, 27–29 Apr 2009

Madland, M.V., Midtgarden, K., Manafov, R., Korsnes, R.I., Kristiansen, T.G., Hiorth, A.: The effect of temperature and brine composition on the mechanical strength of kansas chalk. Paper SCA2008-55 Presented at the International Symposium of the Society of Core Analysts, Abu Dhabi, UAE, 29 Oct–2 Nov 2008

Madland, M.V., Hiorth, A., Omdal, E., Megawati, M., Hildebrand-Habel, T., Korsnes, R.I., Evje, S., Cathles, L.M.: Chemical alterations induced by rock-fluid interactions when injecting brines in high porosity chalks. Transp. Porous Media **87**, 679–702 (2011)

Maury, V., Piau, J.M., Halle, G.: Subsidence induced by water injection in water sensitive reservoir rocks: the example of Ekofisk. Paper SPE 36890 Presented at the SPE European Petroleum Conference, Milan, Italy, 22–24 Oct 1996

Megawati, M., Andersen, P.Ø., Korsnes, R.I., Evje, S., Hiorth, A., Madland, M.V.: The effect of aqueous chemistry pH on the time-dependent deformation behavior of chalk experimental and modelling study. In: Pore2Fluid International Conference. 16–18 Nov, Paris, France (2011)

Megawati, M., Hiorth, A., Madland, M.V.: The impact of surface charge on the mechanical behaviour of high-porosity chalk. Rock Mech. Rock Eng. **46**(5), 1073–1090 (2012)

Megawati, M., Madland, M.V., Hiorth, A.: Mechanical and physical behavior of high-porosity chalks exposed to chemical perturbation. J. Pet. Sci. Eng. **133**, 313–327 (2015). https://doi.org/10.1016/j.petrol.2015.06.026

Mimran, Y.: Fabric deformation induced in Cretaceous chalks by tectonic stresses. Tectonophysics **26**(3–4), 309–316 (1975). https://doi.org/10.1016/0040-1951(75)90097-9

Minde, M.W., Haser, S., Korsnes, R.I., Zimmermann, U., Madland, M.V.: Comparative studies of mineralogical alterations of three ultra-long-term tests of onshore chalk at reservoir conditions. In: 19th European Symposium on Improved Oil Recovery/IOR Norway 2017. European Association of Geoscientists and Engineers (2017). ISBN 978-94-6282-209-2

Nagel, N.B.: Ekofisk field overburden modelling. Paper SPE 47345 Presented at the SPE/ISRM Rock Mechanics in Petroleum Engineering, Trondheim, Norway, 8–10 July 1998

Nermoen, A., Korsnes, R.I., Haug, S., Hiorth, A., Madland, M.V.: The dynamic stability of chalks during flooding of non-equilibrium brines and CO_2, Stavanger. In: Fourth EAGE CO_2 Geological Storage Workshop, Demonstrating Storage Integrity and Building Confidence in CCS (2014)

Nermoen, A., Korsnes, R.I., Hiorth, A., Madland, M.V.: Porosity and permeability development in compacting chalks during flooding of non-equilibrium brines: insights from long-term experiment. J. Geophys. Res. Solid Earth (2015). https://doi.org/10.1002/2014jb011631

Nermoen, A., Korsnes, R.I., Aursjø, O., Madland, M.V., Kjørslevik, T.A.C., Østensen, G.: How stress and temperature conditions affect rock-fluid chemistry and mechanical deformation. Front. Phys. (2016). https://doi.org/10.3389/fphy.2016.00002

Nermoen, A., Korsnes, R.I., Storm, E.V., Stødle, T., Madland, M.V., Fabricius, I.L.: Incorporating electrostatic effects into the effective stress relation: insights from chalk experiments. Geophysics **83**(3), 1–13 (2018)

Neveux, L., Grgic, D., Carpentier, C., Pirnon, J., Truche, L., Girard, J.P.: Influence of hydrocarbon injection on the compaction by pressure solution of a carbonate rock: an experimental study under triaxial stresses. Mar. Pet. Geol. **55**, 282–294 (2014a)

Neveux, L., Grgic, D., Carpentier, C., Pironon, J., Truche, L., Girard, J.P.: Experimental simulation of chemomechanical processes during deep burial diagenesis of carbonate rocks. J. Geophys. Res. Solid Earth **119**(2), 984–1007 (2014b). https://doi.org/10.1002/2013JB010516

Papamichos, E., Brignoli, M., Santerelli, F.J.: An experimental and theoretical study of a partially saturated collapsible rock. Mech. Cohesive-frict. Mater. Int. J. Exp. Model. Comput. Mater. Struct. **2**(3), 251–278 (1997)

Piau, J.M., Maury, V.: Mechanical effects of water injection in chalk reservoirs. In: SPE/ISRM Rock Mechanics in Petroleum Engineering, Delft, Netherlands (1994)

Risnes, R.: Deformation and yield in high porosity outcrop chalk. Phys. Chem. Earth (A) **26**, 53–57 (2001)

Risnes, R., Haghighi, H., Korsnes, R.I., Natvik, O.: Chalk-fluid interactions with glycol and brines. Tectonophysics **370**, 213–226 (2003)

Sachdeva, J.S., Nermoen, A., Korsnes, R.I., Madland M.V.: Chalk surface area evolution during flow of reactive brines: Does oil play a role? Submitted to *Energy & Fuels*, publication under review (2019)

Sachdeva, J.S., Sripal, E.A., Nermoen, A., Korsnes, R.I., Madland, M.V., James, L.A.: A laboratory scale approach to wettability restoration in chalk core samples. In: SCA2018-020 Paper Presented at the International Symposium of the Society of Core Analysts, Trondheim, Norway, 27–30 Aug 2018

Schroeder, C., Bois, A-P., Maury, V., Halle, G.: Water/chalk (or collapsible soil) interaction: part II. Results of Tests in laboratory on lixhe chalk to calibrate water/chalk models. In: Paper SPE 47587 Presented at the SPE/ISRM Rock Mechanics in Petroleum Engineering, Trondheim, Norway, 8–10 July 1998

Schroeder, C., Shao, J.: Plastic deformation and capillary effects in chalks. In: Proceedings of the 5th North Sea Chalk Symposium, Reims, France (1996)

Standnes, D.C., Austad, T.: Wettability alteration in chalk: 1. Preparation of core material and oil properties. J. Pet. Sci. Eng. **28**(3), 111–121 (2000a)

Standnes, D.C., Austad, T.: Wettability alteration in chalk: 2. Mechanism for wettability alteration from oil-wet to water-wet using surfactants. J. Pet. Sci. Eng. **28**(3), 123–143 (2000b)

Stipp, S.L.S.: Toward a conceptual model of the calcite surface: hydration, hydrolysis and surface potential. Geochim. Cosmochim. Acta **63**(19/20), 3121–3131 (1999)

Strand, S., Standnes, D.C., Austad, T.: New Wettability test for chalk based on chromatographic separation of SCN^- and SO_4^{2-}. J. Pet. Sci. Eng. **52**, 187–197 (2006)

Strand, S., Hjuler, H.L., Torsvik, R., Pedersen, J.I., Madland, M.V., Austad, T.: Wettability of chalk: impact of silica, clay content and mechanical properties. Pet. Geosci. **13**(1), 69–80 (2007)

Sulak, R.M.: Ekofisk field: the first 20 years. J. Pet. Technol. **43**(10), 1–265 (1991)

Sulak, R.M., Danielsen, J.: Reservoir aspects of Ekofisk subsidence. J. Pet. Technol. **41**(7), 709–716 (1989)

Sylte, J.E., Thomas, L.K., Rhett, D.W., Bruning, D.D., Nagel, N.B.: Water induced compaction in the Ekofisk field. Paper SPE 56426 Presented at the SPE Annual Technical Conference and Exhibition, Houston, Texas, 3–6 Oct 1999

Tang, G., Firoozabadi, A.: Effect of pressure gradient and initial water saturation on water injection in water-wet and mixed-wet fractured porous media. SPE Reserv. Eval. Eng. **4**(6), 516–524 (2001)

Teufel, L.W., Rett, D.W., Farrell, H.E.: Effect of reservoir depletion and pore pressure drawdown in situ stress and deformation in the Ekofisk field, North Sea. In: Proceedings of the 32nd U.S. Rock Mechanics Symposium, pp. 63–72, Norman, Oklahoma, 10–12 July 1991

Thomas, L.K., Dixon, T.N., Evans, C.E., Vienot, M.E.: Ekofisk waterflood pilot. J. Pet. Technol. **39**(02), 221–232 (1987)

Voake, T., Nermoen, A., Ravnås, C., Korsnes, R.I., Fabricius, I.L.: Influence of temperature cycling and pore fluid on tensile strength of chalk. J. Rock Mech. Geotech. Eng. Publication in print (2019)

Zhang, P., Austad, T.: The relative effects of acid number and temperature on chalk wettability. Paper SPE 92999 Presented at SPE International Symposium on Oilfield Chemistry, Houstan, Texas, USA, 2–4 Feb 2005

Zhang, P., Tweheyo, M.T., Austad, T.: Wettability alteration and improved oil recovery in chalk: the effect of calcium in the presence of sulfate. Energy Fuels **20**, 2056–2062 (2006)

Zhang, P., Tweheyo, M.T., Austad, T.: Wettability alteration and improved oil recovery by spontaneous imbibition of seawater into chalk: impact of the potential determining ions Ca^{2+}, Mg^{2+}, and SO_4^{2-}. Colloids Surf. A **301**(1–3), 199–208 (2007)

Zimmermann, U., Madland, M.V., Nermoen, A., Hildebrand-Habel, T., Bertolino, S.A.R., Hiorth, A., Korsnes, R.I., Audinot, J.N., Grysan, P.: Evaluation of the compositional changes during flooding of reactive fluids using scanning electron microscopy, nano-secondary ion mass spectrometry, X-ray diffraction and whole rock geochemistry. Am. Assoc. Pet. Geol. Bull. **99**(5), 791–805 (2015). https://doi.org/10.1306/12221412196

Affiliations

Jaspreet S. Sachdeva[1,2] · Anders Nermoen[1,3] · Reidar I. Korsnes[1,2] · Merete V. Madland[1,2]

Anders Nermoen
aner@norceresearch.no

[1] The National IOR Centre of Norway, University of Stavanger, Stavanger, Norway

[2] Department of Energy Resources, University of Stavanger, Stavanger, Norway

[3] NORCE - Norwegian Research Centre AS, Essendrops gate 3, 0368 Oslo, Norway

Paper II

Sachdeva, J.S., Muriel, H., Nermoen, A., Korsnes, R.I., and Madland, M.V. (2019). Chalk Surface Area Evolution during Flow of Reactive Brines: Does Oil Play a Role? *Energy & Fuels*, **33**(6), 4890-4908. https://doi.org/10.1021/acs.energyfuels.9b00515.

energy&fuels

Article

Cite This: Energy Fuels XXXX, XXX, XXX−XXX

pubs.acs.org/EF

Chalk Surface Area Evolution during Flow of Reactive Brines: Does Oil Play a Role?

Jaspreet S. Sachdeva,*[,†,‡] Herman Muriel,[§] Anders Nermoen,[†,∥] Reidar I. Korsnes,[†,‡] and Merete V. Madland[†,‡]

[†]The National IOR Centre of Norway and [‡]Department of Energy Resources, University of Stavanger, Ullandhaug, 4036 Stavanger, Norway

[§]Department of Process Engineering, Memorial University of Newfoundland, St. John's, Newfoundland A1C 5S7, Canada

[∥]Norwegian Research Centre AS, 0368 Oslo, Norway

ABSTRACT: Prolonged injection of magnesium chloride ($MgCl_2$) brine into water-wet chalk cores leads to dissolution of calcite and precipitation of magnesium-bearing minerals. In low permeable and highly porous chalk, the mineral surfaces dominate multiphase flow properties. The hydrophobic/hydrophilic behavior of these mineral surfaces is subject to changes when aged in oil at high temperature over time, and from mineral dissolution and precipitation processes. In this study, we evaluate to which extent chemical interactions induced by the continuous $MgCl_2$ brine injection modify the water wetness of chalk samples saturated by oil/water mixtures and compare the evolving results to a 100% water-saturated parallel reference test. The potential of $MgCl_2$ brine to improve the oil recovery after the freely movable hydrocarbons are produced is also assessed. In situ wettability measurements were carried out during the injection program using chromatographic separation, where the delay in the increase of effluent concentration of the adsorbing sulfate ion was compared to a nonaffine tracer. These measurements were performed every 10 days to estimate the evolution in mineral surface area in contact with water. The results show an increased delay time for the sulfate ion, linked to an increase of the mineral surface area. This is observed in both water-wet and mixed-wet cores, but is found to be more dominating in the mixed-wet samples. This implied that oil, which was adsorbed on the mineral surfaces, got mobilized in addition to an increased overall specific surface area as new magnesium-bearing minerals precipitated and grew during the $MgCl_2$ brine flow. This is supported by continuous effluent analysis displaying a reduced magnesium and increased calcium concentration. Petrophysical analysis of cores before and after flow displayed trends along the axis of the sample. Changes in density and specific surface area were more dominant on the inlet side than the outlet side. Even though magnesium (Mg^{2+}) ions in the injection brine increased the available water-wet area in the samples, the nonequilibrium chemical reactions did not lead to additional oil recovery.

1. INTRODUCTION

To understand how hydrocarbons are extracted from a reservoir, it is important to consider how hydrocarbons are trapped during secondary production by water injection. Two effects that lead to nonzero residual oil saturation as water is injected are (a) Young−Laplacian trapping, when the hydraulic pressure difference across an oil ganglia is insufficient to overcome the oil/water surface tension of water-wet and narrow pore throats and (b) unconnected oil films bonded to mineral surfaces are immobile when hydraulic pressure gradients are imposed. In both cases, nonzero oil residuals are expected whether the mineral surfaces in the porous media are water- or oil-wet.

The way in which fluids partition inside each pore is dictated by the surface affinity to the different fluids; water-wet hydrophilic surfaces attract water molecules, oil-wet hydrophobic surfaces attract oil, while neutral wet surfaces have either no energetic preference to oil or water or if a sample consists of a mixture of minerals, this may give rise to a mixture of water- and oil-wet mineral surfaces.

There are several ways in which the surface wetness can be estimated. In Sachdeva et al.,[1] a series of measurement techniques (contact angle, United States Bureau of Mines (USBM), and scanning electron microscopy-mineral liberation analysis (SEM-MLA)) were applied to Kansas chalk exposed to the same wettability alteration technique with increasing aging time. It was found that a stable mixed-wet state was obtained after 21 days of aging. Contact angle method is used to obtain a measure of the wetting preference of a solid by a liquid. A droplet of a liquid is placed onto a flat solid surface using a syringe. Depending on the movement of the droplet, an advancing or a receding contact angle can be measured.[2−4] This procedure of estimating wettability using contact angle is limited to the availability of flat surfaces as any roughness and angularity of the surface would alter the measurement.

The Amott method[5] combines imbibition and forced displacement to measure the average wettability of a core sample. The method is based on the observation that a wetting fluid will imbibe spontaneously into the core, displacing the nonwetting fluid.[4] The original Amott method procedure starts with the centrifuge of oil saturated core with brine until residual oil saturation (S_{or}) is reached. In the modified Amott−Harvey method,[6] the core is centrifuged first with brine and then with oil to reduce the plug to irreducible water saturation

Received: February 20, 2019
Revised: April 24, 2019
Published: May 9, 2019

DOI: 10.1021/acs.energyfuels.9b00515
Energy Fuels XXXX, XXX, XXX−XXX

(S_{wi}). The USBM method also measures the average wettability of core plugs by quantifying the work necessary for one fluid to displace the other. The work is proportional to the area under the drainage and imbibition capillary pressure curves.[4,7−9]

Strand et al.[10] developed another method to quantify wettability in chalk using chromatographic tests, where a brine containing surface-active sulfate ions and inert thiocyanate tracer ions is injected (after a period of flooding by a brine without sulfate and tracer). Since sulfate ions adsorb on the calcite surfaces in contact with water, the increase in sulfate concentration in the effluent is delayed compared to the increase in concentration of the nonaffine tracer. The dynamics at which surface-active ions are retained within the sample during brine flow are assumed to be proportional to the amount of surface in contact with water.[10,11]

In addition, there are other qualitative methods, such as SEM-MLA,[1,12,13] cryo-scanning electron microscopy, environmental scanning electron microscopy,[14−20] and flotation method,[21,22] of wettability determination that are found in the literature.

Considerable research has been carried out concerning chalk behavior since the detection of subsidence in the Ekofisk field at the Norwegian North Sea around 30 years ago.[23−34] In 1987, seawater injection was commenced in the Ekofisk field as means of pressure maintenance and improved oil recovery.[35] Research has shown that injection of seawater and other simplified brines through chalk leads to irreversible chemical reactions because of nonequilibrium of the surface at the rock−brine contact. These reactions lead to dissolution−precipitation processes within chalk if magnesium (Mg^{2+}) ions are present in the brine.[32,36−42] Sulfate ions present in the seawater also contribute to the formation of anhydrite, which enhances calcite dissolution.[31,32,43−46] It is assumed that these nonequilibrium processes can only occur when the water is in direct contact with the rock surface. As such, the amount of ion exchange, because of chemical reactions between the rock surface and the pore water, in wettability-altered samples is reduced.

It has been previously shown that when $MgCl_2$ brine is flooded through chalk, dissolution of calcite $CaCO_3$ and precipitation of magnesite $MgCO_3$ occur.[32,38−42,47] The precipitated minerals that were not present in the samples originally grow from nucleation seeds. It has been further suggested that chemical reactions between the injected brine and chalk surface lead to additional oil recovery from chalk.[46] Further, the divalent Mg^{2+} ions have also shown to adsorb on available sites leading to desorption of calcium (Ca^{2+}) ions from the internal calcite surface.[48−50] This results in stiffening of chalk due to a lower internal repulsive electrostatic force.

The specific surface area (SSA) of a given amount of substance depends on the size of minerals. For monodisperse spherical grains, the SSA (in units m^2/g) scales with $1/r$, where r is the radius of the grains. As an example, a 1 μm spherical grain of density 2.71 g/cm^3 would correspond to an SSA of 2.21 m^2/g. Even though chalk possesses a variability in particle size of angular grains, the scaling of SSA with respect to particle size is maintained. As such, the precipitation of new minerals from nucleation seeds and their growth at the expense of calcite dissolution would affect the SSA in a nontrivial way. A basic premise of this paper is that the oil and/or water wetness of the porous medium is a dynamic property that can be experimentally tuned via aging procedures.[51−54] Aging is performed by saturating the samples with oil and water and leaving the fluids in the samples to redistribute over time at elevated fluid pressure and temperature, thereby changing the affinity of the mineral surface. It is further assumed that the divalent surface-active sulfate ions are adsorbed onto the charged calcite surface, an assumption supported by a range of studies.[34,50] As such, the concentration of sulfate ions that exit the sample reaches the injected concentration at a later stage than an inert tracer traveling through the sample without adsorbing onto minerals. The sulfate adsorption dynamics were plotted together with thiocyanate (SCN^-) tracer in retention plots. The SCN^- tracer has been shown to be inert[10] to the charged calcite surface. In our investigation, we assumed that the mineral surface area in contact with water is proportional to the area spanned by the sulfate and SCN^- curves.

We report results of four flow-through and surface area experiments on outcrop Kansas chalk: (a) one completely water-saturated sample that has never been exposed to oil, which therefore was water-wet throughout the experiment, and (b) three mixed saturated samples (27−28% irreducible water saturation) that were wettability-altered in aging cells at high temperature before the flow-through experiments started. The mobile oil from these three samples was produced initially during the injection of a nonreactive brine until no more oil could be produced before the chemically reactive $MgCl_2$ brine was injected. This was done to explore if chemical reactions due to nonequilibrium flow would lead to additional oil recovery in the late state of production. After every 10 days of $MgCl_2$ flow, the water-wet surface area was measured to evaluate how wettability modification correlated to additional oil production. We will display experimental results that describe the relation between an evolving surface area induced by the chemical reactions and how solid volume, pore volume, and oil/water volumes evolve with time.

The mineral surface area evolution as a function of time is estimated from the combination of the ion chromatography (IC) data and SSA measurements using the Brunauer−Emmett−Teller (BET) before and after flow-through tests. This evolution is correlated to the changes in the retained area between the thiocyanate and sulfate ions of the effluent data. It is further assumed that the injected $MgCl_2$ brine contacted entire pore volume of the chalk cores giving 100% microscopic sweep efficiency and no viscous fingering occurred.

2. MATERIALS AND METHODS

This section presents an overview of the materials and experimental procedures used in this test study.

2.1. Test Material. Outcrop chalk samples of Late Cretaceous age from a quarry in west central Kansas (USA) were used in this study. The Kansas chalk type is reported to have a noncarbonate content of 1−3%.[34,55] Cylindrical core samples were drilled in parallel from a single chalk block and were radially adjusted to a diameter of 38.1 mm using a lathe. The samples were cut to desired lengths, end pieces were stored, and the cylindrical samples were dried at 110 °C overnight, after which the initial dry mass was measured. The samples were then placed in a vacuum chamber and saturated by distilled water (DW), before taken out for saturated mass measurement. The weight difference between the dry and saturated samples was used to estimate the saturated pore volume (see Table 1).

The four chalk samples (KA1−KA4) used in this study had a saturation porosity of 35.2−37.7% (Table 1). The sample labeled KA1 was completely water-wet, whereas the samples labeled KA2−KA4 were saturated by both oil and water before being wettability-altered to a mixed-wet state (section 2.3).

DOI: 10.1021/acs.energyfuels.9b00515
Energy Fuels XXXX, XXX, XXX−XXX

Table 1. Basic Data of the Samples Used in This Study

sample	KA1	KA2	KA3	KA4
wetting state	water wet	mixed wet	mixed wet	mixed wet
length (mm)	68.6	73.2	72.5	71.7
diameter (mm)	38.1	38.1	38.1	38.1
dry mass (g)	136.8	140.8	139.2	137.9
saturated mass (g)	164.4	172.2	170.4	168.1
pore volume (mL)	27.6	31.4	31.2	30.2
bulk volume (mL)	78.2	83.5	82.7	81.7
saturation porosity (%)	35.3	37.6	37.7	36.9
solid volume (mL)	50.6	52.1	51.5	51.5

2.2. Description of Fluids Used. Five brines were used in this study. Two of these brines, SW0T and SW1T, are based on North Sea seawater composition and were used to determine the wettability at frequent intervals through each test. The SW1T brine contained both sulfate (SO_4^{2-}) and thiocyanate (SCN^-) tracers, while the SW0T brine did not; hence, the other salt concentrations were increased in SW0T such that the total dissolved solids (TDSs) were the same for SW0T and SW1T (see Table 2). The three other brines used in this study were

- 1.1 M NaCl sodium chloride brine for initial saturation, to simulate initial resident formation fluids (Table 2). This brine has also shown to weakly interact with chalk.[32,56,57]
- 0.657 M NaCl and 0.219 M $MgCl_2$ magnesium chloride brines, injected during the flow-through tests in triaxial cells. These two brines have the same ionic strength as seawater (0.657) and were used to simulate fluid injection that have taken place in the Ekofisk reservoir (Table 2).

All brines were mixed on a magnetic stirrer and filtered through 0.65 μm filters before use.

The oil mixture used, together with the 1.1 NaCl brine to saturate the KA2−KA4 samples, consisted of a 60−40% volume mixture of crude oil from the Heidrun field offshore, Norway, and heptane. The acid number of the Heidrun oil was measured in our lab to be 2.82 mg KOH/g, while that of the oil mixture was 2.12 mg KOH/g using titration procedure developed by Fan and Buckley.[58]

2.3. Initial Saturation and Wettability Alteration by Aging. The water-wet sample KA1 was saturated by 1.1 M NaCl brine, while the samples KA2−KA4 were prepared according to the following procedure

(i) Saturation by 1.1 M NaCl brine.
(ii) Mounted in Hassler cell and heated to 50 °C.
(iii) Flooded two pore volumes (PVs) in each direction by the oil mixture at a back pressure of 0.7 MPa and a confining pressure of 1.6 MPa. During flooding, the produced brine was collected and its volume was measured to estimate the irreducible water saturation S_{wi}.
(iv) The samples were then submerged in the same oil mixture in aging containers where they were left for 21 days at 90 °C with the entry valves on each side closed (so that the thermal expansion of the oil leads to an internal pressure—remark that cores are permeable so drained conditions were met, and the thermal expansion of the oil leads to negligible local pressure buildup differences inside the cores).

As the differences in the thermal expansion coefficient and compressibility of the oil and water phases at different temperatures and pressures play a role in determining the oil/water saturation, we assume that these effects are not at play in this study and hence consider the oil/water saturations to be equal at both 50 and 90 °C. From here on, the cores KA2−KA4 are referred to as "mixed-wet cores" or "wettability-altered cores".

2.4. Tracer Tests for Wettability Determination Using Chromatographic Separation. Strand et al.[10] developed the chromatographic separation test to estimate the wettability for altered chalk samples. Tracer tests have previously been carried out using Hassler sample holder,[11] but in this study, the triaxial cells were used. The procedure is based on the idea that the water-wet areas of the chalk surface attract sulfate ions (SO_4^{2-}) that are present in the injected brine, i.e., sulfate ions adsorb on the calcite surfaces that are in contact with water. Therefore, when a brine containing sulfate and thiocyanate tracer is injected (into a sample saturated by nonsulfate and nontracer brine), the sulfate is delayed compared to the nonaffine tracer during frequent sampling of the effluent fluids. The key premise in this work is that the area spanned by the sulfate concentration curve compared to the tracer curve of the effluent samples is proportional to the surface area available for the sulfate ions to adsorb. The ratio of the area between curves for a mixed-wet sample divided by the reference area of a water-wet sample defines the wetting index (W_i)

$$W_i = \frac{A_{mw}}{A_{ww}} \tag{1}$$

where A_{mw} and A_{ww} are the areas between the SO_4^{2-} and SCN^- curves for mixed-wet and water-wet samples, respectively. The areas under the SO_4^{2-} and SCN^- curves were determined using the trapezoid method. Sachdeva et al.[11] provide a detailed conceptual description of this technique.

The tracer tests were performed before the injection program started and at frequent intervals along each test. The procedure of each tracer test for wettability determination was as follows: (i) switch off the heating cap allowing the cell to cool down to below 30° (ca. 6−7 h) (remark: the cell was already at ambient temperature for the first tracer test), then (ii) four initial pore volumes (here after termed PV_i) of SW0T brine were injected over approximately 1−3 days to saturate the sample, followed by (iii) the injection of SW1T brine for 500 min with a 0.2 mL/min flow rate. During SW1T injection, 40 samples were collected using Gilson GX-271 fraction sampler. Each sample contained 2 mL of fluid, i.e., the sampling time for each

Table 2. Composition of Brines Used in the Tracer Tests (TTs) and during Flow-Through Tests

	for tracer tests		during flow-through		
ions	SW0T (mol/L)	SW1T (mol/L)	1.1 M NaCl (mol/L)	0.657 M NaCl (mol/L)	0.219 M $MgCl_2$ (mol/L)
HCO_3^-	0.002	0.002	0	0	0
Cl^-	0.583	0.492	1.1	0.657	0.438
SO_4^{2-}	0	0.024	0	0	0
SCN^-	0	0.024	0	0	0
Mg^{2+}	0.045	0.045	0	0	0.219
Ca^{2+}	0.013	0.013	0	0	0
Na^+	0.46	0.393	1.1	0.657	0
Li^+	0	0.024	0	0	0
K^+	0.01	0.034	0	0	0
ionic strength	0.643	0.647	1.1	0.657	0.657
TDS (g/L)	33.39	33.39	64.28	38.40	44.52

DOI: 10.1021/acs.energyfuels.9b00515
Energy Fuels XXXX, XXX, XXX−XXX

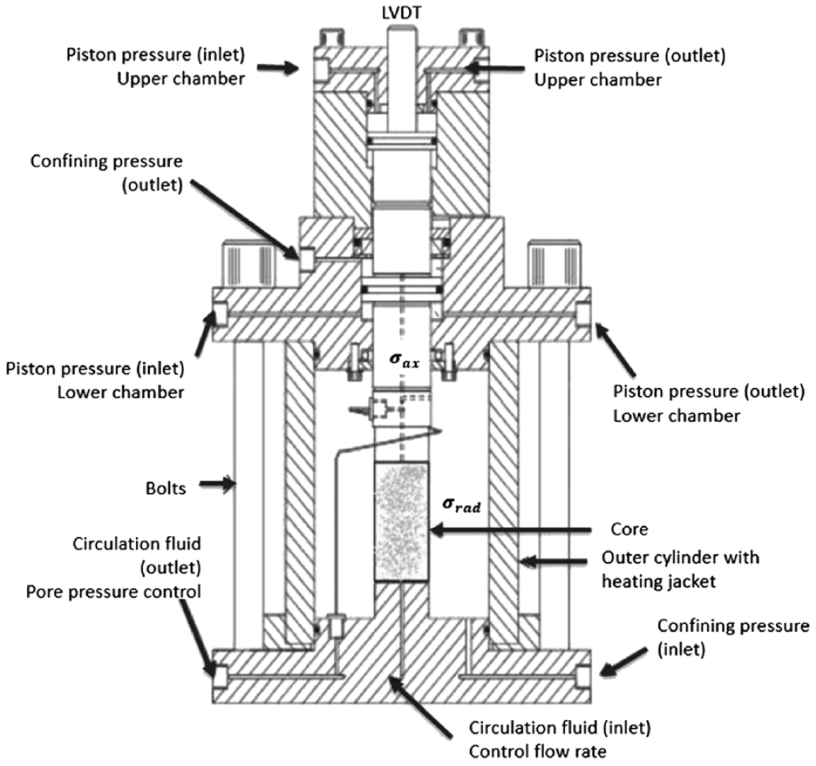

Figure 1. Sketch of the triaxial cell.

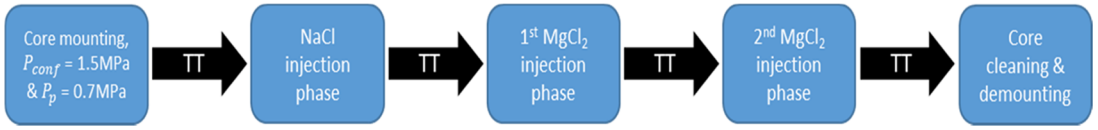

Figure 2. Sketch of the experimental procedure for water-wet sample KA1. The abbreviation TT denotes when tracer tests were performed.

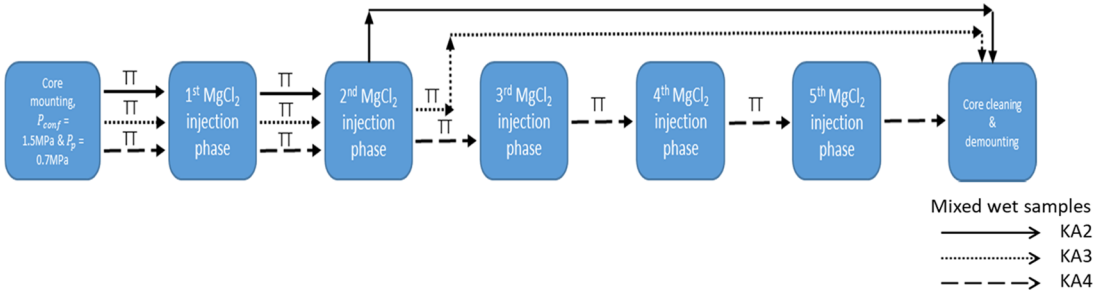

Figure 3. Sketch of the experimental procedure for mixed-wet samples KA2 (solid lines), KA3 (dotted lines), and KA4 (dashed lines). The abbreviation TT denotes when tracer tests were performed.

sample was 10.0 min with a 2.5 min delay between each sample. The concentrations of thiocyanate and sulfate for all samples were determined using IC. Each tracer test (TT) lasted 5−6 days and was performed at ambient temperature.

2.5. Triaxial Test Setup. The chalk samples were mounted into a triaxial cell (Figure 1), which was equipped with a heating element and a regulating system with precise temperature control. Two pumps were connected to the triaxial cell to control the confining pressure (σ_{rad}) and flooding rate (Q). A back-pressure regulator was used on the downstream side to ensure a constant pore pressure (P_p) of 0.7 MPa and to allow the sampling of effluent fluids coming out of the samples that can be tested using IC.

2.6. Experimental Procedure with Time. The experimental procedures followed for the water-wet sample KA1 and the mixed-wet samples KA2−KA4 are mentioned below.

2.6.1. Water-Wet Sample. The experiment conducted on the water-wet KA1 sample was performed according to the following procedures (see the illustration in Figure 2):

1. The KA1 sample saturated by 1.1 M NaCl brine was mounted into the triaxial cell, and the confining pressure (P_{conf}) and pore pressure (P_p) were set to 1.5 and 0.7 MPa, respectively.
2. First tracer test was performed as described in Section 2.4 and was termed "initial/first tracer test".
3. After the tracer test, the sample was saturated by SW1T, which was removed by flooding 4 PV_is of 0.657 M NaCl brine at a rate of 1 PV_i/day at ambient temperature.
4. Increased temperature to 130 °C.
5. Flooded 0.657 M NaCl brine (seawater ion strength) at a rate of 1 PV_i/day at 130 °C for 7.5 days ("NaCl injection phase").

DOI: 10.1021/acs.energyfuels.9b00515
Energy Fuels XXXX, XXX, XXX−XXX

6. Reduced temperature to ambient to perform a "second tracer test".
7. Flooded 4 PV_is of 0.219 M $MgCl_2$ brine at a rate of 1 PV_i/day at ambient temperature to remove SW1T brine.
8. Increased temperature to 130 °C.
9. Injected 0.219 M $MgCl_2$ brine at a rate of 1 PV_i/day at 130 °C for 7 days ("first $MgCl_2$ injection phase").
10. Reduced temperature and performed a "third tracer test".
11. Repeated steps 7−10 and performed a "fourth tracer test": 4 day flow of 0.219 M $MgCl_2$ at ambient temperature to remove SW1T brine, heating to 130 °C and 0.219 M $MgCl_2$ injection for 7 days ("second $MgCl_2$ injection phase").
12. After the fourth tracer test, distilled water (DW) was injected at a rate of 1 PV_i/day to displace leftover salts.

2.6.2. Mixed-Wet Samples. The experimental procedure for the mixed-wet samples (KA2−KA4) was the same as for the water-wet sample, except steps 3−6, i.e., the samples were not flooded by 0.657 M NaCl, and after the first tracer test, the SW1T brine was expelled by 0.219 M $MgCl_2$ brine. The sketch of the experimental procedure is given in Figure 3. The following procedure applied:

1. The wettability-altered samples were mounted into the triaxial cell, and the confining pressure (P_{conf}) and pore pressure (P_p) were set to 1.5 and 0.7 MPa, respectively.
2. First tracer test, described in Section 2.4, termed initial/first tracer test, was performed.
3. After the tracer test, the sample was saturated by SW1T, which was displaced by 4 PV_is of 0.219 M $MgCl_2$ brine at a rate of 1 PV_i/day at ambient temperature.
4. Increased temperature to 130 °C.
5. Injected 0.219 M $MgCl_2$ brine at a rate of 1 PV_i/day at 130 °C for 10 days (first $MgCl_2$ injection phase).
6. Reduced temperature and performed a second tracer test.

From here on, the different samples were treated differently. We will go through from step 7 and describe the procedure for each sample accordingly.

Mixed-wet sample KA2:

7. Switched from SW1T brine to $MgCl_2$ brine flooding for another 7.7 days (second $MgCl_2$ injection phase).
8. Afterward, DW was injected at a rate of 1 PV_i/day to displace leftover salts.

Mixed-wet sample KA3:

7. Repeated steps 3−6 for a second $MgCl_2$ injection phase to perform a third tracer test.
8. After the tracer test, DW was injected at a rate of 1 PV_i/day to displace leftover salts.

Mixed-wet sample KA4:

7. Repeated steps 3−6 three more times for second, third, and fourth $MgCl_2$ injection phases and performed third, fourth, and fifth tracer tests (third tracer test, fourth tracer test, and "fifth tracer test").
8. After the fifth tracer test, switched to $MgCl_2$ brine flooding for another 5.3 days ("fifth $MgCl_2$ injection phase").
9. Afterward, DW was injected at a rate of 1 PV_i/day to displace leftover salts.

During the flow of $MgCl_2$ brine, effluents were collected two to three times per week for IC analysis. This analysis enables the estimation of the amount of chemical reactions taking place at the rock−fluid interface.

From the start of SW0T flooding at step 2 during initial/first tracer test to the end of experiments, the volume of oil produced from the samples was measured. Before finishing the tests, the mixed-wet samples were cleaned using toluene, which was later flushed out by methanol and DW, here referred to as initial cleaning.

2.7. Basic Analysis after Test. After initial cleaning, the samples were demounted from the triaxial cell so that the wet mass, dry mass, length, and diameter could be measured. Afterward, the samples were cut into six sections of almost equal length and tested for density and specific surface area (see Sections 2.10 and 2.11).

After the sections were tested for SSA, they were further cleaned using Soxhlet extraction with toluene as solvent to remove expected traces of oil in the samples. The extraction continued for more than 1 week until no change in the color of toluene was observed, and it remained transparent. The samples were later flooded by methanol to remove toluene, which was later flushed out using DW. Afterward, all sections were again tested for density and SSA. The change in density and SSA before and after the Soxhlet extraction is reported.

2.8. Estimation of Pore Volume after Test. During the triaxial tests, the volume of oil produced and ion composition of the $MgCl_2$ effluent flow were measured. After demounting the samples, oil residuals were expected (even though the initial cleaning was carried out with toluene and methanol). Since the external stress imposed to the samples was insufficient to induce a large volume deformation, the pore volume change was mainly attributed to chemical reactions. In this case, the following apply:

$$V_b = V_p + V_s$$
$$\Delta V_b = \Delta V_p + \Delta V_s \quad (2)$$

Considering that there was no volume deformation in the samples due to the imposed stress

$$\Delta V_b = 0 \quad (3)$$

any change in the solid volume equals the corresponding change in the pore volume, and eq 2 becomes

$$\Delta V_s = -\Delta V_p \quad (4)$$

The pore volume at any time is given by the initial pore volume plus its change

$$V_p = V_{p,o} + \Delta V_p \quad (5)$$

such that we may use the solid volume estimate to calculate the pore volume after test

$$V_p = V_{p,o} - \Delta V_s \quad (6)$$

Here, V_b, V_p, and V_s are the bulk, pore, and solid volumes at any given time; $V_{p,o}$ is the original pore volume; and ΔV_b, ΔV_p, and ΔV_s are the changes in the bulk, pore, and solid volumes, respectively, at any given time.

The change in the solid volume comes from the dissolution of calcite and precipitation of magnesium-bearing minerals during the flow of $MgCl_2$ brine.[38,47] In these one-phase studies, the mass and density measurements were not obstructed by the presence of oil. Hence, it can be assumed that

$$\left(\frac{n_{Ca}}{\Delta V_s}\right)_{\text{Nermoen et al.}^{38}/\text{Andersen et al.}^{47}} = \left(\frac{n_{Ca}}{\Delta V_s}\right)_{\text{this study}} \quad (7)$$

where n_{Ca} is the number of moles of calcium dissolved during $MgCl_2$ flow integrated from the ion concentrations obtained from the IC analysis. For our study, we use this correlation to estimate ΔV_s, and hence V_p according to eq 6, after test in relation to Andersen et al.,[47] which used the same Kansas outcrop chalk type and flooded it with the same $MgCl_2$ brine at the same flooding rate as in this study.

With the solid volume after test estimated from IC and the mineral density estimated using pycnometer (after Soxhlet cleaning), the dry mass of samples KA2−KA4 could be estimated. The weighted average of density ρ_{avg}, used for the dry mass calculation, was estimated using

$$\rho_{avg} = \frac{\sum_{i=1}^{6} m_{dry,i}\rho_i}{\sum_{i=1}^{6} m_{dry,i}} \quad (8)$$

where $m_{dry,i}$ and ρ_i are the dry mass and density of the section i of the sample, respectively. After testing, the samples were nonhomogeneously deformed such that the bulk volume, V_b, was given by the sum of truncated wedges

DOI: 10.1021/acs.energyfuels.9b00515
Energy Fuels XXXX, XXX, XXX−XXX

$$V_b = \sum_i \frac{\pi h_i}{12}(D_i^2 + D_{i+1}^2 + D_i D_{i+1}) \quad (9)$$

where we measure the diameter D_i along the length of the sectioned sample at intervals h_i.

2.9. Ion Chromatography (IC) Procedure. The ion compositional analysis of all effluent samples taken during the experiments were performed using the Dionex IC S-5000+ Ion Chromatography System. The IC process allows the separation and quantification of ion concentrations based on their affinity to the ion exchanger.

To perform the IC analysis, the effluent samples were diluted 500 times with deionized water to meet the linear regime of the Dionex IC S-5000+ Ion Chromatography System. The dilution of the samples was performed using the Gilson GX-271 liquid handler operated using the Trilution software. Once the analysis was finished, a series of peaks, corresponding to each ion in the effluent sample, was obtained. The area under each peak was assumed to be proportional to the corresponding ion concentration in the fluid compared to known standard with known concentrations.

2.10. Mineral Density Determination. The mineral density was estimated by gas pycnometry. Cut sections of all samples were kept in an oven at 110 °C overnight before the mineral density was estimated. The following morning, these sections were taken out and kept in a vacuum-sealed container to cool down to room temperature. The dry mass of each section was measured and inserted, one-by-one, into the Micromeritics AccuPyc II 1340 gas pycnometer (using helium) to measure the solid volume, and hence the average mineral density of each section.

2.11. Specific Surface Area (SSA) Determination. The SSA was estimated by the Brunauer–Emmett–Teller (BET) theory, which works on the principle of physical adsorption of gas molecules on a solid surface.[59] The SSA measurements were carried out on Micromeritics TriStar II instrument. Liquid nitrogen was used for the measurement purpose, as it does not chemically react with chalk. Powdered chalk (2 g) was added to the sample glass tube and degassed for 5 h at 110 °C on Micromeritics VacPrep 061 Sample Degas System. A stable vacuum pressure of around 20–30 mTorr was attained for all tested samples. Afterward, these sample tubes were attached to the BET apparatus and the SSA was measured automatically by the TriStar II 3020 software.

3. RESULTS

The experimental results are presented in different sections: (i) Measurement of irreducible water saturation for mixed-wet samples; (ii) water-wet area evolution with time from chromatographic separation (tracer) tests for all samples; (iii) oil volume development with time for the mixed-wet samples; (iv) effluent sample analysis using IC for all samples; and (v) analysis of samples after tests.

3.1. Measurement of Irreducible Water Saturation (S_{wi}) for Mixed-Wet Samples. The irreducible water saturations for the three mixed-wet samples KA2–KA4 were estimated during the wettability alteration procedure within the Hassler cell. The irreducible water saturations were found to be remarkably similar, i.e., 28.3, 27.2, and 27.1%, respectively (Table 3).

3.2. Chromatographic Separation for the Water-Wet Sample (KA1). The initial tracer test was performed on the water-wet sample KA1 before the injection process started; thereafter, tracer tests were performed after NaCl brine had been injected for 7.5 days, and after two injection periods of $MgCl_2$ brine for 7 days each. During injection of $MgCl_2$ and NaCl, the temperature was 130 °C such that chemical reactions could occur. The aim was to quantify how the two brines affected the area spanned by the sulfate–thiocyanate concentration curves. Figure 4a displays the normalized concentration data along y axis and PV_i of SW1T injected along x axis. It can be seen how thiocyanate concentration increases ahead of the sulfate concentration and the rise in sulfate concentration is delayed in comparison. The area spanned between the thiocyanate and sulfate curves is displayed in Figure 4b, whereas the area per gram of the core is reported in Table 4. The integrated area between the curves is given in units of PV per gram to capture the sample size effect. The time (in PVs) required to reach half the integrated area is also reported in Table 4.

The initial tracer test yielded an area (orange curve in Figure 4b) of 1.45×10^{-3} PV/g, while after NaCl injection for 7.5 days, the curve changed its shape, but the area increased insignificantly to 1.46×10^{-3} PV/g, i.e., an increase of 0.7%. After $MgCl_2$ brine was injected for 7 days, the second tracer test was performed and the area (black curve) increased to 1.60×10^{-3} PV/g, i.e., an increase of 10.3%. After a second $MgCl_2$ brine injection phase for another 7 days, the area increased to 1.75×10^{-3} PV/g, i.e., 20.7% increase compared to the initial tracer test and 9.4% compared to the first $MgCl_2$ injection phase. These results show how the surface area that plays a role in sulfate adsorption increases with time. This area is not necessarily the same as the surface area measured by helium adsorption using BET technique.

Figure 4b also displays how the difference evolves through time, where the curves shift toward the right, and the maximal difference between the thiocyanate and sulfate tracer increases each time.

3.3. Chromatographic Separation for the Mixed-Wet Samples (KA2–KA4). Three mixed-wet samples, KA2–KA4, were used to test the hypothesis that $MgCl_2$ brine could modify the wetting state of mixed-wet chalk and thereby eventually lead to increased oil recovery (in our case, more oil being displaced from the cores). For the three samples, one, two, and four tracer tests were performed. Each tracer test was performed after $MgCl_2$ brine was injected for 10 days in each phase at a rate of 1 PV_i/day at 130 °C.

For KA2–KA4, the initial tracer test yielded areas of 0.81×10^{-3}, 0.86×10^{-3}, and 0.86×10^{-3} PV/g, respectively. This implies water wetnesses of 0.56, 0.59, and 0.59 for the three cores (using eq 1), respectively, by using the area estimated for the water-wet reference sample KA1 (1.45×10^{-3} PV/g).

For the three cores after 10 days $MgCl_2$ injection at 130 °C, the area between thiocyanate and sulfate concentration curves changed to 1.41×10^{-3}, 1.38×10^{-3}, and 1.35×10^{-3} PV/g, respectively. The corresponding wetting indices changed to 0.97, 0.95, and 0.93 for KA2–KA4, which corresponds to an increase in the water-wet surface area by factors of 1.73, 1.61, and 1.57 compared to the surface area before $MgCl_2$ injection started. Then, KA2 was dismantled for analysis while further $MgCl_2$ injection of KA3 and KA4 continued.

After another 10 days of $MgCl_2$ injection at 130 °C, the water-wet surface area of KA3 and KA4 increased to 1.50×10^{-3} and 1.55×10^{-3} PV/g, respectively, namely, an increase of the water-wet surface available for sulfate adsorption by

Table 3. Oil/Water Volume Estimate from Hassler Cell Flow

mixed-wet sample	KA2	KA3	KA4
irreducible water volume (mL)	8.9	8.5	8.2
irreducible water saturation S_{wi} (%)	28.3	27.2	27.1
initial oil volume (mL)	22.5	22.7	22.0

DOI: 10.1021/acs.energyfuels.9b00515
Energy Fuels XXXX, XXX, XXX–XXX

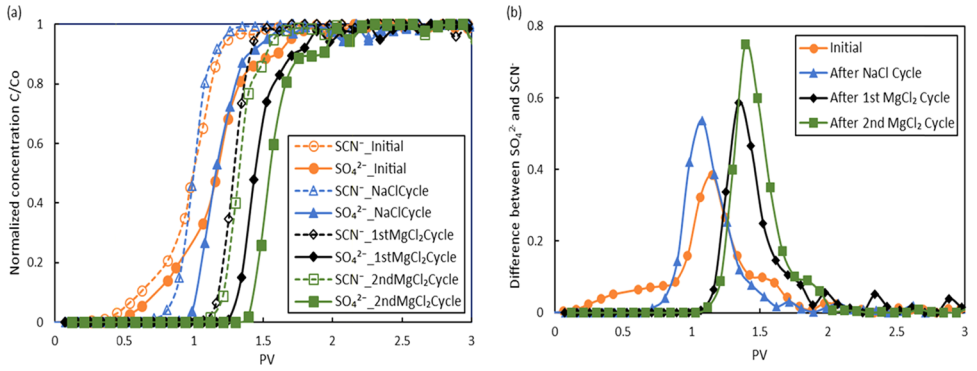

Figure 4. (a) Chromatographic separation during SW1T injection at ambient temperature on KA1. The normalized concentrations for thiocyanate (dashed curves) and sulfate (solid curves) ions are shown for initial tracer test (orange), after 7.5 days of NaCl injection (blue), after 7 days of first $MgCl_2$ injection (black), and after 7 days of second $MgCl_2$ injection (green). The integrated areas between thiocyanate and sulfate are given in Table 4. (b) Difference between SCN^- and SO_4^{2-} as a function of PVs injected for each tracer test.

Table 4. Estimated Integrated Areas Per Gram of the Sample for Water- and Mixed-Wet Samples, and the Corresponding Wettability Indices[a]

sample	timing of tracer test	number of injection days at 130 °C	area between sulfate and SCN (PV)	integrated sulfate tracer area per gram sample (10^{-3} PV/g)	time to half area[b] (PV)	wetting index (W_i)
KA1 water wet	initial tracer test	0	0.20	1.45	1.40	1.00
	NaCl inj.	7.5	0.20	1.46	1.39	1.01
	first $MgCl_2$ inj.	14.5	0.21	1.60	1.42	1.10
	second $MgCl_2$ inj.	21.5	0.24	1.75	1.47	1.21
KA2 mixed wet	initial tracer test	0	0.11	0.81	0.94	0.56
	$MgCl_2$ inj.	10.0	0.20	1.41	1.12	0.97
KA3 mixed wet	initial tracer test	0	0.12	0.86	0.95	0.59
	first $MgCl_2$ inj.	10.0	0.19	1.38	1.22	0.95
	second $MgCl_2$ inj.	20.0	0.21	1.50	1.31	1.03
KA4 mixed wet	initial tracer test	0	0.12	0.86	0.86	0.59
	first $MgCl_2$ inj.	10.0	0.19	1.35	1.21	0.93
	second $MgCl_2$ inj.	20.0	0.21	1.55	1.29	1.07
	third $MgCl_2$ inj.	30.0	0.22	1.62	1.31	1.12
	fourth $MgCl_2$ inj.	40.0	0.24	1.71	1.33	1.18

[a]NaCl and $MgCl_2$ were injected at 130 °C for chemical reactions to occur while tracer test was conducted at ambient temperature. [b]Time to half area represents number of PVs of SW1T brine flooded during the corresponding tracer test to reach half of the area (between thiocyanate and sulfate concentration curves) obtained during the test.

factors of 1.74 and 1.80 compared to initial measurement. Both these values are greater than the KA1 reference of 1.45×10^{-3} PV/g, implying that the water-wet surface area increased to more than the surface area of 100% water-wet core, even though significant oil remains in the core (see later sections of the oil production observation). After this second $MgCl_2$ injection phase, the KA3 sample was dismantled for further analysis.

Third and fourth $MgCl_2$ injection phases of 10 days each were conducted for KA4. Here, the integrated area between the thiocyanate and sulfate curves increased to 1.62×10^{-3} and 1.71×10^{-3} PV/g, which correspond to an increase by factors of 1.88 and 1.99, compared to the initial value. The left column of Figure 5a,c,e displays normalized sulfate and thiocyanate concentrations, and the right column ((b), (d), and (f)) displays the difference between sulfate and thiocyanate concentrations as a function of number of PVs of SW1T injected for different tracer tests performed on mixed-wet samples KA2−KA4, respectively.

The plots in Figures 4 and 5 show how the increase in sulfate concentration is delayed compared to the thiocyanate concentration when SW1T brine is injected. Table 4 summarizes the values of the area obtained between the sulfate and thiocyanate ions during tracer tests for all samples.

The evolution in the areas spanned by the SCN^- and SO_4^{2-} curves per gram of the water-wet KA1 sample in Figure 4b and the mixed-wet samples KA2−KA4 in Figure 5b,d,f is displayed together in Figure 6. Here, in Figure 6a, it can be seen how the

DOI: 10.1021/acs.energyfuels.9b00515
Energy Fuels XXXX, XXX, XXX−XXX

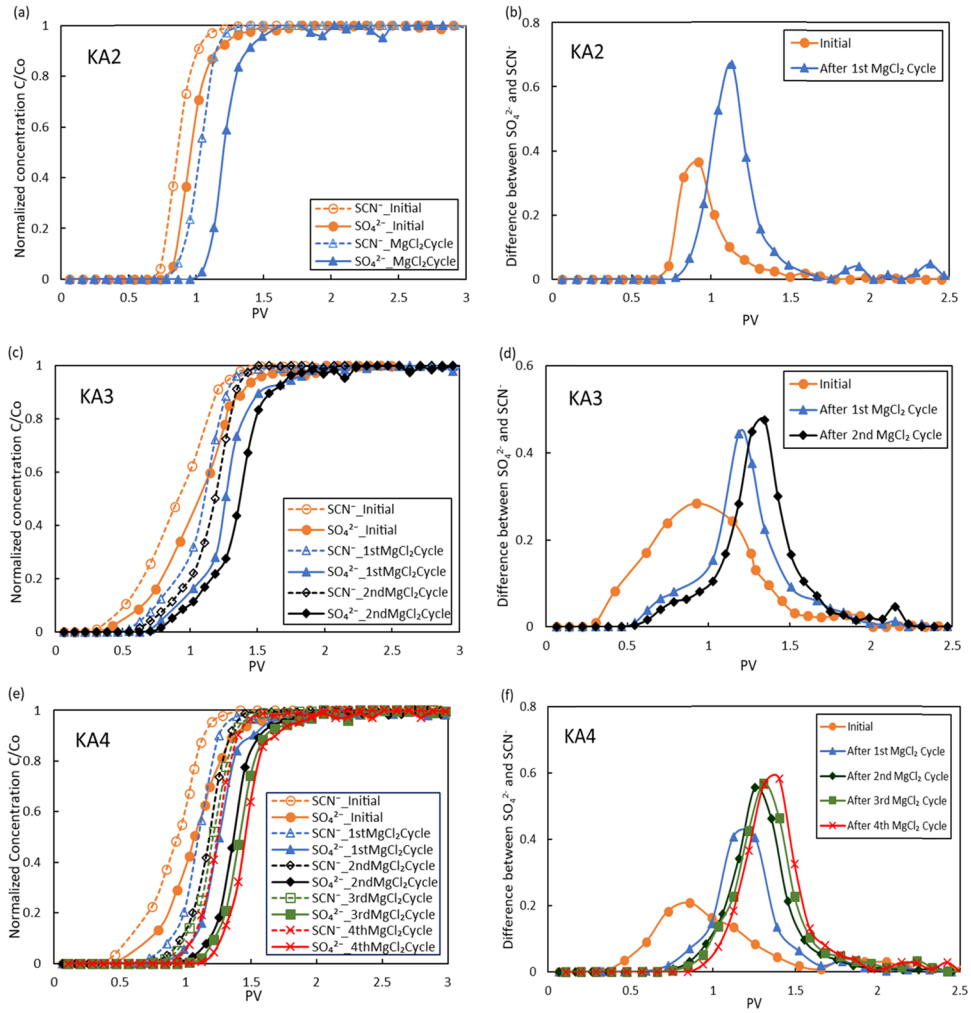

Figure 5. Chromatographic separation test at ambient temperature for the mixed-wet samples KA2−KA4. The left column ((a), (c), and (e)) displays normalized concentrations for thiocyanate (dashed curves) and sulfate (solid curves) and are shown for the initial tracer test (orange), and after first (blue), second (black), third (green), and fourth (red) injection phases of $MgCl_2$ brine each lasting 10 days. The right column ((b), (d), and (f)) displays the difference between sulfate and thiocyanate. Clear trends in the difference are seen, the area increases, the peak increases, and the curve is shifted to the right for each curve (see Table 4 and Figure 6).

continuous $MgCl_2$ injection at 1 PV_i/day evolved the water-wet area available for sulfate adsorption. The amount of fluids required to reach half of the area between the thiocyanate and sulfate (given by the time to half area) as a function of test time at 130 °C is plotted in Figure 6b. As the amount of surface area increased in the core, the required time (i.e., fluid necessary) increased. Further on, the estimated wetting index, compared to the initial surface area of the 100% water-wet core, evolved with increased amount of $MgCl_2$ injection (Figure 6c). After 20 days of $MgCl_2$ injection, both KA3 and KA4 had a surface area exceeding the initial area of KA1, implying that the amount of water-wet area in the core has increased. This is an indication that new mineral phases were growing from nucleation seeds within the core, which is in line with what has been observed for water-wet chalk samples flooded by $MgCl_2$ brine previously.[47]

3.4. Accuracy of the Area Estimate. An assessment of the accuracy of the area estimate was obtained by perturbing each sample in the curve by adding and subtracting a random number drawn from a flat distribution for 5% accuracy, i.e., a random number in the range of −2.5 to +2.5% was added to the normalized concentration (Figure 7a). This number reflects the accuracy of each IC estimate. The accuracy is also supported by the direct observations of the natural variation between nearby samples at the beginning and at the end of the SW1T injection, i.e., from 0 to 0.5 PV and from 2 to 4 PV in Figure 5a. Thus, a variation in this range is seen. The corresponding difference between the curves under which the area was obtained is shown in Figure 7b, where the dashed line represents the actual IC data and the solid blue line represents the perturbed data set. The natural sample accuracy provides a natural accuracy limit of the area estimate. We perturbed the whole data set, as noted above, 50 times such that an average and a standard deviation could be obtained. In this example, the actual data provided an area of 0.199 PV/g using the rapezoid method, while the 50 perturbed data sets provided an average of 0.200 ± 0.008 PV/g (see Figure 7c). As such, a natural accuracy of 0.008 PV/g in the area estimate has been used, and changes within this range are considered insignificant.

3.5. Oil Volume Development with Time for Mixed-Wet Samples. The oil produced during flow of SW0T, SW1T, and $MgCl_2$ brines was collected in a burette placed on the downstream side of the experimental setup and read by eye

DOI: 10.1021/acs.energyfuels.9b00515
Energy Fuels XXXX, XXX, XXX−XXX

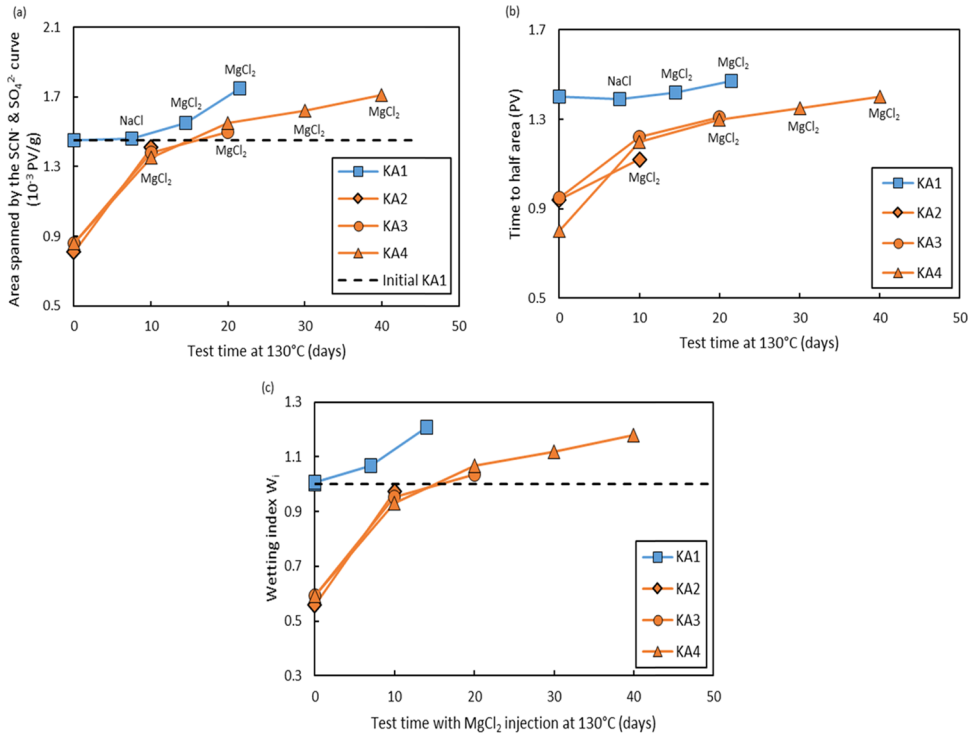

Figure 6. (a) Area spanned by the thiocyanate and sulfate concentration curves for water-wet sample KA1 (blue) and mixed-wet samples KA2−KA4 (orange) as a function of test time at 130 °C. (b) Time required to reach half of the area between thiocyanate and sulfate concentration curves as a function of test time at 130 °C for all samples. (c) Evolution of wetting index as a function of $MgCl_2$ brine injection days at 130 °C for all samples. The black dotted line in (c) gives the wetting index of a completely water-wet core (equal to 1).

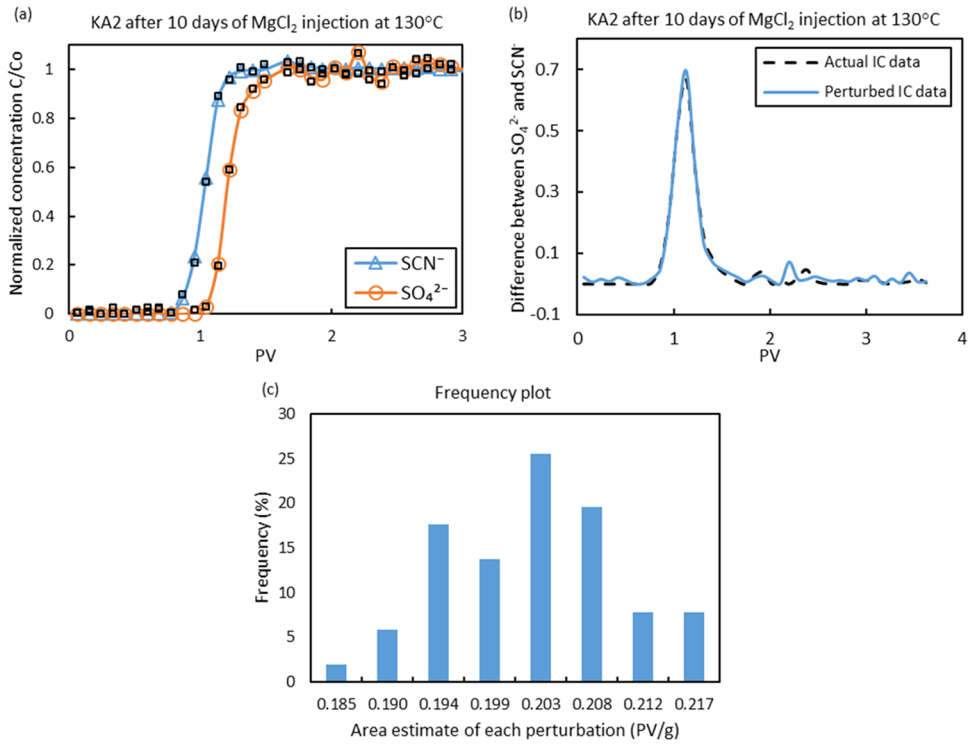

Figure 7. (a) Actual IC data and perturbed IC data by adding 5% noise to each data point (solid squares), (b) the corresponding difference between the SCN^- and SO_4^{2-}, (c) frequency plot of the perturbed areas (50 times), where *x* axis displays the area estimate of each perturbation.

at frequent intervals. The readings were taken more frequently in the starting, and then the frequency of taking readings was reduced. Initially, from the preparation of the samples, the KA2−K4 samples contained 22.5, 22.7, and 22.0 mL of oil, respectively, corresponding to initial water saturations of 28.3, 27.2, and 27.1%. The total amounts of oil produced from KA2−KA4 at the end of tests were 8.5, 11.1, and 7.1 mL, respectively, and all of the oil was produced during the initial

DOI: 10.1021/acs.energyfuels.9b00515
Energy Fuels XXXX, XXX, XXX−XXX

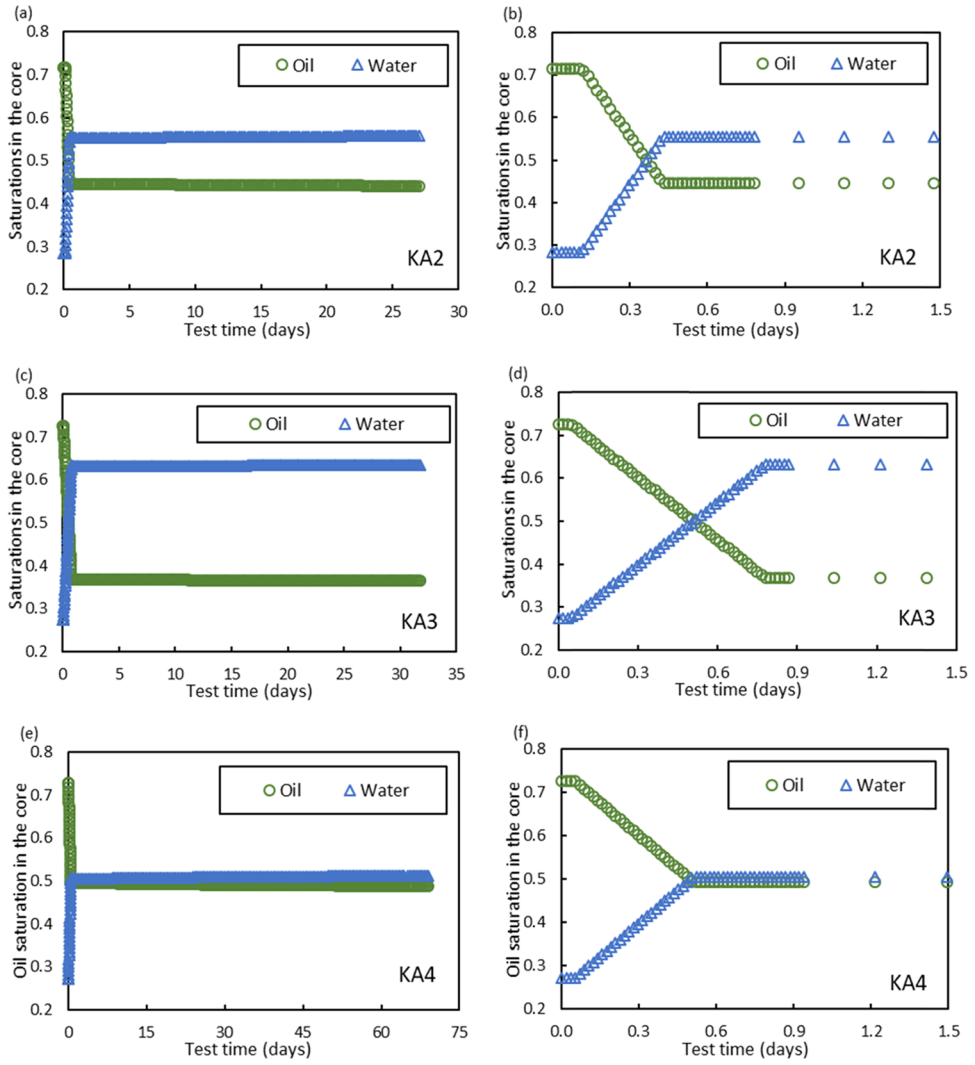

Figure 8. Left column (a, c, e): oil and water saturations in the mixed-wet samples KA2−KA4 (green and blue markers, respectively) during the duration of the test; right column (b, d, f): zoomed version of the oil and water saturations in the samples from the start to 1.5 days.

flooding of the sample by SW0T brine for the initial tracer test. No more oil was produced during flooding of brines during later tracer tests and during flow-through of $MgCl_2$ brine.

The left column of Figure 8 gives the oil and water saturations in the mixed-wet samples at any given time during the test, and the right column shows a zoomed version of these saturations from the start of flooding up to 1.5 days of flooding. As can be seen from the figures in the left column, the oil saturation decreased and the water saturation increased with time. This is because the pore volume increased with time, but no more oil produced. Hence, the sample expanded by increasing the water volume, while the oil volume remained constant.

Sample KA2 was dismantled after a total of 17.7 days of $MgCl_2$ injection, while KA3 and KA4 were dismantled after days and 45.3 days of $MgCl_2$ injection, respectively. The total volume of oil produced during tests and hence the amount of oil remaining in the samples are reported in Table 5.

3.6. Effluent Analysis Using Ion Chromatography for All Samples. Effluent fluid samples were acquired during the injection of brines. The ion concentration of each sample was estimated in the ion chromatograph and compared to the injected ion concentration to quantify the amount of nonequilibrium rock−fluid interactions that take place between the injected fluid and the rock. In all, two to three samples were acquired per week for all tests.

Table 5. Measured Final Oil Volumes for the Mixed-Wet Samples after Test

mixed-wet sample	KA2	KA3	KA4
oil produced at the end of test (mL)	8.5	11.1	7.1
oil volume left in the sample (mL)	14.0	11.6	14.9
oil saturation after test (%)	45.3	37.5	50.3
amount of $MgCl_2$ injected (L) (and pore volumes)	0.55 (17.8)	0.61 (19.7)	1.25 (40.8)

3.6.1. Ion Concentration of the Effluent from Water-Wet Sample KA1. The time evolution of the effluent Mg^{2+} and Ca^{2+} concentrations and the injected Mg^{2+} concentration during the flow of NaCl and $MgCl_2$ brines through the water-wet sample KA1 is shown in Figure 9.

During flooding of NaCl brine, the magnesium concentration is zero as expected, while minute increase in the calcium concentration can be seen (Figure 9). During the subsequent injection of $MgCl_2$, we observe a decrease in the

DOI: 10.1021/acs.energyfuels.9b00515
Energy Fuels XXXX, XXX, XXX−XXX

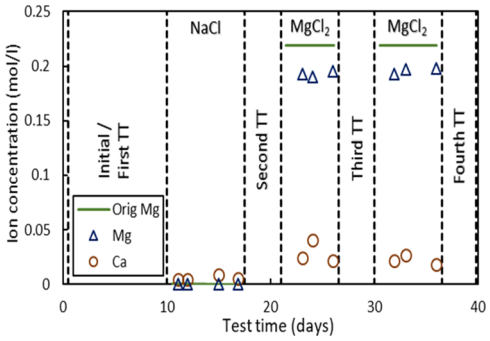

Figure 9. Effluent-ion concentrations of calcium and magnesium ions, and the injected magnesium-ion concentration over time for the water-wet sample KA1. TT stands for tracer test.

magnesium concentration and an increase in calcium concentration. These trends are in line with previous observations as nonequilibrium between the calcite surface and $MgCl_2$ brine leads to dissolution of calcite and precipitation of magnesium-bearing minerals.[32,38−42,47,60−62] The magnesium-ion concentration stabilized around 0.19−0.20 mol/L, and the calcium-ion concentration varied between 0.02 and 0.04 mol/L.

The integrated total magnesium retained for the water-wet sample KA1 was 0.006 mol, which corresponds to a gain of 0.15 g of Mg that gets precipitated as secondary minerals in the sample. Similarly, an amount of 0.008 mol corresponding to 0.32 g of calcium dissolved from the core. In all, a weight loss of −0.17 g was expected from the IC analysis.

3.6.2. Ion Concentration of the Effluent from Mixed-Wet Samples KA2−KA4. The time evolution of the effluent Mg^{2+} and Ca^{2+} concentrations and the injected Mg^{2+} concentration during $MgCl_2$ flow through the mixed-wet samples KA2−KA4 is shown in Figure 10. Despite being saturated by oil, the same observations as the 100% water-saturated KA1 can be inferred from the analysis of these samples. The retention of magnesium (i.e., lower produced concentration than injected) is observed during $MgCl_2$ injection, and the produced magnesium concentration gets stabilized around 0.20 mol/L. Similarly, calcium is lost from the sample as calcium carbonate ($CaCO_3$) dissolves and eventually the calcium concentration decreases to reach a plateau around 0.015 mol/L. The integrated total magnesium retained for the mixed-wet sample KA2 was 0.015 mol (0.35 g), and the calcium dissolved and produced was 0.015 mol (0.59 g). The integrated total magnesium retained for the mixed-wet samples KA3 and KA4 were 0.012 mol (0.28 g) and 0.028 moles (0.68 g), respectively. Similarly, the calcium dissolved and produced from KA3 and KA4 were 0.012 mol (0.47 g) and 0.024 mol (0.97 g), respectively.

The integrated amounts of calcium produced from the core and magnesium retained in the core are obtained from the curves in Figures 9 and 10. These results are given in Table 6. The expected change in solid volume and the corresponding pore volume after test for the mixed-wet samples KA2−KA4 are estimated using eqs 7 and 6, respectively. In Andersen et al.,[47] n_{Ca} = 0.046 mol, and the corresponding change in the solid volume ΔV_s = 0.95 mL. These values have been used in eq 7 to estimate the solid volume change here. The measured pore volume for all samples from saturation tests, explained in Section 3.7, is also reported in Table 6. The difference between the estimated pore volume using eq 6 and the corresponding value from saturation tests give an estimate of the oil volume left after initial cleaning of the mixed-wet samples in the triaxial cell (see section 3.7).

3.7. Analysis of Samples after Test. Basic measurements were carried out on all four samples after the completion of

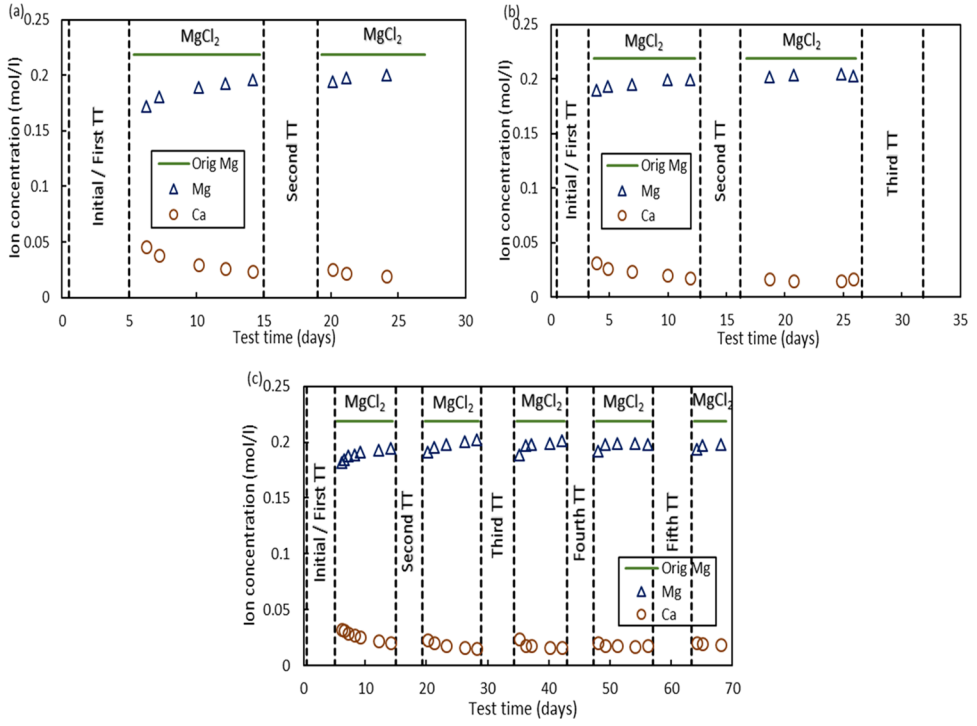

Figure 10. Effluent-ion concentrations of calcium and magnesium ions, and the injected magnesium-ion concentration over time for the mixed-wet samples (a) KA2, (b) KA3, and (c) KA4. TT stands for tracer test.

DOI: 10.1021/acs.energyfuels.9b00515
Energy Fuels XXXX, XXX, XXX−XXX

Table 6. Estimated Magnesium Retained and Calcium Produced from the IC Analysis Obtained during the Tests

sample	magnesium retained n_{Mg} (mol)	calcium produced n_{Ca} (mol)	expected solid volume change from Andersen et al.[47] (eq 7) (mL)	estimated pore volume after test (eq 6) (mL)	measured pore volume from saturation test (mL)	oil volume left after initial cleaning in the triaxial cell (mL)
KA1	0.006	0.008			27.8	
KA2	0.015	0.015	0.31	31.7	30.9	0.8
KA3	0.012	0.012	0.25	31.4	30.9	0.5
KA4	0.028	0.024	0.49	30.7	29.6	1.1

Table 7. Basic Properties of Samples Measured after Tests[a]

		KA2		KA3		KA4	
sample	KA1	after initial cleaning	after additional Soxhlet cleaning	after initial cleaning	after additional Soxhlet cleaning	after initial cleaning	after additional Soxhlet cleaning
length (mm)	68.6 (0.0)	73.1 (−0.1)		72.4 (−0.1)		71.7 (0.0)	
average diameter (mm)	38.1 (0.0)	38.1 (0.0)		38.1 (0.0)		38.0 (−0.1)	
dry mass (g)	136.0 (−0.8)	141.8 (+1.0)	139.8 (−1.0)	140.8 (+1.6)	138.4 (−0.8)	138.7 (+0.8)	135.2 (−2.7)
new bulk volume (cm^3)	78.1 (−0.1)	83.2 (−0.3)		82.5 (−0.2)		81.4 (−0.3)	
new pore volume (cm^3)	27.8 (+0.2)	30.9 (−0.5)	31.7 (+0.3)	30.9 (−0.3)	31.4 (+0.2)	29.6 (−0.6)	30.7 (+0.5)
saturated mass (g)	163.8	172.7	171.5	171.7	169.8	168.3	165.9
new saturation porosity (%)	35.6 (+0.3)	37.1 (−0.5)	38.1 (+0.5)	37.5 (−0.2)	38.1 (+0.4)	36.4 (−0.5)	37.7 (+0.8)
new solid volume (mL)	50.3 (−0.3)	52.3 (+0.2)	51.5 (−0.6)	51.6 (+0.1)	51.1 (−0.4)	51.8 (+0.3)	50.7 (−0.8)
test time (days)	39.9	27.0		31.8		69.0	
test time with $MgCl_2$ injection (days)	12.1	17.7		20		45.3	
mineral density after test (pycnometry, g/cm^3)	2.72	2.67	2.72	2.68	2.71	2.66	2.71
pore volume (mL) and porosity (%) (from pycnometry)	28.1 and 36.0	30.1 and 36.2	31.8 and 38.2	30 and 36.4	31.4 and 38.1	29.3 and 36.0	31.5 and 38.7

[a]Changes compared to initial amount are shown in parenthesis.

Table 8. SSA Measured along the Length of the Samples after Tests[a]

		mixed-wet						
	water-wet	KA2		KA3		KA4		
	KA1	SSA (m^2/g)		SSA (m^2/g)		SSA (m^2/g)		
sample section	SSA (m^2/g)	after initial cleaning	after additional Soxhlet cleaning	after initial cleaning	after additional Soxhlet cleaning	after initial cleaning	after additional Soxhlet cleaning	remarks
outlet end piece	2.19	2.07		2.05		1.85		unflooded
6	1.29	1.07	2.02	1.07	2.08	1.36	2.08	
5	1.65	1.07	2.13	1.09	2.09	1.34	2.16	
4	2.76	1.09	2.45	1.13	2.31	1.46	2.34	flooded sections of the sample
3	2.81	1.12	2.31	1.23	2.17	1.46	2.50	
2	2.60	1.14	2.22	1.32	2.15	1.65	2.45	
1	2.34	1.13	1.96	1.39	2.11	1.61	2.17	
average of 1−6	2.24	1.10	2.18	1.20	2.15	1.48	2.28	
inlet end piece	2.19	2.11		2.07		2.00		unflooded

[a]Mixed-wet samples have SSA values in two columns: the left column gives the value after cleaning the samples with one iteration of toluene and methanol (initial cleaning), and the right column gives the value after additional cleaning in a Soxhlet extractor with the same solvents.

tests, and are reported in Table 7. The water-wet sample was cleaned by DW, while the mixed-wet samples were initially cleaned by toluene, followed by methanol and then DW to flush out methanol. Immediately after demounting, the saturated mass of the samples was determined and the samples were dried in an oven overnight before measuring the dry mass. The difference between these measured values of dry mass and saturated mass gave the pore volume after test. The bulk volume was estimated for all samples from the measurements of length and average diameter (estimated using truncated wedge method; eq 9) after test. Afterward, all four samples were cut into six sections of almost equal length. The sections for the mixed-wet samples KA2−KA4 were further cleaned using Soxhlet extraction. There are two columns shown in Table 7 for the mixed-wet samples KA2−KA4. The left column gives the basic properties of the samples tested after initial cleaning, whereas the right column gives the same properties after the second cleaning using Soxhlet extraction. The pore volume and dry mass of these three mixed-wet samples after the second cleaning were estimated using eqs 2−8. The porosity was estimated from the ratio of the pore volume to the bulk volume.

DOI: 10.1021/acs.energyfuels.9b00515
Energy Fuels XXXX, XXX, XXX−XXX

Measurements of the SSA of unflooded end pieces of these samples, left after cutting the cylindrical cores, and of the tested samples are given in Table 8. The specific surface areas were measured using the BET method. Section 1 represents the section closest to the inlet side, and section 6 represents the outlet section (see Figure 11). There are two values shown for each mixed-wet sample in Table 8. The left column defines the SSA measurement of the pieces that had gone through initial cleaning only in the triaxial cell, and the right column displays the SSA measurements after the pieces were cleaned using Soxhlet extraction. The second Soxhlet cleaning increased specific surface area for all samples, which indicates that oils were left in the core. This was then reflected in the DW saturation tests for pore volume determination in Table 6.

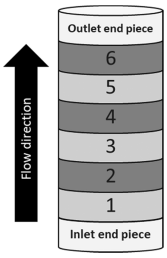

Figure 11. SSA tested along sections acquired from the axis of the sample.

In the water-wet sample KA1, the SSA increased from 2.34 m^2/g at the flooded inlet section to 2.81 m^2/g at the middle, and then decreased to 1.65 and 1.29 m^2/g at the outlet sections of the sample, indicative of how the injected fluid reacts differently with the mineral phases along the length of the sample. The slices of the mixed-wet samples produced a large increase in the specific surface areas after the second cleaning. In all mixed-wet samples, the SSA measurements followed a similar trend to the one followed in the water-wet sample KA1, wherein the SSA increased from the inlet to the middle and then decreased toward the outlet of the samples (Table 8). This may further reveal how different mineral phases and how differently sized minerals react differently with the injected brine.

4. DISCUSSION

Wettability plays a vital role in determining the flow characteristics in a reservoir. Core restoration procedures for the cleaned reservoir samples or water-wet outcrop samples, to establish the original wetting state of a reservoir, are not standardized. There are several procedures reported in the literature about how to establish the initial wetting state of reservoir samples.[1,5−10,21,22,63−65] Simulating experimentally millions of years of interactions between the crude oil, formation water, and reservoir rock within a short restoration procedure will remain a daunting task. Before oil migrates and accumulates in the reservoir rock, the rock is presumed to be completely water-wet. However, when oil gets trapped in the reservoir rock, a new chemical equilibrium is established in reservoir. Reservoir cores are, unfortunately, rarely available for experimentation, so outcrop cores are used to mimic reservoir processes.

Kansas outcrop chalk was used in this study. Water-wet Kansas outcrop chalk samples were flooded with an oil mixture to change the wetting state, simulating the interactions that took place when oil invaded the initially water-wet reservoir rock. To obtain the same initial conditions of the cores after the aging process, all of the mixed-wet samples were prepared with the same methodology that involved the flooding of same volumes of the same fluids in each direction, followed by aging at the same temperature and pressure conditions and for the same duration. This study is the first to visualize how the chemical reaction dynamics are in line with changes in the water-wet surface area with time.

The wettability was determined using the chromatographic separation technique.[10] The results obtained from the samples KA2−KA4 gave initial wettability indices of 0.56, 0.59, and 0.59, respectively (Table 4). This shows that a mixed-wet state was obtained with great repeatability and gives credibility to the estimated evolution in water-wet surface area that was acquired at frequent intervals during the test (every 10 days of $MgCl_2$ flow).

For the water-wet sample KA1, the area obtained between the thiocyanate and sulfate curves remained the same after flooding NaCl brine as before the flooding, supporting the notion that Na^+ and Cl^- ions are inert to weakly reactive to the mineral surfaces in chalk. This is in line with Madland et al.[32] and Sachdeva et al.[11] Later, when the same sample was flooded by $MgCl_2$ brine, an increase in this area was observed with time (Table 4). The time-dependent chemical reactions between the brine and calcite minerals displayed in Figures 9 and 10 are interpreted as (a) magnesium adsorption on available surface sites and (b) dissolution of calcite and precipitation of secondary magnesium-bearing minerals, where the effluent magnesium concentration never reaches the injected concentration and triggers mineralogical changes in the chalk framework. The same behavior has been reported in other similar experimental studies.[11,32,36−41,47,61]

The mixed-wet samples KA2−KA4, which were also flooded by $MgCl_2$ brine, showed similar results in both IC data and evolution of water-wet area, where the brine flow increased the water wetness of the cores, as the water-wet surface area increased after each 10 day $MgCl_2$ flooding cycle (Table 4). The wettability index of samples KA3 and KA4 exceeded 1 after the second $MgCl_2$ injection phase, implying that the available water-wet surface area in these samples exceeded the total mineral area available for the water-wet reference sample KA1. From the effluent analysis of these mixed-wet samples (Figure 10), it is observed that calcium is produced and magnesium is retained in the samples throughout the injection period, in line with the continuous dissolution/precipitation processes taking place in water-saturated samples. Precipitated minerals have been documented to grow using field emission gun-scanning electron microscopy and energy-dispersive X-ray spectroscopy studies.[32,37−42,47,61]

The increase in water-wet area estimated from the tracer tests in all samples during $MgCl_2$ brine injection does not necessarily imply that oil films adsorbed on the mineral surfaces are mobilized. These tracer tests measure the available water-wet adsorption area. Thus, this area will also change due to precipitation and growth of new minerals, e.g., magnesite or talc. Zimmermann et al.,[39] Minde et al.,[41,42] Andersen et al.,[47] and Wang et al.[61] showed occurrence of magnesite crystals, and the absence of coccolith remains in outcrop chalk flooded by $MgCl_2$ brine. Here, we are the first to do the same flow-test analysis of cores saturated by mixture of oil and water, and in the same test program to use 100% water-saturated tests for comparison. Our results indicate that the overall amount of

DOI: 10.1021/acs.energyfuels.9b00515
Energy Fuels XXXX, XXX, XXX−XXX

magnesium-bearing minerals precipitated in a sample was found to be insensitive to the presence of oil. Further on, from Table 4, we observe that the increase in water-wet surface area estimated from the tracer tests is larger for the mixed-wet samples than the water-wet sample. This may imply that the increase in surface area is also dictated by the release of oil films in addition to the precipitation of new mineral surfaces.

The precipitation of magnesium-bearing minerals occurs only onto the water-wet areas. As such, the area available for precipitation of these minerals, in the mixed-wet samples, was smaller to start with due to the oil bonded to some parts of the calcite mineral surface. Now the magnesium retained in the cores is found to be similar for water-wet and mixed-wet samples from the effluent analysis. Hence, for a given amount of magnesium precipitates, the increase in surface area is larger for mixed-wet samples than in water-wet samples.

The changes in Mg- and Ca-ion concentrations in the produced effluents are not only determined by dissolution and precipitation, but also surface processes related to adsorption and desorption occur. This stems from a description of how charges are distributed on the calcite mineral surface. The calcite surface possesses an equal number of positively charged Ca^{2+} and negatively charged CO_3^{2-} surface sites, each with a charge of 1/3 or −1/3,[66] which leads to the adsorption of negative and positive ions from the pore fluid. When $MgCl_2$ brine is flooded through chalk, a new surface equilibrium between the mineral surface and the brine is established. Assuming five negative adsorption sites per nm^2 of sample and that Mg^{2+} ions only adsorb to half the negative sites,[49] it is estimated that 0.20 PV of $MgCl_2$ was required for Mg^{2+} adsorption to occur on all available sites, taking into account an average value of SSA from Table 8 (2.21 m^2/g). The number of Mg^{2+} ions adsorbed in a sample (of approximate average mass 139 g; Table 1) was estimated to be 7.7×10^{20}. Hence, it may be concluded that desorption and adsorption dynamics occurred within the first pore volumes of $MgCl_2$ injected (which was found to be dependent on the ion concentration of the injected brine) and later dissolution and precipitation processes dominated the calcium and magnesium concentrations in the effluents.

Even though nonequilibrium chemical reactions occurred between the brine and the calcite surface (as seen from the IC data of the effluents and the mineral density difference in pycnometry measurements) and the water wetness of the three mixed-wet samples was found to be increasing after each $MgCl_2$ injection phase, no additional oil production was noted from any of these samples. Only a few traces of oil were obtained in the first effluent sample every time the temperature was increased to 130 °C after each tracer test. These traces of oil produced amounted to even less than 0.1 mL in total for all samples. It is assumed that the thermally induced oil mobilization may be explained by the temperature-dependent oil viscosity, allowing oils to be displaced with less energy, or that the temperature variation perturbate the oil/water partitioning on the pore wall and in the pore body. After these experiments, a clear observation is that the ongoing chemical reactions at 130 °C induced by $MgCl_2$ do not contribute to drive oil out of the sample.

Minde et al.[42] and Andersen et al.[47] demonstrated how chemical reactions were more pronounced at the inlet side of the core compared to the outlet slices. The same observation is made in the presented SSA results (Table 8), where SSA increased from the inlet to the middle sections of the samples while it decreased toward the outlet signifying how chemical replacement dynamics occur inhomogeneous along the core due to the dynamics of the flow. We may safely say that the way in which minerals dissolve and precipitate is a function of both the kinetic rates and the kinetics of the flow along the core. These kinetic constants are different for the dissolution and precipitation processes. As $MgCl_2$ moves through porous rock, it will dissolve calcite, and then depending on the nucleation dynamics (the seeds for crystal growth), the new minerals may grow. As such, more precipitation is likely to occur downstream. It has been shown by Minde et al.[42] and Andersen et al.[47] that magnesium-bearing minerals precipitate all the way from inlet to outlet along the length of the core.

Tables 7 and 8 display how solid volume, pore volume, and SSA measurements after test changed for the mixed-wet samples (after initial cleaning compared to their corresponding initial values). According to the experience gained from earlier one-phase studies,[38,47] the change in pore volume is not controlled by compaction and pore collapse in the low effective stress experiments (0.8 MPa in our case), rather the continuous injection of $MgCl_2$ at 130 °C will reduce the solid, hence creating pore volume since the total bulk volume is unaffected. Therefore, it was deduced that oil residuals remained within the samples, i.e., one iteration of toluene and methanol was insufficient for cleaning. Therefore, the samples were cleaned using Soxhlet extraction and the SSA after the second cleaning program provided comparable results to the water-wet sample showing that chemical replacement also occurs when oil is present in the pores. For the mixed-wet cores, we observe that the maximum increase in SSA was achieved for the mixed-wet KA4 sample (from 1.93 originally to 2.28 m^2/g afterward; Table 8). This was the core that was flooded for the longest duration with $MgCl_2$ brine. The other mixed-wet samples, KA2 and KA3, with 17.7 and 20 days, showed an increase in the surface area from 2.09 to 2.18 m^2/g and from 2.06 to 2.15 m^2/g, respectively. Hence, it may seem that the increase in the surface area depends on the quantity of $MgCl_2$ brine flooded through the sample. Multiplying the SSA (the original and final average values) by the dry mass (before and after test) gives the total surface area for each sample (in m^2). This value was correlated with the increase in the integrated areas between the tracer tests (see Figure 12) displaying how the two distinct methods, both of which are used to estimate the surface area, are in line with each other.

In Figure 12, we observe that the slope between the increased integrated surface area (from chromatographic separation along x axis) and the BET surface area (along y axis) is the same for the water-wet sample KA1 and the two mixed-wet samples KA2 and KA3 with test duration of about 20 days (around 20 PV_i's injected). However, for the longest 45 day test, the mixed-wet KA4 has a distinct higher slope (Figure 12). We present evidence here that the $MgCl_2$ injection changes the BET surface area (Table 8), petrophysical properties and mineral density (Table 7), the dynamic ion chromatography (Figures 9 and 10), and the dynamic change in area spanned in the chromatographic separation technique (Figures 4 and 5). The observations are in line and the trends are the same irrespective of the presence of oil inside the cores as long as water come in contact with the rock surfaces inside the porous medium. This provides support to applicability of the petrophysical results obtained in the last few decades, even though they were primarily on 100% water-saturated samples. The change in the petrophysical properties

DOI: 10.1021/acs.energyfuels.9b00515
Energy Fuels XXXX, XXX, XXX−XXX

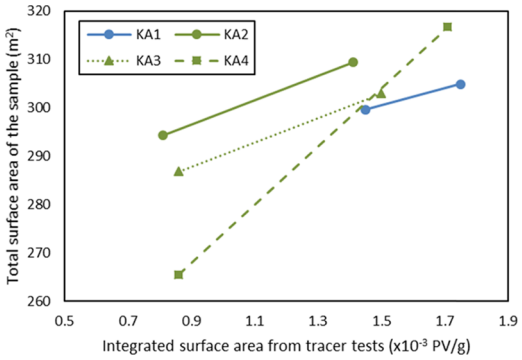

Figure 12. Total surface area of the sample obtained from BET SSA measurements (before and after test) and the increase in the integrated surface area obtained from tracer tests (from Figures 4 and 5). This plot shows how the two distinct methods correlate. The water-wet sample KA1 is shown in blue, and the mixed-wet samples KA2–KA4 are shown in green (solid, dotted, and dashed lines, respectively).

during compaction and reactive flow has shown to be affected by $MgCl_2$ brine due to dissolution of calcite and precipitation of magnesium-bearing minerals in both short- and long-term flooding experiments.[11,32,37−42,47,61]

4.1. Resolving Time-Dependent Dynamics. Since it is not possible to perform BET SSA measurements during the test, while measurements using chromatographic separation technique are possible, the correlations in Figure 12 may become increasingly useful to resolve time-dependent behavior during reactive flow. Further, assuming that grain crushing is not occurring during the test and the change in the overall surface area occurs due to dissolution/precipitation, it is also possible to estimate the change in SSA from the chemical reactions measured by IC (Figures 9 and 10). The IC also enables dynamic estimates of the solid mineral volume, given the mineral densities from pycnometry tests before and after the experiment.

At the same time, the pore volumes were monitored throughout the tests to understand how porosity evolved with time for all samples (Figure 13). These estimates compared to the saturation porosity in Table 7 display a remarkable accuracy, providing support to dynamic estimate of porosity during reaction and flow that was developed by Nermoen et al.[38] We observe an increase in porosity for all samples. During NaCl flow through the water-wet sample KA1 (Figure 13a), the porosity increased marginally from 35.17 to 35.23%, but when $MgCl_2$ was injected, a steeper increase in the porosity was observed. Similar observations were made from the mixed-wet samples where a steep increase in porosity occurred during $MgCl_2$ injection. The chemical reactions, as in this case, lead to the precipitation of denser minerals and mass loss, which both lead to lowering of the solid volume. Since the bulk volume remains the same at these low effective stresses, the dynamics led to an increased porosity. Previous 1072 day-long $MgCl_2$ flooding experimental study at high stress (11.1 MPa)[38] showed that the porosity decreased for the first 150 days before increasing to end up with the final porosity equaling the initial porosity. In our study, the duration of injecting $MgCl_2$ brine is very short compared to the study by Nermoen et al.,[38] and here the bulk volume remains the same since the hydrostatic effective stress is low (0.8 MPa). We have assumed here that there is no porosity change during tracer test (TT) since the tracer test is performed at ambient temperature.

4.2. Estimating Ion Adsorption on Surfaces. The number of sulfate ions adsorbed on calcite surface during SW1T brine flooding was estimated for all samples and was found to increase with increasing number of $MgCl_2$ injection phases (Table 9), signifying the formation of new water-wet surfaces. For the water-wet sample KA1, the number of sulfate ions adsorbed remained unchanged between the initial tracer

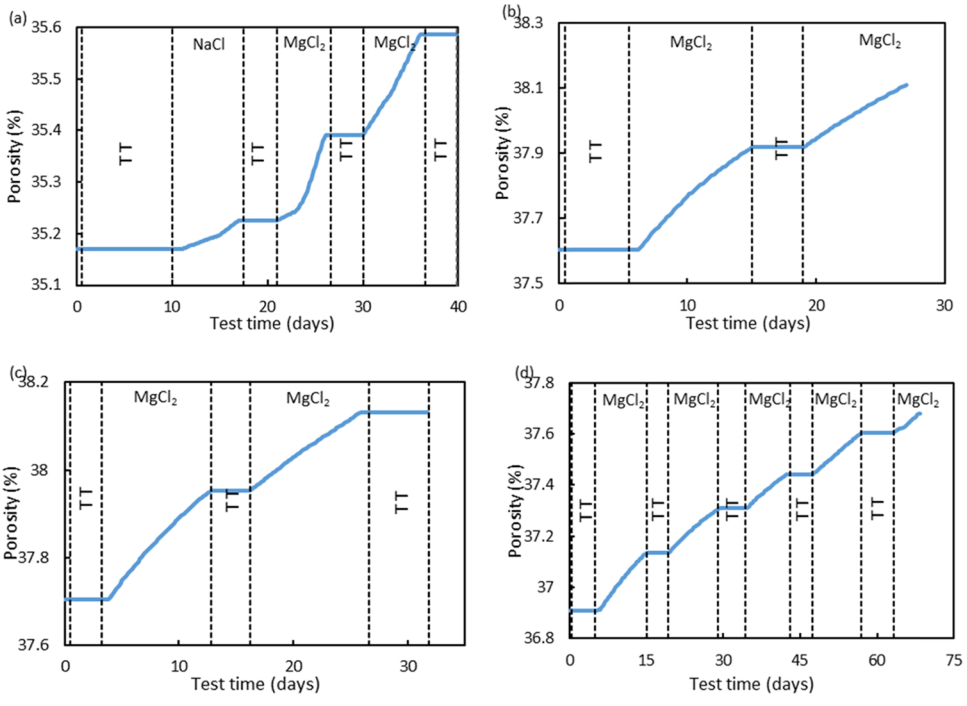

Figure 13. Porosity evolution with time for (a) water-wet sample, KA1, and mixed-wet samples (b) KA2, (c) KA3, and (d) KA4. The abbreviation TT stands for tracer test.

DOI: 10.1021/acs.energyfuels.9b00515
Energy Fuels XXXX, XXX, XXX−XXX

Table 9. Number of Sulfate SO_4^{2-} Ions Adsorbed in Water-Wet and Mixed-Wet Samples during SW1T Brine Flooding[a]

sample	timing of tracer test	estimated area between sulfate and SCN (PV)	initial PV of the samples (mL)	amount of SW1T flooded through sample to obtain the estimated area (mL)	number of sulfate ions adsorbed (10^{-4} mol)
KA1 water wet	initial tracer test	0.199	27.5	5.5	1.3
	NaCl inj.	0.200		5.5	1.3
	first $MgCl_2$ inj.	0.212		5.8	1.4
	second $MgCl_2$ inj.	0.240		6.6	1.6
KA2 mixed wet	initial tracer test	0.114	31.4	3.6	0.9
	$MgCl_2$ inj.	0.199		6.2	1.5
KA3 mixed wet	initial tracer test	0.120	31.2	3.7	0.9
	first $MgCl_2$ inj.	0.192		6.0	1.4
	second $MgCl_2$ inj.	0.209		6.5	1.6
KA4 mixed wet	initial tracer test	0.118	30.2	3.6	0.9
	first $MgCl_2$ inj.	0.186		5.6	1.3
	second $MgCl_2$ inj.	0.213		6.4	1.5
	third $MgCl_2$ inj.	0.224		6.8	1.6
	fourth $MgCl_2$ inj.	0.236		7.1	1.7

[a]The original concentration of SO_4^{2-} in SW1T brine is 0.024 mol/L.

test and the tracer test after the NaCl injection, implying that negligible to minor chemical reactions occurred from the NaCl flow. When $MgCl_2$ was injected, the adsorbed sulfate ions increased from 1.3×10^{-4} initially to 1.4×10^{-4} and 1.6×10^{-4} mol (or 0.13−0.14 and 0.16 mmol), an increase of 0.01 and 0.02 mmol in the two phases. For the mixed-wet cores, the amount of adsorbed sulfate ions was initially smaller than the 100% water-wet sample, i.e., 0.09, 0.09, and 0.09 mmol for the three mixed-wet samples. After the first $MgCl_2$ phase, the adsorbed sulfate ions increased by 0.06, 0.05, and 0.04 mmol, respectively, i.e., significantly different from the 100% water-saturated sample. We interpret this to be related to the mobilization of oil adsorbed on the mineral surfaces that initially inhibited the occurrence of sulfate adsorption. The large change observed from the $MgCl_2$ flow in the first injection phase seems to alter the way in which the oil partitions within the pores.

Further, the change in the number of ions adsorbed from the first to the second and third (and fourth) $MgCl_2$ injection phases follows a decreasing trend, which is interpreted to be associated with dissolution and precipitation rather than mobilization of oil. The trends in the areas are displayed in Figure 6.

The combined observations of increase in water-wet surface area estimated through tracer tests and change in SSA through time indicate that the presence of oil in the porous body in the mixed-wet samples does not really obstruct the path of the brines. However, not all surfaces are available for sulfate adsorption as changes are observed from the initial tracer test to the tracer test after the first $MgCl_2$ injection phase. Remark that no additional oil is produced from the core during the $MgCl_2$ flow, so the brine-induced reactive processes only lead to alterations in which the fluid is partitioned spatially within the pore. The presence of oil after the test, even in small quantities, however, does have an impact on the SSA measurements that needs to be further explored as Soxhlet extraction was necessary to obtain reasonable SSA and pycnometry data. The spatial partitioning of oil and water in the samples after aging also needs to be further investigated to better understand how reactive brines impact oil recovery from chalk.

5. CONCLUSIONS

The focus in this paper has been to investigate how the injection of $MgCl_2$ brine containing divalent ions impacts (a) the wetting state of chalk, (b) specific surface area, and (c) oil production with time. The experiments were performed on a reference water-wet sample and three mixed-wet chalk samples. The wettability of all mixed-wet samples was altered in the same manner, keeping the brine and oil composition, aging time, and aging temperature fixed.

Injecting $MgCl_2$ brine into chalk induced chemical reactions due to nonequilibrium between the calcite surface and the injected brine. These reactions led to a change in the thiocyanate and sulfate retention curves, hence a change in the water wetness of the chalk surface. The available water-wet surface area was found to be increasing with time for both water-wet and mixed-wet samples. The chemical replacement observed by the IC was found to be insensitive to the presence of oil in the pores, indicating that the dissolution−precipitation processes do not depend on the wettability of the samples.

BET measurements showed a reduction in the specific surface areas after the initial cleaning performed in the triaxial cell. When the samples were cleaned using Soxhlet extraction, the specific surface area of the samples increased in line with the tracer tests performed during the experiment. It was shown that this correlation exists irrespective of the initial fluid saturation of the samples. This is an important insight because

DOI: 10.1021/acs.energyfuels.9b00515
Energy Fuels XXXX, XXX, XXX−XXX

it shows that applying the results of one-phase rock−fluid chemical interactions between the injected brine and the chalk also applies to cases in which oil is present in the pores.

It was further observed that the chemical reactions between the brine and the rock did not lead to additional oil recovery. This observation has been linked to the incapability of $MgCl_2$ brine to mobilize oil adsorbed on the mineral surfaces, even though magnesium ions may have an indirect effect on oil recovery when present together with sulfate ions in other injection brines. No additional oil recovery may also have been caused due to the lack of enough pressure difference across oil ganglia in the center of pores to overcome the Young−Laplacian surface forces. Hence, it is of utmost importance to understand, in the future, how oil and water are partitioned in the pores after aging to interpret how reactive seawater-like brines improve the oil recovery rates.

AUTHOR INFORMATION

Corresponding Author

*E-mail: jaspreet.s.sachdeva@uis.no.

ORCID

Jaspreet S. Sachdeva: 0000-0002-4159-6125

Notes

The authors declare no competing financial interest.

ACKNOWLEDGMENTS

The authors acknowledge the Research Council of Norway and the industry partners, ConocoPhillips Skandinavia AS, Aker BP ASA, Eni Norge AS, Equinor ASA, Neptune Energy Norge AS, Lundin Norway AS, Halliburton AS, Schlumberger Norge AS, Wintershall Norge AS, and DEA Norge AS, of the National IOR Centre of Norway for support. They thank Ali Mehrabi at NORCE AS for performing the Soxhlet extraction on the samples.

REFERENCES

(1) Sachdeva, J. S.; Sripal, E. A.; Nermoen, A.; Korsnes, R. I.; Madland, M. V.; James, L. A. In *A Laboratory Scale Approach to Wettability Restoration in Chalk Core Samples*, SCA2018-020 Paper Presented at the International Symposium of the Society of Core Analysts, Trondheim, Norway, Aug 27−30, 2018.

(2) Morrow, N. R. The effects of surface roughness on contact angle with special reference to petroleum recovery. *J. Can. Pet. Technol.* **1975**, *14*, 42−53.

(3) Ma, S.; Mason, G.; Morrow, N. R. Effect of contact angle on drainage and imbibition in regular polygonal tubes. *Colloids Surf., A* **1996**, *117*, 273−291.

(4) McPhee, C.; Reed, J.; Zubizarreta, I. *Core Analysis: A Best Practice Guide*; Elsevier: Amsterdam, Netherlands, 2015; Vol. *64*, pp 313−345.

(5) Amott, E. Observations Relating to the Wettability of Porous Rock. *Trans. AIME* **1959**, *216*, 156−162.

(6) Boneau, D. F.; Clampitt, R. L. A surfactant system for the oil-wet sandstone of the North Burbank Unit. *J. Pet. Technol.* **1977**, *29*, 501−506.

(7) Donaldson, E. C.; Thomas, R. D.; Lorenz, P. B. Wettability Determination and Its Effect on Recovery Efficiency. *SPE J.* **1969**, *9*, 13−20.

(8) Donaldson, E. C.; Kendall, R. F.; Pavelka, E. A.; Crocker, M. E. *Equipment and Procedures for Fluid Flow and Wettability Tests of Geological Materials (No. DOE/BETC/IC-79/5)*; Department of Energy, Energy Technology Center: Bartlesville, OK, 1980.

(9) Donaldson, E. C. Oil-water-rock wettability measurement. *Am. Chem. Soc., Div. Pet. Chem., Prepr.* **1981**, *26*.

(10) Strand, S.; Standnes, D. C.; Austad, T. New Wettability Test for Chalk Based on Chromatographic Separation of SCN^- and SO_4^{2-}. *J. Pet. Sci. Eng.* **2006**, *52*, 187−197.

(11) Sachdeva, J. S.; Nermoen, A.; Korsnes, R. I.; Madland, M. V. Impact of Initial Wettability and Injection Brine Chemistry on Mechanical Behaviour of Kansas Chalk. *Transp. Porous Media* **2019**, *128*, 755−795.

(12) Sripal, E.; James, L. A. In *Application of an Optimization Method for Restoration of Core Samples for SCAL Experiments*, Paper SCA2016-002 Presented at the International Symposium of the Society of Core Analysts, Snowmass, Colorado, Aug 22−26, 2016.

(13) Sripal, E.; James, L. A. Application of an Optimization Method for the Restoration of Core Samples for SCAL Experiments. *Petrophysics* **2018**, *59*, 72−91.

(14) Pesheck, P. S.; Scriven, L. E.; Davis, H. T. Cold stage scanning electron microscopy of crude oil and brine in rock. *Scanning Electron Microsc.* **1981**, *1*, 515−524.

(15) Sutanto, E. In *Cryo SEM of Liquid-Bearing Rock*, Proceedings of the 46th Annual Meeting of the Electron Microscopy Society of America, San Francisco; Bailey, G. W.San Francisco Press: San Francisco, 1988.

(16) Fassi-Fihri, O.; Robin, M.; Rosenberg, E. In *Visualization of Oil and Brine in Porous Media by Cryo-scanning Electron Microscopy*, IFP—Fundamentals of Fluid Transport in Porous Media, Institut Français du Pétrole Exploration and Production Research Conference, 1, 15−18, Arles, May 14−18, 1990.

(17) Fassi-Fihri, O.; Robin, M.; Rosenberg, E. Wettability Studies at the Pore Level: A New Approach by the Use of Cryo-Scanning Electron Microscopy. *SPE Form. Eval.* **1995**, *10*, 11.

(18) Robin, M.; Rosenberg, E.; Fassi-Fihri, O. Wettability studies at the pore level: A new approach by use of Cryo-SEM. *SPE Form. Eval.* **1995**, *10*, 11−19.

(19) Robin, M.; Combes, R.; Rosenberg, E. In *Cryo-SEM and ESEM: New Techniques to Investigate Phase Interactions within Reservoir Rocks*, Paper SPE 56829 Presented at the SPE Annual Technical Conference and Exhibition, Houston, Texas, Oct 3−6, 1999.

(20) Robin, M. Interfacial Phenomena: Reservoir Wettability in Oil Recovery. *Oil Gas Sci. Technol.* **2001**, *56*, 55−62.

(21) Mwangi, P.; Thyne, G.; Rao, D. In *Extensive Experimental Wettability Study in Sandstone and Carbonate-Oil-Brine Systems: Part 1−Screening Tool Development*, Presented at the International Symposium of the Society of Core Analysts Held in Napa Valley, California, Sept 16−19, 2013.

(22) Erzuah, S.; Fjelde, I.; Omekeh, A. V. In *Wettability Characterization Using the Flotation Technique Coupled with Geochemical Simulation*, Presented at the IOR 2017—19th European Symposium on Improved Oil Recovery, Stavanger, Norway, 2017.

(23) Johnson, J. P.; Rhett, D. W. In *Compaction Behavior of Ekofisk Chalk as a Function of Stress*, Paper SPE 15872 Presented at the European Petroleum Conference, London, United Kingdom, Oct 20−22, 1986.

(24) Heugas, O.; Charlez, P. In *Mechanical Effect of the Water Injection on Ekofisk Chalk*, Third North Sea Chalk Symposium, Copenhagen, Denmark, 1990.

(25) Andersen, M. A.; Foeged, N.; Pedersen, H. F. In *The Link between Waterflood-Induced Compaction and Rate-Sensitive Behavior in a Weak North Sea Chalk*, Proceedings of the Fourth North Sea Chalk Symposium, Deauville, France, Sep, 1992.

(26) Brignoli, M.; Santarelli, F. J.; Righetti, C. In *Capillary Phenomena in an Impure Chalk*, RockMechanics in Petroleum Engineering, Delft, Netherlands, 1994.

(27) Delage, P.; Schroeder, C.; Cui, Y. J. In *Subsidence and Capillary Effects In Chalks*, ISRM International Symposium, Torino, Italy; Eurock, 1996; pp 1291−1298.

(28) Schroeder, C.; Bois, A.-P.; Maury, V.; Halle, G. In *Water/Chalk (or Collapsible Soil) Interaction: Part II. Results of Tests in Laboratory on Lixhe Chalk to Calibrate Water/Chalk Models*, Paper SPE 47587 Presented at the SPE/ISRM Rock Mechanics in Petroleum Engineering, Trondheim, Norway, July 8−10, 1998.

DOI: 10.1021/acs.energyfuels.9b00515
Energy Fuels XXXX, XXX, XXX−XXX

(29) Risnes, R. Deformation and Yield in High Porosity Outcrop Chalk. *Phys. Chem. Earth* **2001**, *26*, 53−57.
(30) Risnes, R.; Haghighi, H.; Korsnes, R. I.; Natvik, O. Chalk-Fluid Interactions with Glycol and Brines. *Tectonophysics* **2003**, *370*, 213−226.
(31) Madland, M. V.; Midtgarden, K.; Manafov, R.; Korsnes, R. I.; Kristiansen, T. G.; Hiorth, A. In *The Effect of Temperature and Brine Composition on the Mechanical Strength of Kansas Chalk*, Paper SCA2008-55 Presented at the International Symposium of the Society of Core Analysts, Abu Dhabi, UAE, Oct 29−Nov 2, 2008.
(32) Madland, M. V.; Hiorth, A.; Omdal, E.; Megawati, M.; Hildebrand-Habel, T.; Korsnes, R. I.; Evje, S.; Cathles, L. M. Chemical Alterations Induced by Rock-Fluid Interactions when Injecting Brines in High Porosity Chalks. *Transp. Porous Media* **2011**, *87*, 679−702.
(33) Korsnes, R. I.; Madland, M. V.; Austad, T.; Haver, S.; Røsland, G. The Effects of Temperature on the Water Weakening of Chalk by Seawater. *J. Pet. Sci. Eng.* **2008**, *60*, 183−193.
(34) Megawati, M.; Hiorth, A.; Madland, M. V. The Impact of Surface Charge on the Mechanical Behaviour of High-Porosity Chalk. *Rock Mech. Rock Eng.* **2013**, *46*, 1073−1090.
(35) Hermansen, H.; Landa, G. H.; Sylte, J. E.; Thomas, L. K. Experiences after 10 years of waterflooding the Ekofisk Field, Norway. *J. Pet. Sci. Eng.* **2000**, *26*, 11−18.
(36) Madland, M. V.; Hiorth, A.; Korsnes, R. I.; Evje, S.; Cathles, L. In *Rock Fluid Interactions in Chalk Exposed to Injection of Seawater, $MgCl_2$, and NaCl Brines with Equal Ionic Strength*, Paper A22 Presented at the 15th European Symposium on Improved Oil Recovery, Paris, France, April 27−29, 2009.
(37) Megawati, M.; Andersen, P. Ø.; Korsnes, R. I.; Evje, S.; Hiorth, A.; Madland, M. V. In *The Effect of Aqueous Chemistry pH on the Time-dependent Deformation Behavior of Chalk Experimental and Modelling Study*, Pore2Fluid International Conference, Paris, France, 16−18 Nov, 2011; SPE, 2011.
(38) Nermoen, A.; Korsnes, R. I.; Hiorth, A.; Madland, M. V. Porosity and Permeability Development in Compacting Chalks during Flooding of Non-Equilibrium Brines: Insights from Long-Term Experiment. *J. Geophys. Res.: Solid Earth* **2015**, *120*, 2935.
(39) Zimmermann, U.; Madland, M. V.; Nermoen, A.; Hildebrand-Habel, T.; Bertolino, S. A. R.; Hiorth, A.; Korsnes, R. I.; Audinot, J. N.; Grysan, P. Evaluation of the compositional changes during flooding of reactive fluids using scanning electron microscopy, nano-secondary ion mass spectrometry, X-ray diffraction and whole rock geochemistry. *AAPG Bull.* **2015**, *99*, 791−805.
(40) Minde, M. W.; Haser, S.; Korsnes, R. I.; Zimmermann, U.; Madland, M. V. In *Comparative Studies of Mineralogical Alterations of Three Ultra-long-term Tests of Onshore Chalk at Reservoir Conditions*, 9th European Symposium on Improved Oil Recovery/IOR Norway 2017, European Association of Geoscientists and Engineers, 2017.
(41) Minde, M. W.; Zimmermann, U.; Madland, M. V.; Korsnes, R. I.; Schulz, B.; Gilbricht, S. Mineral Replacement in Long-Term Flooded Porous Carbonate Rocks. *Geochim. Cosmochim. Acta*, submitted for publication, 2018.
(42) Minde, M. W.; Wang, W.; Madland, M. V.; Zimmermann, U.; Korsnes, R. I.; Bertolino, S. R.; Andersen, P. Ø. Temperature effects on rock engineering properties and rock-fluid chemistry in opal-CT-bearing chalk. *J. Pet. Sci. Eng.* **2018**, *169*, 454−470.
(43) Heggheim, T.; Madland, M. V.; Risnes, R.; Austad, T. A chemical induced enhanced weakening of chalk by seawater. *J. Pet. Sci. Eng.* **2005**, *46*, 171−184.
(44) Hiorth, A.; Cathles, L. M.; Kolnes, J.; Vikane, O.; Lohne, A.; Madland, M. V. In *Chemical Modelling of Wettability Change in Carbonate Rocks*, Presented in the 10th Wettability Conference, Abu Dhabi, UAE, 27−28 Oct, 2008.
(45) Hiorth, A.; Cathles, L. M.; Kolnes, J.; Vikane, O.; Lohne, A.; Korsnes, R. I.; Madland, M. V. In *A Chemical Model for the Seawater−CO_2−Carbonate System—Aqueous and Surface Chemistry*, Presented at the International Symposium of the Society of Core Analysts, Abu Dhabi, UAE, SCA2008-18, 29 Oct—2 Nov, 2008.
(46) Hiorth, A.; Cathles, L. M.; Madland, M. V. The impact of pore water chemistry on carbonate surface charge and oil wettability. *Transp. Porous Media* **2010**, *85*, 1−21.
(47) Andersen, P. Ø.; Wang, W.; Madland, M. V.; Zimmermann, U.; Korsnes, R. I.; Bertolino, S. R. A.; Minde, M.; Schulz, B.; Gilbricht, S. Comparative Study of Five Outcrop Chalks Flooded at Reservoir Conditions: Chemo-mechanical Behaviour and Profiles of Compositional Alteration. *Transp. Porous Media* **2018**, *121*, 135−181.
(48) Ahsan, R.; Fabricius, I. L. In *Sorption of Magnesium and Sulfate ions on Calcite*, 72nd EAGE Conference and Exhibition Incorporating SPE EUROPEC 2010, Extended Abstracts, SP13; SPE, EAGE, 2010.
(49) Alam, M. M.; Ahsan, R.; Shaik, A. K.; Fabricius, I. L. In *Surface Charge of Calcite and Its Influence on the Electrical Conductivity in Chalk*, SEG International Exposition and 80th Annual Meeting, Denver, Colorado 2010, 17−22 October 2010. Vol. Expanded Abstracts. CD-ROM; Society of Exploration Geophysicists, 2010; pp 2686−2691.
(50) Nermoen, A.; Korsnes, R. I.; Storm, E. V.; Stødle, T.; Madland, M. V.; Fabricius, I. L. Incorporating electrostatic effects into the effective stress relation - Insights from chalk experiments. *Geophysics* **2018**, *83*, MR123−MR135.
(51) Anderson, W. G. Wettability Literature Survey-Part 1: Rock/Oil/Brine Interactions and the Effects of Core Handling on Wettability. *J. Pet. Technol.* **1986**, *38*, 1125−1144.
(52) Jadhunandan, P. P.; Morrow, N. R. Spontaneous imbibition of water by crude oil/brine/rock systems. *In Situ* **1991**, *15*, 319−345.
(53) Zhou, X. M.; Torsæter, O.; Xie, X.; Morrow, N. R. The effect of crude-oil aging time and temperature on the rate of water imbibition and long-term recovery by imbibition. *SPE Form. Eval.* **1995**, *10*, 259−266.
(54) Graue, A.; Viksund, B. G.; Baldwin, B. A. Reproducible wettability alteration of low-permeable outcrop chalk. *SPE Reservoir Eval. Eng.* **1999**, *2*, 134−140.
(55) Tang, G.; Firoozabadi, A. Effect of pressure gradient and initial water saturation on water injection in water-wet and mixed-wet fractured porous media. *SPE Reservoir Eval. Eng.* **2001**, *4*, 516−524.
(56) Ricci, M.; Spijker, P.; Stellacci, F.; Molinari, J. F.; Voïtchovsky, K. Direct visualization of single ions in the Stern layer of calcite. *Langmuir* **2013**, *29*, 2207−2216.
(57) Hofmann, S.; Voïtchovsky, K.; Spijker, P.; Schmidt, M.; Stumpf, T. Visualising the molecular alteration of the calcite (104) − water interface by sodium nitrate. *Sci. Rep.* **2016**, *6*, No. 21576.
(58) Fan, T.; Buckley, J. S. Acid number measurements revisited. *SPE J.* **2007**, *12*, 496−500.
(59) Brunauer, S.; Emmett, P. H.; Teller, E. Adsorption of gases in multimolecular layers. *J. Am. Chem. Soc.* **1938**, *60*, 309−319.
(60) Megawati, M.; Madland, M. V.; Hiorth, A. Mechanical and physical behavior of high-porosity chalks exposed to chemical perturbation. *J. Pet. Sci. Eng.* **2015**, *133*, 313−327.
(61) Wang, W.; Madland, M. V.; Zimmermann, U.; Nermoen, A.; Korsnes, R. I.; Bertolino, S. R. A.; Hildebrand-Habel, T. Evaluation of porosity change during chemo-mechanical compaction in flooding experiments on Liège outcrop chalk. *Geol. Soc. London, Spec. Publ.* **2016**, *435*, 217−234.
(62) Borromeo, L.; Egeland, N.; Minde, M. W.; Zimmermann, U.; Andò, S.; Madland, M. V.; Korsnes, R. I. Quick, Easy, and Economic Mineralogical Studies of Flooded Chalk for EOR Experiments Using Raman Spectroscopy. *Minerals* **2018**, *8*, No. 221.
(63) Slobod, R. L.; Blum, H. A. Method for determining wettability of reservoir rocks. *J. Pet. Technol.* **1952**, *4*, 1−4.
(64) Tang, G. Q.; Morrow, N. R. Influence of brine composition and fines migration on crude oil/brine/rock interactions and oil recovery. *J. Pet. Sci. Eng.* **1999**, *24*, 99−111.
(65) Erzuah, S.; Fjelde, I.; Omekeh, A. V. In *Wettability Estimation by Oil Adsorption Using Quartz Crystal Microbalance with Dissipation QCM-D*, Presented at the 80th EAGE Annual Conference & Exhibition 2018, SPE-190882-MS; European Association of Geoscientists and Engineers: Copenhagen, Denmark, 2018.

DOI: 10.1021/acs.energyfuels.9b00515
Energy Fuels XXXX, XXX, XXX−XXX

(66) Stipp, S. L. S. Toward a conceptual model of the calcite surface: Hydration, hydrolysis and surface potential. *Geochim. Cosmochim. Acta* **1999**, *63*, 3121−3131.

DOI: 10.1021/acs.energyfuels.9b00515
Energy Fuels XXXX, XXX, XXX−XXX

Paper III

Sachdeva, J.S., Nermoen, A., Korsnes, R.I., and Madland, M.V. (2019). Effect of Initial Wettability on Rock Mechanics and Oil Recovery: Comparative Study on Outcrop Chalks. Submitted to *Transport in Porous Media*, publication under review.

Effect of Initial Wettability on Rock Mechanics and Oil Recovery: Comparative Study on Outcrop Chalks

Jaspreet S. Sachdeva*[1,2], Anders Nermoen[1,3], Reidar I. Korsnes[1,2], Merete V. Madland[1,2]

[1]The National IOR Centre of Norway, University of Stavanger, Stavanger, Norway
[2]Department of Energy Resources, University of Stavanger, Stavanger, Norway
[3]Norwegian Research Centre AS, Oslo, Norway
*Corresponding author: Jaspreet Singh Sachdeva (jaspreet.s.sachdeva@uis.no)

Keywords:
- Improved Oil Recovery
- Water flooding
- Chalk compaction
- Wettability
- Geomechanics
- Oil production measurements

ABSTRACT

Brines containing surface-active divalent ions such as Ca^{2+}, Mg^{2+} and SO_4^{2-} impact the stiffness, strength and time-dependent deformation of water wet outcrop chalk from various locations. This study documents how stiffness and strength of wettability-altered oil and water saturated (mixed wet) chalk compares to water saturated samples during hydrostatic loading. During hydrostatic creep, the strain rate response to magnesium chloride ($MgCl_2$) brine injection is compared for water wet and mixed wet samples. For the mixed wet samples, the oil production was estimated during compaction and $MgCl_2$ flow. The results presented here were then compared to a similar test series on Kansas outcrop chalk. The differences were interpreted in terms of difference in physical parameters such as porosity and pore size.

The samples were wettability altered and tested in parallel at hydrostatic conditions and 130°C. It was found that the initial wettability controlled the plastic strength measurements of Mons chalk with initial resident fluids inside the pores but to a lesser extent than the corresponding Kansas chalk. Afterwards, when Mons cores were hydrostatically loaded to a stress level approximately 1.5 times yield, both water wet and wettability-altered Mons chalk samples gave comparable trends during a stagnant phase and a following $MgCl_2$ injection phase at varying flow rates. Similar observations were reported for water wet and wettability-altered Kansas chalk as well. It was also shown that the non-equilibrium chemical reactions were insensitive to the initial wettability for both Kansas and Mons chalks. The oil production observations, however, showed that 43% of the total oil was recovered during early-stage compaction from Mons chalk with no flow, whereas Kansas chalk did not produce any oil. No tail-end oil production was observed due to compaction or non-equilibrium brine flow in any of the two chalk types.

INTRODUCTION

The physico-chemical interactions between resident fluids and reservoir rock have an impact on the mechanical rock properties. This has led to considerable investigations towards searching for more optimal injection fluids. Chalk is a highly porous and a low permeable rock. Due to the large surface area in chalk, surface processes (dissolution/precipitation and adsorption/ desorption) dominate the bulk mechanical behaviour. Studies have shown that the injection of seawater into chalk lead to enhanced compaction of the reservoir rock and hence acts as an important driving mechanism to mobilise pore fluids towards production facilities, thereby leading to improved oil recovery rates (Sulak and Danielsen 1989; Sulak 1991; Hermansen et al. 2000). The enhanced reservoir compaction has also shown to induce seafloor subsidence which raises serious concerns related to the safety of personnel on the platforms and the equipment in the wellbore (Sulak and Danielsen 1989; Maury et al. 1996; Nagel 1998; Sylte et al. 1999; Gauer et al. 2002). This compaction has been found to be caused by both pore pressure depletion early in the field life and water weakening induced by seawater injection during the later stages (Gauer et al. 2002).

Research on how chalk mechanics was affected by pore fluid composition intensified after the detection of subsidence at Ekofisk field (Norwegian Continental Shelf). A key research question had been to find how the mechanical chalk properties were affected by aqueous chemistry, with focus on elastic stiffness, plastic strength and time-dependent creep deformation rates (Risnes 2001; Hellmann et al. 2002a, 2002b; Risnes et al. 2003; Korsnes et al. 2006a, 2006b, 2008; Madland et al. 2008, 2011; Megawati et al. 2011, 2013; Neveux et al. 2014a, 2014b). The relationship between chalk mechanics and pore fluid chemistry has been important to the petroleum industry (Hermansen et al. 2000; Nagel 2001; Fabricius and Borre 2007).

Until now, the rock-mechanical studies have concentrated mostly on water wet and water saturated systems. It has been shown that the surface-active divalent ions, such as magnesium (Mg^{2+}) and sulphate (SO_4^{2-}), have a huge effect on the mechanical behaviour. Heggheim et al. (2005) observed that sulphate ions in the injected synthetic seawater (SSW) brine led to a reduced yield and caused weakening of chalk. Korsnes et al. (2008) also observed the same effect by demonstrating that flooding SSW containing sulphate ions through chalk yielded at a significantly lower stress compared to the samples flooded by SSW without sulphate ions. Megawati et al. (2011) showed that the reduction in yield is due to its adsorption on the charged calcite surface, which leads to a disjoining pressure at the grain-grain contacts and causes pore collapse failure at lower stresses.

When magnesium chloride ($MgCl_2$) brine is injected through chalk, dissolution of calcite $CaCO_3$ and precipitation of magnesite $MgCO_3$ occur (Madland et al. 2011; Nermoen et al. 2015; Zimmermann et al. 2015; Minde et al. 2017, 2018a, 2018b; Andersen et al. 2018). These dissolution/precipitation processes lead to enhanced bulk volume creep rates in chalk compared to when flooded with weakly reactive sodium chloride (NaCl) brine (Madland et al. 2009, 2011). Further, Nermoen et al. (2015) showed that the compaction rate was sensitive to the injection rate. At higher flooding rates, the rate of dissolution of calcite and precipitation of Mg-bearing minerals increased. The solid volume changed because the sample lost mass and the mineral density increased (density of magnesite is 3.0 g/cm^3 and calcite 2.7 g/cm^3). Further, the solid volume changes led to a reduction in bulk volume and the grains unlocked and reorganised to reduce pore volume. Long-term $MgCl_2$ flooding tests (516 days and 1072 days) on Liège water wet chalk (Belgium) altered the mineralogy from calcite to Mg-bearing minerals dominated by magnesite (Nermoen et al. 2015; Zimmermann et al. 2015; Minde et al. 2017; Borromeo et al. 2018). Mg^{2+} ions have also shown to adsorb on the calcite surface leading to desorption of calcium ions (Ahsan and Fabricius 2010; Alam et al. 2010; Nermoen et al. 2018). Nermoen et al. (2018) showed

that adsorption of magnesium ions onto the charged calcite surface caused less weakening than when sulphates were present in the injection brine.

It has also been suggested that chemical reactions between the injected non-equilibrium brines and chalk surface lead to additional oil recovery (Hiorth et al. 2010) either due to rock dissolution or change in the surface charge during brine injection that affects rock wettability. For chemical reactions to be non-negligible, tens (or hundreds) of pore volumes are required. So, for chemical reactions to play a role in enhancing the oil recovery, it must be to mobilise oil after the initial displacement. This idea was tested in a recent study by Sachdeva et al. (2019). Here, however, no oil was produced during tail-end oil production through $MgCl_2$ flow even though chemical reactions and pore volume compaction occurred.

Megawati et al. (2015) and Andersen et al. (2018) studied five different chalk types and found a dependence of the non-carbonate content on how the mechanical creep behaviour was affected by $MgCl_2$ brine injection. Injecting this brine into impure chalks (Liège, Aalborg and Kansas) led to an immediate increased creep rate. However, in pure chalks (Mons and Stevns Klint) the creep response was delayed by a time lag of several weeks before a tertiary-like creep developed. These rock samples were never exposed to oil, which enabled the aqueous solution to contact the minerals directly. A question that has been raised is to what extent these results are applicable to actual chalk reservoirs. Chalk wettability has been studied extensively to understand how different wetting states affect multiphase fluid flow with focus on oil recovery (Standnes and Austad 2000a, 2000b; Zhang and Austad 2005; Strand et al. 2007). In the present study, we also focus on the mechanical stiffness, strength and creep rate dependencies upon brine injection into wettability-altered chalk, besides oil recovery.

Sachdeva et al. (2019) studied how wettability affected the mechanical behaviour of Kansas outcrop chalk saturated by oil-water mixture. It was found that the elastic stiffness and plastic strength were higher for mixed wet samples compared to water wet samples, and that when $MgCl_2$ brine was injected the on-going rock-fluid interactions led to enhanced creep rates, which was found to be applicable for both water wet and mixed wet samples. However, after the initial oil displacement during the first 2-3 pore volumes (PVs) injected, no additional oil was produced from the samples even though the chemical reactions from the rock-fluid interactions took place. Further, ongoing pore volume compaction also did not mobilise any additional oil from the samples.

This study shares the same objective as Sachdeva et al. (2019), but here we perform experiments on Mons chalk which is mineralogical purer than Kansas. The geochemical analyses carried out by Andersen et al. (2018) showed that the unflooded and untested chalk samples from these two quarries were dominated by CaO as expected. Kansas chalk samples were found to contain CaO between 54.2 and 55.1 weight percent (wt%) and relatively small amounts of non-carbonate phases such as SiO_2 (between 1.1 and 1.5 wt%), K_2O (0.1 wt%) and Al_2O_3 (0.3 to 0.5 wt%). Trace elements, such as Rb, Zr and Y, were also found to be in minute quantities with concentrations below 5 ppm. Mons chalk contained a slightly lower SiO_2 (0.98 wt%) than chalk cores from Kansas with CaO amounting to around 55 wt%. With Al_2O_3 as low as 0.2 wt% and even lower trace element concentrations, this chalk type was concluded to be cleaner than the Kansas chalk.

The premise of this study was to alter the wettability, test the reproducibility in the wettability alteration, document the relation between wettability and stiffness, strength and time-dependent mechanical behaviour, and finally to determine how tail-end oil recovery is affected by compaction and continuous flow of reactive brine. The wetting state of Mons chalk cores was altered to a mixed wet state prior to mechanical testing at high effective stresses and 130°C temperature. The results from how wettability-altered Mons chalk responded to $MgCl_2$ injection are compared to those carried out on Kansas chalk by Sachdeva et al. (2019).

This study emphasises on how differences in the initial pore fluid saturations and wettability affect the mechanical response of Mons chalk. It further highlights the effect of mineralogical changes on chalk mechanics. The bulk, solid and pore volumes as well as oil and water volumes are monitored continuously to observe how the volume dependencies are linked to deformations and injection of reactive $MgCl_2$ brine.

MATERIALS AND METHODS

Rock sample material

Chalk samples from a single block obtained from the Trivières Formation in Mons (Belgium) were used. This chalk belongs to Late Cretaceous age and is very pure (> 99 wt% calcite).

Ten cylindrical samples were cored, radially adjusted to 38.1 mm diameter, cut at desired lengths and dried at 110°C overnight before dry mass was measured. The samples were then vacuumed and saturated by distilled water (DW) to measure saturated mass. The mass difference between the dry and saturated sample was used to estimate pore volume and saturation porosity (Table 1).

The samples were divided into two test series:

- Six samples were used for wettability determination. Three samples were kept water wet and 100% water saturated (Mww) for reference, and the other three were wettability altered (Mmw), Table 1.
- Four samples were used in triaxial test program (M1 to M4). Two samples were kept water wet and 100% water saturated, and the other two were wettability altered, Table 1.

Table 1. Basic properties of samples used for wettability determination and triaxial tests.

	Core ID	Wetting state	Core length (mm)	Core diameter (mm)	Dry mass (g)	Saturated mass (g)	Pore volume (ml)	Bulk volume (ml)	Saturation porosity ϕ (%)
Wettability determination program	Mww1	Water wet	72.4	38.1	126.7	162.1	35.4	82.5	42.9
	Mww2		69.9	38.1	122.3	156.5	34.2	79.7	42.9
	Mww3		73.2	38.1	130.2	165.4	35.2	83.5	42.2
	Mmw1	Mixed wet	72.4	38.1	123.9	159.3	35.4	82.5	42.9
	Mmw2		68.9	38.1	122.1	156.3	34.2	78.6	43.5
	Mmw3		69.4	38.1	120.9	155.0	34.1	79.1	43.1
Triaxial test program	M1	Water wet	72.7	38.1	129.4	164.4	35.0	82.9	42.2
	M2		68.9	38.1	119.9	153.8	33.9	78.6	43.2
	M3	Mixed wet	68.9	38.1	119.7	153.7	34.0	78.6	43.3
	M4		68.8	38.1	122.0	155.0	33.0	78.4	42.1

Description of fluids

Four brine compositions were used. In the wettability determination program, two different versions of artificial seawater were used: SW1T brine contained sulphate (SO_4^{2-}) and thiocyanate (SCN^-) tracer while SW0T did not (Table 2). The total dissolved solids of SW1T and SW0T were equal to synthetic sea water (SSW). The two other brines used during the triaxial tests program (Table 2) were:

- 1.1 M NaCl brine for initial saturation to resemble resident formation fluids. NaCl brine moderately interacts with chalk (Madland et al. 2011; Ricci et al. 2013; Hofmann et al. 2016).
- 0.219 M $MgCl_2$ brine used as a flooding brine with equal ionic strength as seawater. This is injected to trigger dissolution/precipitation effects from the Ca-Mg exchange (Madland et al.

2009, 2011) and adsorption effects of magnesium ions on the calcite surface (Ahsan and Fabricius 2010; Alam et al. 2010; Nermoen et al. 2018; Liu et al. 2018).

A 60%-40% volume mixture of crude oil from the Heidrun field offshore Norway and heptane was used. The acid number of the Heidrun oil was measured to be 2.82 mg KOH/g, while the acid number of the oil mixture was 2.12 mg KOH/g measured according to the Fan and Buckley (2007) procedure.

Table 2. Composition of brines used in the wettability determination program and for core flooding in the triaxial test program.

	Wettability determination program		Triaxial test program	
Ions	**SW0T**	**SW1T**	**1.1 M NaCl**	**0.219 M $MgCl_2$**
	mol/l	**mol/l**	**mol/l**	**mol/l**
HCO_3^-	0.002	0.002	0	0
Cl^-	0.583	0.492	1.1	0.438
SO_4^{2-}	0	0.024	0	0
SCN^-	0	0.024	0	0
Mg^{2+}	0.045	0.045	0	0.219
Ca^{2+}	0.013	0.013	0	0
Na^+	0.460	0.393	1.1	0
Li^+	0	0.024	0	0
K^+	0.010	0.034	0	0
Ionic Strength	0.643	0.647	1.1	0.657
TDS (g/l)	33.39	33.39	64.28	44.52

Wettability alteration and fluid saturations

Five wettability-altered samples (three for wettability determination and two for triaxial tests) were treated according to the following procedure:

- Saturated by 1.1 M NaCl brine.
- Mounted in a Hassler cell and heated to 50°C. Flooded two pore volumes (PVs) of the oil mixture in each direction during which the produced brine was collected to estimate the initial water saturation S_{wi}.
- Submerged the samples in the same oil mixture in aging containers and left for 21 days at 90°C.

The wettability-altered samples were termed Mmw1 to Mmw3 in the wettability determination program and M3 & M4 in the triaxial test program. The water wet samples were simply saturated by 1.1M NaCl brine and were termed Mww1 to Mww3 in the wettability determination program and M1 & M2 in the triaxial test program.

Chromatographic separation for wettability determination

The chromatographic separation technique for wettability determination used here, and developed by Strand et al. (2006a), refers to how the effluent concentration profile of non-affine tracers differ from that of surface-active ions. The surface-active divalent sulphate anions (SO_4^{2-}) replace the monovalent anions on the positively charged calcite surface sites. Sulphate adsorption occur on mineral surface areas

in contact with water, hence a key premise is that mineral surfaces covered by oil will not capture the injected sulphate ions. By co-injecting sulphate anions and non-affine thiocyanate (SCN^-) tracer, after being flooded by a brine stripped of these ions, the two effluent concentration profiles split as the increased concentration of the adsorbed ion is delayed compared to the non-affine tracer. The split, measured by the area spanned by the two concentration profiles, as a function of pore volumes (PVs) injected is proportional to the mineral surface in contact with water. When oil is bound to calcite mineral surfaces in mixed wet samples, the separation area is reduced compared to water wet samples if the specific surface area is the same. The ratio of areas for mixed wet sample (A_{mw}) and water wet sample (A_{ww}) defines the wettability index (W_i),

$$W_i = \frac{A_{mw}}{A_{ww}} \tag{1}$$

A wettability index of 1 imply that the sample has the same number of surface sites for sulphate adsorption as the reference case, making it 100% water wet. A W_i of zero (overlapping sulphate and tracer curves) imply no sulphate ions adsorption making the sample 100% oil wet. Other values of W_i imply that the minerals are partially covered by oil (mixed wet). Rock fluid interactions also changes the specific surface area. Dissolution and precipitation reactions can increase or decrease the specific surface area, thereby changing the number of surface sites even when oil is present, hence leading to a mixed wet state.

Quantifying the wettability alteration by aging

The wettability alteration procedure was equivalent for all samples in both the 'wettability determination program' and 'triaxial test program'. Wettability determination could not be done on samples for the triaxial tests because the flow of fluids used to determine wettability displaces oil and alters the wettability, since sulphate has shown to modify wettability (Strand et al. 2006b; Zhang and Austad 2006; Zhang et al. 2007). We assume that the wettability determined for the three aged cores in the wettability determination program is the same as the two aged cores in the triaxial test program.

Wettability determination was performed in a Hassler cell by (i) flooding four PVs of SW0T brine, (ii) injecting SW1T brine for 500 minutes with a flow rate of 0.2 ml/min. During the SW1T injection, 40 samples were collected using a Gilson fraction sampler. Each sample contained 2 ml of fluids collected over 10.0 minutes, with 2.5 minutes waste time between each sample. For each fluid sample, the thiocyanate and sulphate concentrations were determined using ion chromatography (IC). The concentration c_k of each species k (SCN^- and SO_4^{2-}) is rescaled by the SCN^- and SO_4^{2-} concentrations of SW0T c_{k0} (in this case zero) and SW1T $c_{k1} = 0.024$ mol/liter, such that a reduced concentration $\hat{C}_k$ could be obtained,

$$\widehat{C_k} = \frac{c_k - c_{k0}}{c_{k1} - c_{k0}} \tag{2}$$

This reduced concentration varies between zero and one, and when the effluent concentration equals the inlet concentration, $\widehat{c_k} = 1$ enabling the thiocyanate and sulphate curves to be plotted together. The area between the curves was estimated by integration using the trapeze method. Further, larger cores will have a larger *total* surface area than smaller ones, so the areas are reported in per gram of the core for accurate comparison (Table 3).

Ion Chromatography (IC)

The effluent samples acquired were diluted 500 times with nanopure water (of specific resistance 18.2 MΩ-cm at 25°C) to meet the linear regime of the Dionex IC S-5000+ Ion Chromatography System. The samples were diluted using the Gilson GX-271 liquid handler operated by the Trilution software. Once

the IC analysis finalised, a series of peaks, corresponding to each ion in the effluent sample, was obtained. The area under each peak was assumed to be proportional to the ion concentration in the fluid, when compared to known standards with known concentrations.

The triaxial cell setup for mechanical flow-through tests

The samples were mounted into the triaxial cell allowing for continuous measurements of axial and radial strains at elevated stresses and temperature (Figure 1). The triaxial cell was equipped with a heating element and a regulating system with temperature control (0.1°C precision). Three pumps were used to control the axial piston pressure (P_{pist}), confining pressure (σ_{rad}) and flow rate (Q). The pore pressure (P_p =0.7 MPa), was controlled by a back-pressure regulator ensuring constant pore pressure on the downstream side. An external Linear Voltage Differential Transducer (LVDT), placed on top of the moving piston, monitored the change in sample length (L) and an internal extensometer monitored the change in diameter (D).

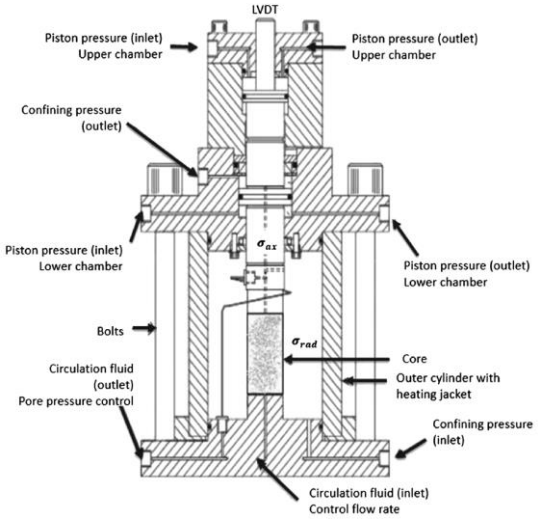

Figure 1. Sketch of the triaxial cell

The axial stress was calculated using radial stress, piston pressure, frictional pressure of the piston movement in the triaxial cell, and an area factor (f_{area} = 1.28) for the piston pressure chamber and the cross area of the plug,

$$\sigma_{\mathrm{ax}} = \sigma_{rad} + f_{area}\left(P_{pist} - P_{fric}\right) \tag{3}$$

In the hydrostatic phase the stresses are equal in all directions, so the bulk modulus K is given by,

$$K = {}^{\Delta\sigma'_{ax}}/_{\Delta\varepsilon_{vol}} \tag{4}$$

Here, $\Delta\sigma'_{ax}$ is the change in effective stress in axial direction and $\Delta\varepsilon_{vol}$ is the change in volumetric strain (see equation 7). The effective stress is given by the imposed stress in a spatial direction minus a fraction α times the pore pressure ($\sigma' = \sigma - \alpha P_{pore}$). We assume the Biot coefficient $\alpha = 1$ hereon.

Constitutive equations

The bulk, pore and solid volumes are linked through the constitutive equation $V_b = V_s + V_p$. During the test, the pore volume is not directly measured. Since porosity is determined by the ratio of pore volume (V_p) to bulk volume (V_b),

$$\phi = \frac{V_p}{V_b} = 1 - \frac{V_s}{V_b} \tag{5}$$

the solid volume (V_s), estimated from the IC analysis, and the bulk compaction can be used to estimate porosity evolution using (Nermoen et al. 2015),

$$\phi(t) = \frac{\phi_o + \varepsilon_{vol} - \Delta V_s / V_{b,o}}{1 + \varepsilon_{vol}} \tag{6}$$

where ϕ_o is the original porosity, ε_{vol} is the volumetric strain and $V_{b,o}$ defines the original bulk volume.

Evolution in bulk volume with time

The radial strain was measured only at the middle of the core. Since radial deformation is non-equal along the length of the cores even in in hydrostatic tests (Nermoen et al. 2015), we introduced the factor X, assumed to be constant through the test, to improve the volumetric strain estimates from axial strain measurements,

$$\varepsilon_{vol} = X\varepsilon_{ax} \tag{7}$$

The factor X was determined from the ratio of length and volume changes measured with a sliding caliper directly on the core sample after test. As such, the bulk volume can be estimated via,

$$V_{b,t} = V_{b,o}(1 - \varepsilon_{vol}) = V_{b,o}(1 - X\varepsilon_{ax}) \tag{8}$$

Evolution in solid volume with time

The solid mass evolution over time $M_s(t)$ is calculated from the difference in the concentrations of the injected fluid and the produced effluent fluids (from ion chromatography) times the flow rate q_{in} and molar mass of Mg and Ca (n_{Mg}=24 g/mol and $n_{Ca} = 40$ g/mol),

$$M_s(t) = M_{s,0} + \eta \int_0^t q_{in}(n_{Mg}(c_{in,Mg} - c_{out,Mg}) - n_{Ca}(c_{in,Ca} - c_{out,Ca}))dt \tag{9}$$

This is used to interpolate between the measured mass before and after test, and η is a fitting parameter that makes the observed replacement of Ca by Mg from IC data match the observed mass loss (measured on a scale) in dry weight.

The solid density is measured before and after test, and we used the calcium produced from the sample $m_{Ca}(t)$, at time t to interpolate between the initial ($\rho_{s,o}$) and final ($\rho_{s,f}$) densities via,

$$\rho_s(t) = \rho_{s,o} + ((\rho_{s,f} - \rho_{s,o})(m_{Ca}(t)/m_{Ca,total})) \tag{10}$$

Using equations 9 and 10 the change in solid volume ΔV_s can be estimated,

$$\Delta V_s(t) = \frac{M_s(t)}{\rho_s(t)} - \frac{M_{s,o}}{\rho_{s,o}} \tag{11}$$

Evolution in porosity and pore volume with time: The pore volume is not directly monitored in the test, so it is estimated from the bulk volume (equation 8) minus the solid volume (equation 11) using,

$$V_p(t) = V_b(t) - V_s(t) = V_b(t) - V_{s,0} - \Delta V_s(t) \tag{12}$$

The water volume in the sample is not directly measured. So, to estimate the water volume as function of time we use,

$$V_b = V_p + V_s = V_w + V_o + V_s \tag{13}$$

where V_w and V_o are the volumes of water and oil. When this equation is re-shuffled for water volume, which is the unknown parameter in this experimental design, the measured quantities, namely the bulk volume, solid volume, and oil volume inside the sample, are used. The oil volume in the sample at any

time is estimated from the initial oil volume minus the oil volume produced in a vertically oriented gravity glass separator. The oil (S_o) and water (S_w) saturations in the sample are then given by,

$$S_o(t) = \frac{V_o(t)}{V_p(t)} \text{ and } S_w(t) = \frac{V_w(t)}{V_p(t)} \quad (14)$$

These equations implicitly obey the requirement that $S_o + S_w = 1$.

Triaxial test program

The mechanical tests were performed according to the following procedure:

1. Mounted the cores in the triaxial cell with bypass valve open (no flow through the cores).
2. Simultaneously increased confining pressure (σ_{rad}) to 1.2 MPa and pore pressure (P_p) to 0.7 MPa.
3. Increased temperature to 130°C.
4. Increased hydrostatic stress to approximately 1.5 times yield at 0.045 MPa/min loading rate while observing volumetric strain to determine stiffness and strength. The stiffness measurements were carried out during loading conditions and hereon referred to as 'bulk modulus'.
5. Observed volumetric creep and oil production with constant pore pressure and hydrostatic stress with bypass valve open the first 15 days.
6. On the 16th creep day the bypass valve was closed and $MgCl_2$ brine was flooded at 0.010 ml/min flow rate.
7. Increased $MgCl_2$ brine flow rate to 0.040 ml/min after a certain number of days.
8. Decreased flow rate back to 0.010 ml/min.
9. Cleaned the cores with four PVs of DW at the end of the test.
10. Decreased temperature to room temperature. Used toluene to remove leftover oil from cores M3&M4, followed by methanol flooding to remove toluene. Multiple iterations of toluene and methanol flooding were performed till the effluent became completely transparent in colour.
11. Used DW to remove methanol from these cores.
12. Chromatographic separation tests were performed on all four samples.
13. Demount cores from the triaxial cell and measured saturated mass. Kept them in an oven at 110°C overnight.
14. Measured dry weights, lengths and diameters the day after.
15. Cut the cores into 6 sections of almost equal lengths. The density and specific surface area of these sections and of the unflooded end pieces were measured using gas pycnometer and Brunauer–Emmett–Teller (BET) theory, respectively.

Effluent samples were taken two to three times a week during steps 5 to 9. The ionic composition was estimated using ion chromatography. The oil production was measured for mixed wet cores M3 and M4 using a separator on the downstream side of the triaxial cell. Due to pore pressure fluctuations during the M3 test, the oil volume measurements were disregarded because of emulsification of the produced oil. Pore volume was estimated from the solid volume estimate and bulk volume measurement. With the oil production from core M4 known, the remaining oil volume inside the core was estimated.

Mineral density and specific surface area determination

The mineral density and specific surface area were estimated by Gas Pycnometry and Brunauer–Emmett–Teller (BET) technique, respectively.

Before the mineral density was measured, the cut sections for all samples were kept in the oven at 110°C overnight. Next morning these sections were taken out and placed in a vacuum sealed container to cool

down. Each section was weighted and inserted, one-by-one, into the Micromeritics AccuPyc II 1340 Gas Pycnometer (using helium) to measure the solid volume. With mass and solid volume known, the mineral density of each section was estimated.

BET theory works by determining the adsorption of gas molecules on a solid surface (Brunauer et al. 1938). The specific surface area measurements were carried out on Micromeritics TriStar II instrument using liquid nitrogen, as it does not chemically react with the chalk. Two grams of powdered chalk was added to the sample glass tube and degassed for 5 hours at 110°C on Micromeritics VacPrep 061 Sample Degas System. A stable vacuum pressure of 20-30 mTorr was attained for all tested samples before the sample tubes were attached to the BET apparatus. The specific surface area was measured automatically by the TriStar II 3020 software.

RESULTS

The experimental results are presented in the following way: (i) Wettability determination program based on 3 reference water wet and 3 mixed wet samples, (ii) stiffness and strength measurements from the hydrostatic loading tests, (iii) volumetric deformation during creep, (iv) effluent sample analyses using ion chromatography, (v) oil volume development for the mixed wet samples, (vi) analyses of all cores used in the triaxial test program after tests, and (vii) wettability by chromatographic separation tests after triaxial tests on all samples.

Wettability determination based on 6 samples

Figure 2(a) and (b) show an example of two chromatographic separation tests performed on a completely water wet sample (Mww2) and a mixed wet sample (Mmw3). Here, the reduced ion concentration is plotted against PVs of SW1T flooded. Each dot represents a single effluent sample and the corresponding thiocyanate ion and sulphate ion concentrations. The separation between thiocyanate and sulphate ions can be seen. Figure 2(c) displays the difference between the thiocyanate and sulphate concentrations for the water wet sample (Mww2, blue) and mixed wet sample (Mmw3, green). The green curve has a smaller area and is shifted to the left of the blue. The integrated areas between the two curves were divided by the weight of the core to provide accurate comparison for differently sized cores. The average areas for water wet and mixed wet samples were 1.48 ± 0.08 PV/g and 0.93 ± 0.04 PV/g, respectively. This corresponds to an average W_i of 0.63 ± 0.07 for the wettability-altered samples. The estimated areas for all samples are reported in Table 3 displaying great repeatability. The initial irreducible water saturation ranged from 0.31 to 0.38.

Table 3. Estimated integrated areas per gram of the core for water wet and mixed wet samples, and the corresponding wettability indexes.

	Core	Estimated area between sulphate and tracer (PV)	Integrated sulphate – tracer area per gram core (10^{-3} PV/g)	Wettability index (W_i)	Irreducible water saturation (S_{wi})
Water wet	Mww1	0.201	1.59	1	1
	Mww2	0.175	1.43	1	1
	Mww3	0.184	1.41	1	1
	Average		1.48±0.08		
Mixed wet	Mmw1	0.112	0.88	0.60±0.03	0.31
	Mmw2	0.114	0.93	0.63±0.03	0.38
	Mmw3	0.118	0.98	0.66±0.04	0.37
	Average		0.93±0.04	0.63±0.07	

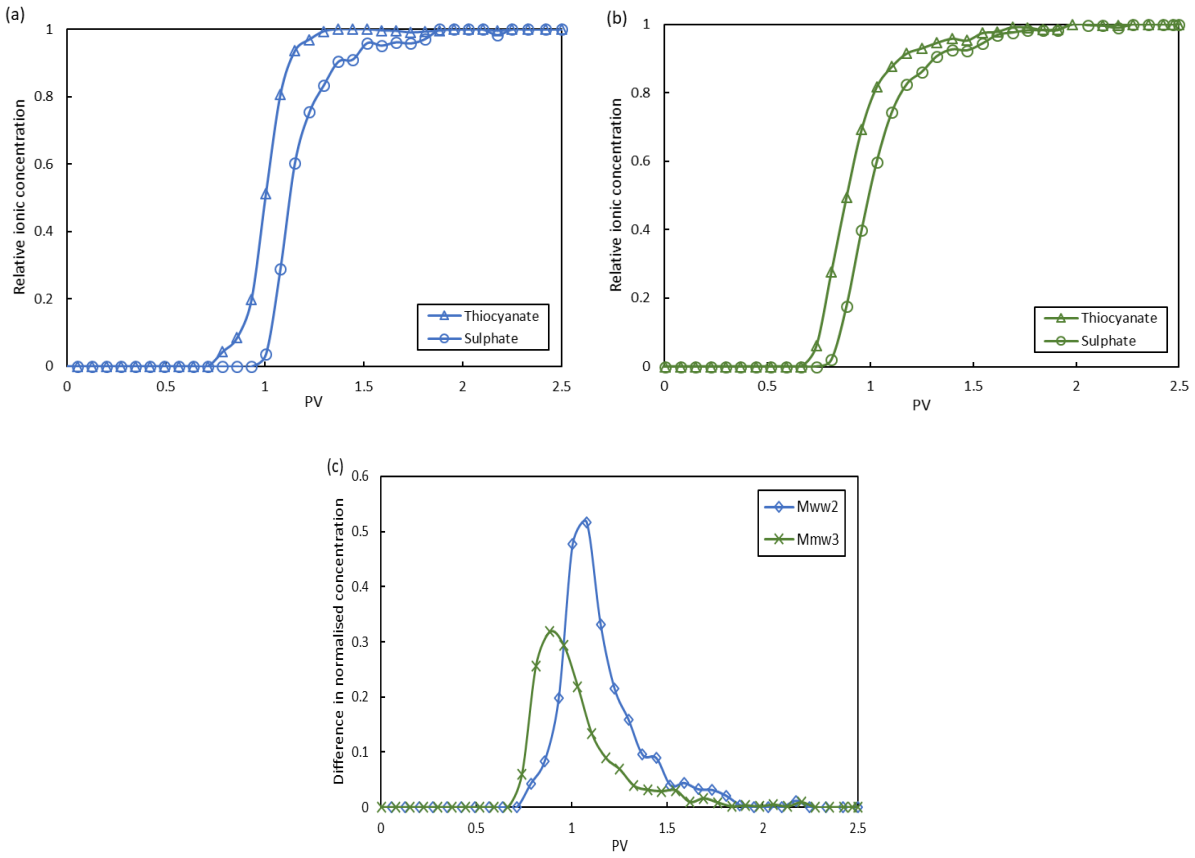

Figure 2. Chromatographic separation on (a) water wet core (Mww2, blue) and (b) mixed wet core (Mmw3, green). The plots (a) and (b) show how the increase in sulphate concentration is delayed compared to the thiocyanate concentration after SW1T is injected. The plot (c) shows the difference in normalised concentrations between the thiocyanate and sulphate curves for the water wet (blue) and mixed wet cores (green). The integrated separation areas for Mww2 and Mmw3 were 1.43×10^{-3} *PV/g and* 0.98×10^{-3} *PV/g, respectively, (Table 3).*

It is assumed that the W_i of the mixed wet samples used in the triaxial test program, drilled from the same block and altered in the same way, was also 0.63 ± 0.07.

Stiffness and strength determination from hydrostatic loading tests

The volumetric strain was measured during hydrostatic loading from 1.2 MPa to approximately 1.5 times the yield at 130°C and 0.7 MPa pore pressure. The onset of yield stress was determined at the point when the stress – strain curve deviated by more than 0.5 MPa from the initial straight elastic line used to determine the loading bulk modulus (K). The stress-strain curve during loading and the yield stresses for all four cores are shown in Figure 3(a), and the yield stress, bulk modulus and creep stress used further are reported in Table 4 that also display the initial water saturation.

Table 4. Bulk modulus, onset of yield stress and creep stress of M1 to M4 samples from hydrostatic loading at 130°C, 0.7 MPa pore pressure and with the bypass kept open.

Core	Wetting state	Initial water saturation (fraction)	Onset of yield stress (MPa)	Creep stress (MPa)	Bulk modulus (GPa)	Uncertainty in bulk modulus ($\times 10^{-1}$ GPa)	Creep stress/yield stress factor
M1	Water wet	1	14.4	21.5	1.3	0.08	1.49
M2		1	13.4	19.3	1.8	0.24	1.44
M3	Mixed wet	0.34	12.4	17.8	1.0	0.06	1.44
M4		0.36	12.3	18.3	1.1	0.09	1.49

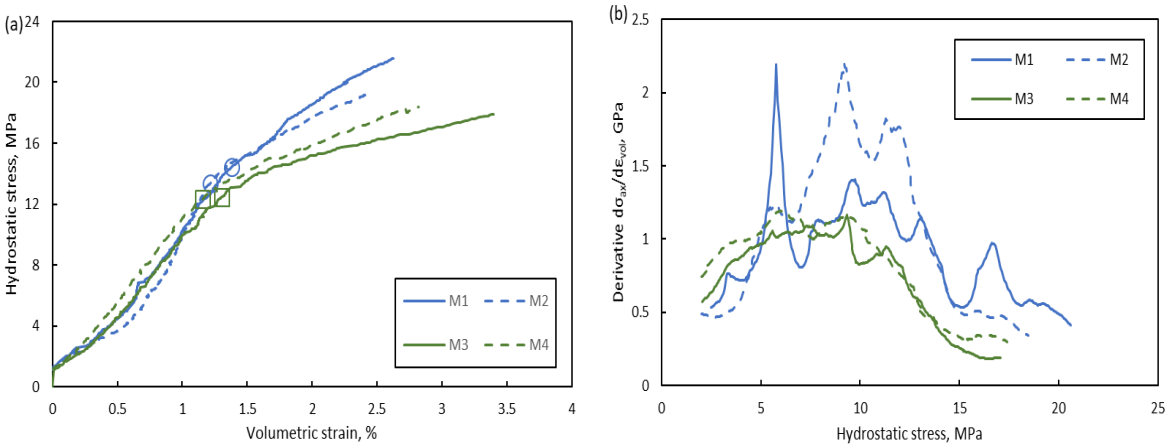

Figure 3. (a) Hydrostatic stress versus volumetric strain for all samples in the triaxial test program. Yield stresses are displayed on the curves. (b) Slope of stress-strain curve plotted as a function of stress. Blue and green lines represent water wet and mixed wet samples, respectively.

Stiffness observations

The loading bulk modulus was estimated from hydrostatic loading curves from 7 MPa to 11 MPa hydrostatic stress interval via equation 4 (reported in Table 4 and Figure 3(a)). The bulk moduli of the water wet samples (M1 and M2) were 1.3 GPa and 1.8 GPa, which were higher than the mixed wet samples (M3 and M4) that had stiffnesses of 1.1 GPa and 1.0 GPa, respectively. When the loading bulk modulus was measured in three other stress intervals, 2 - 10 MPa, 4 - 8 MPa and 4 - 10 MPa, the mixed wet samples M3 and M4 attained the same values (1.0 GPa and 1.1 GPa, respectively). However, the slopes in the stress-strain curves varied for the water wet samples, where M1 varied from 0.9 GPa to 1.8 GPa and M2 varied from 1.0 GPa to 1.3 GPa. Thus, it cannot be claimed that the stiffness is significantly altered by the aging procedure and wettability alteration. This is emphasised in Figure 3(b) where the slopes of the stress-strain curves obtained in +/- 0.5 MPa intervals is plotted against the hydrostatic stresses. Here, the variation in slope during loading is displayed. Stiffness estimates during simple loading are attributed with significant lack of imprecision and it has been discussed to what extent this is a valid method. The yield stress, however, can potentially be interpreted with greater certainty as seen in Figure 3(b) where the slope decreases systematically for all samples.

Strength observations

The yield stresses for all cores are reported in Table 4 and shown on the loading curves in Figure 3. The water wet cores (M1 and M2) yielded at 13.90 ± 0.50 MPa, while the mixed wet cores (M3 and M4)

yielded at 12.35 ± 0.05 MPa. The yield stresses were also measured using the same elastic regions defined in the 'Stiffness observations' and were found to be varying in a range of ± 1 MPa. Even though the actual numbers obtained suggest that the water wet samples are stronger than the mixed wet samples, we cannot claim the differences observed to be significant since the certainty of the experimental method and interpretation is above or in the same range as the differences. Hence, the yield strength of water wet and mixed wet samples were found to be almost similar. Figure 4 shows the relationship between strength and stiffness based on the data reported in Table 4.

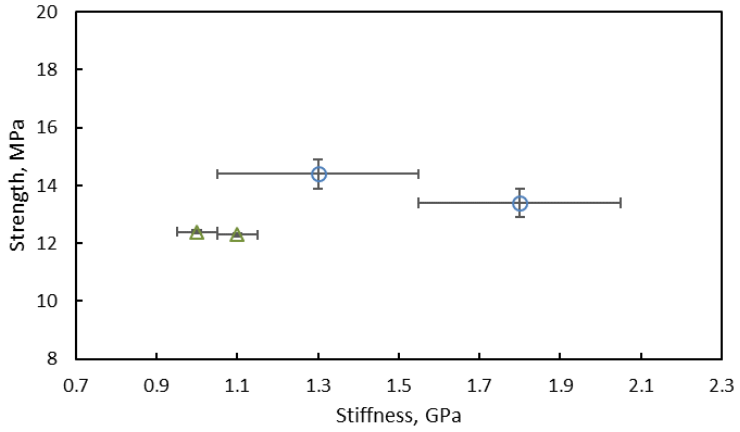

Figure 4. Plastic strength (onset of yield) versus stiffness (bulk modulus).

Volumetric deformation during creep

The creep stress was set to approximately 1.5 times yield stress. Since the yield stress was determined by naked eye during loading, the actual creep stresses deviated from the 1.5 factor when the yield stress was determined systematically. A variation between a factor of 1.44 and 1.49 times yield stress was used (Table 4). The creep strains and creep strain rates are shown in Figure 5 and Figure 6, respectively, for all four cores. The volumetric creep strain for different wettability cores followed a similar trend during the stagnant fluid creep period (black dotted lines in Figure 5 and all dotted lines in Figure 6). At the start of $MgCl_2$ flow at a rate of 0.010 ml/min, we observe that the strain rate decreased for approximately 15 days before an acceleration phase is observed for all cores (red dashed lines in Figure 5 and all solid lines in Figure 6). It is also observed that the creep curves obtained for the water wet core M2 and the mixed wet core M3 were almost parallel to each other (Figure 5). These two had a saturation porosity before test of 43.2% and 43.3%, respectively. The two other curves for the samples M1 and M4, with a porosity of 42.2% and 42.1% respectively, were also parallel. This may indicate how porosity can determine mechanical property, and further that the chalk mechanical behaviour is independent of the presence of oil in the cores but rather dependent on the solid framework and/or mineralogy of chalk. After increasing the flow rate four times to 0.040 ml/min in all cores, a flow rate induced accelerated strain (dark gray solid lines in Figure 5 and all dashed lines in Figure 6) is observed for all cores.

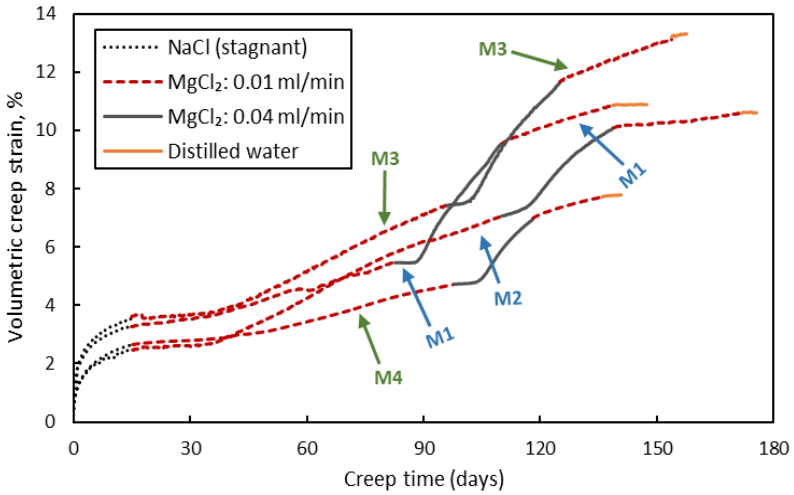

Figure 5. Volumetric creep strain with time for 100% brine saturated water wet cores M1 and M2 (blue arrows), and oil and brine saturated mixed wet cores M3 and M4 (green arrows).

Afterwards, the flow rate was reduced back to 0.010 ml/min leading to a rapid reduction in strain rate for all cores. The strain rate for all cores dropped to the original value obtained during the first flooding period at 0.010 ml/min. Before demounting, all cores were flooded by DW to remove salts from the pores and a sudden drop to almost zero in the creep strain rate for all cores was obtained (orange solid lines in Figure 5 and all dash-dotted lines in Figure 6). Hence, the slope of the creep curves was observed to be different for all cores, but the response to any changes in brine and flow rates was similar. The final volumetric creep strains at the end of the tests for cores M1 to M4 are 10.9% (after 147.5 creep days), 10.6% (after 175.7 creep days), 13.3% (after 157.7 creep days) and 7.8% (after 141.8 creep days), respectively.

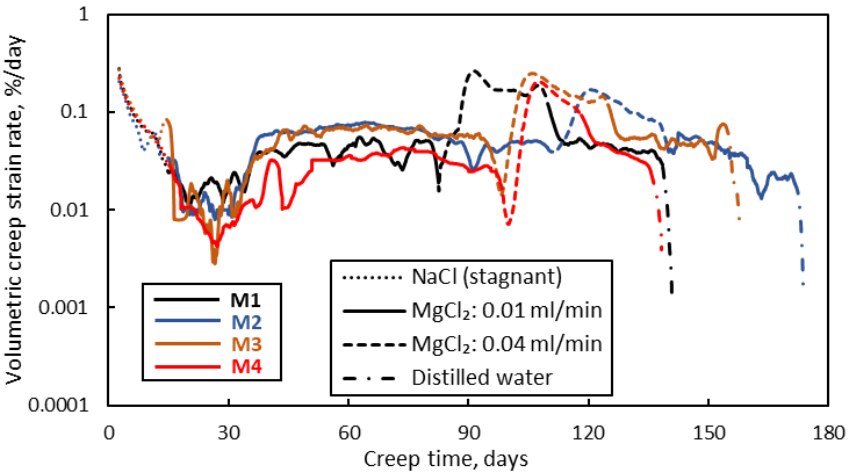

Figure 6. Volumetric creep strain rate with time for 100% brine saturated water wet cores M1 (black) and M2 (dark blue), and oil and brine saturated mixed wet cores M3 (brown) and M4 (red). The different brines are shown by (a) dotted lines for NaCl brine, (b) solid lines for $MgCl_2$ brine at a flow rate of 0.010 ml/min, (c) dashed lines for $MgCl_2$ brine at a flow rate of 0.040 ml/min, and (d) dash-dotted lines for DW.

Effluent ion concentration during $MgCl_2$ brine flow

Rock-fluid interactions changes the ion concentration of the effluent brine. Effluents were sampled two to three times per week during creep phase. The ion concentrations of the two most important ions, calcium and magnesium, for the water wet (M1 and M2) and mixed wet (M3 and M4) cores are shown in Figure 7.

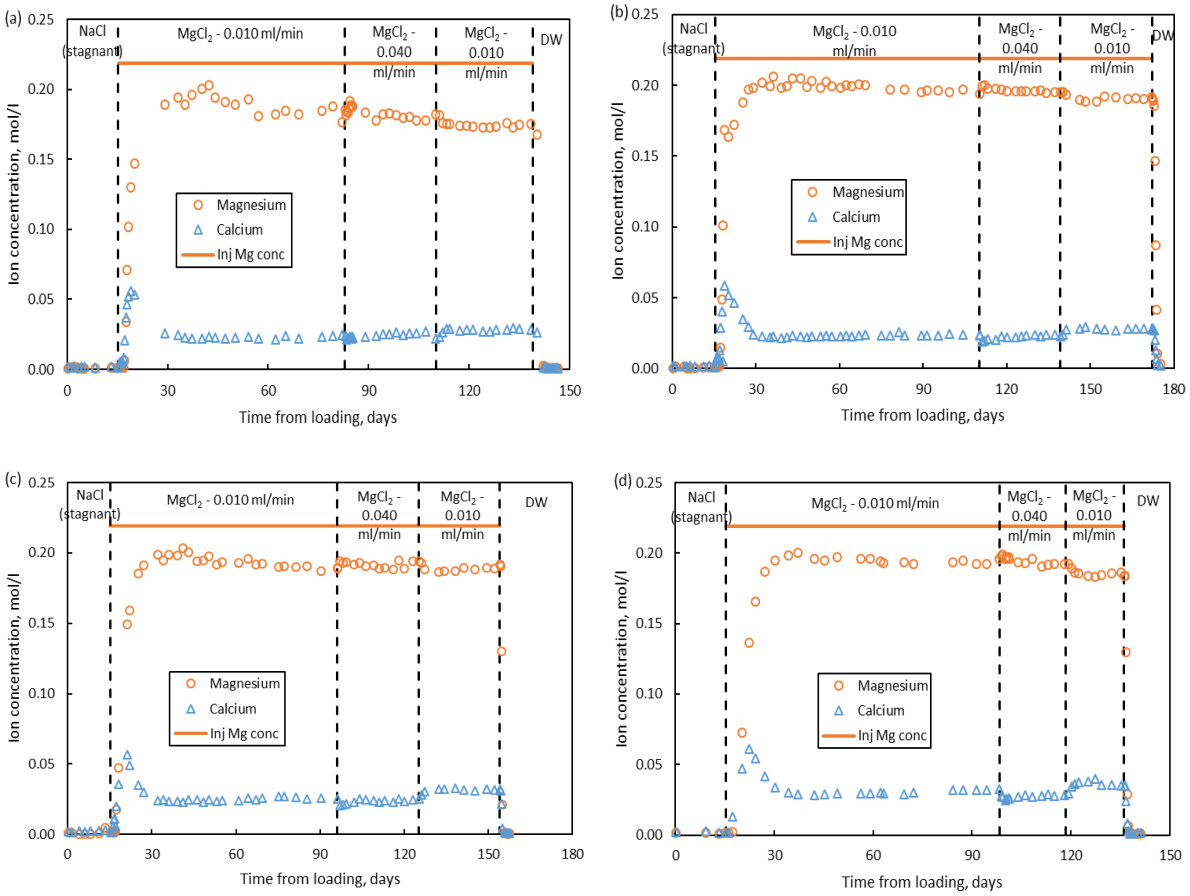

Figure 7. Samples flooded by 0.219M $MgCl_2$ brine. Effluent ion concentrations of calcium and magnesium and the injected magnesium concentration are shown for water wet cores (a) M1 and (b) M2, and mixed wet cores (c) M3 and (d) M4.

In all four plots in Figure 7, the magnesium concentration decrease compared to the injected concentration. This is a result of adsorption of magnesium ions on the mineral surface and desorption of calcium ions, and precipitation of magnesium-bearing mineral phases and dissolution of calcium carbonate (Madland et al. 2011; Nermoen et al. 2015; Zimmermann et al. 2015; Minde et al. 2017, 2018a, 2018b; Andersen et al. 2018; Sachdeva et al. 2019).

From 15 days onward when $MgCl_2$ brine flow started, a transient period in the calcium production and magnesium retention is seen until around 30 days, after which the production/retention stabilised. From 15 to 30 days the retention and production are interpreted to be a combination of dissolution/precipitation and adsorption/desorption processes. The retained magnesium concentration stabilised at 0.190-0.195 mol/l for all four samples irrespective of the wettability and initial saturations. The produced calcium concentration stabilised at 0.020-0.025 mol/l and 0.025-0.030 mol/l for water wet and mixed wet cores, respectively, i.e. the water wet samples displayed a slightly larger calcium production than the mixed wet samples. Further, in Figure 7(b), (c) and (d), when $MgCl_2$ flooding rate was increased four-fold to 0.040 ml/min, the produced calcium concentration decreased to around 0.020-

0.022 mol/l, whereas it remained almost unchanged for water wet sample M1 (Figure 7(a)). The change in magnesium concentration was found to be less sensitive to flow rate than for calcium and the flow rate sensitivity for magnesium ions was found to be similar for both water wet and mixed wet samples. Afterwards when the flow rate was decreased back to 0.010 ml/min, the magnesium concentration also decreased to around 0.180-0.185 mol/l for all four cores and the calcium concentration was found to have increased to a value around 0.025-0.030 mol/l and 0.033-0.038 mol/l for water wet and mixed wet cores, respectively. Same trends were seen for $MgCl_2$ flow through Kansas chalk (Sachdeva et al. 2019).

During cleaning, the calcium and magnesium concentrations fall drastically to almost zero for all cores, confirming that negligible to minor interactions occurred during DW flooding.

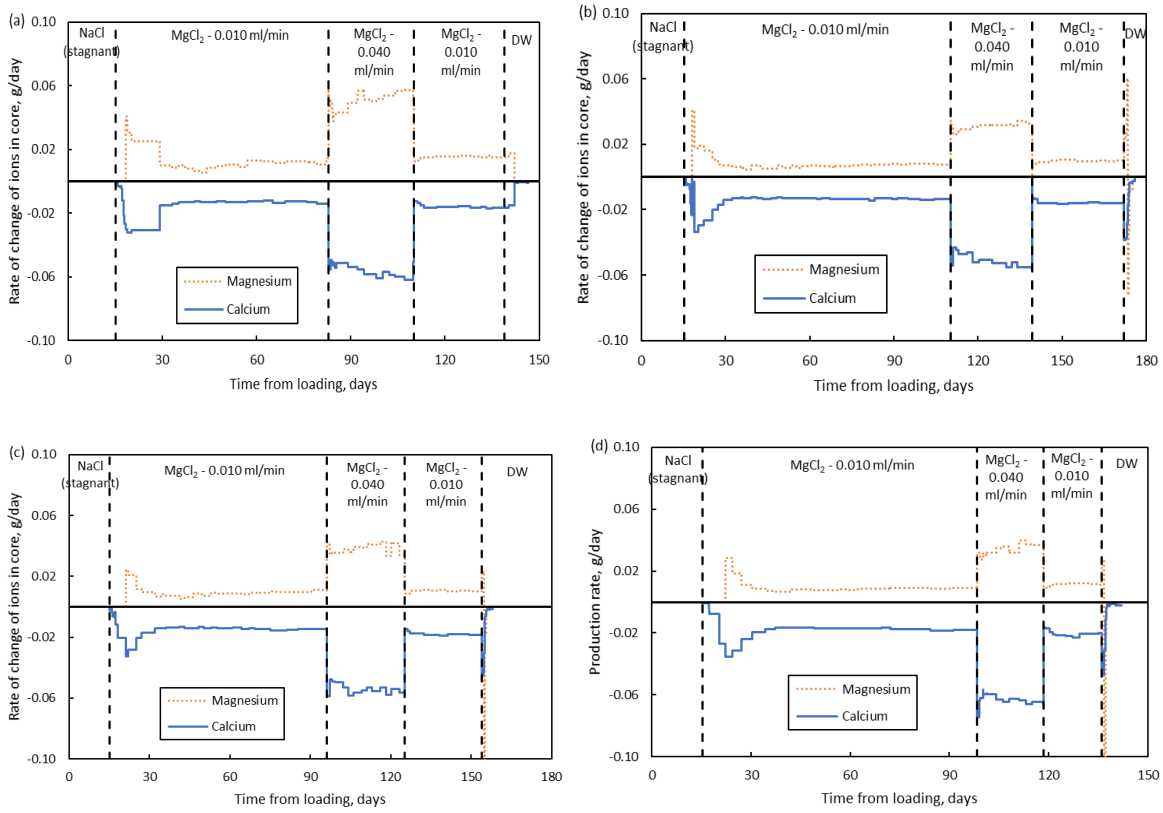

Figure 8. Samples flooded by 0.219M $MgCl_2$ brine. Evolution of rate of change of calcium and magnesium ions in the core (g/day) as a function of time is shown for 100% brine saturated water wet cores (a) M1 and (b) M2, and oil and brine saturated mixed wet cores (c) M3 and (d) M4.

The production rate of calcium and retention rate of magnesium, in units of gram per day shown in Figure 8, are obtained from a product of the ion concentration change, molar weight and flow rate. The analysis was done from the core perspective, hence the magnesium retained is positive and calcium produced is negative. For all cores, the rate of change of these two ions was zero during bypassing of NaCl brine for the first 15 days as the flow rate through the cores was zero. When $MgCl_2$ injection started through the cores at a rate of 0.010 ml/min, a peak in the retention and production rates of magnesium and calcium is seen. The magnesium retention rate stabilised around 0.010 g/day, whereas the calcium production rate stabilised around 0.013-0.016 g/day after 15 days of flooding (molecular weights of Ca^{2+} and Mg^{2+} are 40 g/mol and 24 g/mol, respectively). In all the effluent samples indicated that the dry mass reduced during $MgCl_2$ flow.

When the flow rate increased four times to 0.040 ml/min, the retention rate of magnesium increased to 0.029 – 0.057 g/day and the calcium dissolution rate to 0.047 – 0.060 g/day. Hence, an increase of 3 to 6 times in the magnesium retention rate and 3 to 4 times in the calcium production rate was observed. When the flow rate reduced to 0.010 ml/min, the magnesium retention and calcium production rates dropped to 0.013 g/day and 0.017-0.023 g/day, respectively. When DW was injected, the magnesium retention and calcium production rates fell to zero. The sensitivity to flow rate in the gain of magnesium and loss of calcium (from core perspective) was independent of the wettability and presence of oil implying that sufficient water wet areas existed for the fluid to equilibrate within the core.

The integrated total magnesium retained for the water wet cores was 0.114 moles (2.74 g) for M1 and 0.082 moles (1.96 g) for M2. For the mixed wet cores it was 0.088 moles (2.11 g) for M3 and 0.066 moles (1.58 g) for M4. Similarly, the integrated total calcium dissolved and produced from the cores was 0.078 moles (3.13 g) for M1, 0.086 moles (3.45 g) for M2 for the water wet cores, while for the mixed wet cores 0.085 moles (3.38 g) for M3 and 0.080 moles (3.19 g) for M4 of Ca^{2+} was produced.

Oil production from the mixed wet core (M4) during $MgCl_2$ flow

Oil production as function of time for the core M3 were omitted due to uncertainty in the oil volume readings because of emulsification of the produced fluids. Hence, only measurements for the M4 test are presented here (Table 5). The oil produced, because of $MgCl_2$ flow and compaction, was measured in a gravity separator on the downstream side of the experiment. Readings were recorded from digital photographs taken at frequent time intervals.

Table 5. Initial and final oil and water volumes in mixed wet cores M3 and M4 during $MgCl_2$ brine flow.

Core	M3	M4
Irreducible water volume before test	11.5 ml	12.0 ml
Irreducible water saturation S_{wi}	33.7%	36.4%
Initial oil volume	22.5 ml	21.0 ml
Total oil produced at the end of test	N.A.	11.2 ml
Oil volume after test	N.A.	9.8 ml
Oil Saturation after test S_{or}	N.A.	41.4%
Pore volume before and after test	34.0 ml and 20.4 ml	33.0 ml and 23.7 ml

The irreducible water saturations of M3 and M4 were estimated to be 33.7% and 36.4% with an initial oil in place of 22.5 ml and 21.0 ml before test. For the M4 test, 0.3 ml of oil was produced due to expansion of oil during temperature increase from ambient to 130°C. Figure 9(a) shows the oil with time together with the water volume estimated from equation (13) where the bulk volume, solid volume and pore volume used are displayed in Figure 10, which also displays the porosity evolution with time. In Figure 9(b) the oil saturation inside the core throughout the test from the start of hydrostatic loading using equation (14) is plotted. Before loading, when the sample was mounted, the oil and water volumes were 20.7 ml and 12.3 ml. 1.4 ml of oil was produced during hydrostatic loading to 1.5 times yield, reducing the oil volume to 19.3 ml. During the no-flow period, 3.3 ml of oil was produced due to compaction, which led the oil volume inside the core to further decrease to 16.0 ml by the end of 15th day, in all 4.7 ml oil was produced. During this time, the bulk volume of the sample reduced from 78.4 ml before (Table 1) to 74.2 ml (Figure 10(c)) at 15 days, i.e. a 4.2 ml reduction. Given that the solid

volume is constant, the bulk volume reduction equals the reduction in pore volume ($\Delta V_b = \Delta V_p$). This imply that oil is primarily being produced during compaction, while the water is stagnant inside the core during mechanical loading and creep with no flow.

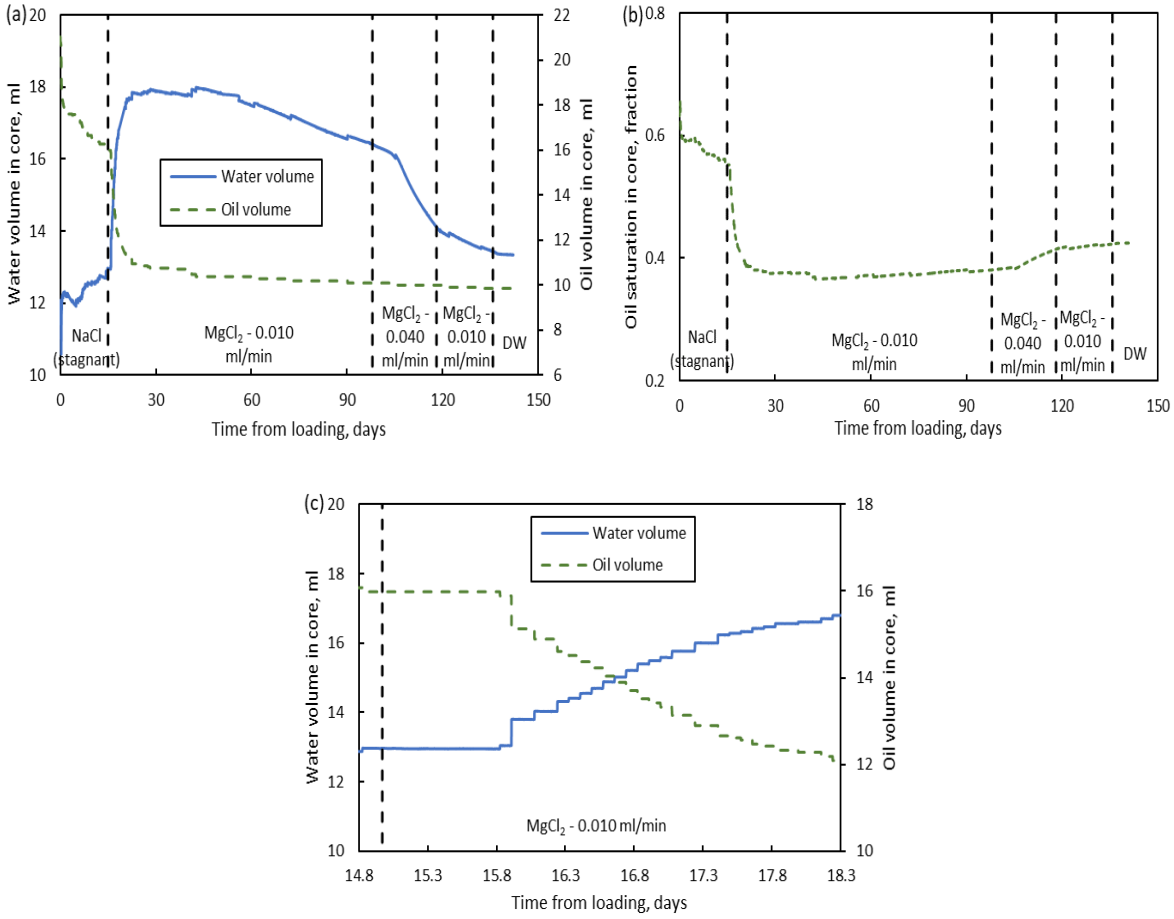

Figure 9. Oil and water volumes with time in the mixed wet sample (M4). (a) Oil and water volumes from measurements of oil volume (separator), bulk volume (compaction) and solid volume (IC effluent analysis), (b) oil saturation in the core with time, and (c) zoomed into oil and water volumes in the core from 14.8 days to 18.3 days. Black dashed vertical lines depict the time when brine composition and/or flow rate changed.

When $MgCl_2$ injection started, a total of 4.8 ml of oil was produced in the first five days (approximately 2.5 PVs), followed by another 1.1 ml in the next 78 days while flooding and compaction co-existed. After increasing the rate to 0.040 ml/min, only 0.2 ml oil produced during the next 20 days, and another 0.1 ml oil produced after reducing it to 0.010 ml/min. At the end of the $MgCl_2$ injection phase the oil volume in the core reduced to 9.8 ml. Figure 9(c) displays a zoomed version of the oil and water volumes in the core at the start of $MgCl_2$ injection phase after the no-flow period. The bulk volume changed during compaction (see equation 9), and the solid volume changed due to non-equilibrium flow (see equation 10).

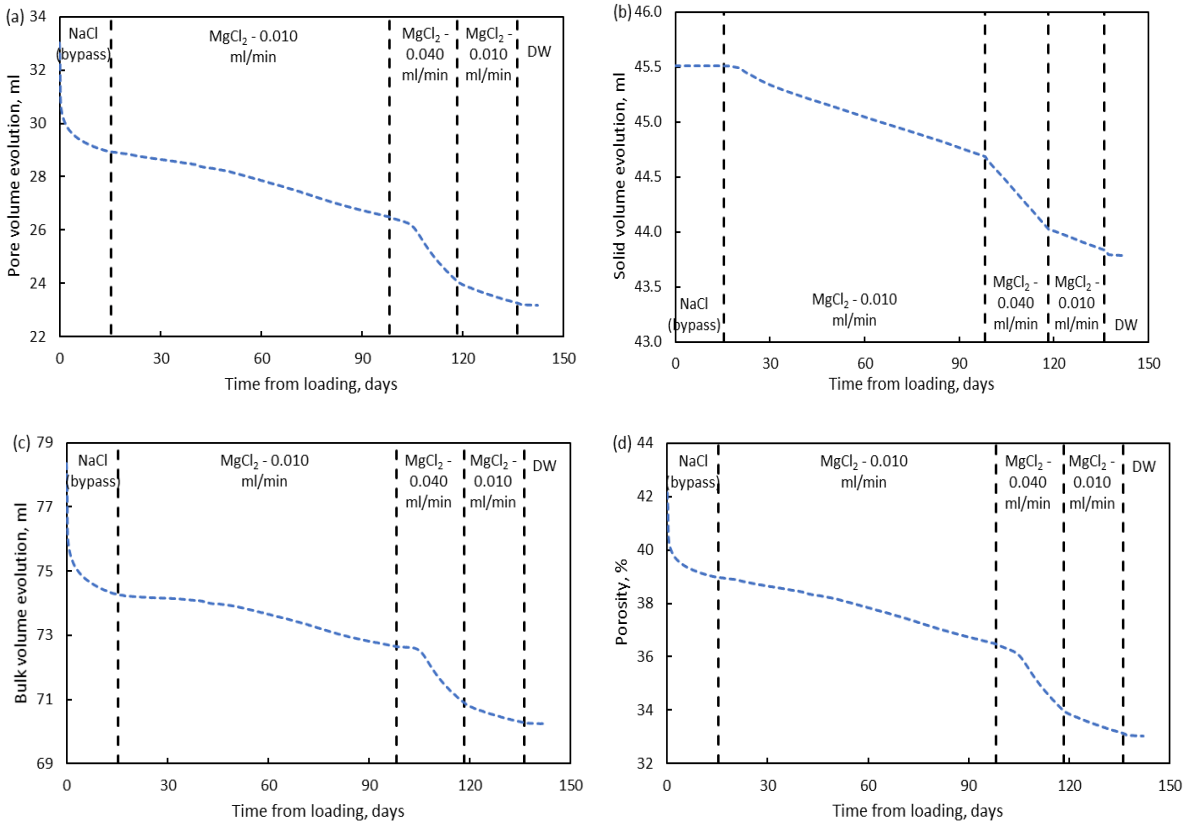

Figure 10. (a) Pore volume, (b) solid volume, (c) bulk volume and (d) porosity evolution with time for mixed wet Mons core M4.

The increase in $MgCl_2$ flow rate to 0.04 ml/min on the 98th day did not lead to any significant additional oil production. At the same time, as presented in (Figure 8), the calcium dissolution and magnesium retention rates (in g/day) increased by a factor of 3 to 6. This did not affect the oil recovery rate. Further on, though pore volume decreased with time because of compaction, only water was expelled from the core. Consequently, the oil saturation increased from 90 days and onwards (Figure 9(b)).

Chromatographic separation test after mechanical test

Chromatographic separation for wettability determination was performed on all four cores after the mechanical tests completed, but before the samples were dismantled from the triaxial cell. The thiocyanate and sulphate concentrations versus PVs of SW1T flooded are shown in Figure 11(a) to (d). The integrated areas between thiocyanate and sulphate curves for all samples are given in Table 6.

Table 6. Integrated areas between thiocyanate and sulphate curves estimated using chromatographic separation tests performed on all samples after mechanical tests. For comparison, water wet cores had an integrated area of 1.41 to 1.59 $\times 10^{-3}$ PV/g and the mixed wet cores had an area of 0.88 to 0.98 $\times 10^{-3}$ PV/g in the wettability determination program (Table 3).

Core	Initial wetting state	Estimated area between sulphate and tracer (PV)	Integrated sulphate – tracer area per gram core ($\times 10^{-3}$ PV/g)	Total $MgCl_2$ flooded (litres)
M1	Water wet	0.238	1.84	2.96
M2		0.294	2.45	3.51
M3	Mixed wet	0.202	1.69	3.26
M4		0.170	1.39	2.61

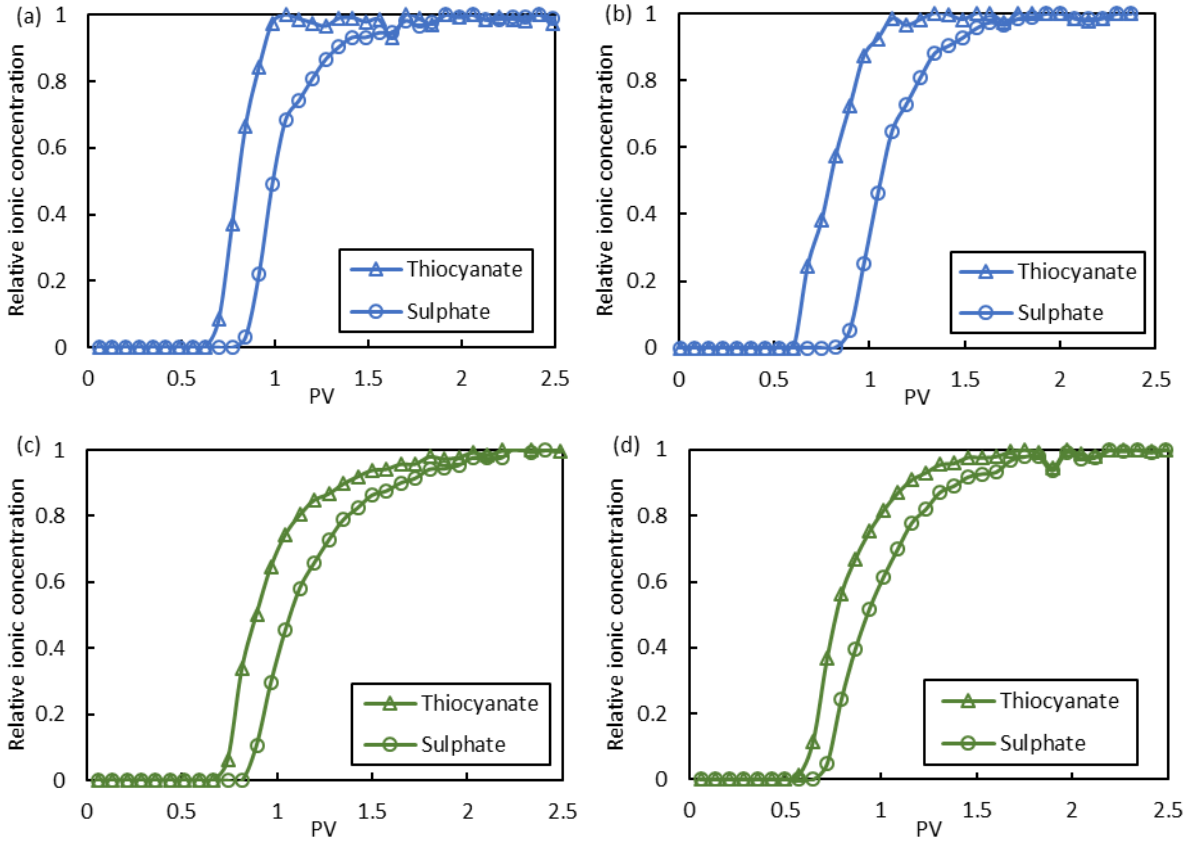

Figure 11. Chromatographic separation tests performed on water wet cores (a) M1 and (b) M2, and mixed wet cores (c) M3 and (d) M4 at ambient temperature after mechanical tests. The plots show reduced ion concentrations of the thiocyanate and sulphate ions for SW1T brine plotted as a function of PVs injected.

All cores showed an increase in the integrated areas compared to the areas obtained in the wettability determination program (Table 3), assumed to be the same for the samples before the mechanical tests. It is observed that the available water wet area increases when more $MgCl_2$ brine is flooded through the cores. From Table 6, the amount of $MgCl_2$ flooded through water wet sample M2 (3.51 litres) is more than that flooded through sample M1 (2.96 litres). The corresponding available water wet area after the mechanical test is also higher for the M2 sample (2.45×10^{-3} PV/g) compared to the M1 sample (1.84×10^{-3}PV/g) (Table 6). The same dependencies are also seen for the mixed wet samples, where more $MgCl_2$ brine through sample M3 (3.26 litres) gave a higher water wet area after the triaxial test (1.69×10^{-3} PV/g) compared to the sample M4 (1.39×10^{-3} PV/g) flooded by 2.61 litres. Dissolution and precipitation processes changes the amount of available mineral surfaces in contact with water and is the only factor at play in the water wet cases, while in the mixed wet cases the increase can also be related to the mobilisation of oil adsorbed on the mineral surfaces.

Analysis of core after test

Basic measurements on all four cores after the mechanical tests are reported in Table 7. The dry mass reduced by 1.3 to 2.1 g for all samples while the solid density increased by 0.02-0.04 g/cm^3, thereby reducing solid volume by 0.8 to 1.4 ml. The samples compacted so bulk volume reduced by 8.2 to 12.7 ml. Thus, the pore volume reduced by 9.3 to 13.6 ml.

Table 7. Basic properties of cores measured after tests. Changes compared to the corresponding initial values are given in parenthesis.

Core	M1	M2	M3	M4
Length (mm)	70.2	66.0	66.1	66.9
Average diameter (mm)	36.2	36.3	35.6	35.8
New dry mass (ΔM_s) (g)	128.1 (-1.3)	118.3 (-1.6)	117.6 (-2.1)	120.3 (-1.7)
Saturated mass (g)	152.8	142.7	138.0	144.0
New bulk volume (ΔV_b) (cm^3)	71.7 (-11.2)	68.2 (-10.4)	65.9 (-12.7)	70.2 (-8.2)
New pore volume (ΔV_p) (cm^3)	24.7 (-10.3)	24.4 (-9.5)	20.4 (-13.6)	23.7 (-9.3)
New porosity (%)	34.4 (-7.8)	35.8 (-7.4)	31.0 (-12.3)	33.8 (-8.3)
New solid density ($\Delta \rho_s$) (g/cm^3) (Pycnometry)	2.72 (0.02)	2.71 (0.04)	2.71 (0.04)	2.71 (0.03)
New solid volume (ΔV_s) (cm^3) (Pycnometry)	47.1 (-0.8)	43.7 (-1.2)	43.4 (-1.4)	44.4 (-1.1)
Ratio of volumetric to axial strain (X)	3.87	3.12	3.99	3.84
Test time (days)	147.9	176.0	158.1	142.2

The tested samples were cut into six sections of almost equal lengths with sections numbered from the inlet (Figure 12). The specific surface area along the sample sections and untested end pieces are reported in Table 8.

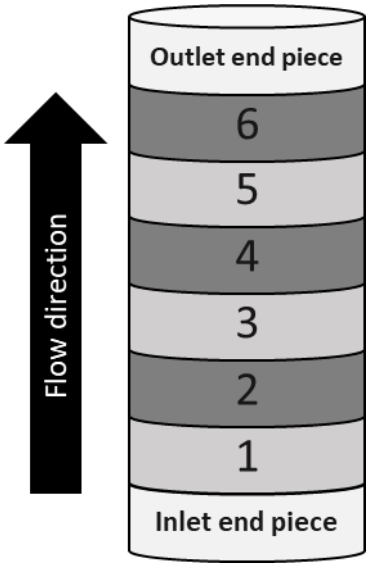

Figure 12. Specific surface area tested along the length of the sample.

Table 8. Specific surface area measurements of unflooded core material from both sides of the core, and for sections along the length of the cores M1 to M4 after tests.

Core	M1	M2	M3	M4
Core section	Water wet		Mixed wet	
	SSA, m^2/g	SSA, m^2/g	SSA, m^2/g	SSA, m^2/g
Outlet end piece (unflooded)	1.82	1.98	2.11	1.96
6	2.33	2.26	2.20	2.02
5	2.47	2.43	2.14	2.08
4	2.45	2.49	2.39	2.44
3	2.45	2.46	2.55	2.45
2	2.47	2.49	3.05	2.82
1	2.18	2.40	3.35	3.02
Inlet end piece (unflooded)	2.13	2.05	2.22	2.17

The SSA of water wet cores M1 and M2 increased from the inlet to the middle and then decreased towards the outlet. Specific surface areas of sections 1 of M1 and M2 were 2.18 m^2/g and 2.40 m^2/g compared to 2.13 m^2/g and 2.05 m^2/g for the unflooded end pieces. They increased to 2.45 m^2/g and 2.49 m^2/g at the middle and then decreased to 2.33 m^2/g and 2.26 m^2/g at the outlet for M1 and M2, respectively. Mixed wet cores M3 and M4 showed a large increase in the SSA of the inlet sections (3.35 m^2/g and 3.02 m^2/g, respectively, compared to 2.22 m^2/g and 2.17 m^2/g for the unflooded end pieces), followed by a gradual decrease from the inlet to the outlet of the flooded samples. The SSA decreased to 2.20 m^2/g and 2.02 m^2/g at the outlet for M3 and M4, respectively.

DISCUSSION

The grain sizes in chalk range from sub-micron to 2-3 microns. This leads to large specific surface areas compared to many other reservoir materials, so that surface interactions with pore fluids become increasingly important to the observed sample dynamics. In effect, water weakening is more likely to occur in chalk than in other reservoir rocks. Wettability of reservoir rock affects the flow and distribution of fluids in the porous media and hence the recovery of oil.

The effect of wettability on stiffness, strength and time-dependent deformation of Mons chalk is documented, and then the results are compared to the Kansas chalk reported in Sachdeva et al. (2019). The key premise is perturbing the experimental conditions (aging time, aging temperature, oil composition, brine composition etc.) to alter the forces at particle level that integrate to the overall core scale geomechanical properties.

Wettability alteration

In the wettability determination program, chromatographic separation was performed on three mixed wet and three reference water wet Mons chalk samples. Based on these measurements, we assume the wettability index of the mixed wet samples in the triaxial test program to be 0.63 ± 0.07 (Table 3). Two aged wettability-altered and two water wet samples were loaded hydrostatically and kept at 1.5 times yield stress over time, and later flooded by $MgCl_2$ brine at varying rate.

Impact of wettability on elastic stiffness and plastic strength

A significant difference in the loading stiffness and yield strength, beyond the experimental uncertainty, was not observed. The initial soft behaviour at low stresses, i.e. the initial large strains of the water wet samples, can be caused by closure of micro-cracks and fractures formed due to the sample handling. Further experiments are required to identify if the mechanical parameters for Mons samples can be altered by aging, e.g. with a more acidic oil, higher aging temperature/time, or by lowering S_{wi} even more before oil is injected.

Oil adsorption impact particle-particle contact forces

The thickness of the charged diffusive layer on calcite surfaces is characterised by the Debye length (Lyklema 2005; Megawati et al. 2013; Voake et al. 2019) that increases with increasing temperature (Andreassen and Fabricius 2010). A thickening of the layer (Debye length) increases the repulsive area between particles causing further weakening of water-saturated samples. Voake et al. (2019) further reported a Debye length of around 200 nm at 130°C using Debye-Huckel theory.

The force between particles in the presence of water is dictated by the sum of attractive van der Waals forces and repulsive electrostatic forces from the overlapping diffusive layer. When oil replace water on surface areas where the double layers would otherwise interact (regions with electrostatic repulsion), the disjoining pressure would reduce and the overall force balance between particles would change. When the normal force between two grains increase (in the case of oil adsorption), it becomes harder for particles to re-organise. This seems to have occurred in Kansas (Sachdeva et al. 2019), which has a Biot coefficient of 0.91 (Voake et al. 2019) and smaller pore size (characterised by the lower relaxation time T_2 estimated from the NMR studies, Voake et al. 2019) than Mons with a Biot coefficient of 0.95 (Figure 13(a) and Table 9 in appendix). If oil adsorbs on mineral surfaces but not on nearby particle contacts, the geomechanical parameters would remain un-affected. This seems to have occurred in Mons (Figure 13(b)).

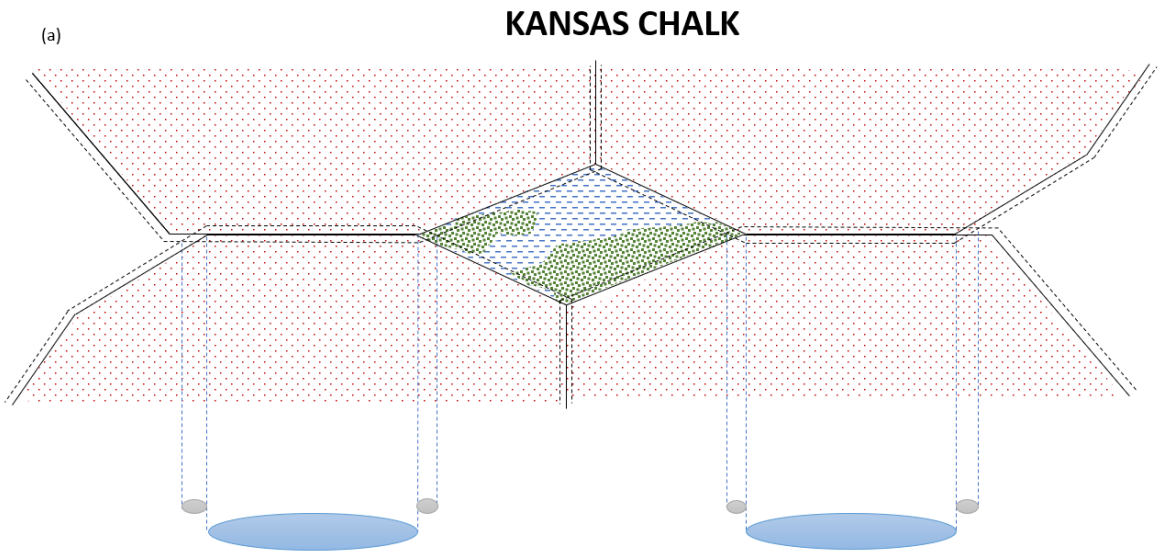

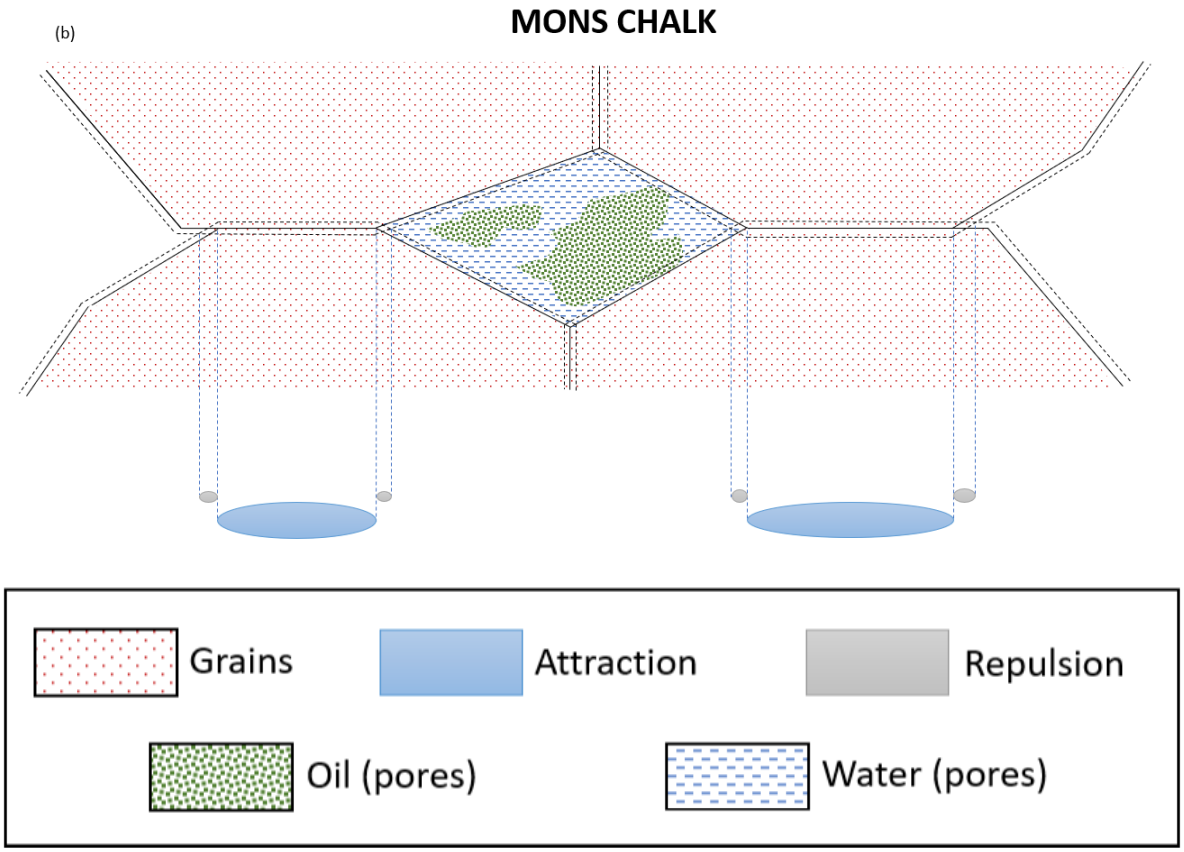

Figure 13. Partitioning of oil and water in pores for (a) Kansas and (b) Mons chalks. Attractive van der Waals and repulsive electrostatic forces present between calcite grains are also shown. Mons chalk has larger pore size and Biot coefficient compared to Kansas chalk (Voake et al. 2019).

With the same oil, brine composition and aging temperature as here, Sachdeva et al. (2018) reported that Kansas chalk remains water wet if the aging time is less than 6 days, and aging for 21 days was enough to obtain a stable mixed wettability. It remains to be tested how mechanical parameters changed for the same oil/water saturation for unaged samples. If the aging conditions were modified, the Mons chalk may become more mixed/oil wet thereby affecting stiffness and strength differently than in this study.

Impact of wettability on creep behaviour during $MgCl_2$ injection

The volumetric creep strain at constant creep stresses (in Table 4) followed a comparable trend for all samples throughout the creep period (Figure 5). The injection of $MgCl_2$ brine induce chemical reactions leading to additional creep rates (Nermoen et al. 2015). When $MgCl_2$ brine was injected at 0.010 ml/min, the strain rate curve continued to follow a decreasing trend for around 15 days, after which it stayed constant (Figure 6). This has also been seen for other clean chalks, e.g. Mons and Stevns Klint (Andersen et al. 2018). All cores showed an accelerated strain when the flow rate was increased to 0.040 ml/min (Figure 5), the strain rate increased by a factor of 3 to 8, and the calcium production and magnesium retention increased by a factor 3 to 6 (Figure 8). This shows how chemical reactions drive solid volume changes (reduce solid mass and increase mineral density), and how this behaviour links to bulk creep strain rate, also seen in Nermoen et al. (2016) and Andersen et al. (2018).

During DW flooding the strain rate dropped down to zero instantly depicting that the electrostatic repulsion between neighbouring particles, when the pores are saturated by salty brines, vanish. It is important to notice that both the chemical reaction dynamics observed by IC analysis and the sensitivity

of the creep rate to the chemical reactions are independent of the oil/water saturation and the initial wetness. This is interpreted to be caused by a shift in the overall force balance between particles, occurring in all samples, where the particle-particle dynamics are controlled by the attractive van der Waals forces and a varying electrostatic repulsion. When the electrostatic repulsion is reduced, the particle-particle friction overcome the local shear stresses, thereby halting the re-organisation.

Calcite-NaCl brine interactions during hydrostatic loading and creep

When NaCl brine was injected into Liège chalk, dissolution of calcite was observed (Madland et al. 2011). In our case, the samples were only saturated by NaCl, and not flooded, and as shown in Figure 7 the concentration of calcium produced was in the range 0.001 – 0.003 mol/l. This means that around 0.0001 moles (0.01 g) of calcite dissolved from a 100% NaCl brine saturated core (with a PV of approximately 34 ml), which amounted to approximately 0.01% in mass compared to the initial dry mass of the samples (approximately 125 g). This percentage would be even less for the mixed wet samples due to the initial irreducible water saturation ranging from 31% to 38%. Therefore, the NaCl brine / rock interactions can be neglected.

Adsorption/desorption dynamics on the calcite surfaces

The calcite mineral surface possesses positively charged Ca^{2+} and negatively charged CO_3^{2-} surface sites (Stipp 1999) that leads to the adsorption of positive and negative ions from the pore fluid. When the pore fluid composition is changed, a new surface-equilibrium between the mineral surface and the ion concentration of the pore is established. The desorption and adsorption dynamics occur typically within the first pore volumes injected, dependent upon the ion concentration of the injected brine. When $MgCl_2$ brine was injected through all cores a plateau in the concentration of the produced effluent was established after approximately 15 days (from 16th day till around 30th day i.e. approximately 6.5 PVs injected, Figure 7), after which the magnesium and calcium concentrations are dominated by dissolution and precipitation processes.

Interactions of calcite with DW during sample cleaning

The solubility of calcite in DW at 25°C is 0.013 g/l (Voake et al. 2019) which decreases with increase in temperature (Coto et al. 2012). If the PV is 34 ml, 0.00044 g of calcite could dissolve per PV during DW flow at 25°C. In this study, four PVs of DW were flooded for cleaning at 130°C. Therefore, the dissolved calcite would be less than 0.0018 g, i.e. less than 0.0015% of the initial dry mass (approximately 125 g). Hence, any calcite dissolved during DW flooding can be neglected, as is also shown in the effluent analysis (Figure 7 and Figure 8).

Chemical alterations along the axis of the core

The non-homogeneous chemical replacement dynamics are observed in the specific surface area measurements (Table 8). The SSA of water wet core increases towards the middle of the core and then decreases towards the outlet, whereas the SSA of the mixed wet cores decreases towards the outlet with the highest value observed at the inlet of the samples. Andersen et al. (2018) demonstrated that the SSA of the water wet Mons chalk also decreased from the inlet to the outlet. This difference in our results may be linked to the initial spatial variability in grain size through the cores. The non-homogenous chemical replacement dynamics were also observed in the SSA measurements of Kansas cores as reported in Sachdeva et al. (2019), where the change in SSA was non-uniform through the core. The trends obtained in Kansas cores were not clear, except that the SSA increased from the inlet towards the middle of the samples.

Dynamic bulk, solid and pore volume measurements

Figure 10 shows how $MgCl_2$ flow rate affect the different volumes with time. Solid volume decreases due to the dissolution of larger calcium ions, which forms the solid framework of chalk, and precipitation

of smaller magnesium ion forming secondary minerals. Pore volume decreases due to compaction and non-equilibrium flow. The rate of decrease in these volumes is larger when the injection rate of $MgCl_2$ is higher (0.040 ml/min). There is also a transition period of around 5 days observed in the pore volume and bulk volume evolution when the flow rate of $MgCl_2$ is increased from 0.010 ml/min to 0.040 ml/min. During this period the pore and bulk volumes decrease at almost the same rate as before, followed by a decrease at an accelerated rate. This transient period in Figure 10 (also observed in Figure 5 at the start of $MgCl_2$ flooding at a higher rate of 0.040 ml/min) shows the delayed weakening during reactive flow of $MgCl_2$, i.e. a delay in the accelerated strain by increased pore collapse rate at constant stress and temperature conditions. The rock framework (acting as force chains) can withstand the chemical reactions for some time, which are dependent upon stresses focussing the dissolution to the load bearing parts (which in our case is the solid framework or the grain-grain contacts following the force chains) of the material, and thus a delayed failure occurs. During the flooding of DW before demounting, no change in the pore volume, solid volume and bulk volume is observed.

Comparing the observed mechanical response with Kansas chalk

Kansas chalk is coccolithic mudstone or wackestone characterised by moderately preserved coccolithopores, whereas Mons chalk is pure coccolithic mudstone (Andersen et al. 2018). Both Kansas and Mons chalks are from Cretaceous age. Mons chalk has > 99 wt% calcite content, whereas Kansas chalk has around 95-97 wt% calcite content. Kansas chalk has gone through a higher degree of diagenesis (Finn and Johnson 2005) than the Mons chalk (Pirson et al. 2008). Previous XRD analyses of the clay fraction (< 2 μm) from these two chalk types have shown differences in their mineralogical assemblage, indicative of different diagenetic conditions (Bertolino et al. 2013; Andersen et al. 2018).

The mechanical parameters of Mons chalk obtained in this study are compared to those obtained from Kansas chalk reported by Sachdeva et al. (2019). We observe that these chalk types differ in their wettability values with the same aging procedure and their mechanical response to chalk at imposed stresses at 130°C. The wettability for the mixed wet Kansas chalk was reported to be 0.55 ± 0.05, whereas mixed wet Mons chalk gave the wetting indices of 0.63 ± 0.07 (Table 3). During loading with stagnant and inert fluids inside the pores, the behaviour observed for Mons differs from Kansas chalk, where a clear difference in both stiffness and strength in response to wettability alteration between the mixed wet samples and water wet samples were seen (Sachdeva et al. 2019).

During time-dependent creep period, water wet and mixed wet Kansas chalk gave a similar creep trend irrespective of the presence of oil (Sachdeva et al. 2019). Similar comparable trends were observed for Mons chalk as well. Strain rates reduced for all Mons cores at the start of $MgCl_2$ flood (Figure 6). It was followed by an increase in strain rates for all cores after approximately 15 days of $MgCl_2$ injection. All strain rates increased even more when flow rate was increased four-fold, followed by a reduction in strain rates when flow rate was reduced again. These rates dropped down to zero for all cores during DW injection. The creep slope was observed to be not the same for all cores, but the response to change in brine and flow rates was the same. Similar observations were also documented for Kansas cores (Sachdeva et al. 2019).

Oil production during compaction and flow

During hydrostatic loading and no-flow creep period (up to 15th day), 4.7 ml oil was produced from mixed wet Mons M4 core. Hence, deformation contributed to 43% of the total oil recovered after the initial thermal expansion. This value is comparable to the bulk volume loss of the sample (i.e. $\Delta V_s = \Delta V_p = \Delta V_{oil}$). Given that the water was not mobilised implies that oil was the mobile phase during compaction. After the first 15 days of creep, $MgCl_2$ was injected. In this phase, all the oil was oil was produced during the initial 2-3 PVs, and after which despite the ongoing chemical reaction and

compaction negligible oil volume was produced from the core. This shows that the non-equilibrium rock-fluid interactions between the calcite surface and $MgCl_2$ brine did not contribute to any tail-end recovery after the initial viscous displacement. When the observed oil production is compared to the chromatographic separation tests after mechanical tests, it can be deduced that the observed increase in the integrated area of the mixed wet samples is related to the creation of new mineral phases due to precipitation rather than the mobilisation of oil volumes wetting the mineral phases.

On the other hand, no oil was produced during the loading and the creep phase due to compaction and further, no oil was recovered during $MgCl_2$ injection through mixed wet Kansas chalk after the initial displacement (Sachdeva et al. 2019). The recovery of oil from Mons chalk due to compaction is likely due to the fact that it is more water wet (W_i of 0.63 ± 0.07, Table 3) to start with compared to the mixed wet Kansas chalk (W_i of 0.55 ± 0.05). Mixed wet Mons M4 core also have a larger volumetric strain during loading and creep in the stagnant phase compared to the Kansas mixed wet cores, which could also have resulted in production of oil. Kansas chalk also has a smaller pore size than Mons (Voake et al. 2019) and due to the capillary forces, they need the extra flow energy from the injection brine to produce oil. However, it remains to be tested how compaction-driven multiphase flow and geomechanical properties are changed for unaged oil/water saturated Kansas and Mons chalk samples.

Summary of the discussion

The results on Mons and Kansas chalks have shown that the initial wettability and oil/water saturation does not play a role in determining the effect of pore fluids on chalk mechanics. Even though $MgCl_2$ brine leads to weakening of chalk, it does not lead to any additional recovery of oil at the defined flow rates, which is likely due to one of these two reasons as reported by Sachdeva et al. (2019): (a) even though a change in the wetting state is observed for mixed wet Mons cores M3 and M4, $MgCl_2$ brine was not able to mobilise the oil stuck on the walls, meaning the new surfaces formed due to precipitation of magnesium-bearing minerals were all in contact with the water phase, and/or (b) pressure difference across the oil ganglia is insufficient to overcome capillary forces. Hence the combined observations from Kansas chalk showed that both compaction and non-equilibrium flow do not contribute to oil production after the initial displacement (Sachdeva et al. 2019), whereas these observations from Mons showed that compaction contributes to oil production up to a certain extent, but non-equilibrium flow does not. It will be important to study, in the future, the effect of increasing the flow rate even more to study the potentiality of $MgCl_2$ brine to improve oil recovery at higher rates.

CONCLUSIONS

We have investigated how injection of $MgCl_2$ brine through hydrostatically compacted Mons chalk impact a) stiffness and strength, b) time-dependent deformation at constant stresses, and c) oil production rates. All samples were loaded to a stress level of 150% of the compaction yield stress. The experiments were performed on both water wet and mixed wet samples. We have compared the observed mechanical response to a similar test series conducted on a different chalk type (Kansas) to display how petrophysical differences impact the overall dynamics.

The water wet and wettability-altered Mons samples were found to have a similar strength, but further investigations are required to define the stiffness relationship. On the other hand, the wettability altered Kansas samples were stiffer and stronger than their water wet counterparts. Hence, the initial wettability was shown to control the elastic stiffness and plastic strength measurements in both chalk types.

The volumetric creep strain and creep strain rate for different wettability cores followed a comparable trend during the stagnant fluid period. The creep response to the injection of $MgCl_2$ brine was also the same, irrespective of the wettability and oil/water saturation. These observations were found for both

the Kansas and Mons chalks. The results seem to indicate that the presence of oil in pores does not prevent brines to access intergranular contacts, i.e. the water weakening by $MgCl_2$ injection prevails.

Further, IC analysis displayed that the chemical reactions were also insensitive to oil in the samples implying that the injected brine can interact with the mineral surfaces. The chemical replacement observed by ion chromatography was insensitive to the presence of oil in the pores, so the outcome from experiments performed on water wet samples can be applied to actual oil reservoir scenarios.

The oil production with time measurements due to compaction in Mons chalk showed a 43% additional oil recovery before the start of reactive brine flooding, whereas no additional oil recovery was seen during this stage in Kansas chalk. After the initial oil was produced during the first 2-3 PVs of $MgCl_2$ injection, neither compaction nor chemical interactions through both the Kansas and Mons chalks led to additional oil recovery.

ACKNOWLEDGEMENT

The authors acknowledge the Research Council of Norway and the industry partners, ConocoPhillips Skandinavia AS, Aker BP ASA, Eni Norge AS, Equinor ASA, Neptune Energy Norge AS, Lundin Norway AS, Halliburton AS, Schlumberger Norge AS, Wintershall Norge AS, and DEA Norge AS, of The National IOR Centre of Norway for support.

AVAILABILITY OF DATA

The data that support the findings of this study are available on request from the corresponding author.

APPENDIX

The main differences between Kansas and Mons chalk types used to discuss the results are reported in Table 9.

Table 9. Differences between Kansas and Mons chalk types.

	Kansas	**Mons**
Carbonate content, %	95-97	> 99
Initial wettability index (Sachdeva et al. 2019)	0.55 ± 0.05	0.63 ± 0.07
Biot coefficient (Voake et al. 2019)	0.91	0.95
Initial porosity, % (Sachdeva et al. 2019)	35-38	42-44
Initial water saturation, % (Sachdeva et al. 2019)	26-29	31-38
Relaxation time T_2 from NMR studies, ms (Voake et al. 2019)	15-80	35-200

REFERENCES

Ahsan, R. and Fabricius, I.L., 2010. Sorption of magnesium and sulfate ions on calcite. In 72nd EAGE Conference and Exhibition incorporating SPE EUROPEC 2010, Extended Abstracts, SP13.

Alam, M.M., Ahsan, R., Shaik, A.K., and Fabricius, I.L., 2010. Surface charge of calcite and its influence on the electrical conductivity in chalk. In 80th Annual International Meeting, Society of Exploration Geophysicists, Expanded Abstracts, 2686-2691.

Andersen, P.Ø., Wang, W., Madland, M.V., Zimmermann, U., Korsnes, R.I., Bertolino, S.R.A., Minde, M., Schulz, B., and Gilbricht, S., 2018. Comparative Study of Five Outcrop Chalks Flooded at Reservoir Conditions: Chemo-mechanical Behaviour and Profiles of Compositional Alteration. *Transport in Porous Media*, **121**(1), 135-181.

Andreassen, K.A. and Fabricius, I.L., 2010. Biot critical frequency applied to description of failure and yield of highly porous chalk with different pore fluids. *Geophysics*, **75**(6), E205-E213.

Bertolino, S.A.R., Zimmermann, U., Madland, M.V., Hildebrand-Habel, T., Hiorth, A., and Korsnes, R.I., 2013. Mineralogy, geochemistry and isotope geochemistry to reveal fluid flow process in flooded chalk under long term test conditions for EOR purposes. In XV International Clay Conference, Brasil, **676**.

Borromeo, L., Egeland, N., Minde, M.W., Zimmermann, U., Andò, S., Madland, M.V. and Korsnes, R.I., 2018. Quick, Easy, and Economic Mineralogical Studies of Flooded Chalk for EOR Experiments Using Raman Spectroscopy. *Minerals*, **8**(6), 221. ISSN 2075-163X. DOI: https://doi.org/10.3390/min8060221.

Brunauer, S., Emmett, P.H., and Teller, E., 1938. Adsorption of gases in multimolecular layers. *Journal of the American Chemical Society*, **60**(2), 309-319.

Coto, B., Martos, C., Peña, J. L., Rodríguez, R., and Pastor, G., 2012. Effects in the solubility of $CaCO_3$: Experimental study and model description. *Fluid Phase Equilibria*, **324**, 1-7.

Fabricius, I.L. and Borre, M.K., 2007. Stylolites, porosity, depositional texture, and silicates in chalk facies sediments. Ontong Java Plateau–Gorm and Tyra fields, North Sea. *Sedimentology*, **54**(1), 183-205.

Fan, T. and Buckley, J.S., 2007. Acid number measurements revisited. *SPE Journal*, **12**(04), 496-500.

Finn, T.M. and Johnson, R.C., 2005. Niobrara Total Petroleum System in the Southwestern Wyoming Province. Chapter 6 of *Petroleum Systems and Geologic Assessment of Oil and Gas in the Southwestern Wyoming Province, Wyoming, Colorado, and Utah*, U.S. Geological Survey Digital Data Series DDS-69-D, U.S. Geological Survey, Denver, Colorado.

Gauer, P.R., Sylte, J.E., and Nagel, N.B., 2002. Ekofisk Field Well Log Decompaction. Paper SPE/ISRM 78177 presented at the Rock Mechanics Conference, Irving, Texas, October 20-23.

Heggheim, T., Madland, M.V., Risnes, R., and Austad, T., 2005. A Chemical Induced Enhanced Weakening of Chalk by Seawater. *Journal of Petroleum Science and Engineering* **46**, 171-184.

Hellmann, R., Renders, P.J.N., Gratier, J.P., and Guiguet, R., 2002a. Experimental pressure solution compaction of chalk in aqueous solutions. Part 1. Deformation behavior and chemistry. *Water-Rock Interactions, Ore Deposits, and Environmental Geochemistry: A Tribute to David A. Crerar*, **7**(7), 129–152.

Hellmann, R., Gaviglio, P., Renders, P.J.N., Gratier, J.P., Bekri, S., and Adler, P., 2002b. Experimental pressure solution compaction of chalk in aqueous solutions. Part 2. Deformation examined by SEM, porosimetry, synthetic permeability, and X-ray computerized tomography. *Water-Rock Interactions, Ore Deposits, and Environmental Geochemistry: A Tribute to David A. Crerar*, **7**(7), 153–178.

Hermansen, H., Landa, G.H., Sylte, J.E., and Thomas, L.K., 2000. Experiences after 10 years of waterflooding the Ekofisk field, Norway. *Journal of Petroleum Science and Engineering*, **26**, 11–18.

Hiorth, A., Cathles, L.M., and Madland, M.V., 2010. The impact of pore water chemistry on carbonate surface charge and oil wettability. *Transport in porous media*, **85**(1), 1-21.

Hofmann, S., Voïtchovsky, K., Spijker, P., Schmidt, M., and Stumpf, T., 2016. Visualising the molecular alteration of the calcite (104) – water interface by sodium nitrate. *Scientific reports*, **6**, 21576.

Korsnes, R.I., Madland, M.V., and Austad, T., 2006a. Impact of Brine Composition on the Mechanical Strength of Chalk at High Temperature. *Eurock 2006: Multiphysics Coupling and Long Term Behaviour in Rock Mechanics*, Taylor and Francis, London, 133-140.

Korsnes, R.I., Strand, S., Hoff, O., Pedersen, T., Madland, M.V., and Austad, T., 2006b. Does the Chemical Interaction between Seawater and Chalk affect the Mechanical Properties of Chalk? *Eurock 2006: Multiphysics Coupling and Long Term Behaviour in Rock Mechanics*, Taylor and Francis, London: p. 427-434.

Korsnes, R.I., Madland, M.V., Austad, T., Haver, S., and Røsland, G., 2008. The Effects of Temperature on the Water Weakening of Chalk by Seawater. *Journal of Petroleum Science and Engineering*, **60**, 183-193.

Liu, J., Wani, O.B., Alhassan, S.M., and Pantelides, S.T., 2018. Wettability Alteration and Enhanced Oil Recovery Induced by Proximal Adsorption of Na^+, Cl^-, Ca^{2+}, Mg^{2+}, and SO_4^{2-} Ions on Calcite. *Physical Review Applied*, **10**(3), 034064.

Lyklema, J., 2005. *Fundamentals of interface and colloid science: soft colloids,* **5**. San Diego, USA: Elsevier, Academic Press.

Madland, M.V., Hiorth, A., Korsnes, R.I., Evje, S., and Cathles, L., 2009. Rock Fluid Interactions in Chalk Exposed to Injection of Seawater, $MgCl_2$, and NaCl Brines with Equal Ionic Strength. Paper A22 presented at the 15th European Symposium on Improved Oil Recovery, Paris, France, April 27-29.

Madland, M.V., Hiorth, A., Omdal, E., Megawati, M., Hildebrand-Habel, T., Korsnes, R.I., Evje, S., and Cathles, L.M., 2011. Chemical Alterations Induced by Rock-Fluid Interactions when Injecting Brines in High Porosity Chalks. *Transport in Porous Media*, **87**, 679-702.

Madland, M.V., Midtgarden, K., Manafov, R., Korsnes, R.I., Kristiansen, T.G., and Hiorth, A., 2008. The Effect of Temperature and Brine Composition on the Mechanical Strength of Kansas Chalk. Paper SCA2008-55 presented at the International Symposium of the Society of Core Analysts, Abu Dhabi, UAE, October 29-November 2.

Maury, V., Piau, J.M., and Halle, G., 1996. Subsidence induced by water injection in water sensitive reservoir rocks: The example of Ekofisk. Paper SPE 36890 presented at the SPE European Petroleum Conference, Milan, Italy, October 22-24.

Megawati, M., Andersen, P.Ø., Korsnes, R.I., Evje, S., Hiorth, A., and Madland, M.V., 2011. The effect of aqueous chemistry pH on the time-dependent deformation behavior of chalk experimental and modelling study. In: Pore2Fluid International Conference. 16–18 Nov, Paris, France.

Megawati, M., Hiorth, A., and Madland, M.V., 2013. The impact of surface charge on the mechanical behavior of high-porosity chalk. *Rock Mechanics and Rock Engineering*, **46**(5), 1073-1090.

Megawati, M., Madland, M.V., and Hiorth, A., 2015. Mechanical and physical behavior of high-porosity chalks exposed to chemical perturbation. *Journal of Petroleum Science and Engineering*, **133**, 313–327. http://dx.doi.org/10.1016/j.petrol.2015.06.026.

Minde, M.W., Haser, S., Korsnes, R.I., Zimmermann, U., and Madland, M.V., 2017. Comparative Studies of Mineralogical Alterations of Three Ultra-long-term Tests of Onshore Chalk at Reservoir Conditions. In: 19th European Symposium on Improved Oil Recovery/IOR Norway 2017. European Association of Geoscientists and Engineers. ISBN 978-94-6282-209-2.

Minde, M.W., Zimmermann, U., Madland, M.V., Korsnes, R.I., Schulz, B. and Gilbricht, S., 2018a. Mineral Replacement in Long-Term Flooded Porous Carbonate Rocks. Submitted to *Geochimica et Cosmochimica Acta*, publication under review.

Minde, M.W., Wang, W., Madland, M.V., Zimmermann, U., Korsnes, R.I., Bertolino, S.R., and Andersen, P.Ø., 2018b. Temperature effects on rock engineering properties and rock-fluid chemistry in opal-CT-bearing chalk. *Journal of Petroleum Science and Engineering*, **169**, 454-470.

Nagel, N.B., 1998. Ekofisk Field Overburden Modelling. Paper SPE 47345 presented at the SPE/ISRM Rock Mechanics in Petroleum Engineering, Trondheim, Norway, July 8-10.

Nagel, N.B., 2001. Compaction and subsidence issues within the petroleum industry: From Wilmington to Ekofisk and beyond. *Physics and Chemistry of the Earth, Part A: Solid Earth and Geodesy*, **26**(1-2), 3-14.

Nermoen, A., Korsnes, R.I., Hiorth, A. and Madland, M.V., 2015. Porosity and Permeability Development in Compacting Chalks during Flooding of Non-Equilibrium Brines: Insights from Long-Term Experiment. *Journal of Geophysical Research: Solid Earth*, **120**, doi: 10.1002/ 2014JB011631.

Nermoen, A., Korsnes, R.I., Aursjø, O., Madland, M.V., Kjørslevik, T.A., and Østensen, G., 2016. How stress and temperature conditions affect rock-fluid chemistry and mechanical deformation. *Frontiers in Physics*, **4**, 2.

Nermoen, A., Korsnes, R.I., Storm, E.V., Stødle, T., Madland, M.V., and Fabricius, I.L., 2018. Incorporating electrostatic effects into the effective stress relation - Insights from chalk experiments. *Geophysics*, **83**(3), MR123-MR135.

Neveux, L., Grgic, D., Carpentier, C., Pirnon, J., Truche, L., and Girard, J.P., 2014a. Influence of hydrocarbon injection on the compaction by pressure solution of a carbonate rock: An experimental study under triaxial stresses. *Marine and Petroleum Geology*, **55**, 282–294.

Neveux, L., Grgic, D., Carpentier, C., Pironon, J., Truche, L., and Girard, J.P., 2014b. Experimental simulation of chemomechanical processes during deep burial diagenesis of carbonate rocks. *Journal of Geophysical Research: Solid Earth*, **119**(2), 984–1007. https://doi.org/10.1002/2013JB010516

Pirson, S., Spagna, P., Baele, J.M., Damblon, F., Gerrienne, P., Vanbrabant, Y., and Yans, J., 2008. An Overview of the Geology of Belgium. *Memoirs of the Geological Survey of Belgium*, **55**(5), 26.

Ricci, M., Spijker, P., Stellacci, F., Molinari, J.F., and Voïtchovsky, K., 2013. Direct visualization of single ions in the Stern layer of calcite. *Langmuir*, **29**(7), 2207-2216.

Risnes, R., 2001. Deformation and Yield in High Porosity Outcrop Chalk. *Phys. Chem. Earth* (A), **26**, 53-57.

Risnes, R., Haghighi, H., Korsnes, R.I., and Natvik, O., 2003. Chalk-Fluid Interactions with Glycol and Brines. *Tectonophysics*, **370**, 213-226.

Sachdeva, J.S., Nermoen, A., Korsnes, R.I., and Madland, M.V., 2019. Impact of Initial Wettability and Injection Brine Chemistry on Mechanical Behaviour of Kansas Chalk. *Transport in Porous Media*. https://doi.org/10.1007/s11242-019-01269-z

Sachdeva, J.S., Sripal, E.A., Nermoen, A., Korsnes, R.I., Madland, M.V., and James, L.A., 2018. A Laboratory Scale Approach to Wettability Restoration in Chalk Core Samples. SCA2018-020 paper

presented at the International Symposium of the Society of Core Analysts, Trondheim, Norway, August 27-30.

Standnes, D.C. and Austad, T., 2000a. Wettability alteration in chalk: 1. Preparation of core material and oil properties. *Journal of Petroleum Science and Engineering*, **28**(3), 111-121.

Standnes, D.C. and Austad, T., 2000b. Wettability alteration in chalk: 2. Mechanism for wettability alteration from oil-wet to water-wet using surfactants. *Journal of Petroleum Science and Engineering*, **28**(3), 123-143.

Stipp, S.L.S., 1999. Toward a conceptual model of the calcite surface: Hydration, hydrolysis and surface potential. *Geochimica et Cosmochimica Acta*, **63**(19/20), 3121 – 3131.

Strand, S., Standnes, D.C., and Austad, T., 2006a. New Wettability Test for Chalk Based on Chromatographic Separation of SCN^- and SO_4^{2-}. *Journal of Petroleum Science and Engineering*, **52**, 187-197.

Strand, S., Høgnesen, E.J., and Austad, T., 2006b. Wettability alteration of carbonates - Effects of potential determining ions (Ca^{2+} and SO_4^{2-}) and temperature. *Colloids and Surfaces A: Physicochemical and Engineering Aspects*, **275**(1-3), 1-10.

Strand, S., Hjuler, H.L., Torsvik, R., Pedersen, J.I., Madland, M.V., and Austad, T., 2007. Wettability of chalk: Impact of silica, clay content and mechanical properties. *Petroleum Geoscience*, **13**(1), 69-80.

Sulak, R.M., 1991. Ekofisk Field: The First 20 Years. *Journal of Petroleum Technology*, **43**(10), 1-265.

Sulak, R.M. and Danielsen, J., 1989. Reservoir Aspects of Ekofisk Subsidence. *Journal of Petroleum Technology*, **41**(7), 709-716, SPE 17852-PA.

Sylte, J.E., Thomas, L.K., Rhett, D.W., Bruning, D.D., and Nagel, N.B., 1999. Water Induced Compaction in the Ekofisk Field. Paper SPE 56426 presented at the SPE Annual Technical Conference and Exhibition, Houston, Texas, October 3-6.

Voake, T., Nermoen, A., Ravnås, C., Korsnes, R.I., and Fabricius, I.L., 2019. Influence of temperature cycling and pore fluid on tensile strength of chalk, *Journal of Rock Mechanics and Geotechnical Engineering*, https://doi.org/10.1016/j.jrmge.2018.12.004.

Zhang, P. and Austad, T., 2005. The Relative Effects of Acid Number and Temperature on Chalk Wettability. Paper SPE 92999 presented at SPE International Symposium on Oilfield Chemistry, Houstan, Texas, USA, February 2-4.

Zhang, P. and Austad, T., 2006. Wettability and oil recovery from carbonates: Effects of temperature and potential determining ions. *Colloids and Surfaces A: Physicochemical and Engineering Aspects*, **279**(1-3), 179-187.

Zhang, P., Tweheyo, M. T., and Austad, T., 2007. Wettability alteration and improved oil recovery by spontaneous imbibition of seawater into chalk: Impact of the potential determining ions Ca^{2+}, Mg^{2+}, and SO_4^{2-}. *Colloids and Surfaces A: Physicochemical and Engineering Aspects*, **301**(1-3), 199-208.

Zimmermann, U., Madland, M.V., Nermoen, A., Hildebrand-Habel, T., Bertolino, S.A.R., Hiorth, A., Korsnes, R.I., Audinot, J.N., and Grysan, P., 2015. Evaluation of the compositional changes during flooding of reactive fluids using scanning electron microscopy, nano-secondary ion mass spectrometry, x-ray diffraction and whole rock geochemistry. *AAPG (Am. Assoc. Pet. Geol.) Bulletin*, **99**(5), 791–805. http://dx.doi.org/10.1306/12221412196.

Paper IV

Sachdeva, J.S., Sripal, E.A., Nermoen, A., Korsnes, R.I., Madland, M.V., and James, L.A. (2018). A Laboratory Scale Approach to Wettability Restoration in Chalk Core Samples. Paper SCA2018-117 presented at the International Symposium of the Society of Core Analysts, Trondheim, Norway, 27-30 August.

A LABORATORY SCALE APPROACH TO WETTABILITY RESTORATION IN CHALK CORE SAMPLES

Jaspreet S. Sachdeva[1,2], Edison A. Sripal[3], Anders Nermoen[1,2,4], Reidar I. Korsnes[1,2], Merete V. Madland[1,2], Lesley A. James[3]
[1]The National IOR Centre of Norway
[2]University of Stavanger
[3]Department of Process Engineering, Memorial University of Newfoundland
[4]International Research Institute of Stavanger
Corresponding Author: Dr. Lesley A. James (ljames@mun.ca)

This paper was prepared for presentation at the International Symposium of the Society of Core Analysts held in Trondheim, Norway, 27-30 August 2018

ABSTRACT

Wettability in chalk has been studied comprehensively to understand fluid flow mechanisms impacting coreflooding experiments. Wettability becomes paramount in understanding the parameters influencing chalk-fluid interactions. The main objective of this work is to evaluate as to which degree the wettability in chalk core samples can be controlled in the laboratory. Kansas chalk samples saturated with brine (1.1 M/64284 ppm NaCl) and an oil mixture (60% - 40% by volume of Heidrun oil and heptane) were aged at a constant temperature of 90^{o}C with aging time as the laboratory control variable. A multimodal method incorporating contact angle measurements, wettability index via USBM test, and SEM-MLA analysis was applied in evaluating wettability. A systematic approach was applied with the three different methods to quantify the degree of uncertainty linked to a) wettability estimation and b) the aging procedure to control wettability alteration of Kansas chalk. With a comprehensive suite of samples, we were successfully able to alter the wettability of chalk cores.

INTRODUCTION

Wettability is the tendency of one fluid to spread on, or adhere to, a solid surface in the presence of another immiscible fluid. Wettability is of paramount importance in oil recovery from low permeability chalk as it controls the flow and distribution of fluids [1]. In the past, numerous studies have indicated a number of factors influencing wettability including the composition of oil, rock mineralogy, fluid saturation, brine composition, temperature, and time of aging [2]. Although carbonate reservoirs tend to be intermediate to strongly oil wet, in the laboratory restoration to oil wet characteristics is fraught with uncertainties [3].

One of the simplest experimental control variables is the aging time. Anderson [2] indicated that 1000 hours (40 days) of aging at reservoir temperature is sufficient for wettability

equilibrium for sandstones. In order to ensure that brine chemistry are not ignored during the aging process it is important to saturate the core with brine prior to any flooding of oil.

Wettability can be quantified using contact angle measurements of a drop placed on top of the surface and/or the USBM method (United States Bureau of Mines). For a reservoir rock to be termed oil wet, the contact angle in an oil-brine-rock system should be greater than 105° [2,4,5], or the wettability index for the USBM method to be close to -1, calculated from drainage and imbibition capillary pressure vs saturation curves. Robin et al. [6] developed a qualitative description of how to differentiate between oil wet and water wet capillary pressure curves. In addition to the contact angle and USBM methods, Scanning Electron Microscopy (SEM) analyses using Cryo Scanning Electron Microscope (Cryo-SEM) and Environmental Scanning Electron Microscope (ESEM) methods [6,7] have been used to determine wettability in rocks and packed glass beads saturated with reservoir fluids. These analyses had uncertainties as it often compromised the sample integrity due to extreme changes in the physical state because of cooling and polishing. In a newly developed method [8], SEM-MLA (Mineral Liberation Analysis) has been applied by testing the samples without any changes to their physical state.

In this paper we try to determine the threshold duration beyond which the aging does not change the wetting state of outcrop chalk. After aging the chalk cores at high temperature for varying periods of time, wettability determination was performed using contact angle measurements, USBM method and SEM-MLA analysis. Specifically, the study was carried out on outcrop chalk samples as laboratory core flooding and SCAL experiments are routinely performed on core samples from restored state [9]. Similar work had been carried out previously on Rørdal chalk samples [1] wherein the chalk samples were submerged into crude oil for wettability alteration, and then after aging the crude oil was flushed out by decahydronapthalene, which subsequently was flushed out by decane for imbibition tests. Graue et al. [1] reported that a stable wettability was obtained for cores aged more than 14 days using a different set of fluids.

EXPERIMENTAL METHODODLOGY

Porous Medium

The porous media used for this work was outcrop chalk from Kansas, from the Niobrara formation, Fort Hays Member, USA (Late Cretaceous). The Kansas chalk used here displayed a permeability ranging from 1.90 to 2.10 mD, and a porosity ranging from 36.93 to 38.57 %. Its carbonate content is approx. 95-97%, the Biot coefficient is 0.91 and the induration is H3 [10,11], which imply that Kansas chalk is partially cemented compared to other high porous chalks.

Fluids

The physical properties of the 1.1 M NaCl-brine used to determine the saturation porosity, brine-permeability, and for initial saturation are presented in Table 1. Heidrun (offshore Norway) dead crude oil with 6 cP viscosity and 858 kg/m^3 density was mixed with n-

heptane (60% - 40% by volume) and used as the non-wetting phase. The total acid number (TAN) of the Heidrun crude oil was analyzed and found to be 2.82 mg KOH/g (reported to be 3 mg KOH/g in [12]), while the mixture obtained an acid number of 2.12 mg KOH/g using potentiometric titration method. The oil mixture was filtered (5 μm filter paper) and degassed by vacuuming for 48 hours to prevent gas production during the drainage. The physical properties of Heidrun crude oil are tabulated in Table 2. The composition of the oil mixture was analyzed using *Agilent 7890A Gas Chromatograph with Simulated Distillation* (SIMDIS) system (see Table 3).

Experimental Method

Sample Preparation and Basic Sample Characterization

7 full sized cylindrical core samples ('cores') of 1.5" (38.1 mm) diameter and 2" (50 mm) lengths, and 5 mm length end pieces from both ends (top and bottom, 14 in total) were drilled out from a single block. The cores and end pieces were sonicated to remove fines and then dried at 90^{o}C for two days. Then the dry weight of the cores was measured before being vacuumed and saturated by NaCl brine for wet weight measurements. The saturation porosity could then be estimated (the porosity of the end pieces was assumed to be the same). The 7 cores were mounted in flow-cells and the brine-permeability was estimated from differential pressure measurements and Darcy's law. The saturation porosity and brine permeability estimates are given in Table 4.

Centrifuge for Primary Drainage

The 7 brine saturated cores including the 14 top and bottom end pieces with filter paper in between, were mounted into the core holders of the centrifuge (*Rotosilenta 630RS* centrifuge from Vinci Technologies). An overburden/confining pressure of 200 psi (1.38 MPa) was used, and the centrifuge was operated in drainage mode to displace the brine with oil to irreducible water saturation. Drainage was performed in 7 steps from 500 rpm to 3500 rpm in increments of 500 rpm with 3 hours of equilibration time for each step. The capillary pressure was calculated at any position, r, along the core length using the Hassler-Brunner equation [13]:

$$P_c(r) = \frac{1}{2}\Delta\rho\omega^2(r_1^2 - r^2) \quad (1)$$

where $\Delta\rho = \rho_{out} - \rho_{in}$ is the density difference between the fluid expelled from the core (ρ_{out}) and the fluid entering the core (ρ_{in}), ω is the angular rotation speed of the centrifuge, and $r_1 \simeq 22.1$ cm (for drainage mode of centrifuge) and 16.5 cm (for imbibition mode of centrifuge) and r (varying from 0 to 5 cm) are the distances from the rotational axis to the outlet face and any point along the core length, respectively. In addition to Hassler Brunner method, Forbes and Forbes-splines method were also applied, but there was no significant improvement in the model fit. According to Forbes [16], it is assumed that the pressure field in the core is linear, (neither radial nor centrifugal), and gravity is neglected. These assumptions can be satisfied for very short and narrow samples spun far from the rotation axis. In the case of Vinci centrifuge, the geometry is such that (sample being far from the rotation axis), the pressure field in the core is almost linear which is not the case with other

centrifuge's (Beckmans). Hence this was determined to be reason for very little difference between the results of Hassler Brunner and Forbes equations in our case.

After reaching an equilibrium between the oil/water saturation and capillary pressure, hence when no more brine is being produced, the brine expelled from the core was measured and the average water saturation for each rotation speed was obtained. This water saturation (%) was plotted against the capillary pressure estimated from equation (1) to produce the capillary pressure curve.

Aging

After the centrifuge the confining pressure was reduced to 100 psi and then the core holders with cores and end pieces inside were placed in the oven to age at 90°C for aging time ranging from 6 to 30 days (Table 4).

After aging, the 7 full sized cores were used for USBM wettability measurement, and the 7 top and 7 bottom end pieces were used for the contact angle measurements and SEM-MLA analyses, respectively.

Wettability determination by USBM of cores

After the primary drainage (oil displaced brine) and aging, the NaCl brine was forcibly imbibed (primary imbibition) into the cores using the centrifuge in imbibition mode to obtain residual oil saturation S_{or} – before a secondary drainage (oil displaced brine) was performed to reach the irreducible water saturation, as described by McPhee et al. [14]. The receiving tubes coupling cups to core holders, were saturated by the same fluid as the cups holding the fluid that enters the cores. A confining pressure of 200 psi and 7 centrifugal steps from 500 to 3500 rpm at 500 rpm increments for 3 hours equilibration time was used. Areas under the secondary drainage curve (A_1) and primary imbibition curve (A_2), when plotting the capillary pressure against water saturation enabled us to estimate the wettability index I_w via:

$$I_w = log\ (A_1/A_2) \quad (2)$$

The trapezoidal method was used to estimate the area under the curves. In conjunction to the formula above, the wettability index I_w is greater than 0 for water wet, smaller than 0 for oil wet and around 0 for neutral wet systems.

Wettability determination by Contact Angle Measurements of the top end pieces

The top end piece of the aged core sample was mounted in a *Vinci IFT 700* instrument to measure the contact angle by sessile drop method. The same NaCl brine (Table 1) was used as the droplet fluid and each droplet was of size $\sim 5 \cdot 10^{-4}$ ml (radius of 0.5 mm). The sessile drop method uses a contact angle goniometer, which allows the user to measure the contact using digital photography for immobile and permanently attached droplets placed by a syringe onto the chalk end piece surface. 8-10 photographs were acquired over 2 minutes each enabling us to observe how the droplet obtained a stable geometry over time. The contact angle measurement was done on trimmings that were on top of the consolidated

sample. These trimmings were at the oil front during the primary imbibition process. Hence it was assured that the saturation was uniform. Contact angle was measured at multiple spots (about 10 to 12) on the surface of the trimming and an average value was taken as the contact angle for that particular samples resulting in 150 to 300 data points for each sample. Initially, brine drops were left for a longer duration to observe the change in contact angle, but this largely due to evaporation of the brine droplet. Also, leaving the brine droplet for a longer duration resulted in formation of salt crystals on the surface causing discrepancies in the contact angle measurements. Hence, contact angle measurement at multiple spots on the rock surface was performed an average value of the contact angle measurement is reported. On the other hand it was understood that roughness will impact contact angle measurements. It is understood that the contact angles measured are effective and will vary depending on surface treatment. But in this case all samples were treatment the same way and that the contact angles can be compared. All the sample trimmings were cut with the same saw using SS blade (1/16”). The chalk samples that were used for contact angle and SEM-MLA were also cut in the same way. We don’t believe the surface roughness influenced the contact angle measurement within our measurements as the shape of the droplet did not change from sample to sample or within a sample.

Wettability determination by SEM-MLA analysis of the bottom end pieces

In the last stage, the bottom end piece of the aged core sample was used for SEM-MLA analysis [8]. A *FEI Quanta 650 FEG* SEM, equipped with Bruker high throughput Energy Dispersive X-ray (EDX) system and backscattered electron detectors was used for this purpose. Imaging of the flat sample surfaces was carried out at very low vacuum conditions (0.6 Torr) [15]. Additionally, the end pieces were not subjected to any metallic or carbon coating on the surface, which is a standard procedure for SEM-MLA analysis, except for liquid graphite coating on the sample holder. The instrument conditions and parameters were: high voltage of 25 kV, spot size of 5.75, working distance of 13.5 mm, 10 nA beam current, 16 µs BSE dwell time, 10-pixel minimum size (400-pixel frame resolution for 1 mm High Full Well (HFW) capacity), and 12 ms spectrum dwell for EDX. The MLA acquisitions were performed using the 3.1.4.683 MLA™ software and each acquisition took between 3 and 4 hours per sample. Minerals and fluids in the core sample were calculated through a custom classification script that accounted for porosity and mineralogy. The results for individual samples were acquired as a digital map of the minerals and a data table listing their mineral composition. Prior to testing the individual aged end pieces, two pure chalk pieces; one with a drop of the oil mixture and another with a drop of 1.1M NaCl-brine on it, were analyzed to determine the oil and NaCl-brine (termed ‘halite’) signature and added to the SEM mineral database. The aged end pieces were then analyzed to determine the relative quantity of oil, halite and carbonate in percent. The premise is to link the oil/halite concentrations to the overall wetness of the mineral surface, which in this study is controlled by the aging time.

RESULTS AND DISCUSSION

The premise of this work was to measure wettability of aged Kansas chalk using three techniques at varying aging time while keeping brine and oil composition, and aging temperature fixed.

Before aging, the samples were brought to irreducible water saturation (S_{wi}) using the primary drainage method. From trial and error, it was found that a confining pressure of 200 psi (1.38 MPa) was optimal to avoid disintegration of the cores during centrifuge tests. The irreducible water saturation was found to be 54.15 to 64.71% for all cores (Table 4).

After the samples were aged they were imbibed by NaCl brine (primary imbibition) from S_{wi} to the residual oil saturation (S_{or}, see Figure 1 and Table 4). The area under the P_c vs S_w curve during primary imbibition is termed A_2. Then, the cores were taken out of the holders which were switched to drainage mode before secondary drainage was performed (in which oil expelled brine). The area spanned by the P_c vs S_w curve is termed A_1.

The wettability index I_w from USBM method was estimated using the log10 of the ratio A_1 by A_2 in equation (2). From the WI reported in Table 4, it can be seen that, except from chalk number 5 (18 days), an increasing aging time leads to a lowered wettability index, ranging from 0.36 and 0.51 for 6 and 9 days aging to around zero for 12, 15 and 21 days, and -0.15 for 30 days aging. Figure 2 (left) gives a plot of wettability index estimated by USBM method as a function of aging time. The abnormality with result from sample aged 18 days is quite uncertain. But during the USBM tests it was observed that number of tests have to be repeated as the samples disintegrated due to excess overburden pressure. This resulted in additional tests to optimize the confining pressure required for successful drainage and imbibition tests on the samples. Even though the confining pressure was optimized by trial and error, and the confining pressure used for the sample with 18 days aging time is the same as the other samples, we suspect that this outlier may have been caused by natural fractures present in chalk which led to further disintegration during the primary imbibition and secondary drainage that was not visible during the initial tests.

In summary each method provided a conclusion that could not be perceived as unanimous. This discrepancy in the experimental data may have originated mainly from the USBM method. Although the data shows only 7 samples with 7 aging times, more than 30 samples were tested with almost half of them breaking apart. Initially the samples were not able to withstand the confining pressure and with that reduced and optimized, we had samples coming out intact in the primary drainage stage. The core samples (used for USBM) went through further damage during the primary imbibition and secondary drainage. Hence it was with great difficulty we were able to get reliable data for the USBM method. This was not the case for the trimmings used for the contact angle measurement and the SEM-MLA analysis. In these cases, the trimmings being just a few millimeters, we were able to get a saturated and a more reliable sample after few attempts. The trimmings for the SEM-MLA

were selected once the primary drainage test was found to be reliable as the data was similar for all the samples. For SEM-MLA analysis, the trimmings being barely few millimeters were put though the primary drainage process and selected for aging. This again took number of attempts to eventually select the 7 samples and age them.

The top end pieces were analyzed with contact angle measurement in which a brine droplet was placed on the sample. It was found impossible to place a stable droplet onto the samples aged for 6 and 9 days, as the droplet initially had a maximal contact angle of around 65°, but within only a few seconds, it started to spread out and got sucked into the chalk developing into a contact angle of 0° in time. Hence, obtaining a stable, time independent, contact angle measurement was not possible for samples with 6 and 9 aging days. For samples aged for 12 days and 30 days the sessile droplets formed enabling stable contact angle measurements. For the 12 and 15 days samples contact angles of 78° and 85° were found respectively. Increasing the aging time to 18, 21 and 30 days the contact angle increased to 102, 110, and 108°, respectively (Figure 2 (right) and Figure 3, Table 4). Hence, as the aging time is increased to 18 days and beyond, the contact angle reached a plateau of more than 100° which is in-line with oil wet characteristics, said to be greater than 105° [2,4,5]. Figure 2 (right) gives a plot of contact angle as a function of aging time.

The lower end pieces were analyzed using SEM–MLA in which the oil/brine content of the surface of the samples was determined (Table 5). The use of a pre-defined signature of the oil, calcite mineralogy and brine in the MLA-database simplified the analysis compared to a similar study using Berea sandstone [8]. Based on the individual surface measurements (reported in Table 5) for the amount of oil/brine/calcite of the aged chalk samples, we report the SEM-MLA wettability estimate in Table 4. Figure 4 provides two examples of mineral/fluid MLA maps and SEM images of samples aged for 6 days and 30 days showing how an increasing aging time results in an increased oil signature on the chalk samples.

The wettability measurements reported here, from all three methods, imply that an aging time exceeding 21 days was sufficient to ensure that the Kansas chalks are oil wet when the samples were saturated by 1.1 M NaCl-brine and 2.12 mg KOH/g oils and aged at 90°C.

CONCLUSIONS

1. 7 outcrop Kansas chalk cores together with 5 mm thick top and bottom end pieces were acquired from the same block and their wettability were altered by aging for varying durations. The aging temperature, brine and oil compositions were kept fixed for all 7 aged samples.
2. Wettability was measured using three different methods viz. contact angle, wettability index via USBM method and oil saturation using SEM-MLA analysis.
3. USBM method: Increasing oil wet characteristics, i.e. close to zero meaning that the ratio of A_1 by A_2 equals 1, was observed with increasing aging time from 12 days onward. The 18 days' experiment seemed to be an outlier result as it did not match the 12 and 15 days' (close to zero, positive value), and 21 and 30 days tests (close to zero,

negative value). To ensure that the sample remained intact a confining pressure of 200 psi had to be used to prevent disintegration of the sample.

4. Contact angle measurement: With increasing aging time, the chalk samples indicated increasing oil wet characteristics, especially after 12 days aging and onwards. Contact angle values varied from 65° (unstable readings from 6 and 9 days tests – water wet) to 110° (very stable readings for 18, 21 and 30 days test – oil wet).
5. The newly developed SEM-MLA method for oil/brine chalk surface determination provided a direct observation of the chemical composition of the end-pieces. An increasing amount of oil present on the samples was measured using MLA analysis. It was found that the oil fraction increased steadily from 10% to 46% when aging time was increased from 6 to 30 days. Interestingly MLA analysis on chalk samples was straight forward compared to Berea as the mineral list was limited.
6. Based upon the three presented measures, an aging time exceeding 21 days, at 90°C saturated by 1.1 M NaCl-brine and 2.12 mg KOH/g oils, was sufficient to ensure that the Kansas chalks are oil wet. This conclusion was largely driven by the contact angle results indicating a wettability condition above 21 days. The USBM method indicated oil wet characteristics starting from 21 days added to the discrepancy on 18 days was forcing us to lean towards 18 days timeline to ensure oil wet characteristics. Hence a timeline of 21 days have been conclude to restore oil wet characteristics in chalk.
7. The tests can further be strengthened by varying brine salinity, aging temperature and the wettability tests broadened to include Amott tests in addition.

ACKNOWLEDGEMENTS

The authors acknowledge the Research Council of Norway and the industry partners, ConocoPhillips Skandinavia AS, Aker BP ASA, Eni Norge AS, Total E&P Norge AS, Equinor ASA, Neptune Energy Norge AS, Lundin Norway AS, Halliburton AS, Schlumberger Norge AS, Wintershall Norge AS, and DEA Norge AS, of The National IOR Centre of Norway for support. The authors would also like to thank Chevron Canada, Hibernia Management and Development Company (HMDC), Research and Development Corporation of Newfoundland and Labrador (RDC), Natural Sciences and Engineering Research Council of Canada (NSERC), and the Canadian Foundation for Innovation (CFI) for financial support. We thank our colleagues in the Hibernia EOR Research Group for technical support.

REFERENCES

1. Graue, A., Viksund, B.G., & Baldwin, B.A., “Reproducible Wettability Alteration of Low-Permeable Outcrop Chalk,” (1999), Society of Petroleum Engineers. doi:10.2118/55904-PA
2. Anderson, W.G., “Wettability Literature Survey - Part 1: Rock/Oil/Brine Interactions and the Effects of Core Handling on Wettability”. *Journal of Petroleum Technology*, (1986) **38,** 10, 1125-1144.

3. Zangiabadi, B., Korsnes, R.I., Madland, M.V., Hildebrand-Habel, T., Hiorth, A., & Kristiansen, T.G., "Mechanical Properties of High And Lower Porosity Outcrop Chalk At Various Wetting States," (2009), Presented at Asheville 2009, the 43rd US Rock Mechanics Symposium and 4th US-Canada Rock Mechanics Symposium, Asheville, NC, 28 June-1 July.
4. Andersen, P.O., Ahsan, R., Evje, S., Bratteli, F., Madland, M.V., & Hiorth, A., "A Model for Brine-Dependent Spontaneous Imbibition Experiments with Porous Plate," (2013), Society of Petroleum Engineers. doi:10.2118/164901-MS
5. Cuiec, L.E., Bourbiaux, B., & Kalaydjian, F., "Oil Recovery by Imbibition in Low-Permeability Chalk," (1994), Society of Petroleum Engineers. doi:10.2118/20259-PA
6. Robin, M., Combes, R., Degreve, F., & Cuiec, L., "Wettability of Porous Media from Environmental Scanning Electron Microscopy: From Model to Reservoir Rocks", (1997), Paper SPE-37235, Presented at the International Symposium on oilfield Chemistry, Houston, Texas, USA, 18-21 February.
7. Schmatz, J., Klaver, J., Jiang, M., & Urai, J.L., "Nanoscale Morphology of Brine/Oil/Mineral Contacts in Connected Pores of Carbonate Reservoirs: Insights on Wettability From Cryo-BIB-SEM," (2017), Society of Petroleum Engineers. doi:10.2118/180049-PA
8. Sripal, E., & James, L.A., "Application of an Optimization Method for the Restoration of Core Samples for SCAL Experiments," *Petrophysics*, (2018) **59,** 1, 72-81.
9. Hirasaki, G.J., Rohan, J.A., Dubey, S.T., & Niko, H., "Wettability Evaluation During Restored-State Core Analysis," (1990), Paper SPE-20506, Presented at the SPE Annual Technical Conferences and Exhibition, New Orleans, Louisisana, USA, 23-26 September.
10. Henriksen, A.D., Fabricius, I.L., Borre, M.K., Korsbech, U., Theilgaard, A.T., & Zandbergen, J.B., "Core density scanning, degree of induration and dynamic elastic moduli of Palaeogene limestone in the Copenhagen area," *Quarterly Journal of Engineering Geology and Hydrogeology*, (1999) **32**, 107-117.
11. Voake, T., Nermoen, A., Ravnås, C., Korsnes, R.I., & Fabricius, I.L., "The influence of temperature cycling and pore fluid on the tensile strength of chalk," Submitted for publication, (2018).
12. Warner, R., "Western European refineries and acidity in crude oil," S&P Global Platts, (2017), Available at https://www.platts.com/IM.Platts.Content/InsightAnalysis/IndustrySolutionPapers/SR-western-european-refineries-and-acidity-in-crude-oil.pdf [Accessed 26 April 2018].
13. Hassler, G.L., & Brunner, E. "Measurement of capillary pressures in small core samples," Trans. AIME, (1945) **160**, 114-123.
14. McPhee C., Reed, J., & Zubizarreta, I., *Core Analysis: A Best Practice Guide*, Elsevier, Amsterdam, Netherlands, (2015), **64**, 313-345.
15. Kumar, M., Fogden, A., Senden, T., & Knackstedt, M.A., "Investigation of Pore-Scale Mixed Wettability," Paper SPE-129974, *SPE Journal*, (2012), **17,** 1, 20–30. doi: 10.2118/129974-PA.
16. Frobes,P.L., 1997, Centrifuge Data Analysis Techniques: An SCA Survey on the Calculation of Drainage Capillary Pressure Curves from Centrifuge Measurements,

paper SCA 1997 – 14, Presented at The International Symposium of the Society of Core Analysts, Calgary, Canada.

Table 1. Composition and properties of brine at 25°C

Brine Salinity (ppm)	Density (kg/m^3)	Viscosity (cP)	IFT with oil (Nm/m)
64,284	1060	1.05	70.8

Table 2. Properties of Heidrun Crude oil at 25°C

Color	Density (kg/m^3)	Viscosity (cP)	TAN (mg KOH/g)	Asphaltene content (%)
Light brown	858	6	2.82	< 1

Table 3. Composition of the 60-40 Heidrun/Heptane oil mixture from GC-analyses

Component	Mass fraction	Mole fraction	Volume fraction
CO_2	0.0000	0.0000	0.0000
N_2	0.0000	0.0000	0.0000
C1	0.0000	0.0000	0.0000
C2	0.0000	0.0000	0.0000
C3	0.0002	0.0009	0.0003
i-C4	0.0003	0.0012	0.0005
n-C4	0.0018	0.0070	0.0026
i-C5	0.0028	0.0086	0.0040
n-C5	0.0054	0.0165	0.0075
C6	0.0163	0.0427	0.0206
C7+	0.9732	0.9231	0.9646

Table 4. Experimental measurements for Kansas chalk

Core No.	Sat. porosity (%)	Brine Permeability (mD)	Aging Time (days)	S_{wi} (%)	S_{or} (%)	Contact Angle (°)*	SEM-MLA oil %	I_w (USBM)
1	38.57	2.10	6	64.71	19.23	65 (29.4)	10	0.368
2	38.49	1.90	9	54.32	13.82	66 (26.8)	19	0.510
3	37.76	2.01	12	58.10	6.10	78 (9.1)	27	0.005
4	36.93	1.92	15	62.61	8.81	85 (7.5)	37	0.053
5	38.04	1.96	18	54.15	4.13	102 (6.2)	37	0.864
6	38.06	2.00	21	54.33	4.28	110 (4.2)	39	-0.018
7	37.63	1.95	30	58.64	2.15	108 (4.5)	46	-0.165

** 150 to 300 data points were collected with average value presented and the standard deviation presented in brackets*

Table 5. Mineral list from the SEM-MLA analysis for Kansas chalk samples 1 to 7, number of aging days in parenthesis: 1(6), 2(9), 3(12), 4(15), 5(18), 6(21) and 7(30).

Colour	Mineral	% Area Coverage by Sample						
		#1 6 days	#2 9 days	#3 12 days	#4 15 days	#5 18 days	#6 21 days	#7 30 days
	Carbonate	8	21	61	3	57	50	31
	Halite	82	60	12	60	6	11	23
	Oil	10	19	27	37	37	39	46
	Others	0	3	3	4	3	1	2

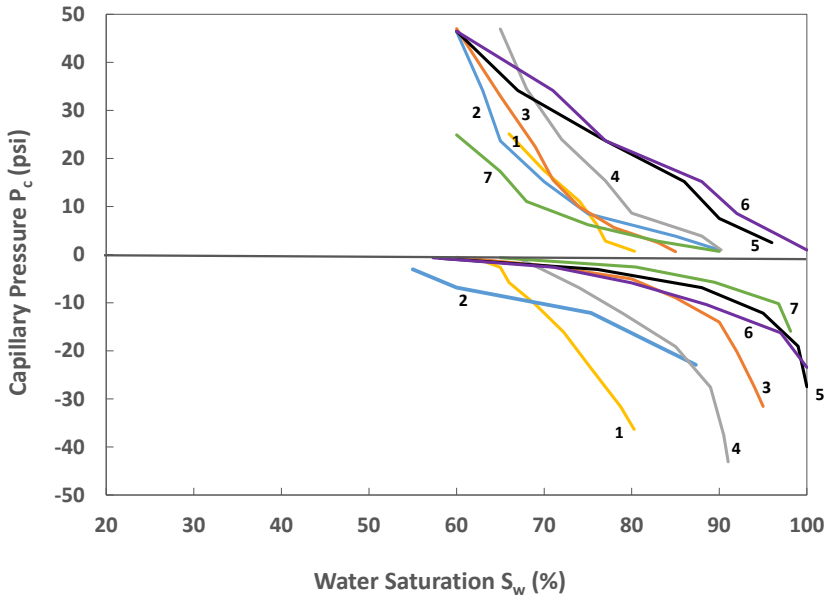

Figure 1. Primary imbibition (brine displacing oil, $P_c < 0$) and secondary drainage (oil displacing brine, $P_c > 0$) for Kansas chalk samples 1 to 7, number of aging days in parenthesis: 1 (6-yellow), 2 (9-blue), 3 (12-orange), 4 (15-grey), 5 (18-black), 6 (21-purple) and 7(30-green).
Note: For samples 5 and 6, the primary imbibition data was adjusted to 100% maximum saturation as the experiments overestimated the saturations to beyond 100%. The S_{or} reported for samples 5 and 6 in Table 4 are assumed to be the penultimate points after the saturations were adjusted to 100%.

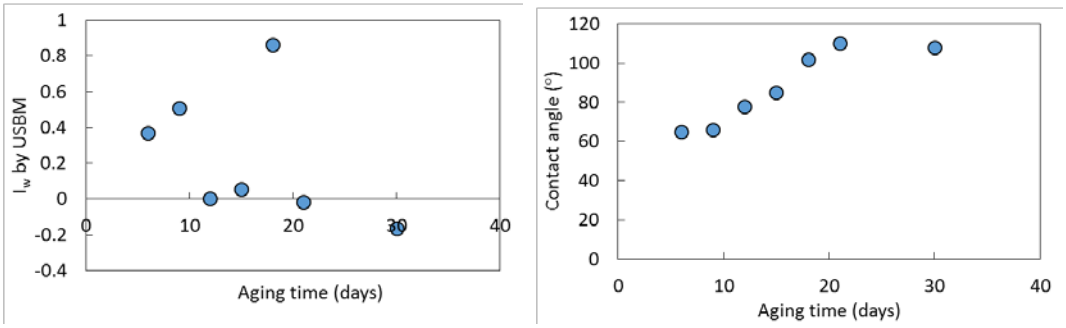

Figure 2. Left: Wettability index measurement using USBM method as a function of aging time. Right: Contact angle on the top end piece of aged chalk cores as a function of aging time.

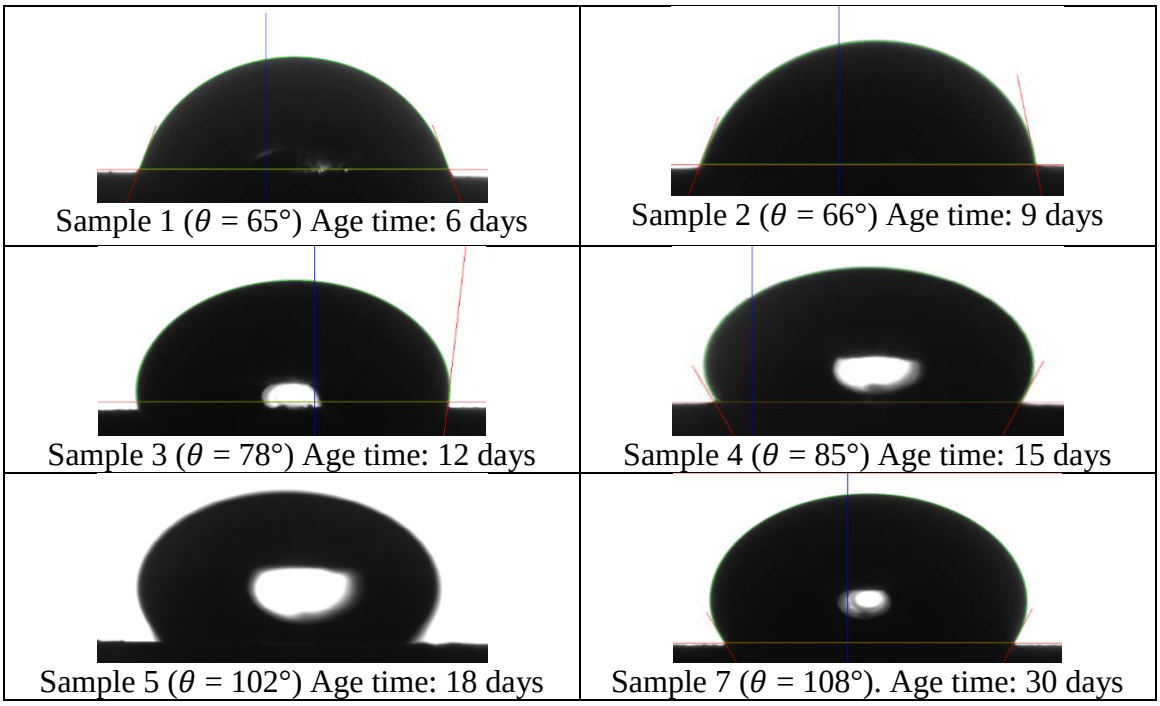

Figure 3. Brine droplet of size $\sim 5 \cdot 10^{-4}$ ml placed onto the aged top end piece. The contact angle is shown for differently aged chalk samples.

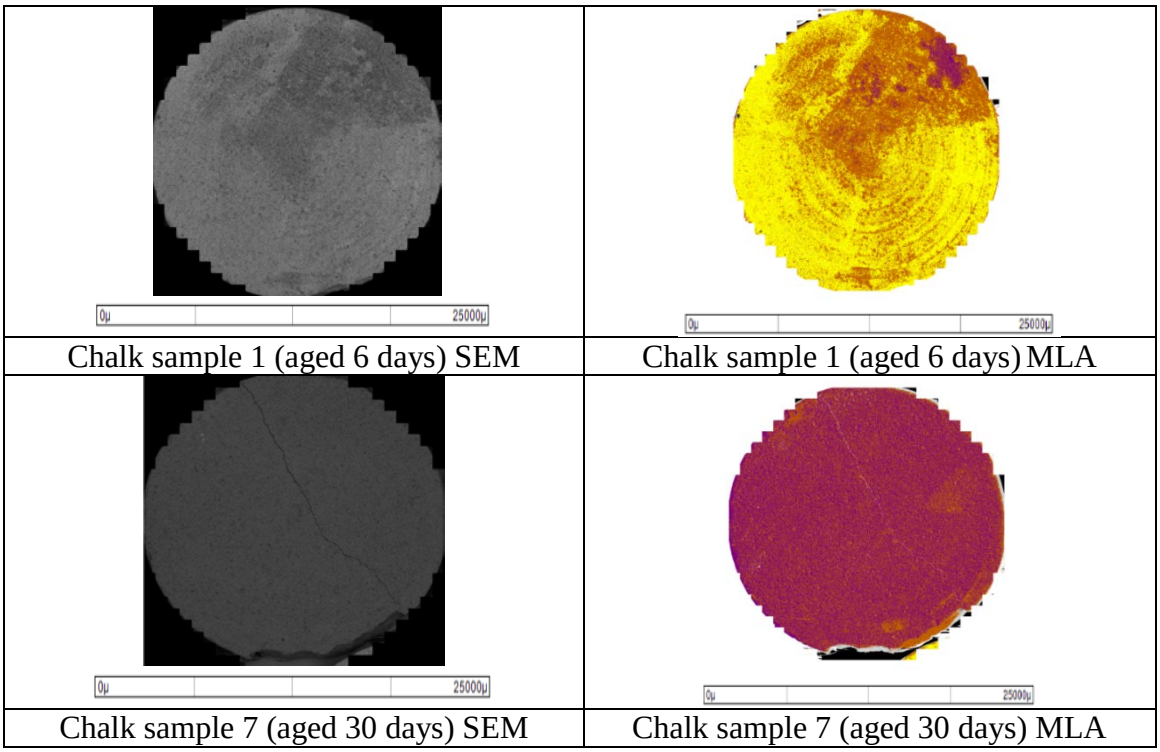

Figure 4. SEM Images and MLA image of different aged chalk samples

Paper V

Sachdeva, J.S., Nermoen, A., Korsnes, R.I., and Madland, M.V. (2017). Elastic and Plastic Behavior of Chalks at Deviatoric Stress Condition: Experiments Performed with Four Different Brines. Paper Tu P030 presented at the IOR Norway 2017 – 19th European Symposium on Improved Oil Recovery, Stavanger, Norway, 24-27 April.

Tu P030

Elastic and Plastic Behavior of Chalks at Deviatoric Stress Condition: Experiments Performed with Four Different Brines

J.S. Sachdeva* (The National IOR Centre of Norway, UiS), A. Nermoen (The National IOR Centre of Norway, UiS, IRIS), M.V. Madland (The National IOR Centre of Norway, UiS) & R.I. Korsnes (The National IOR Centre of Norway, UiS)

SUMMARY

This paper deals with exploring elastic (bulk modulus and Young's modulus) and plastic parameters (yield stress, creep and rebound) during deviatoric loading and time-dependent deformation. A series of experiments were carried out at Ekofisk reservoir temperature (130°C) to study the effect of four different fluids, viz., distilled water (DW), NaCl-brine, MgCl2-brine and seawater (SSW), on Mons outcrop chalk. The cores were deviatorically loaded and left to creep at a constant value of 69-73% of the axial yield stress obtained from reference tests with the same brine. Variations in the bulk modulus and Young's modulus were observed as function of saturation fluid, although the significance of these observations require more data. SSW had the lowest yield stress followed by NaCl and MgCl2, and highest for DW, which conforms the results from earlier studies. The final creep strain was highest for SSW and was 1.3-1.5 times higher than for other brines. The core initially saturated by SSW showed the highest plastic component of the total strain inferring that the ions in SSW does play an important role in inducing permanent damage.

Introduction

Chalk is an important reservoir rock in the Norwegian Continental Shelf. It is characterized as a highly porous and a low permeable rock. The injection of seawater into North Sea chalk reservoirs has proved to be an important driving mechanism for pushing the residence fluids towards production facilities and, hence, of great potential for improving oil recovery. However, injection of seawater-like brines into the chalk reservoirs lead to enhanced compaction of the reservoir rock, which has shown to induce seafloor subsidence.

Mechanical strength of chalk has been of great focus for several decades now after Ekofisk subsidence problem was discovered (Hermansen et al., 1997; Kristiansen et al., 2005; Doornhof et al., 2006). Seawater injection was initiated in 1987 to re-pressurize the reservoir, to halt subsidence problem and to improve oil recovery. The oil production was improved significantly (Doornhof et al., 2006), but the compaction problem in the reservoir continued in the water flooded areas, even though at a smaller pace compared to before the seawater injection. This water-induced compaction phenomenon is described as water weakening of chalk.

Several studies have been carried out to fill the important gap of understanding how pore fluid chemistry affects the mechanical strength of chalk (Risnes, 2001; Hellmann et al., 2002a, 2002b; Risnes et al., 2003; Madland et al., 2006; Korsnes et al., 2008; Neveux et al., 2014a, 2014b). These studies have been performed to gain knowledge about the effect of aqueous chemistry on mechanical stiffness and failure strength during, and after, hydrostatic stress buildup. The studies done so far have shown that the injected brines are not in equilibrium with the rock surface, hence they alter the rock mineralogy. They have shown that elastic bulk modulus, yield stress, and time-dependent deformation at a constant stress condition depends on the pore fluid composition (Korsnes et al., 2006a, 2006b, 2008; Madland et al., 2008, 2011; Megawati et al., 2011, 2012).

Previous studies performed at hydrostatic conditions on Stevns Klint (Korsnes et al., 2006a, 2006b, 2008; Megawati et al., 2012), Liège (Madland et al., 2011) and Kansas (Madland et al., 2008; Megawati et al., 2012) outcrop chalks have shown that the presence of sulfate ions in the pore fluid causes a significant weakening of the chalk framework and has a huge impact on the mechanical properties. Madland et al. (2011) and Megawati et al. (2011) demonstrated that magnesium in seawater triggered precipitation of secondary magnesium-bearing minerals (viz. carbonates and silicates) that lead to enhanced dissolution of chalks.

In this study, we evaluate the effect of aqueous chemistry on the mechanical parameters that define stiffness and strength of chalk during deviatoric loading and time dependent deformation. What is the relation between the brine composition and chalk mechanics during non-hydrostatic loading? How does the brine composition affect chalk mechanics if the cores are only saturated, and not flooded? How can the observed deformation be partitioned? What is the relation between the observed creep and the elastic-plastic strains? Analyzing strain partitioning may shed additional insight into how strain is accumulated in chalk, i.e. how grain re-arrangement and framework compressibility relate. In real field scenarios, the magnitude of elastic rebound determines how the reservoir responds to variations in pore pressure. Is it possible for a chalk reservoir to de-compact if the pore pressure is increased by water flooding, or is the deformation in the reservoir irreversible?

This paper deals with cases where the cores are initially saturated by different brines and are not flooded during the laboratory experiments. In this test series, we evaluate various elastic and plastic parameters during deviatoric loading and time-dependent creep below yield. A series of experiments were carried out at 130°C to study the effect of the brines used in previous studies (Korsnes et al., 2006a, 2006b, 2008; Madland et al., 2011; Megawati et al., 2011, 2012) on pure water-wet Mons outcrop chalk from the Trivieres formation. Furthermore, elastic-plastic partitioning was quantified by carrying out rebound tests.

Materials and Methods

Outcrop chalk from the Trivieres formation in Mons, Belgium was used in this study. The chalk is from the Cretaceous period (Geys, 1980; "Gateway to the Paleobiology Database", 1999) and is considered to be >99% pure (Megawati et al., 2015). Cylindrical plugs were drilled from a Mons chalk block before being radially adjusted to the desired diameter using a lathe machine. The core plugs of desired length were, then, cut and dried in an oven at 110°C overnight to measure the initial dry mass. They were vacuumed before being saturated with distilled water for saturated mass measurements. The difference between the dry and saturated mass gave the pore volume estimate using the density of distilled water (1 g/cc). Porosity was calculated from the ratio of pore volume by the bulk volume (see *Table 1*). The porosity of these cores varied in the range of 41 to 44%.

Table 1 *Basic properties of Kansas chalk cores.*

Core Number	Saturating Brine	Length, mm	Diameter, mm	Pore Volume, ml	Bulk Volume, ml	Porosity, %
C1	DW	70.94	38.08	34.03	80.79	42.1
C2		72.54	38.10	35.12	82.70	42.5
C3	NaCl	71.97	38.09	35.29	82.01	43.0
C4		71.10	38.11	33.35	81.10	41.1
C5	$MgCl_2$	70.93	38.10	34.19	80.87	42.3
C6		71.58	38.10	34.86	81.61	42.7
C7	SSW	70.26	38.09	34.42	80.06	43.0
C8		70.85	38.08	35.20	80.69	43.6

In contrast to experiments documented in earlier works (e.g. Korsnes et al., 2006a, 2006b, 2008; Madland et al., 2011; Megawati et al., 2012) the experiments reported here were performed at non-hydrostatic stresses below yield stress. The axial stress at which shear failure occurred for the given confining stress was obtained by testing equivalent cores in reference tests. In addition, the cores were saturated by four different brines and not flooded during the experiments to analyze the impact of one pore volume of saturation fluid on the chalk network. We used distilled water (DW) and three different brines: NaCl-brine, $MgCl_2$-brine and seawater (SSW) as summarized in *Table 2*.

.

Table 2 Composition of brines used in the experiments.

Ions	Synthetic Seawater (SSW)	0.657 M NaCl	0.219 M $MgCl_2$
	mol/l	mol/l	mol/l
HCO_3^-	0.002	0.000	0.000
Cl^-	0.525	0.657	0.438
SO_4^{2-}	0.024	0.000	0.000
Mg^{2+}	0.045	0.000	0.219
Ca^{2+}	0.013	0.000	0.000
Na^+	0.450	0.657	0.000
K^+	0.010	0.000	0.000
Ionic Strength	0.657	0.657	0.657
TDS, g/l	33.390	38.400	20.840

The Triaxial Cell Setup

The chalk cores were mounted into the triaxial cell (*Figure 1*) that allowed for continuous measurements of the axial strains during mechanical tests performed at elevated stresses and temperatures.

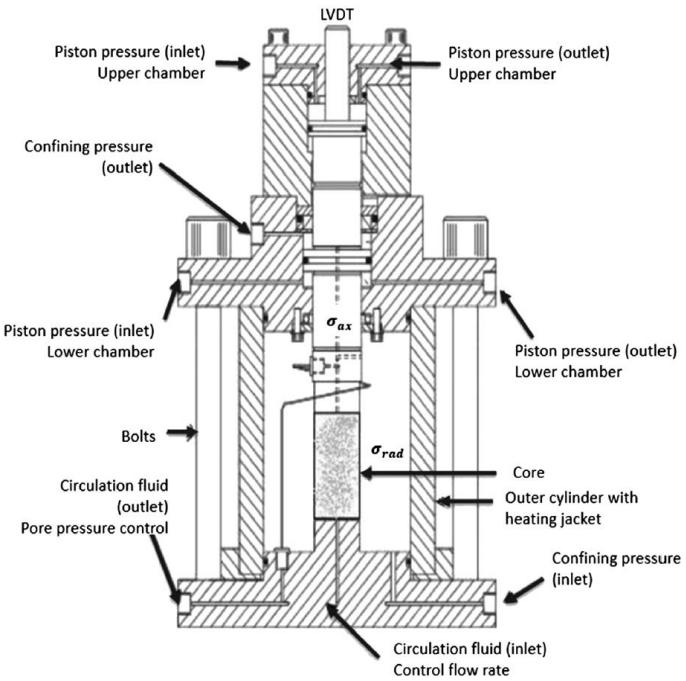

Figure 1 *Sketch of the triaxial cell (Nermoen et al., 2015a).*

The cell was equipped with a heating element and a regulating system with precise temperature control. Three pumps were connected to the triaxial cell to control the piston pressure (P_{pist}), confining pressure (σ_{rad}) and flooding rate (Q). The pore pressure on the downstream side (P_p) was controlled by a back-pressure regulator ensuring a constant pore pressure of 0.7 MPa. An external Linear Voltage Differential Transducer (LVDT) monitored the length change of the plug (L). In these tests, the deformation was measured only in axial direction. The axial stress was calculated using confining pressure (radial stress), piston pressure, frictional pressure of the piston movement in the triaxial cell, and an area factor for the piston pressure chamber and the cross area of the plug ($f_{area} = 1.2855$) using equation 1,

$$\sigma_{ax} = \sigma_{rad} + f_{area}\left(P_{pist} - P_{fric}\right) \quad (1)$$

In the hydrostatic phase ($P_{pist} = P_{fric}$), the stresses are equal in all directions, so the bulk modulus K is given by

$$K = {\Delta\sigma'_{ax}}/{\Delta\varepsilon_{vol}} = {\Delta\sigma'_{ax}}/{(\Delta\varepsilon_{ax} + 2\Delta\varepsilon_{rad})} \quad (2)$$

Here, $\Delta\sigma'_{ax}$ is the change in effective stress in axial direction, where the effective stress is given by the imposed stress in radial and axial direction minus a fraction α times the pore pressure ($\sigma' = \sigma - \alpha P_{pore}$). We assume that the Biot coefficient $\alpha = 1$ in these experiments. $\Delta\varepsilon_{vol}$ is the change in volumetric strain, $\Delta\varepsilon_{ax}$ is the change in strain in axial direction and $\Delta\varepsilon_{rad}$ is the change in strain in radial direction.

In this test series deformation was measured only in one direction, and the radial deformation was assumed equal to the axial deformation. In this case, equation (2) became

$$K = {}^{\Delta\sigma'_{ax}}/_{3\Delta\varepsilon_{ax}} \tag{3}$$

In the deviatoric phase, there is no change in the radial stress, i.e. $\Delta\sigma'_{rad} = 0$. Young's modulus E is, then, given by the slope of the axial stress-strain curve in the deviatoric phase, expressed by

$$E = {}^{\Delta\sigma'_{ax}}/_{\Delta\varepsilon_{ax}} \tag{4}$$

Value of q, used to define one of the basic stress invariants, is given by

$$q = \sigma'_{ax} - \sigma'_{rad} \tag{5}$$

where σ'_{ax} gives the effective axial stress and σ'_{rad} gives the effective radial stress.

Experimental Procedure

In order to understand how the fluid composition affect the below yield behavior, four reference experiments, one for each brine, were performed. They were performed to identify the position of the shear failure stress and were executed according to the following plan:

1. Cores saturated with the pre-scribed brine and mounted into the cell.
2. Pore pressure and confining pressure built up simultaneously to P_{pore} = 0.7 MPa and P_{conf} = 1.2 MPa. Bypass valve was kept open to ensure negligible fluid replacement within the core and at the same time maintain a stable pore pressure.
3. Increased temperature from ambient to 130°C and allowed to stabilize overnight. 130°C was chosen to replicate the same temperature conditions in the laboratory as of the Ekofisk field in North Sea.
4. Loaded hydrostatically from 1.2 to 3 MPa by increasing the confining pressure. The piston pressure was kept just above the friction pressure to ensure close contact between the piston and the core for axial strain measurement. During hydrostatic loading, the bulk modulus was estimated. The bulk modulus was obtained by introducing the value of slope of the stress-strain curve during hydrostatic loading phase $\left({}^{\Delta\sigma'_{ax}}/_{\Delta\varepsilon_{ax}}\right)$ into equation 3.
5. Loaded deviatorically by increasing the piston pressure until failure. During deviatoric loading, the Young's modulus and onset of yield were estimated. The Young's modulus was obtained from the data from the start of deviatoric loading to 1 MPa below yield. The onset of yield was obtained when the absolute difference between the extrapolated line from the elastic domain and the observed stress exceeded 0.3 MPa.

Now the value of the axial yield stress was known. A new set of cores from the same chalk block was studied to investigate the elastic and plastic properties at 69-73% of axial yield stress. In all, four core experiments were performed, one with each brine composition, according to the following plan:

1. Repeated steps 1 to 4 above.
2. Loaded deviatorically to a constant value of 69-73% of axial yield stress obtained from the reference test for the same brine.

3. Left the core to creep for 4.5 days to investigate time-dependent deformation for different brines.
4. Closed the bypass valve and started flooding DW through the core to clean it. 3 PVs of DW were flooded through all cores for cleaning. The permeability of these cores varied in the range of 0.6 mD to 3 mD.
5. Removed the additional axial load by lifting the piston such that hydrostatic conditions were met.
6. The piston was put down again after 40 minutes to obtain a direct reading of how much the core rebounded elastically.

Results

The experimental results are presented in sections starting with (i) hydrostatic and deviatoric loading, followed by (ii) results from creep phase and lastly, results from (iii) rebound tests. Please note that the brines were not flooded through the core, which means no new fluid was getting in contact with chalk during the tests. As such, any differences in experimental results arose from the chemical interactions of 1 PV of the initially saturating fluid.

Hydrostatic and deviatoric loading

For each brine, the stiffness was quantified via bulk modulus (K) and Young's modulus (E) from the hydrostatic phase and deviatoric phase, respectively. Poisson ratio estimates could not be provided since radial strain gauges were not installed. The values of bulk modulus and Young's modulus for cores saturated by the different brines used in both test series 1 (reference test series; odd core numbers) and test series 2 (creep test series at 69-73% of yield; even core numbers) are given in *Table 3*. Here, the values of the axial yield stresses (test series 1) and the corresponding creep stresses (test series 2) are shown. The radial stresses were 3 MPa for all experiments. The stress-strain plots for all brines during hydrostatic and deviatoric loading phases are displayed in *Figure 2*.

Table 3 *Bulk modulus and Young's modulus during hydrostatic and deviatoric loading for cores saturated with different brines. Axial yield stress (odd core numbers) and creep stress (even core numbers) are given in the right column at radial stress of 3 MPa. Experiments performed at 130°C.*

Core Number	Saturating Brine	Bulk Modulus K, GPa	Young's Modulus E, GPa	Axial yield stress, MPa	Creep stress, MPa	Percent of creep stress to axial yield stress, %
C1	DW	0.72	2.00	10.7*		
C2		0.80	2.78		7.7	72.0
C3	NaCl	0.88	2.12	9.1		
C4		0.75	2.12		6.4	70.3
C5	$MgCl_2$	0.70	2.25	9.4		
C6		0.62	1.76		6.5	69.1
C7	SSW	0.69	1.94	7.4		
C8		0.71	1.99		5.4	73.0

**Offset yield parameter for DW core C1 and SSW core C7 was 0.6 MPa instead of 0.3 MPa which was used for cores C3 (NaCl) and C5 ($MgCl_2$).*

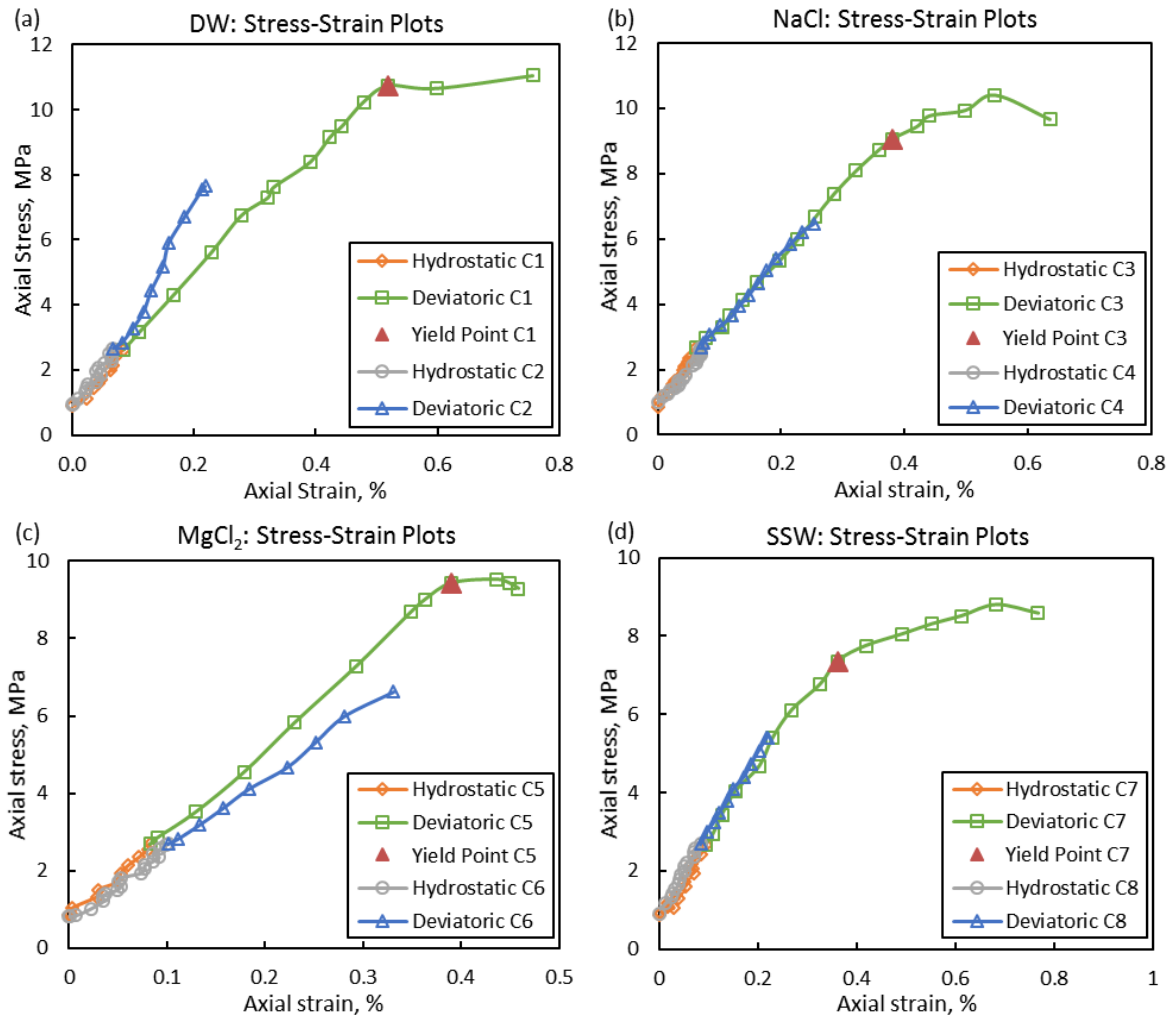

Figure 2 *Stress-strain plots for all cores initially saturated by different brines viz. (a) DW, (b) NaCl, (c) $MgCl_2$ and (d) SSW. The legends denote the core number preceded by the type of the loading phase depicted for that specific core. Yield point for odd numbered reference cores is displayed using a closed triangle in each plot.*

The bulk modulus was found to be lowest for the plugs initially saturated by $MgCl_2$-brine with an average value of 0.66 GPa, followed by the plugs initially saturated by SSW with an average value of 0.70 GPa and DW with an average value of 0.76 GPa. The highest bulk modulus was attained for the core plugs initially saturated by NaCl-brine with an average value of 0.82 GPa. The variation between equal tests range from 0.02 to 0.13 GPa.

Young's modulus was found to be lowest for the plugs initially saturated by SSW with an average value of 1.96 GPa which was moderately lower than the plugs initially saturated by $MgCl_2$ and NaCl (average values of 2.00 GPa and 2.12 GPa, respectively). The highest Young's modulus was attained for the core plugs tested with DW with an average value of 2.39 GPa. The variation between equal tests range from zero to 0.78 GPa.

It was also found that SSW had the lowest yield stress of 7.4 MPa followed by NaCl and $MgCl_2$ with yield stresses of 9.1 MPa and 9.4 MPa, respectively. The highest yield stress was found for the core initially saturated with DW (10.7 MPa) which was approx. 1.45 times higher than SSW.

Creep phase of test series 2 (below yield)

The even number cores (C2 - DW, C4 - NaCl, C6 - $MgCl_2$, C8 - SSW) were loaded deviatorically to 69 to 73% of axial yield stresses as shown in *Table 3* for the same brine (estimated from test series 1). Then the cores were left to creep to investigate the time dependent behavior in the so-called elastic region compared for the different brines. The stress levels during creep were (a) DW: 7.7 MPa; (b) NaCl: 6.4 MPa; (c) $MgCl_2$: 6.5 MPa; and (d) SSW: 5.4 MPa.

Time-dependent deformation for each brine was estimated at constant stress level. In**Error! Reference source not found.** *Figure 3*, the axial creep strain for the different experiments are shown. Please note that the creep stress is not the same, but rather 69-73% of the yield for each brine. The creep phase lasted for 4.5 days.

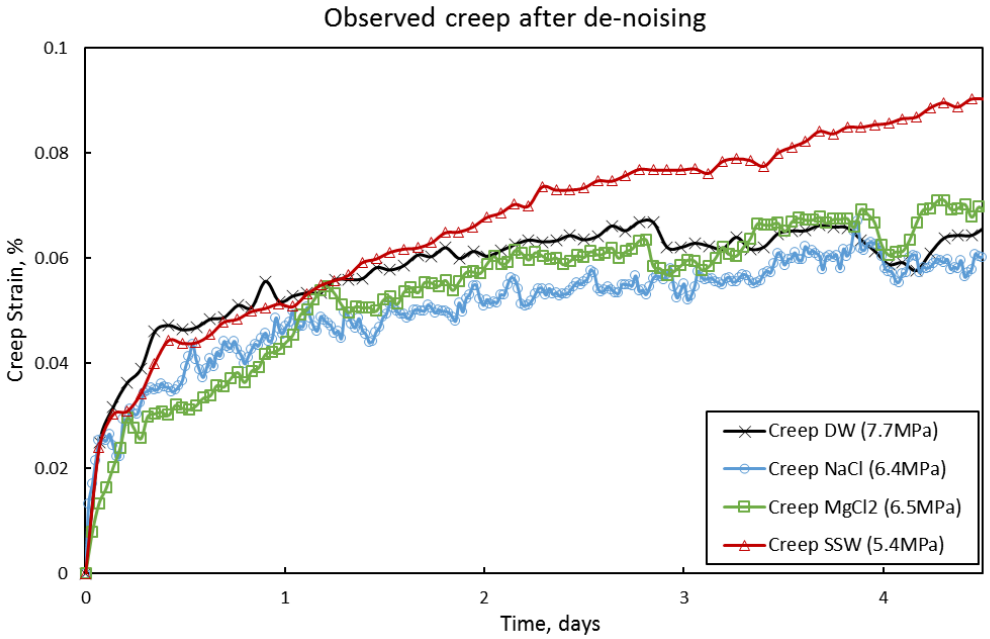

Figure 3 *Observed modified creep with time for the cores saturated with all four different fluids. Here the data is smoothened to remove noise. DW was compacted at 72.0%, NaCl at 70.3%, $MgCl_2$ at 69.1% and SSW at 73.0% of the corresponding axial yield stresses estimated from test series 1.*

Figure 3 shows the observed creep for the cores saturated with different brines. The figure is modified to remove noise from the curves. For this purpose, creep strain was sampled over time and consists of an average creep strain measured over 60 minutes at each time step. As is seen from *Figure 3*, the observed final creep strains are similar for all brines except SSW which attained a final creep strain of 0.09% at the end of creep period. This is approx. 0.02 to 0.03 p.u. higher than other brines, i.e. the SSW sample had a final creep strain that was a factor 1.3 to 1.5 times that of the other brines.

The strain rates measured for the last half a day were $6.0 \cdot 10^{-4}$ %/hour for DW, $5.7 \cdot 10^{-4}$ %/hour for NaCl, $6.6 \cdot 10^{-4}$ %/hour for $MgCl_2$ and $8.6 \cdot 10^{-4}$ %/hour for SSW, which shows that the deformation rate was higher for SSW compared to other brines.

Rebound

After creep, the cores were cleaned by flooding 3 PVs of distilled water at 130°C. The elastic and plastic partitioning was measured by lifting the piston from the core and putting it back on top of the core again after 40 minutes. As defined in *Figure 4*(d), the total axial strain consists of the sum of strains developed in the deviatoric loading and creep phase; creep strain is the strain developed during creep phase only; and, plastic strain is the irreversible strain calculated by subtracting the elastic strain (rebound) from the total strain. The total axial strain, plastic and creep strains, the percent of plastic strain divided by the

total strain (i.e. plastic component of total strain), and creep strain divided by the total strain (creep component of total strain) are given in
Table 4.

Table 4 *Total axial, plastic and creep strains observed in cores saturated with different brines. The strains are defined in the text and in Figure 4(d).*

Core Number	Brine	Tot. axial strain, %	Plastic (and elastic) strain, %	Creep strain, %	Plastic component of tot. strain, %	Creep component of tot. strain, %
C2	DW	0.23	0.10 (0.13)	0.066	43	29
C4	NaCl	0.25	0.11 (0.14)	0.060	44	24
C6	$MgCl_2$	0.34	0.19 (0.15)	0.069	56	20
C8	SSW	0.24	0.17 (0.07)	0.090	71	38

The total and plastic strains are calculated from the plot of q as a function of axial strain shown in *Figure 4*.

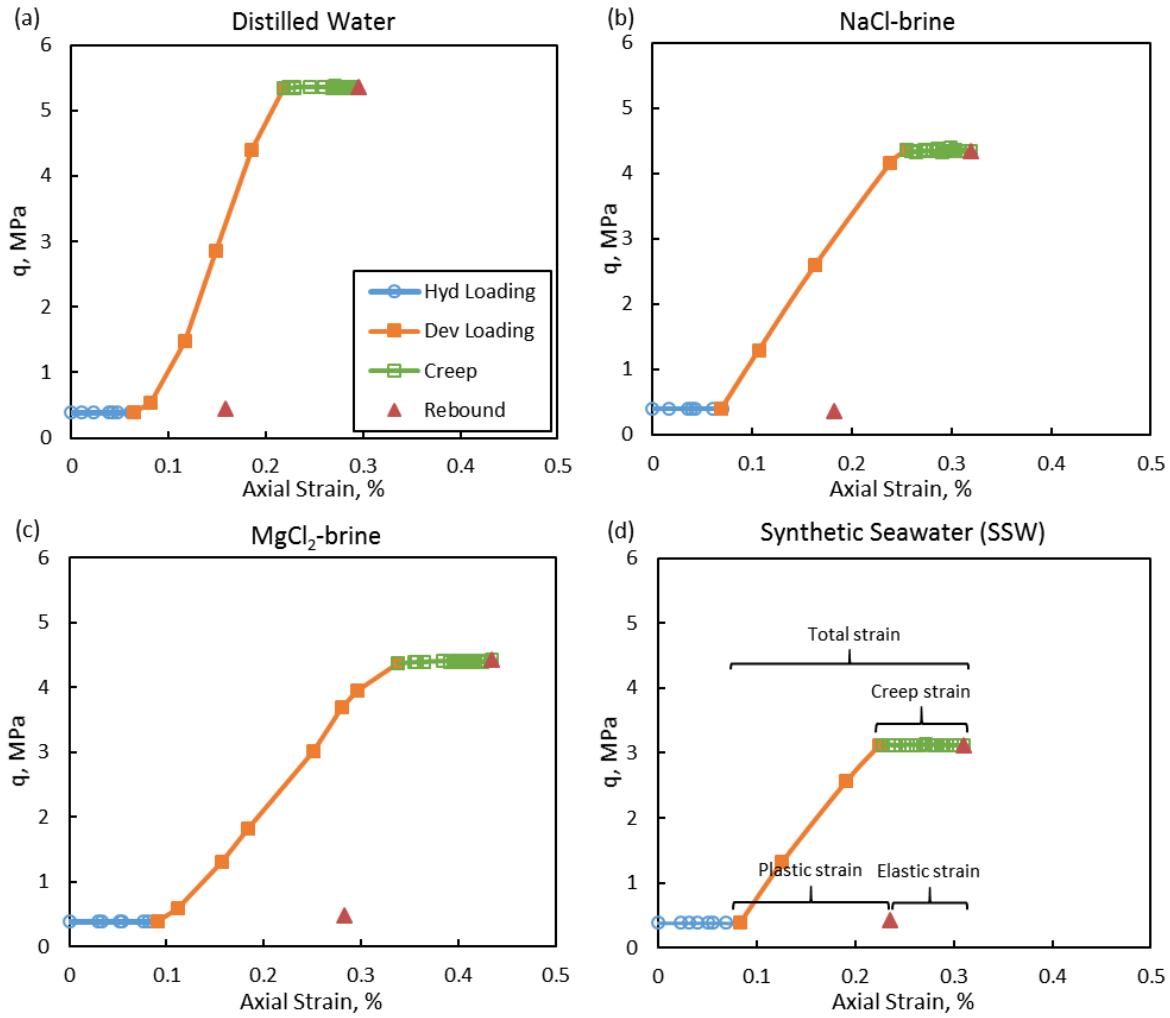

Figure 4 *Plots of q as a function of axial strain to determine elastic and plastic strains for cores saturated with different fluids, viz., (a) DW, (b) NaCl, (c) $MgCl_2$ and (d) SSW. Rebound strain was found by lifting up the piston while waiting 40 minutes before being lowered onto the core – radial stress was 3 MPa in all cases. Legend in (a) apply to all figures. The definition of the elastic and plastic (i.e. reversible and irreversible), and total strains are shown in (d).*

As can be seen from *Figure 4* the elastic strain (see brackets in column 4 in *Table 4*) for the C6 ($MgCl_2$) core (0.15%) is similar to that observed in C2 (DW) and C4 (NaCl) cores, with values 0.13% and 0.14%, respectively. This applies even though core C6 ($MgCl_2$) attained the largest total strain at the end of the creep phase (0.34%).

The plastic and elastic strains, and the corresponding strain components of total strain (*Table 4*), in cores C2 (DW) and C4 (NaCl) were not significantly different. The C6 ($MgCl_2$) core attained a plastic component of the total strain of 56% which was in between the C2 and C4 cores (43 and 44%, respectively) and the C8 (SSW) core which had a plastic component of 71%. The creep component of the total strain was 38% for C8 (SSW), which was significantly higher than the other cores.

Discussion

In real field scenarios, when there is a moderate drop in the pore pressure, the deformation occurs within the elastic domain. For chalk reservoirs, even within the elastic domain, minute grain reorganization can take place that lead to plastic deformation over time. Hence, if the pore pressure is increased to the original level by water flooding, the reservoir would not re-establish its original state. There will be some permanent deformation in the reservoirs even after pore pressure increase. This deformation usually occurs in the axial direction because reservoirs are free to deform vertically but are horizontally constrained by tectonic forces and induce negligible horizontal deformation. Hence, the ratio of the average horizontal stress to the overburden stress, defined by stress ratio $k = \sigma_h'/\sigma_z'$ is below 1. Rhett and Teufel (1992) reported a stress ratio of 0.20 for Ekofisk field in North Sea after 20 years of production. In our case, stress ratio was different for all tests due to equal radial stresses but varying axial stresses. The stress ratio varied in the range 0.28-0.56 for our tests. This means that deviatoric stresses do exist. To gain insight into how reservoirs deform at these conditions, we performed a series of laboratory core scale experiments. The aim was to investigate how strains were accumulated at anisotropic stress conditions within the elastic domain, i.e. at 69-73% of yield stress for the corresponding four brines.

Four yield tests (test series 1: odd number cores) were performed for the four different brines. As shown in *Table 3* the DW saturated core had the highest yield stress (10.7 MPa), followed by $MgCl_2$ and NaCl with almost equal strength (9.4 MPa and 9.1 MPa, respectively), and SSW had the lowest yield stress (7.4 MPa). This is in line with earlier reported studies, in which the adsorption of divalent ions lead to weakening of the chalk (Korsnes et al., 2006b, 2008; Madland et al., 2011; Megawati et al., 2012). The actual value for the onset of yield is sensitive to variations in the cores (Madland et al., 2011), the loading rate (Omdal et al., 2010) and the way in which the experiment is analyzed. Here, it was chosen to determine the onset of yield from the stress at which the extrapolated linear behavior deviated by 0.3 MPa from the observed yield in stress-strain plots (*Figure 2*). Typically, having a higher value for offset yield parameter would lead to a higher onset of yield. The choice of offset yield parameter was chosen to be as small as possible (0.3 MPa); however, the DW and SSW cores had more variation in stress-strain such that a higher value of 0.6 MPa had to be chosen. In all, experience has shown that hydrostatic tests have better repeatability and that the typical variation in the yield stress from core to core from the same block typically lies within a range of 0.2 – 0.5 MPa (Korsnes et al., 2008; Madland et al., 2011; Megawati et al., 2012; Nermoen et al., 2015b). As such, when comparing strength tests any difference beyond 0.5 MPa is considered significant.

We focus the rest of the discussion on the tests performed below yield (test series 2: even number cores). Values of (a) bulk modulus during hydrostatic loading and Young's modulus during deviatoric loading, (b) time-dependent deformation for the four different brines at 69-73% of axial yield stress, and (c) the elastic and plastic part of the total strain are being discussed.

Variations in the bulk modulus and Young's modulus (*Table 3*) as function of brine composition is observed. To estimate the accuracy of the bulk modulus and Young's modulus reported here a two-step analysis was performed. We estimated the standard deviation for the (two) cores saturated with the same brine, and then took the average of the standard deviations. This is because reporting a standard

deviation from only two tests are sensitive with too great uncertainty since the pair of cores can, or cannot, overlap. As is visible from *Figure 2* the curves lie almost on top of each other for hydrostatic loading phase for all four brines, but during deviatoric phase, significant deviation is seen for DW and $MgCl_2$, but they overlap in NaCl and SSW. As such, deviations of 0.05 and 0.23 were calculated for bulk modulus and Young's modulus, respectively. *Figure 5* gives the average values of bulk modulus and Young's modulus as a function of yield stress with an uncertainty quantified by standard deviation.

As can be seen in *Figure 5(b)*, there seems to be a trend between Young's modulus and onset of yield. As for strength, the SSW saturated core had the lowest Young's modulus, while NaCl and $MgCl_2$ had intermediate and DW the highest Young's modulus. The trend between bulk modulus and strength is less visible as seen in *Figure 5(a)*. Organizing the cores from soft to stiff $MgCl_2$ was the weakest followed by SSW and DW, and NaCl had the highest bulk modulus.

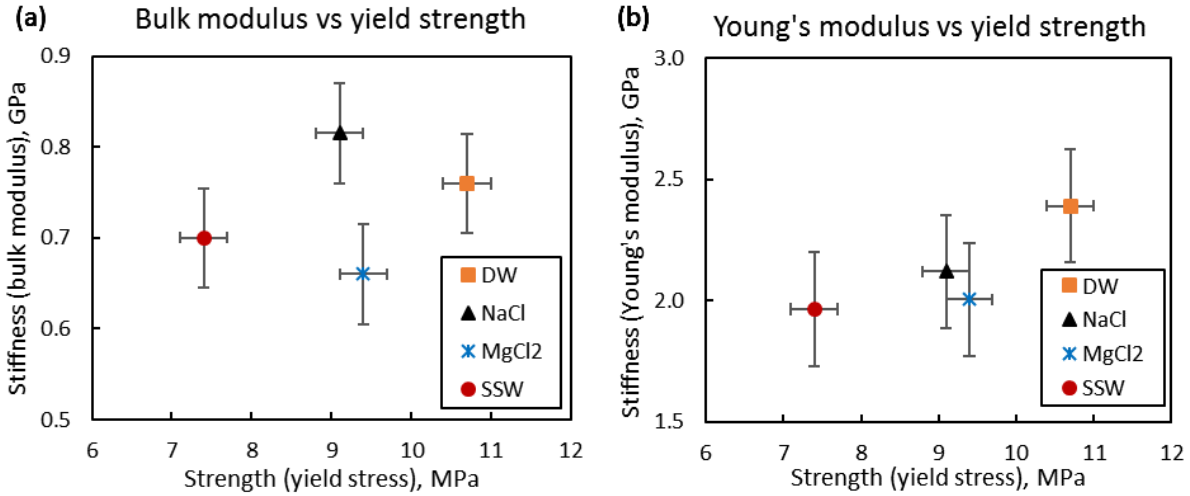

Figure 5 *(a) Bulk modulus and (b) Young's modulus (quantifying stiffness) as a function of yield strength (quantified by yield stress). The average values of bulk modulus and Young's modulus are shown with their standard deviations (quantifying uncertainty) of 0.05 and 0.23, respectively. A standard deviation of 0.3 MPa was chosen for the yield stress.*

The final creep strain observed for the cores loaded deviatorically to 69-73% of axial yield stress was almost similar for all brines except SSW, which displayed approx. 0.02-0.03 p.u. higher final creep strain than for other brines. Remark that this occurred even though it had the lowest creep stress (core C8 saturated by SSW had a creep stress of 5.4 MPa which was 73 % of axial yield stress obtained, i.e. 7.4 MPa, for the reference core C7 saturated by same brine). The observed lowest yield and highest creep strain with SSW can be explained by the way sulfate ions adsorb onto chalk surface. Sulfate adsorption gives rise to significant repulsive forces close to the granular contacts. These forces induce disjoining pressures reducing cohesive forces at the intergranular contacts (Megawati et al., 2012).

It was also observed that even at the lowest creep stress, the strain rate was higher for seawater in the last half day ($8.6 \cdot 10^{-4}$ %/hour) compared to other brines (ranging from $5.7 \cdot 10^{-4}$ to $6.6 \cdot 10^{-4}$ %/hour) leading to a higher deformation rate in the core with SSW.

Even though before rebound tests the cores were cleaned of any salts by flooding 3PVs of DW, the data obtained for total axial and plastic strains (
Table 4) has shown that there is a clear difference in the values of plastic component of the total strain for the four brines. The core with SSW developed a 71% plastic component of the total strain. This value is 1.65 times larger than for DW and NaCl, and 1.27 times larger than for $MgCl_2$. It is also evident from this table that the creep component of total strain is smaller than plastic component of total strain for all four brines. This means that the whole of creep period as well as a part of deviatoric loading phase are accountable for the plastic strain in the cores.

The large value of plastic component of the total strain for the C8 (SSW) core can be interpreted as sign of rock-fluid interactions taking place within the rock, even though the rock was in contact with only one pore volume of SSW during the test. Madland et el. (2011) reported the detection of precipitated magnesium-bearing minerals and formation of anhydrite $CaSO_4$ for the core flooded with SSW using Scanning Electron Microscope (SEM) studies. Besides, sulfate adsorption onto chalk surface and the generation of disjoining pressures (Megawati et al., 2012) also play an important role in facilitating rock deformation.

Conclusion

The effect of distilled water and three brines with different ion compositions on the chalk mechanics has been demonstrated during deviatoric loading and during time-dependent deformation below yield. Variations in the bulk modulus and Young's modulus as function of brine composition is observed, however more data is required to claim that the variations are significant. Yield stress was found to be highest for DW and lowest for SSW, and conforms the results from previous studies. The final creep strain with SSW was approx. 0.02-0.03 p.u. i.e. a factor 1.3 to 1.5 times higher than the other brines. This suggest that rock-fluid interactions can change the mechanical property even only with one pore volume. SSW had also shown to give a large plastic component of total strain. This effect can either be attributed to precipitation of magnesium-bearing silicates and carbonates, and the formation of anhydrite, or, sulfate adsorption onto chalk surface and the generation of disjoining pressures facilitating rock deformation. The strain recovery analyses, i.e. the elastic-plastic partitioning sheds light onto other geomechanical parameters than what has frequently been tested before. The quantitative analysis reported here paves the way for further geomechanical studies relevant to understand the stress-strain behavior during an actual reservoir history. The impact of temperature, pore fluid composition, stress state and time have been shown to be important to the rock stiffness, strength and elastic-plastic partition.

Acknowledgements

The authors acknowledge the Research Council of Norway and the industry partners; ConocoPhillips Skandinavia AS, Aker BP ASA, Eni Norge AS, Maersk Oil Norway AS, DONG Energy A/S, Denmark, Statoil Petroleum AS, ENGIE E&P NORGE AS, Lundin Norway AS, Halliburton AS, Schlumberger Norge AS, Wintershall Norge AS of The National IOR Centre of Norway for support.

References

Doornhof, D., Kristiansen, T.G., Nagel, N.B., Pattillo, P.D., and Sayers, C. [2006] Compaction and Subsidence. *Oilfield Review*, 50–68.

Gateway to the Paleobiology Database [1999]. Retrieved January 02, 2017 from http://fossilworks.org/bridge.pl?a=collectionSearch&collection_no=3919

Geys, J.F. [1980] Phymosomatoid Echinoids from the Campanian and the Maastrichtian of Belgium and the Netherlands. *Paläontologische Zeitschrift*, **54**(3-4), 199-224.

Hermansen, H., Thomas, L.K., Sylte, J.E., and Aasboe, B.T. [1997] Twenty Five Years of Ekofisk Reservoir Management. In: SPE Annual Technical Conference and Exhibition, SPE Paper 38927-MS.

Hellmann, R., Renders, P., Gratier, J.P., and Guiguet, R. [2002a] Experimental Pressure Solution Compaction of Chalk in Aqueous Solutions, Part 1. Deformation Behavior and Chemistry. In: *Water Rock Interactions, Ore Deposits, and Environmental Geochemistry: A Tribute to David A. Crerar*, edited by R. Hellmann and S. A. Wood. Geochemical Society, 129–152.

Hellmann, R., Gaviglio, P., Renders, P., Gratier, J.P., Bèkri, S., and Adler, P. [2002b] Experimental Pressure Solution Compaction of Chalk in Aqueous Solutions, Part 2. Deformation Examined by SEM,

Posimetry, Synthetic Permeability, and X-Ray Computerized Tomography. In: *Water Rock Interactions, Ore Deposits, and Environmental Geochemistry: A Tribute to David A. Crerar*, edited by R. Hellmann and S. A. Wood. Geochemical Society, 153–178.

Korsnes, R.I., Strand, S., Hoff, Ø., Pedersen, T., Madland, M.V., and Austad, T. [2006a] Does the Chemical Interaction Between Seawater and Chalk Affect the Mechanical Properties of Chalk?. In: Cottheim, A.V., Charlier, R., Thimus, J.F., Tshibangu, J.P. (eds.) Eurock, *Multiphysics Coupling and Long Term Behaviour in Rock Mechanics*. Taylor & Francis, London, 427–434.

Korsnes, R.I., Madland, M.V., and Austad, T. [2006b] Impact of Brine Composition on the Mechanical Strength of Chalk at High Temperature. In: Cottheim, A.V., Charlier, R., Thimus, J.F., Tshibangu, J.P. (eds.) Eurock, *Multiphysics Coupling and Long Term Behaviour in Rock Mechanics*. Taylor & Francis, London, 133–140.

Korsnes, R.I., Madland, M.V., Austad, T., Haver, S., and Røsland, G. [2008] The Effects of Temperature on the Water Weakening of Chalk by Seawater. *Journal of Petroleum Science and Engineering*, **60**, 183–193.

Kristiansen, T.G., Barkved, O.I., Buer, K., and Bakke, R. [2005] Production-Induced Deformations Outside the Reservoir and their Impact on 4D Seismic. In: International Petroleum Technology Conference, Doha, Qatar, 21-23 November, IPTC Paper 10818.

Madland, M.V., Finsnes, A., Alkafadgi, A., Risnes, R., and Austad, T. [2006] The Influence of CO2 Gas and Carbonate Water on the Mechanical Stability of Chalk. *Journal of Petroleum Science and Eng*ineering, **51**, 149–168.

Madland, M.V., Midtgarden, K., Manafov, R., Korsnes, R.I., Kristiansen, T.G., and Hiorth, A. [2008] The Effect of Temperature and Brine Composition on the Mechanical Strength of Kansas Chalk. In: International Symposium of the Society of Core Analysts, Abu Dhabi, UAE, 29 October-2 November, SCA Paper SCA2008-55.

Madland, M.V., Hiorth, A., Omdal, E., Megawati, M., Hildebrand-Habel, T., Kornes, R.I., Evje, S., and Cathles, L. [2011] Chemical Alterations Induced by Rock-Fluid Interactions When Injecting Brines in High Porosity Chalks. *Transport in Porous Media*, **87**(3), 679-702.

Megawati, M., Andersen, P.Ø., Korsnes, R.I., Evje, S., Hiorth, A., and Madland, M.V. [2011] The Effect of Aqueous Chemistry pH on the Time-Dependent Deformation Behaviour of Chalk Experimental and Modelling Study. In: Pore2Fluid International Conference, IFP Energies Nouvelles Paris (France), November 16–18.

Megawati, M., Hiorth, A., and Madland, M.V. [2012] The Impact of Surface Charge on the Mechanical Behavior of High-Porosity Chalk. *Journal of Rock Mechanics and Rock Engineering*, **46**(5), 1073-1090.

Megawati, M., Madland, M.V., and Hiorth, A. [2015] Mechanical and Physical Behavior of High-Porosity Chalks Exposed to Chemical Perturbation. *Journal of Petroleum Science and Engineering*, **133**, 313-327.

Nermoen, A., Korsnes, R.I., Hiorth, A., and Madland, M.V. [2015a] Porosity and Permeability Development in Compacting Chalks During Flooding of Nonequilibrium Brines: Insights from Long-Term Experiment. *Journal of Geophysical Research: Solid Earth*, **120**(5), 2935-2960.

Nermoen, A., Korsnes, R.I., Fabricius, I.L., and Madland, M.V., [2015b] Extending the Effective Stress Relation to Incorporate Electrostatic Effects. *SEG Technical Program Expanded Abstracts 2015*, 3239-3243. http://dx.doi.org/10.1190/segam2015-5891149.1

Neveux, L., Grgic, D., Carpentier, C., Pirnon, J., Truche, L., and Girard, J. [2014a] Influence of Hydrocarbon Injection on the Compaction by Pressure Solution of a Carbonate Rock: An Experimental Study Under Triaxial Stresses. *Marine and Petroleum Geology*, **55**, 282–294.

Neveux, L., Grgic, D., Carpentier, C., Pironon, J., Truche, L., and Girard, J. [2014b] Experimental Simulation of Chemomechanical Processes During Deep Burial Diagenesis of Carbonate Rocks. *Journal of Geophysical Research: Solid Earth*, **119**(2), 984–1007.

Omdal, E., Madland, M.V., Kristiansen, T.G., Nagel, N.B., Korsnes, R.I., and Hiorth, A. [2010] Deformation Behavior of Chalk Studied Close to In Situ Reservoir Conditions. *Rock Mechanics and Rock Engineering*, **43**(5), 557-580. http://dx.doi.org/10.1007/s00603-010-0087-4

Rhett, D.W., and Teufel, L.W. [1992] Effect of Reservoir Stress Path on Compressibility and Permeability of Sandstones. In: 67th Annual Technical Conference and Exhibition of the Society of Petroleum Engineers, Washington, DC, USA, 4-7 October, SPE Paper 24756.

Risnes, R. [2001] Deformation and Yield in High Porosity Chalks. *Physics and Chemistry of the Earth (A)*, **26**(1–2), 53–57.

Risnes, R., Haghighi, H., Korsnes, R.I., and Natvik, O. [2003] Chalk-Fluid Interactions with Glycol and Brines. *Tectonophysics*, **370**, 213–226.

Paper VI

Sachdeva, J.S., Nermoen, A., Madland, M.V., and Korsnes, R.I. (2016). How Wetting Conditions Dictate Chalk Mechanics at Uni-axial Strain Conditions – Insights from Experiments Performed at In-situ Stress, Temperature and Pore Pressure. Paper SCA2016-068. *International Symposium of the Society of Core Analysts 2016*, Snowmass, Colorado, USA.

HOW WETTING CONDITIONS DICTATE CHALK MECHANICS AT UNI-AXIAL STRAIN CONDITIONS – INSIGHTS FROM EXPERIMENTS PERFORMED AT IN-SITU STRESS, TEMPERATURE AND PORE PRESSURE

Jaspreet S. Sachdeva[1,2], Anders Nermoen[1,2,3], Merete V. Madland[1,2], Reidar I. Korsnes[1,2]
[1]University of Stavanger, Norway
[2]The National IOR Centre of Norway
[3]International Research Institute of Stavanger, Norway

This paper was prepared for presentation at the International Symposium of the Society of Core Analysts held in Snowmass, Colorado, USA, 21-26 August 2016.

ABSTRACT

This paper document how the mechanical strength of chalk depends on the chemistry of pore fluids. Three experiments with different pore fluid compositions were performed at uni-axial strain conditions maintaining constant overburden stress during pore pressure depletion and subsequent compaction phase. The pore fluids were: i) 100% NaCl-brine, ii) 10%-90% NaCl-brine and oil mixture and iii) 100% oil. Significant differences were observed during the depletion and time-dependent compaction phase. The oil-saturated core was stronger than core saturated by brine-oil mixture, while the brine-saturated core accumulated most strain. During compaction, seawater was injected that led to additional strain; most so in the oil-saturated core, intermediate additional strain in the brine-oil mixed core, and least additional strain was observed in the brine-saturated core. This is in line with earlier results on how the ion composition of seawater significantly impacted chalk mechanics. Other significant observations include the additional side stress required to maintain the zero radial strain requirement, and irrespective of the original fluid composition, it is found that after only 2.5 PVs of seawater injection the creep rate for all three cases attained the same value. This indicates that the seawater induced weakening is abrupt, and it is more prominent when there is less water in the core originally.

INTRODUCTION

During primary phase oil production from a reservoir, the extraction of pressurized fluids reduce the pore fluid pressure leading to an increase in the effective stress, which in turn drives compaction. Reservoirs can be re-pressurized by injecting seawater to reduce the effective stress and mobilize oil. Even though the pressure is maintained, there is still considerable amount of compaction observed in the reservoirs. This compaction has been linked to the interaction of ions in the brines with the rock itself. Considerable research has been carried out concerning this water induced compaction in chalk reservoirs in the past few decades [1-4]. These studies have been carried out on water-wet chalk. This research has primarily shown that the pore fluid composition alters the mechanical

integrity of chalk, as seawater and other simplified brines affect the mechanical strength. Different ions in the water, e.g. sulphates and magnesium ions, change the macroscopic mechanical behaviour of chalk, thus altering the way in which the brines and oils move through the porous rock and hence affecting oil recovery [2-4]. In recent studies of isotropic (hydrostatic) loading tests [5,6], it was shown that values characterizing the mechanical properties of chalk decreased when the wetting state was changed towards more water-wet. However, how do the results in [5,6] apply to high fluid pressures at uni-axial strain condition? In addition, how does the initial water condition dictate the mechanical response after the core has been flooded by seawater? This paper deals with the cases where the cores are initially saturated by different fluids and then the wettability is altered by aging to more mixed-wet state.

MATERIAL, EQUIPMENT, AND EXPERIMENTAL PROGRAM

Test Material and Saturation Fluids

The experiments in this study are performed on an outcrop chalk from a quarry in west-central Kansas in the USA (~39% porosity). The Kansas chalk type is considered to be a pure chalk with a non-carbonate content in the range 1-3% [2,7] and a permeability in the range 1-2 mD. This chalk is from Late Cretaceous geological age. Tang and Firoozabadi [7] argue that it is a good analogue to some clean North Sea reservoir chalks in regards to porosity, capillary pressure, and absolute and relative permeability.

Three different initial fluid saturations were used: Core K01 was saturated and flooded by 1.1M NaCl-brine. NaCl-brine was used as a simplified formation brine to minimize rock-fluid interactions prior to seawater flooding. Core K02 was saturated by approx. 10% NaCl-brine and 90% of Heidrun and Heptane oil that were mixed in 60%-40% (by volume). This oil was filtered through a 6.5μm filter. Core K03 did not contain any brine and was saturated only by the same oil. Both cores K02 and K03 were flooded with two pore volumes of this oil in each direction at 50°C. After the cores, K02 and K03, were saturated, they were submerged into the same oil and aged for 3 weeks at 8 bar and 90°C. The aging was performed to alter the wettability properties of the chalk cores. Wettability was not measured after aging. The aging procedure followed here would yield a wettability along the same lines as the results of Zangiabadi et al. [6] where they aged the cores with the same oil together with 20% brine, which gave a wettability index of 0.65. The wettability index (WI) is a measure of the available sulphate adsorption sites, where a WI equal to 0 means completely oil-wet and 1 means completely water-wet [6]. Strand et al. [8] reported wettability indexes below 0.5 on Stevns Klint chalk that were aged after being completely saturated by 60%-40% Heidrun/heptane mixture without initial water. Zangiabadi et al. [6] also reported acid number 1.92 mg KOH/g oil for the same oil mixture that is used in this study as well. Zangiabadi et al. [6] and Strand et al. [8] conclusively report that by increasing the acid number in the oil, the cores become more oil-wet after aging.

The Triaxial Cell Setup

The chalk cores were mounted into the triaxial cell that allows for continuous measurements of the axial and radial strains during flooding fluids at elevated stresses, pressures, and temperatures. The cell was equipped with a heating element and a regulating system with precise temperature control. Four pumps were connected to the triaxial cell to control the axial stress (σ_{ax}), confining pressure (σ_{rad}), flooding rate (Gilson pump) and pore pressure on the downstream side (P_p). An external linear voltage differential transducer (LVDT) monitored the length of the plug (L). The circumferential diameter on the middle of the core was measured with an extensometer. All the tests were performed at uni-axial strain conditions, with varying radial stress to ensure zero lateral (radial) strain and constant overburden stress such that the stress-path is similar to those that are occurring in the real field scenarios. In these tests, the deformation only took place in the axial direction and a constant axial stress was maintained. The extensometer attached around the core plug measured the radial deformation in the core as a function of time. The signal from extensometer was sent to the computer (LabView software) and was used to change confining pressure for the purpose of avoiding any radial deformation and maintaining zero radial strain. Changes in the confining pressure also affected the axial stress, so the piston pressure was automatically regulated to ensure constant axial stress.

Test Procedure

The experiments were performed at uni-axial strain conditions according to the following procedure: i) Mount the core in the triaxial cell; ii) Increase confining pressure (σ_{rad}) to 1.2 MPa and pore pressure (P_p) to 0.7 MPa simultaneously; iii) Increase temperature to 130°C; iv) Increase σ_{rad} to 40 MPa and P_p to 38 MPa simultaneously; v) Increase axial stress (σ_{ax}) to 42.5 MPa; vi) Start uni-axial strain test. Pore pressure depletion from 38 MPa to 15 MPa; vii) Observe creep at constant overburden; viii) Inject seawater according to the recipe shown in Zangiabadi et al. [6] and observe the creep strain.

During pore pressure depletion in uni-axial strain experiments, Hooke's law is modified such that Young's Modulus is calculated using,

$$E\delta\varepsilon_{ax} = \frac{3\alpha\delta P_p\delta\sigma_{rad} - 2(\delta\sigma_{rad})^2}{\delta\sigma_{rad} - 2\alpha\delta P_p} \quad (1)$$

where E defines the Young's or elastic modulus, δP_p defines the change in the pore pressure from 38 MPa to the point where the core starts to yield, $\delta\sigma_{rad}$ defines the change in the radial stress and $\delta\varepsilon_{ax}$ defines the change in the axial strain corresponding to the same pore pressure values, and α is the Biot coefficient taken equal to 1 for calculations.

RESULTS

Pore Pressure Depletion Phase

Pore pressure depletion is carried out from 38 MPa to 15 MPa at uni-axial strain conditions. The yield, total axial strain and Young's Modulus values for the three cores during the pore pressure depletion phase are given in

Table 1. For the K03 core (100% oil), the yield strength and elastic modulus is found to be 2 and 1.4 times larger, respectively, than the results for the K01 core (100% brine). The total axial strain after loading is 4 times larger for the K01 core compared to the K03 core. The axial stress vs axial strain curves for all cores are given in Figure 1(a).

Uni-Axial Strain Compaction and Seawater Injection

The uni-axial compaction at constant overburden and pore pressures observed for the three cores is shown in Figure 1(b). The uni-axial compaction observed for K01 and K02 is 5.6% and 2.3%, before seawater injection, which goes up to 8.6% and 5.3%, respectively, after injecting seawater for 40 days. No compaction is observed for K03 prior to seawater injection, but shoots up to 7.5% after injecting the seawater for only 15 days. The strain rates before and after seawater injection for all tests are given in Figure 1(c). The strain rates for K01 and K02 prior to seawater injection are 0.05%/day and 0.07%/day, which increase to 0.17%/day and 0.19%/day, respectively, immediately after the start of injection. The strain rate shoots up to 0.77%/day from zero for K03 immediately after the start of seawater injection. After 2.5 PVs (5 days) of injection, all three cores attain the same value of around 0.17%/day strain rate. Please note that the starting time of seawater injection is taken as zero time (reference time) to make it easy to analyse the results.

DISCUSSIONS

The uni-axial compaction experiments, similar to Omdal et al. [9], have been performed, where the radial stress is automatically adjusted to ensure zero radial strain. The experiments have been carried out by depleting pore pressure whilst keeping the overburden stress constant, before the pore pressure was kept constant at 15 MPa over time. This experimental setup opens up for a range of studies in addition to the mechanical consequences reported here. For example, we can simulate the actual reservoir history with respect to stress, temperature and pore fluid composition, how the pore pressure affects the mobility of oil and water at actual PVT-values, and, to which extent adsorption, dissolution and precipitation depend on pore pressure and stress.

As expected from simpler hydrostatic tests reported by e.g. Zangiabadi et al. [6], we observe that K03 (100% oil) obtains the highest elastic modulus and highest yield during pressure depletion and that these values decrease with increasing brine content.

Prior to seawater injection, the side stresses are automatically reduced as the core compacts (Figure 1(d)). This is interpreted as a signature of work hardening during time,

since less stress is required to keep the core at zero radial strain. However, when seawater is injected, the core weakens. Because of that, both the axial strain is increased, and similarly, the side stress required to maintain zero radial strain is increased. The side stress for the oil-saturated core increased by 6.3 MPa whilst the 10% and 100 % brine-saturated cores obtained approx. 3% additional axial strain, and correspondingly, the extra side stress required to sustain zero radial strain was 2.3 MPa and 1.7 MPa, respectively. We expect that a similar phenomenon could occur in reservoir systems when seawater is injected. In these cases, it is expected that the horizontal stresses would increase, since the uni-axial strain condition applies to reservoirs with large width to height ratios.

In Figure 1(c) before seawater injection, the compaction (strain) rate is different for all tests. However, irrespective of the original fluid composition, it is found that after only 2.5 PVs of seawater injection the creep rate for all three cases attained the same value. This shows that the wetting conditions have minor impact on the compaction rate after flooding 2.5 PVs of seawater through the core. In addition, it shows that the seawater induced weakening is abrupt and more prominent when there is almost zero initial water in the core. Thus in mixed wet cores, oil is not blocking seawater access to the intergranular contacts.

CONCLUSIONS

1. Completely oil-saturated core is found to be stronger compared to partially or completely brine-saturated cores.
2. Uni-axial compaction rate accelerates when seawater is injected.
3. The initial accelerated compaction by seawater injection is affected by the initial fluid chemistry.
4. After injecting 2.5 PVs of seawater, initial saturation and wetting state have minor effects on compaction rate.

ACKNOWLEDGEMENTS

The authors would like to thank the Research council of Norway and the industry partners; ConocoPhillips Skandinavia AS, BP Norge AS, Det Norske Oljeselskap AS, Eni Norge AS, Maersk Oil Norway AS, DONG Energy A/S, Denmark, Statoil Petroleum AS, ENGIE E&P NORGE AS, Lundin Norway AS, Halliburton AS, Schlumberger Norge AS, Wintershall Norge AS of the National IOR Centre of Norway for support.

REFERENCES

1. Sylte, J.E., L.K. Thomas, D.W. Rhett, D.D. Bruning and N.B. Nagel, “Water Induced Compaction in the Ekofisk Field”, Presented at the SPE Annual Technical Conference and Exhibition, Houston, Texas, SPE 56426 (1999).
2. Megawati, M., A. Hiorth, and M.V. Madland, “The impact of surface charge on the mechanical behaviour of high-porosity chalk”, *Rock Mechanics and Rock Engineering*, (2012) **46**(5), 1073-1090.

3. Madland, M.V., A. Hiorth, E. Omdal, M. Megawati, T. Hildebrand-Habel, R.I. Korsnes, S. Evje, and L.M. Cathles, "Chemical Alterations Induced by Rock-Fluid Interactions when Injecting Brines in High Porosity Chalks", *Transport in Porous Media*, (2011) **87**, 679-702.
4. Korsnes, R.I., M.V. Madland, T. Austad, S. Haver, and G. Røsland, "The Effects of Temperature on the Water Weakening of Chalk by Seawater", *Journal of Petroleum Science and Engineering*, (2008) **60**, 183-193.
5. Zangiabadi, B., T.A. Davidian, R.I. Korsnes, K.A.N. Vorland, T.G. Kristiansen and M.V. Madland, "The effect of wetting conditions on the mechanical strength of chalk", *Proceedings of the 3rd International Conference on Coupled T-H-M-C Processes in Geo-systems, Lille, France*, (2008), 179-186.
6. Zangiabadi, B., R.I. Korsnes, M.V. Madland, T. Hildebrand-Habel, A. Hiorth and T.G. Kristiansen, "Mechanical Properties of High and Lower Porosity Outcrop Chalk at Various Wetting States", Presented at the 43rd US Rock Mechanics Symposium and 4th U.S.-Canada Rock Mechanics Symposium, Asheville, NC, ARMA 09-139 (2009).
7. Tang, G. and A. Firoozabadi, "Effect of pressure gradient and initial water saturation on water injection in water-wet and mixed-wet fractured porous media", *SPE Reservoir Evaluation & Engineering*, (2001) **4**(6), 516-524.
8. Strand, S., M.L. Hjuler, R. Torsvik, J.I. Pedersen, M.V. Madland and T. Austad, "Wettability of Chalk: Impact of Silica, Clay Content and Mechanical Properties", *Petroleum Geoscience*, (2007) **13**, 69-80.
9. Omdal, E., M.V. Madland, T.G. Kristiansen, N.B. Nagel, R.I. Korsnes and A. Hiorth, "Deformation Behavior of Chalk Studied Close to In-Situ Reservoir Conditions", *Rock Mechanics and Rock Engineering*, (2010) **43**, 557-580.

FIGURES AND TABLES

Table 1: Mechanical properties of the chalk cores

Core		K01	K02	K03
Yield Stress	MPa	8.85	14.92	18.45
Total depletion strain	%	2.72	1.16	0.64
Young's Modulus	GPa	2.81	3.47	4.05

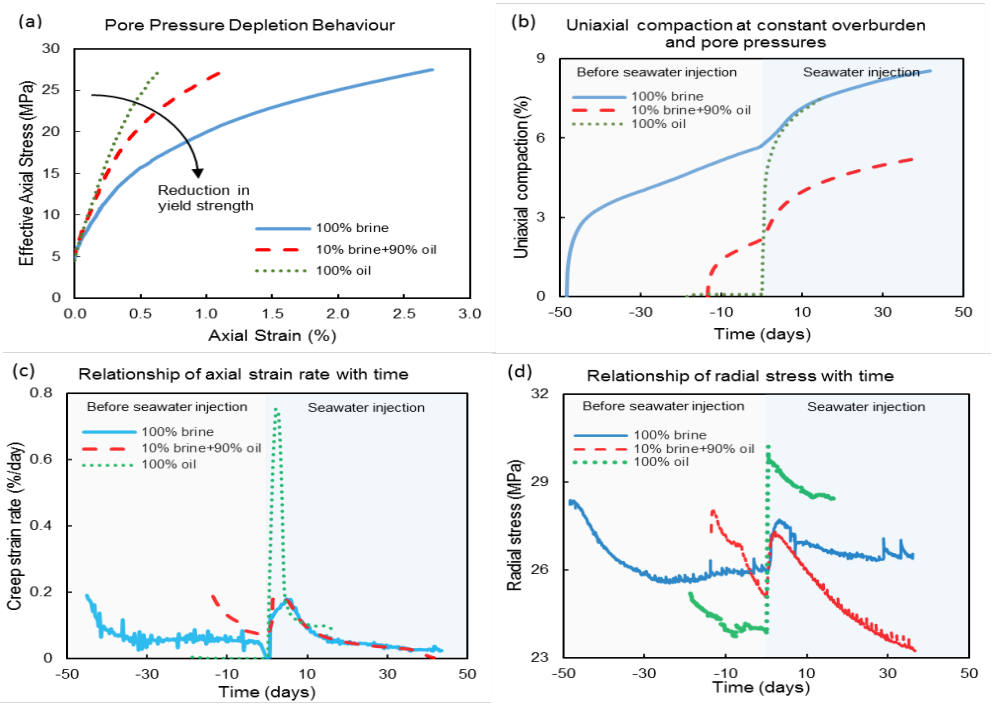

Figure 1: (a) Axial stress vs axial strain for all cores. (b) Compaction curves for all tests. (c) Compaction strain rate for all tests. (d) Radial stress curves for all tests. Please note that the starting time of seawater injection is taken as t=0 days in (b), (c) and (d).